IMPERIAL COLLEGE OF SCIENCE AND TECHNOLOGY

(University of London)

Department of Electrical Engineering

ANTENNAS BASED ON A WIRE PARALLEL TO A REACTIVE PLANE INTERFACE

by

Abdol Hamid Radjy, M.A. Cantab.

A Thesis Submitted for the Degree of

Doctor of Philosophy of the University of London

September, 1974.

ABSTRACT

The thesis is concerned with the evaluation of the characteristics of an antenna which, in its simplest form, consists of a length of conducting wire parallel to a reactive strip; the antenna is energized by a discrete voltage source, and terminated in a matched impedance, connected between the wire and the strip. The study presented is concerned with two forms of this antenna in particular: the Beverage antenna which has been a subject of controversy, although studied extensively in the past; and the Inductive-Plane-Antenna (IPA), which is a new proposal.

The inductive strip employed in the construction of the IPA consists of a conducting plane with uniform periodic corrugations. A new theoretical approach is used to determine the propagation factor of the IPA, and the results are compared with laboratory measurements. The far-field characteristics are determined by analysis, and agreement is obtained with results of field measurements carried out on a test-site. The IPA is a wide-band, directive antenna, with low dispersion; it is suitable for operation in the VHF or UHF bands.

The analysis for propagation constant is applied to the Beverage antenna, for comparison with other theoretical results published to date. A critical survey of the Beverage antenna is presented, and the controversial question of its mode of action is discussed.

Some modifications are proposed for the IPA and their relative merits are considered. Finally, a qualitative appraisal of the IPA characteristics is presented, and various proposals for increasing the efficiency of the Beverage antenna are examined.

ACKNOWLEDGEMENTS

First and foremost, the author would like to express his gratitude towards his parents, Mrs. Shamsi Kalali Radjy and Mr. Abol Hassan Radjy, for their patient understanding and encouragement which have made this research study possible.

The author is indebted to Mr. H. Page for his instructive criticisms and constructive guidance throughout the research program; also for having taught him even his first lessons in antenna engineering.

The author also wishes to thank Dr. A.F. dos Santos (at the Instituto Superior Tecnico, University of Lisbon) for his helpful suggestions, and Professor J. Brown (Head of the Electrical Engineering Department, Imperial College), for useful discussions of related problems.

The author is grateful to Imperial College for providing the research facilities, and for their token of financial support granted from the Metropolitan Vickers Fund. He also wishes to remember with thanks the late Mr. W.A. Gurnhill for his cooperation in the construction of experimental models, measuring devices and apparatus.

Thanks are also extended to the author's colleagues, who continually contributed to many interesting discussions which are so pertinent to sustaining a spirit of inquiry necessary in a research environment; C. Chappas, R.J. Chignell, N. Williams, P.J. Mitchell and T. Ege - to name but a few.

Last but not least, the author wishes to thank Miss E.A. Farmer for typing the final manuscript with efficiency and charming kindness.

"The point is that, whenever we propose a solution to a problem, we ought to try as hard as we can to overthrow our solution, rather than defend it. Few of us, unfortunately, practise this precept; but other people, fortunately, will supply the criticism for us if we fail to supply it ourselves. Yet criticism will be fruitful only if we state our problem as clearly as we can and put our solution in a sufficiently definite form - a form in which it can be critically discussed."

Karl R. Popper

[from the (1959) Preface to 'The Logic of Scientific Discovery']

CONTENTS

	Page:
TITLE	I
ABSTRACT	II
ACKNOWLEDGEMENTS	III
A QUOTATION FROM KARL R. POPPER	IV
CHAPTER I - INTRODUCTION	
1.1 Problem Definition	1
1.2 Development of the Inductive-Plane Antenna (IPA)	4
1.3 The Beverage Antenna	8
Appendix 1A Antenna Noise Considerations	11
References	13
CHAPTER II - PROPAGATION ALONG A WIRE PARALLEL TO A PLANE INTERFACE	
2.1 Introduction	14
2.2 An Appraisal of Studies Related to the Propagation Constant of the Beverage Structure	14
2.3 The Surface Impedance Concept	24
2.4 Propagation Constant Along a Uniform Structure	27
2.5 Effect of Approximations on the Propagation Constant	34
References	39
CHAPTER III - PROPAGATION CONSTANTS OF THE BEVERAGE ANTENNA AND THE IPA	
3.1 Introduction	42
3.2 Evaluation of Integrals in the Expression for Propagation Constant	42
3.2.1. A Priori Assumptions	42
3.2.2. Approximations in the Distribution of Magnetic Field	45
3.2.3. Approximations in the Distribution of E_z	47
3.2.4. Evaluation of Denominator D	50
3.2.5. Determination of the Weighting Function q_2	51
3.2.6. Characteristic Impedance Z_c	52
3.3 Calculations for a Transition-Boundary Interface	55
3.3.1. Approximations Related to Transition-Boundary Parameters	55

Page:

3.3.2. Summary of Equations 59
3.3.3. Propagation Constant of the Beverage Structure: Comparison With Other Theories 62
3.4 Calculations for a Corrugated-Plane Interface 73
3.5 Near-field Measurements on the Inductive-Plane-Antenna 77
3.5.1. Preliminary Experiments 77
3.5.2. Experimental Determination of the Propagation Constant 79
3.6 Comparison Between Theory and Experiment 82
Appendix 3A Diffraction By An Infinitely Long, Perfectly--Conducting Cylinder 91
3A.1 Field Scattered by the Cylinder 91
3A.2 Current Induced in the Wire 95
Appendix 3B Branch Cuts Associated with the Transverse Wave Number h 98
Appendix 3C Propagation Along Parallel Wires Equidistant From A Plane Interface 102
3C.1 Characteristic Impedance of the Coupled Line 103
3C.2 Evaluation of $G = \int_{-\infty}^{\infty} |H_{oy}|^2 dy$ for the Coupled Line 109
References 113

CHAPTER IV - ANALYSIS OF RADIATION CHARACTERISTICS
4.1 Introduction 114
4.2 Radiation Characteristics of the Beverage Antenna : An Historical Survey 117
4.3 Mode of Action of the Beverage Antenna 122
4.4 Considerations of Symmetry 126
4.5 Near-Field Scattering By An Impedance-Strip on Perfect Ground 133
4.5.1. General Considerations 133
4.5.2. Distribution of E_z Along the Position of the Wire 134
4.5.3. Evaluation of Results for Near-Field Scattering 141
4.5.4. Distribution of E_x Near the Impedance-Strip 149
4.6 Radiation Pattern of IPA 152
4.6.1. Problem Definition 152

Page:

4.6.2. Application of the Reciprocity Theorem 155
4.6.3. Principal-Polarization Radiation Pattern; Evaluation of V_p 160
4.6.4. Cross-Polarization Radiation Pattern ÷ Evaluation of V_q 163
4.7 Power Gain of the IPA 164
4.8 Directivity of the IPA 167
Appendix 4A Field of Horizontal Doublet Above Perfectly-Conducting (Plane) Ground 169
Appendix 4B Field of a Vertical Doublet Above Perfectly-Conducting (Plane) Ground 171
References 173

CHAPTER V - FAR FIELD MEASUREMENTS
5.1 Introduction 177
5.2 The Reference Antenna 180
5.3 Test Antenna for E-Plane Measurements 182
5.4 Test Antenna for H-Plane Measurements 187
5.5 Preliminary Measurements 188
5.5.1. Evaluation of the Test-Site 188
5.5.2. Examination of Far-Field Conditions 192
5.5.3. Reference Antenna Characteristics 194
5.6 Comparison of Experimental and Theoretical Results 199
5.6.1. H-Plane Characteristics 199
5.6.2. E-Plane Characteristics 213
5.6.3. Concluding Remarks 228
References 233

CHAPTER VI - APPLICATIONS
6.1 Introduction 234
6.2 Proposals for Increasing the Efficiency of the Beverage Antenna 236
6.3 Proposed Modifications to the IPA 240
6.4 Comparison of the IPA with Other Antennas 243
6.5 Suggestions for Future Work 245
Appendix 6A A Critical Appraisal of "A Leaky-Wave Transmitting Antenna for the Band 3 - 30 MHz" 247
References 252

List Of Principal Symbols 254

CHAPTER I

INTRODUCTION

1.1. Problem Definition

The study described in this thesis is concerned with the evaluation of a class of travelling-wave structures from the view-point of antenna engineering. In its simplest form, the structure considered consists of a finite straight length of perfectly-conducting wire, in free-space, parallel to a plane interface: the system is excited by a discrete voltage source connected between one end of the wire and the interface; the other end of the wire is connected to the interface through a resistance of appropriate value. The configuration is depicted schematically in Fig. 1.1.

The structure generally exhibits guiding characteristics similar to a transmission line, and, by analogy, we shall employ terms from transmission line theory when referring to various aspects of the structure considered.

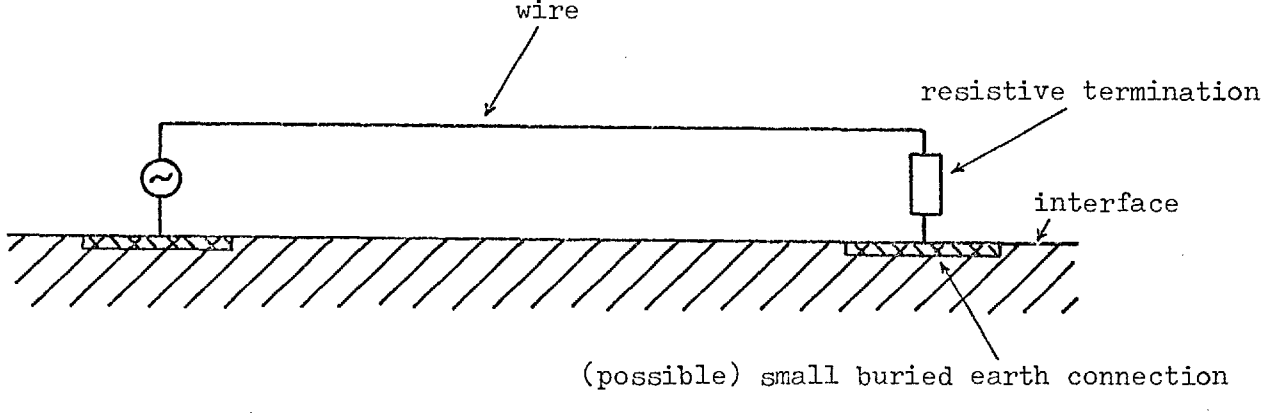


Fig. 1.1. The basic form of the structure considered

The interface may represent a transition boundary between the free--space region and an isotropic homogeneous medium, such as ground. In

this case we obtain the well known Beverage antenna. Alternatively the interface may be a true boundary, such as a reactive plane or a lossy sheet. Another possibility is a transition boundary with a stratified medium, or the upper surface of a slab of (dielectric) material, possibly grounded with a perfectly conducting sheet. However, we shall restrict our study to the Beverage antenna and the case when the interface represents an inductive plane, i.e., when the surface impedance of the plane considered has a positive reactance. We shall refer to the latter as the Inductive Plane Antenna (IPA).

A number of variations are possible in the basic configuration described, both for the Beverage antenna and for the IPA. We shall consider the modified forms of the Beverage antenna in Chapter VI, where various proposals for increasing its radiation efficiency are examined. As for the IPA, two arrangements will be considered in particular, as depicted in Figs. 1.2 and 1.3 (p. 3). We shall describe these arrangements in the next section.

We are primarily interested in the far field, input impedance and dispersion characteristics of the antenna. All of these characteristics are more or less dependent on the mode of propagation of electromagnetic waves along the structure; hence it is important to determine the propagation factor along the antenna. Chapter II is devoted to this problem, where we shall derive a new expression for the propagation constant of electromagnetic waves along a uniform structure. In Chapter III the result will be evaluated both for the Beverage antenna and for the IPA. In Chapters IV and V we shall be concerned with far field considerations, with emphasis on the IPA characteristics. Applications arising from this research study will be examined in Chapter VI.

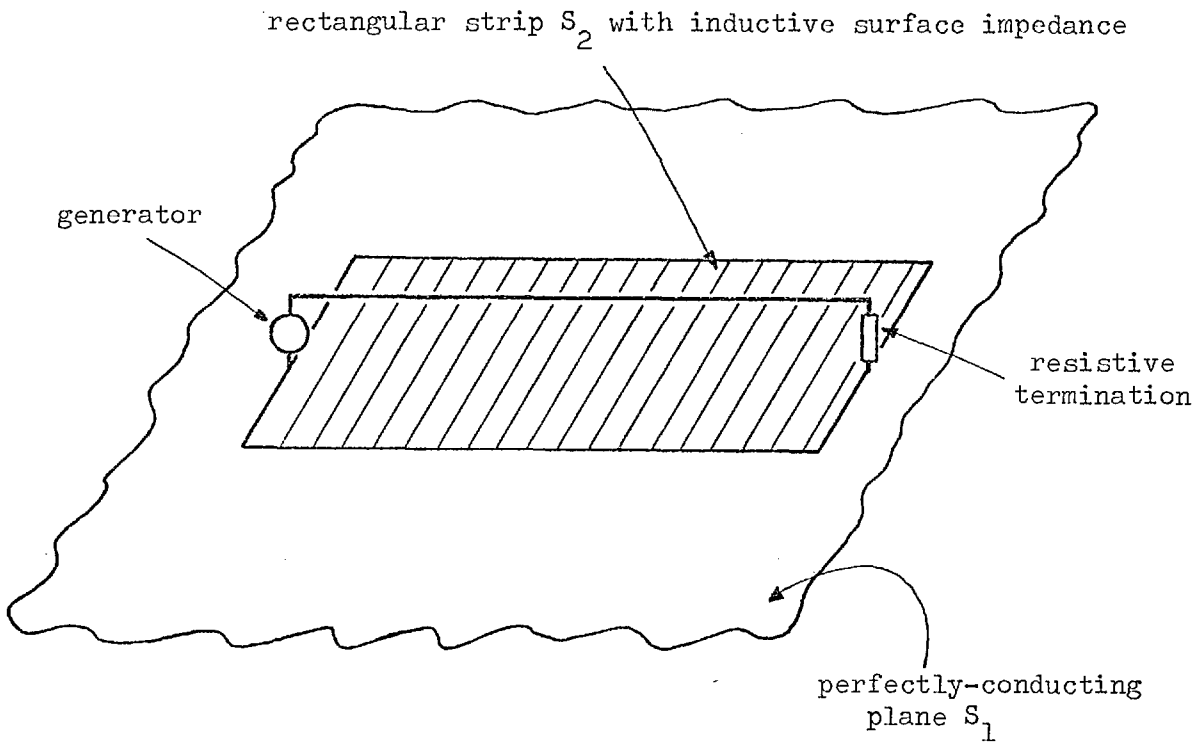


Fig. 1.2 Schematic representation of IPA_1. The inductive strip consists of short-circuited corrugations with perfectly-conducting walls : the walls lie in planes perpendicular to the wire.

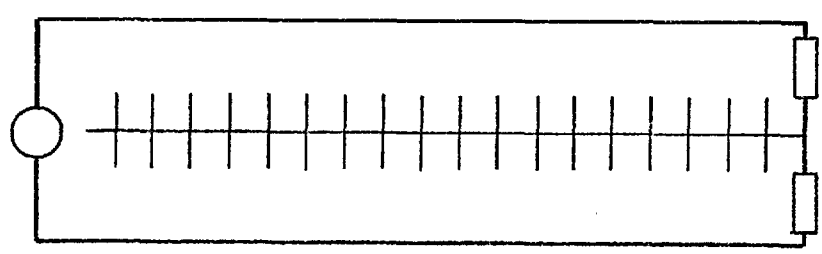


Fig. 1.3 Schematic representation of IPA_2. The rectangular strip (shown edgeon) is inductive on both sides, made of short-circuited corrugations. The generator (or receiver) is connected in series between the two wires.

1.2. Development of the Inductive-Plane Antenna (IPA)

The present study was initiated by a requirement for a directive wide-band antenna for operation in VHF and UHF bands. Originally, a two-element end-fire array of rhombics was considered: however it was found that the radiation pattern was frequency sensitive due to deterioration of the element pattern at lower frequencies, and due to deterioration of the array factor pattern at higher frequencies.

Subsequently it was decided to evaluate the performance of the Beverage antenna at frequencies above 100 MHz due to its wide-band characteristics. It was found that high ohmic losses in the ground resulted in low gain figures and poor directivity. Hence it was proposed to replace the air-ground interface by an artificial impedance plane in order to reduce the antenna losses.

Early in the research program a decision had to be made as to the method of achieving a suitable surface impedance. The first approach was to construct an 'artificial ground' from an appropriate material whose dielectric constant and conductivity could be controlled. A proposal was made to use expanded polyurethane foam loaded with aquadag (a suspension of fine carbon particles in water). Samples of material were prepared using a wide range of concentrations of aquadag. Unfortunately, measurements indicated no significant variation of either conductivity or dielectric constant with concentration of aquadag used. Furthermore, in the frequency range of interest (UHF), theory indicated excessive losses for antennas based on this artificial ground. Eventually this material was only used to simulate real earth in a scaled model of the Beverage antenna [Ref. 1.4].

The inductive-plane used in experimental studies of the IPA consisted of short-circuited corrugations, as shown in Fig. 1.4: the material used was aluminium, and details of construction are given in

Chapter III. This choice has two advantages: firstly, ohmic losses

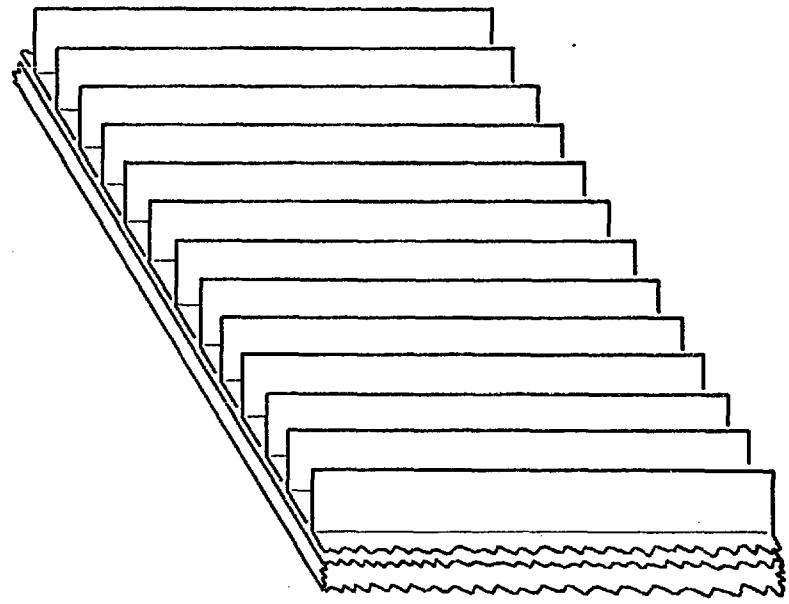


Fig. 1.4. Schematic representation of the corrugated plane used in the construction of IPA

in the surface are negligible; secondly, proper choice of corrugation dimensions ensures that only one dominant mode (TEM) propagates in the corrugations [Ref. 1.5], reducing uncertainties in the value of surface reactance obtained. (The concept of surface impedance is discussed in Section 2.3).

Two particular forms of Inductive Plane Antenna will be considered. The first configuration, IPA_1, is shown in Fig. 1.2 (p. 3): the corrugation walls are in planes perpendicular to the direction of the wire. The depth of corrugations is chosen such that the surface reactance is positive in the rectangular region S_2; the surface impedance over S_1, the remainder of the plane, is zero. This arrangement is suitable for flush-mounting in a conducting surface, or when the antenna is constructed on the surface of ground. In the latter case, the finite conductivity of ground over the region S_1 (in Fig. 1.2) only modifies the far field of the antenna near ground, and causes a

reduction in the antenna gain.

The second arrangement, IPA_2, shown in Fig. 1.3, is equivalent to two IPA_1's placed back-to-back and excited in series. It was thought that IPA_2 might be used as a compact directive antenna with the main beam in the end-fire direction. In fact, this arrangement is a special case of the more general 'wedge configuration', as depicted in Fig. 1.5. The wedge configuration has inherently potential wide-band characteristics, and was considered due to a demand for a wide band directive

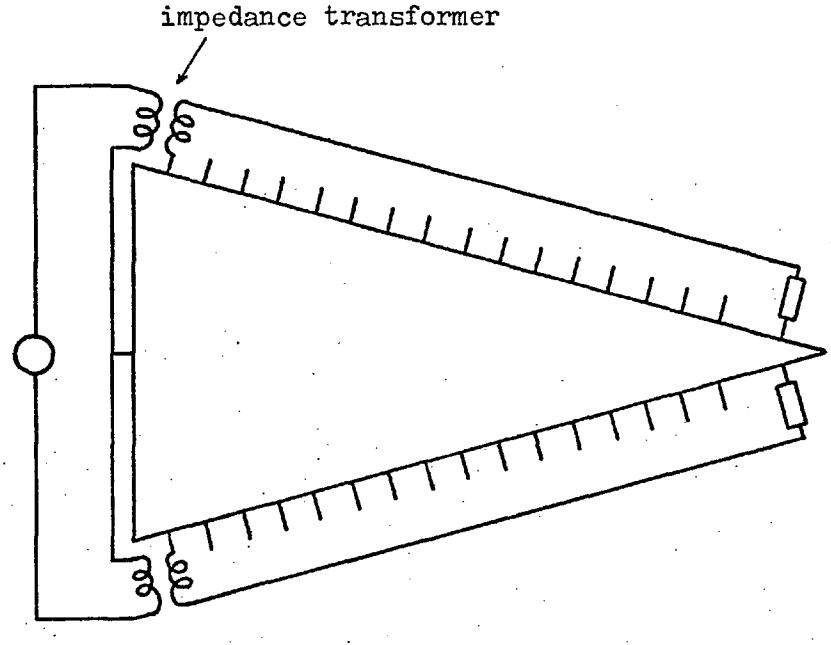


Fig. 1.5. Schematic representation of wedge configuration of IPA

antenna in the frequency bands VHF and UHF. The IPA_2 configuration was chosen for further evaluation primarily due to its comparatively simple construction, but also because the wedge-configuration required a more complex experimental set up.

It should be pointed out that the original requirement which initiated the present study was fulfilled by an alternative antenna in the first stages of this research programme. (The alternative antenna was designed at G.E.C.'s Hirst Research Centre, and consisted of an array of two log-periodic-dipole antennas arranged in the wedge configuration). Nevertheless it was decided to proceed with the research programme, in order to determine the characteristics of the IPA, using the specifications in the original requirement as a frame of reference throughout the work. The broad specification is given below:

Frequency band	:	150 - 1000 MHz
Overall length	:	not greater than 3 m
3-dB beamwidth	:	40° (or 10 dB directivity)
Sidelobes	:	better than - 15 dB
Absolute gain	:	not less than 5 dB
Impedance S.W.R.	:	not greater than 2:1 over the band

As it turned out, the IPA could not fulfill the above specification. This point will be further discussed in Chapter VI.

1.3. The Beverage Antenna

In 1923 an antenna was proposed which consists of a long horizontal wire, supported a short distance above ground, in a straight line. The configuration is shown in Fig. 1.1 (p. 1). When used for reception, the end of the line nearest the transmitting station is terminated in a suitable resistance, corresponding to a nearly matched load; the receiver is connected at the other end, between the wire and ground. Usually a small buried earth system is employed at each end, to ensure proper connections to ground.

This antenna is now commonly referred to as the Beverage antenna, as mentioned in the first section. Originally it was developed for the reception of trans-Atlantic transmissions in the LF band 40-130 KHz [Ref. 1.1]; later applications included VLF [Ref. 1.2], Medium Frequencies [Ref. 1.3], and High Frequencies [Ref. 1.4].

During the last half century, numerous papers have been published on the Beverage antenna. By far the greater volume of attention devoted to this subject has been concerned with theoretical analyses and applications of the system. Fortunately a few experimental studies have also been carried out. Nevertheless, certain aspects of this problem appear to remain a subject of some controversy to the present day. For example, a question which has remained unanswered is whether radiation from the Beverage antenna occurs from the end of the structure or continuously along its length.

Another area of contention has been the propagation constant of the Beverage antenna: sometimes, the desired correlation between experimental work and theoretical results has not been obtained; often, different analyses have led to divergent results; in one instance, even contradictory experimental results have been reported.

In view of the above controversy, in Chapter II we shall make an appraisal of the extensive work published to date relating to the

propagation constant of the Beverage structure. On the other hand, there has been general agreement about methods of calculating the radiation pattern of this antenna; hence, in Chapter IV, we shall merely mention some of the more significant studies reported on this subject. The question of 'the mode of action' of the Beverage antenna will also be dealt with in Chapter IV.

The extensive application of the Beverage antenna for reception is due to its wide-band characteristics, simple construction and low cost. It has a directive radiation pattern with reasonably good sidelobe levels, and bandwidths as large as 10:1 have been envisaged. The radiation efficiency is relatively low (typically less than 25% at HF); however, efficiency is not an important consideration for a receiving antenna when external noise is predominant compared to receiver noise. (This question is considered in Appendix 1A). Hence, for reception at HF and lower frequencies, the directive characteristics of the Beverage antenna are generally sufficient to provide improved signal discrimination against (external) noise and interference. Furthermore, its low cost makes the Beverage antenna suitable for use as the element in a circular receiving array to give a steerable beam [Ref. 1.4].

The Beverage antenna has seldom been considered for the purpose of transmission to date. This is due to an inherent disadvantage of low radiation efficiency which results in relatively low gain figures. The low efficiency arises from comparatively high ohmic losses in the ground. Radiation from this antenna is also directly related to the conductivity of ground; choosing an antenna site with relatively high conductivity, in order to reduce the losses, generally results in lower gain figures, even though the directivity increases. In the limit as ground conductivity tends to infinity, the Beverage antenna approaches

an ideal transmission line, with radiation occuring from the line terminations only.

In view of the advantages mentioned earlier, recently considerable attention has been given to methods of increasing the efficiency of the Beverage antenna : a higher efficiency would make it suitable for transmission, as well as reception, and could also extend its application to the higher frequencies VHF and UHF. The present study was carried out with this important consideration in mind, and the performance characteristics of the IPA have a direct bearing on the efficiency of the Beverage. This approach and other proposals for improving the efficiency of the Beverage are discussed in Chapter VI.

APPENDIX 1A

ANTENNA NOISE CONSIDERATIONS

For a transmitting antenna, the gain G and directivity D can be defined as follows : the antenna gain is the ratio of the maximum power intensity (in the far-field) of the antenna to the maximum power intensity of a reference (lossless) antenna with the same power input. The gain referred to an isotropic radiator is known as the absolute gain G_o. The antenna directivity is the ratio of the maximum power intensity to the average power intensity (in the far-field).

The radiation efficiency η can be defined by the following equation

$$\eta = \frac{G_o}{D} \qquad (1A.1)$$

It should be noted that the efficiency is also the ratio of the total power radiated to the total power input of the antenna.

It can be shown that the signal-to-noise ratio (SNR) at the output of the receiving antenna is given by

$$\frac{S}{N} = D \frac{S_o}{kT_b B} \frac{1}{1 + \frac{(1 - \eta)T_p}{\eta T_b}} \qquad (1A.2)$$

where S_o is the available signal power at the output of an isotropic antenna; k is Boltzmann's constant (1.38×10^{-23} J/°K), and B the receiver bandwidth; T_b, the antenna brightness temperature (related to the external noise); and T_p, the physical temperature of the antenna and its surroundings.

It is evident that the improvement in SNR is approximately equal

to the directivity D provided that

$$\eta T_b \gg (F - \eta)T_p \qquad (1A.3)$$

where F is the noise figure of the preamplifier or receiver.

For example, the maximum efficiency of the Beverage antenna is 25% at HF [Ref. 1.6]: consideration of external noise levels [Ref. 1.7] indicates that, for a given directivity, increasing this efficiency at HF might improve the SNR by approximately 3 dB or less.

Taking into account the receiver noise Figure F, rearrangement of Eq. (1A.2) yields

$$\frac{S}{N} = \eta D \frac{S_o}{kT_p B} \frac{1}{F + \eta(\frac{T_b}{T_p} - 1)} \qquad (1A.4)$$

It is readily seen that when thermal noise or receiver noise predominates over external noise, increasing the antenna gain (= ηD) would lead to a corresponding improvement in the SNR. Consequently, efficiency becomes an important consideration in the design of receiving Beverage antennas at VHF and higher frequencies.

REFERENCES

1.1 Beverage, H.H., Rice, C.W., Kellog, E.W.: "The wave antenna: a new type of highly directive antenna" , A.I.E.E., Vol. 42, pp 215-266, February, 1923.

1.2 Seeley, E.W.: "Optimum reception pattern of the Beverage wave antenna at Very Low Frequencies", Journal of Research of National Bureau of Standards, Vol. 67D, No. 4, pp 387, 395, July-August, 1963.

1.3 Belousov, S.P., Yampolskii, V.G.: "Single-wire medium wave travelling-wave receiver antennas", Radiotekhnika, Vol. 15, pp 16-25, 1960.

1.4 dos Santos, A.F.: "Multi-beam receiving antenna for the band 3-30 MHz", Ph.D. thesis, Dept. of Elec. Engineering, Imperial College, London, September 1970.

1.5 Collin, R.E.: "Field Theory of Guided Waves", McGraw-Hill, 1960, pp 465-8.

1.6 dos Santos, A.F.: Op. Cit., p. 78.

1.7 C.C.I.R.: 'World Distribution and Characteristics of Atmospheric Radio Noise', Report 322, International Telecommunication Union, Geneva, 1964.

CHAPTER II

PROPAGATION ALONG A WIRE PARALLEL TO A PLANE INTERFACE

2.1. Introduction

It is a formidable problem to determine the variation of electromagnetic waves along the length of the antenna considered, be it the Beverage antenna or the IPA. It is easier to obtain the propagation constant for the corresponding structure of infinite or semi-infinite length. This technique gives very good approximations to the desired solution if the antenna length is at least of the order of a wavelength, and if the spacing between the wire and the interface is much less than the antenna length. In all the literature published to date on the Beverage antenna, this technique has been at least implicit in the derivation of expressions for the propagation constant. In section 2.4. we shall derive an expression for the propagation constant of electromagnetic waves along a uniform structure: the results will be evaluated for the Beverage antenna in Section 3.3, and for the IPA in Section 3.4; again the assumption will prevail that results derived for an infinite line are valid for structures of finite length which are of interest.

However, we shall start, in the next section, by presenting an appraisal of the extensive work published to date concerning the propagation constant of the Beverage antenna, with a view to relating differences between the results obtained with differences in assumptions made in the analyses.

2.2. An Appraisal of Studies Related to the Propagation Constant of the Beverage Structure

During the last half century, numerous papers have been published

on the Beverage antenna. By far the greatest volume of attention devoted to this subject been concerned with theoretical analyses and applications of the system. Fortunately, a few experimental studies have also been carried out. Nevertheless, certain aspects of this problem appear to remain a subject of some controversy to the present day. For example, a question which has remained unanswered is whether radiation from the Beverage antenna occurs from the end of the structure, or continuously along its length.

Throughout the discussion of various published papers in this section, the configuration and coordinate system of Fig. 2.2, page **28** , will be used, and not the coordinate systems used in the original (published) papers.

The first paper published on the Beverage antenna was in 1923, by H.H. Beverage, C.W. Rice and E.W. Kellog [Ref. 2.1]. The near-field study was mainly experimental in nature, although recourse was made to transmission-line equations for analysis of measured data, and for extrapolation for design purposes. This excellent paper contains detailed accounts of both measurement techniques and experiments carried out.

The investigation was performed in the VLF band. Beverage's first antenna consisted of an insulated wire, approximately 9 km long, laid over ground in nearly a straight line : the end nearest the transmitting station was grounded, and the receiver was connected at the other end between the wire and ground. Beverage found that, on reception, the signal current in the wire increased towards the receiver, reaching a maximum and then decreasing. By inserting series condensers in the line he was able to shift the current maximum towards the receiver. The receiver was then replaced by an oscillator and the measurements were repeated : the current was found to have a phase velocity much

less than the free-space value, corresponding to the same frequency, and high attenuation was observed along the line. Also, it was found that series capacitive loading increased both the attenuation and the phase velocity along the line.

Later, a more sophisticated line was constructed with a number of wires at different heights, between 5.5 and 9.2 metres, above ground. Values of attenuation constant and phase velocity were calculated from input impedance measurements made with short-circuit and open-circuit terminations.

Unfortunately, Beverage's experimental results cannot be used, with confidence, for checking subsequent analytical results obtained by other theoreticians : this opinion is based on two reasons. Firstly, for any particular set of results, the number and exact heights of wires used are never stated explicitly. Secondly, there is some uncertainty in the effective value of ground conductivity that should be used in computations. Beverage measured the specific resistance of sandy soil in the vicinity of the line, and obtained a value equivalent to a conductivity $\sigma_2 = 5 \times 10^{-5}$ s/m. However, the authors themselves do not regard this as a representative value, for two reasons : firstly, ground water was found to occur at a depth of 30 metres below ground (At 30 KHz, skin depth $\delta \simeq 100$ m for $\sigma_2 = 10^{-3}$ s/m). Secondly, moisture content of ground was judged to be generally higher than in the sample used by Beverage.

If ground conductivity is inferred from Zenneck's formula [Ref. 2.2], using the value for "wave front tilt" as measured by Beverage, we obtain a conductivity $\sigma_2 \simeq 2 \times 10^{-3}$ s/m.

The first significant theoretical analysis of the Beverage problem was by J.R. Carson in 1926 [Ref. 2.3]. He made a series of simplifying assumptions which limited the range of validity of his analysis. These

assumptions were: (i) polarization currents are neglected in the conducting region; (ii) phase variations in the cross section are regarded as negligible in the dielectric region; (iii) only axial currents are considered in the conducting regions; (iv) the wire radius is assumed to be small, and the current distribution is symmetrical in the wire cross section.

Transmission line equations are used to derive expressions for propagation constant γ and characteristic impedance Z_c, in terms of Z_{12}, the series loading effect due to ground of finite conductivity. Z_{12} is obtained by evaluating E_z, the longitudinal component of electric field, at the surface of the wire. E_z is expressed in terms of a scalar potential V and axial component A_z of the magnetic vector potential. V is obtained from the electrostatic solution for perfect ground. A_x and A_y are zero by assumption (iii), and A_z is obtained by integrating H_y in the dielectric region. H_y is formulated in terms of a Fourier integral (y being the transformed variable), for which the transform is derived from continuity of H_x and H_y across the interface (relative permeability μ_r of ground is taken as unity). It is interesting to note that Carson's formulation leads to the continuity of E_z also.

In 1934, W.H. Wise [Ref. 2.4] extended Carson's analysis by removing assumptions (i), (ii) and (iii) above. Wise derived an expression for $\underline{A}$ by integrating the contribution due to a current-element along the wire. In this way he obtained components A_x and A_z for the magnetic vector potential. Like Carson, he expressed E_z in terms of A_z and a scalar potential V, but he defined V by using the Lorentz condition $\nabla \cdot \underline{A} = - j\omega\epsilon\mu V$. Wise's expression for Z_{12} can only be evaluated for zero attenuation along the wire; hence, as a first approximation, he assumes $\gamma = jk$ where k is the free-space wave number

(Carson derived Z_{12} by assuming $k \simeq 0$).

Wise also noted that the distributed capacitance of the line was modified by finite ground conductivity; however, he neglected this effect due to complexity of the associated computational problem.

M. Jenssen's paper [Ref. 2.5] contains two sections with a direct bearing on the question of the propagation constant. Jenssen considers a line consisting of three parallel wires above ground, all at the same height, and with equal spacing. He shows that three modes of propagation are possible, with distinct values of γ^2: the existence of these modes depends on the excitation conditions and the configuration of terminations used. Expressions are given for currents, voltages and impedances associated with the modes. The analysis is based on Wise's results for the single wire.

Also presented are results of attenuation measurements made for the earth-return mode, over a frequency band 0.2 - 1.2 MHz. A graph of attenuation plotted against frequency indicates a smaller slope for the experimental data than for the theoretical curves, although agreement is close.

A selection of graphical results are given, for the propagation constant, in [Ref. 2.6], for applications in the medium frequencies band 150 - 1500 KHz. These results correspond to the analysis given by Wise.

E.W. Seely [Ref. 2.7] has reported an experimental study of velocity ratio, loss and impedance characteristics over the band 10 - 80 KHz. Based on measurements made before and during the rainy season, it is claimed that more moisture in the soil increased the antenna losses, and slowed down the wave along the line. Another surprising (experimental) result is that the variation of attenuation α with frequency f was almost linear (analysis indicates $\alpha \propto f^{\frac{1}{2}}$, approximately, at low frequencies). It must be pointed out that the antenna used consisted of

a length of cable (only the shield was used) lying on the ground in a straight line. It is possible that the anomolous results reported are due to the particular arrangement used, as the measurements would tend to be sensitive to local variations in ground parameters.

H. Kikuchi [Refs. 2.8, 2.9, 2.10] has provided one of the most rigorous solutions to the Beverage boundary-value problem. He starts with the wave equations for the magnetic vector potential $\underline{A}$ and the scalar potential V. Applying Fourier transform techniques, boundary conditions at the interface (continuity of tangential electric and magnetic fields) lead to explicit expressions for the potential functions A_z and V. Then, from the boundary condition for E_z at the wire surface, Kikuchi derives a relation involving the potentials and the wire current I. He rearranges this equation to correspond to transmission-line equations, and thus identifies the equivalent circuit terms for series impedance Z and parallel admittance Y. Like Carson and Wise, Kikuchi defines γ and Z_c in terms of Z and Y; the latter are evaluated using asymptotic expansions. Kikuchi has noted that calculations are also possible in terms of convergent series, but the exercise is regarded as superfluous and therefore omitted.

Experimental work carried out in Japan [Ref. 2.11] strongly support Kikuchi's analysis. In fact, the only possibly significant limitation of Kikuchi's analysis is that his results rely on the validity of transmission-line equations. This leads to certain anomalies, which can generally be disregarded; for example, transmitted power obtained from the characteristic impedance Z_c does not equal power evaluated by integrating the complex Poynting vector. Furthermore, it seems that radiation effects are not included in the analysis. This tentative conclusion is supported by the observation that experimental attenuation results were consistently higher than indicated by

analysis, in the frequency band where ground currents are significant [Ref. 2.11].

A.F. dos Santos [Ref. 2.12] has made a similar analysis without recourse to transmission-line equations. His formulation is in terms of an electric Hertz vector potential $\underline{\pi}$, which has two components only : π_z parallel to the wire axis, and π_x normal to the interface. Like Kikuchi, dos Santos applies Fourier transform techniques; but he solves the dispersion equations directly, using a digital computer to apply numerical methods.

Dos Santos was the first person to realize that two distinct solutions of the dispersion relation are possible. One solution corresponds to a superposition of incoming plane waves above the wire, and satisfies the radiation condition at infinity : this solution has been termed 'the proper mode', for obvious reasons. The second solution, named 'the improper mode', corresponds to a superposition of outgoing plane waves above the wire, without conforming to the radiation condition. Both solutions are based on converging integral representations of potential functions.

Computed results indicate that both modes have similar phase velocities, but different attenuation characteristics : compared to the improper mode, the attenuation of the proper mode exhibits a greater rate of change with frequency, and a higher maximum value. At high frequencies the attenuation for both modes decreases with frequency. In contrast to Kikuchi's analysis, dos Santos' results do not indicate a minimum attenuation value since he neglects the finite conductivity of the wire.

J.R. Wait also takes the credit for providing one of the three most rigorous formulations of the Beverage boundary-value problem [Ref. 2.13], the other formulations being due to Kikuchi and dos Santos.

Wait expresses the total fields in terms of two scalar potentials : the z-components π and π^* of electric and magnetic Hertz vectors respectively. Using integral representations for the potentials, Wait derives the modal equation for propagation constant. This equation has a somewhat complicated form; however, a few justified approximations lead to complete correspondence with Kikuchi's results. Further simplification enables one to retrieve Carson's formula.

It must be noted that, like dos Santos, Wait considers only the case for a thin perfectly-conducting wire. He concludes that writing the modal equation in Carson's form yields the most general representation. For example, unlike Kikuchi's results, there are no limitations on the height b of the wire above the ground, and b can approach zero. For an infinitessimally thin wire located in the interface between two non-magnetic media of wave numbers k_1 and k_2, Wait obtains the simple result for the phase constant β given by

$$\beta = [(k_1^2 + k_2^2)/2]^{\frac{1}{2}}$$

A recent paper using a novel approach to the problem is due to P. Knight [Ref. 2.14]. The problem is formulated by considering a semi-infinite Beverage line, terminated in a matched load. Two pairs of terminals are considered, separated by a distance L, one of which is located at the antenna input. Starting with Monteath's compensation formula [Ref. 2.15], which is a particular form of the reciprocity theorem, Knight derives an expression for the change in the mutual impedance between the two pairs of terminals when perfectly-conducting ground is replaced by a ground of finite conductivity. Allowing L to tend to infinity leads to an expression for γ, in terms of a surface integral of fields evaluated over the interface. On the other hand, an expression for Z_c is obtained by letting L approach zero.

Theoretical results given for velocity ratio and attenuation factor are in agreement with other analyses for frequencies below 10 MHz approximately. Above 10 MHz, Knight's analysis gives attenuation results similar to Wise's theory, in contradiction to results predicted by Kikuchi, dos Santos or Wait. Knight also reports experimental data obtained in the frequency range 0.4 - 2.0 MHz. He presents graphs showing the variation with frequency of velocity ratio, attenuation and characteristic impedance. Correlation between theory and experiment seems excellent, except for theoretical attenuation results which are consistently higher than measured data.

There appear to be two numerical errors in Knight's paper. First, the expression used by Knight for the characteristic impedance Z_{co} of a thin wire parallel to perfectly-conducting ground is

$$Z_{co} = 60 \log_e(b/a)$$

where a is the radius of the wire. In the above expression a factor 2 is missing inside the brackets, i.e., (b/a) should be replaced by (2b/a). For Knight's parameters, this corresponds to an error of 42 ohms, or roughly 10%. Writing $Z_c = R_c + jX_c$ for the characteristic impedance of the Beverage line, and using the correct expression for Z_{co}, experimental results indicate values for R_c less than Z_{co} whereas theoretical values for R_c are greater than Z_{co} [Fig. 5a of Ref. 2.14].

The second error appears in the comparison between Knight's theoretical values and Beverage's measurements, [Table 1, Ref. 2.14]. Knight's theoretical results are calculated for a ground conductivity $\sigma_2 = 5 \times 10^{-3}$ S/m, whereas Beverage had measured "a specific resistance of about 2×10^6 ohms per centimetre cube" (equivalent to $\sigma_2 = 5 \times 10^{-5}$ S/m). Alternatively, based on 'wave front tilt' observations, we obtain $\sigma_2 = 2 \times 10^{-3}$ S/m. Furthermore, experimental results given by Beverage

pertain to antennas consisting of "two wires in multiple, seven to nine metres above ground"; Knight's calculations are based on a single wire eight metres above ground! Theoretical velocity ratios are in agreement with Beverage's figures, but attenuation results are greater by a factor of two.

Compensation theorem is a powerful tool in the solution of certain electromagnetic problems, as shown by Monteath [Ref. 2.15]. On the other hand, if the errors in Knight's paper are corrected, the divergence between theory and experiment seems unexplainable. Thus it is of interest to examine Knight's analysis further, especially as this analysis could easily be extended to the IPA problem.

Knight makes two approximations in particular which do not seem justified. He derives the magnetic field distribution on the interface in terms of a wire current I and its weighted image pI, where p is taken as the Fresnel reflection coefficient for normally incident uniform plane waves. Others have also used, successfully, the reflection coefficient approximation in the solution of similar problems [Ref. 2.16]; however, the reflection coefficient can generally not be taken as constant, and must be evaluated for individual geometric rays.

The second questionable approximation is that in the conducting region $x < 0$ the field is approximated by a predominant plane wave travelling in the x - z plane; however, the field is assumed to have a y variation as given by image theory on the plane $x = 0_+$. This inconsistency leads to a distribution for E_z which is discontinuous across the transition boundary.

It is thought that Knight's approach could yield more accurate results provided a more rigorous technique is employed for arriving at the required approximations.

Certain aspects of analyses by Kikuchi, dos Santos and Knight are discussed further in Section 3.3, using results of the analysis presented

in this thesis (Sections 3.2 and 3.3) as a basis for comparison.

2.3. The Surface Impedance Concept

Surface impedance is defined as the ratio of orthogonal components of tangential electric and magnetic fields at the surface considered [Refs. 2.17, 2.18]. Clearly, for an anisotropic surface the value of surface impedance depends on the direction of electric field, even though surface impedance is not a vector.

Throughout this thesis we make use of the surface impedance concept. However, the validity of this concept in the solution of boundary value problems has been questioned in spite of its frequent and successful applications over the last thirty years. Hence, before proceeding further, we shall briefly describe the development of this concept, and discuss the controversy associated with its applications.

S.A. Schelknnoff [Ref. 2.19, 2.20] has been credited with the proper evaluation of the significance and application of the wave impedance concept. Also, he determined propagation losses in a waveguide by evaluating the component of the complex Poynting vector directed into the guide surface, in terms of the tangential magnetic field and "impedance seen normal to the surface" [Ref. 2.19]. Later, impedance boundary conditions were used in studies dealing with propagation over earth, originally by Russian theoreticians during the nineteen--forties [Ref. 2.21]. Eventually, rigorous definitions of surface impedance appeared in numerous publications concerned with the analysis and application of surface waves, [For example, Refs. 2.17 and 2.18].

Criticism against the usefulness of the surface impedance concept has come from R.A. Waldron [Refs. 2.22, 2.23 and 2.24]. He points out that the value of surface impedance obtained depends not only on the nature and properties of the surface, but also on the configuration of fields near the surface: hence the value of surface impedance can not be

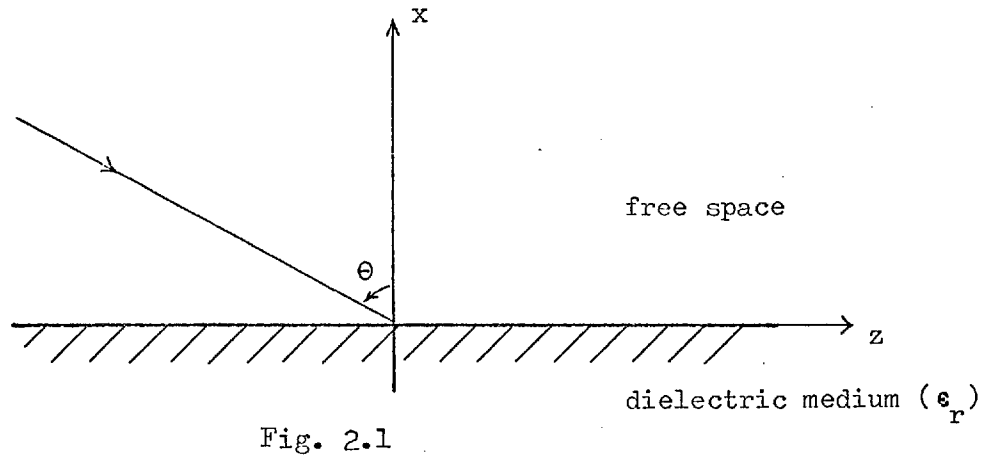


Fig. 2.1

known until the problem has been solved by another method in order to obtain the field distribution. Waldron cites two examples in particular, to demonstrate the invalidity of the surface impedance concept in the solution of boundary-value problems: we shall briefly describe these two examples in order to clarify the nature of Waldron's objections.

In one example [Ref. 2.23], Waldron considers a plane interface at $x = 0$ between free space, in the region $x > 0$, and a homogeneous dielectric medium, in the region $x < 0$, as depicted in Fig. 2.1. The dielectric region is characterised by complex relative permittivity ϵ_r. For a TM surface wave propagating in the z-direction, the surface impedance Z_s is given by

$$Z_s = \frac{Z_o}{(\epsilon_r+1)^{\frac{1}{2}}} \qquad (2.1)$$

Where Z_o is the intrinsic impedance of free-space. However, for a plane wave incident at an angle θ in the x - z plane, as shown in Fig. 2.1, the surface impedance is given as

$$Z_s = \frac{Z_o}{(\epsilon_r - \sin^2\theta)^{\frac{1}{2}}} \qquad (2.2)$$

which differs from eq. (2.1). According to Waldron, this difference demonstrates the ambiguity in the surface impedance value. In fact the above equation is only appropriate to TE polarization, i.e., for the magnetic field lying in the plane of incidence. The correct equation for TM polarization is

$$Z_s = Z_o \frac{(\epsilon_r - \sin^2\theta)^{\frac{1}{2}}}{\epsilon_r} \qquad (2.3)$$

Equations (2.1) and (2.3) appear to be different, but in fact (2.1) is merely a special case of (2.3). This can easily be shown by using the boundary condition corresponding to a pole or zero for the reflection coefficient at the surface, namely the relation

$$Z_o \cos\theta_1 = Z_s \qquad (2.4)$$

Substitution from (2.4) into (2.3) leads to (2.1).

In another example [Ref. 2.22], Waldron considers wave propagation inside a circular waveguide with a wall of finite conductivity. He presents two equations for the dispersion relation : one equation is derived by the application of the surface impedance concept, and the other by invoking the continuity condition for tangential fields at the wall boundary. He points out that there is no value of Z_s which will make the two equations identical. Hence the impedance concept is either not applicable, or only approximately valid. Waldron arives at this misplaced conclusion because he assumed identical values for the transverse and longitudinal surface impedances : at best, this is a good approximation for small values of surface impedance only [Ref. 2.25]; in fact, Waldron's equations yield identical results for the particular case of small surface impedance.

Although Waldron's arguments are essentially correct they do not invalidate the surface impedance concept, or its usefulness, for two reasons : firstly, the concept can be made completely rigorous by taking into account the dependence of the surface impedance on the nature of waves. For example, this has been achieved in the application of transverse resonance techniques to waveguide problems [Ref. 2.26], or to surface waves supported by a corrugated plane [Ref. 2.27].

Secondly, for a plane wave incident in a particular direction on a plane interface, a unique surface impedance can be defined, and the total field can be represented as an angular spectrum of plane waves. In many cases of interest, to a very good approximation, the surface impedance can be taken as a simple function of direction, or even independent of direction if the surface is isotropic. For a boundary between free-space and a material of high (complex) refractive index, the approximations involved in this technique have been evaluated theoretically, and found to be acceptable [Ref. 2.15, 2.28]. Furthermore, where experimental studies have been made, good correlation has been obtained with analysis using the surface impedance concept [for example Ref. 2.29].

The above considerations are regarded as sufficient justification for the judicious application of the surface impedance concept whenever this leads to a simplification or better physical understanding of the boundary-value problem.

2.4. Propagation constant along a uniform structure

In this section we consider a uniform transmission system of infinite length, such as depicted in Fig. 2.2 , with propagation in the positive z-direction, and assuming $\exp(j\omega t)$ time variation of fields. As we consider a uniform cross-section only, the variation of all field

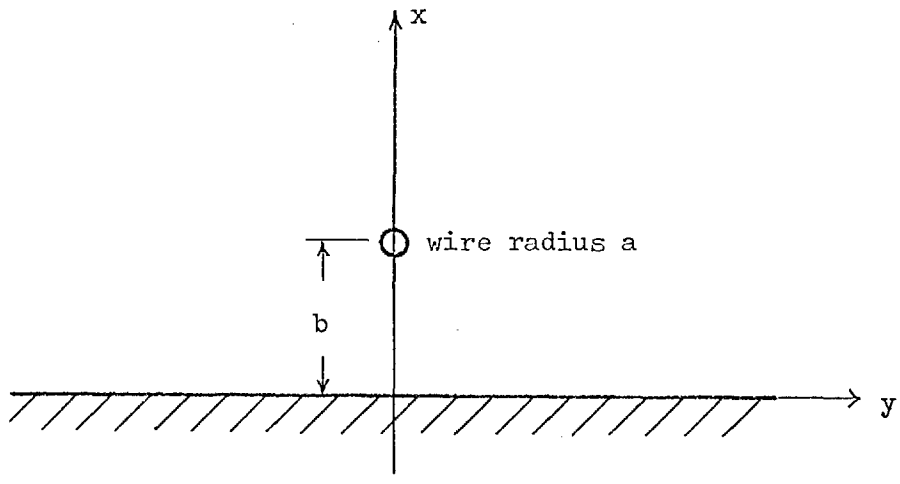


Fig. 2.2

components in the z-direction can be represented by a propagation factor $\exp(-\gamma z)$.

Starting with Maxwell's equations for an isotropic, homogeneous and source free region, in the usual notation,

$$\underline{\nabla} \wedge \underline{E} = - j\omega\mu\underline{H} \tag{2.5}$$

$$\underline{\nabla} \wedge \underline{H} = j\omega\epsilon\underline{E} \tag{2.6}$$

Separating the vectors into transverse and longitudinal components, denoted by subscripts t and z respectively, we can write

$$- j\omega\mu\underline{H}_t = \underline{\nabla}_t \wedge \underline{E}_z + \underline{\nabla}_z \wedge \underline{E}_t \tag{2.7}$$

$$- j\omega\mu\underline{H}_z = \underline{\nabla}_t \wedge \underline{E}_t \tag{2.8}$$

$$j\omega\epsilon\underline{E}_t = \underline{\nabla}_t \wedge \underline{H}_z + \underline{\nabla}_z \wedge \underline{H}_t \tag{2.9}$$

$$j\omega\epsilon\underline{E}_z = \underline{\nabla}_t \wedge \underline{H}_t \tag{2.10}$$

Multiplying (2.7) by $j\omega\epsilon$ and writing $\omega^2\mu\epsilon$ as k^2, where k is the free-space wave number, we obtain,

$$k^2\underline{H}_t = j\omega\epsilon(\underline{\nabla}_t \wedge \underline{E}_z + \underline{\nabla}_z \wedge \underline{E}_t) \tag{2.11}$$

Taking the curl of (2.9) gives the following equations for the longitudinal and transverse components respectively.

$$j\omega\epsilon(\underline{\nabla}_t \wedge E_t) = -\underline{\nabla}_t^2 \underline{H}_z + \underline{\nabla}_z\underline{\nabla}_t \cdot \underline{H}_t \tag{2.12}$$

$$j\omega\epsilon(\underline{\nabla}_z \wedge \underline{E}_t) = \underline{\nabla}_t(\nabla_z H_z) - \nabla_z^2\underline{H}_t \tag{2.13}$$

But

$$\nabla_z H_z = -\gamma H_z$$

and

$$\nabla_z^2\underline{H}_t = \gamma^2\underline{H}_t$$

Hence (2.13) can be written as

$$j\omega\epsilon(\underline{\nabla}_z \wedge \underline{E}_t) = -\gamma\underline{\nabla}_t H_z - \gamma^2 H_t \tag{2.14}$$

substitution from the above into (2.11) yields

$$(\gamma^2 + k^2)\underline{H}_t = j\omega\epsilon\underline{\nabla}_t \wedge \underline{E}_z - \gamma\underline{\nabla}_t H_z \tag{2.15}$$

Multiplying (2.15) by $\underline{H}_t^*$, the complex conjugate of $\underline{H}_t$, and integrating over the cross-section leads to the expression

$$\gamma^2 + k^2 = \frac{j\omega\epsilon\int_A \underline{H}_t^* \cdot (\underline{\nabla}_t \wedge \underline{E}_z)dA - \gamma\int_A \underline{H}_t^* \cdot \underline{\nabla}_t H_z dA}{\int_A \underline{H}_t^* \cdot \underline{H}_t \, dA}$$

$$= \frac{N_1 + N_2}{D} \tag{2.16}$$

The denominator D in the above expression is related to the average power flow along the structure, provided the concept of wave impedance or characteristic impedance is applicable. We shall now proceed to simplify the numerator, to facilitate the application of the above expression to uniform structures of interest.

N_1 can be transformed according to the vector identity

$$\underline{\nabla} \cdot (\underline{A} \wedge \underline{B}) = \underline{B} \cdot \underline{\nabla} \wedge A - \underline{A} \cdot \underline{\nabla} \wedge \underline{B} \tag{2.17}$$

i.e.

$$N_1 = j\omega\varepsilon \int_A \underline{H}_t^* \cdot (\underline{\nabla}_t \wedge \underline{E}_z) dA$$

$$= j\omega\varepsilon \int_A \underline{\nabla}_t \cdot \underline{E}_z \wedge \underline{H}_t^* dA + j\omega\varepsilon \int_A \underline{E}_z \cdot \underline{\nabla}_t \wedge \underline{H}_t^* dA \tag{2.18}$$

Applying the two-dimensional form of the divergence theorem [Ref. 2.30],

$$\int_A \underline{\nabla}_t \cdot E_z \wedge \underline{H}_t^* dA = - \oint_C (\underline{E}_z \wedge \underline{H}_t^*) \cdot \underline{n} \, d\ell \tag{2.19}$$

where A represents the cross-sectional area of the dielectric region (extending to infinity in an open structure), outside the conducting regions; contour C defines the perimeter of area A, and is closed at infinity in an open structure, as indicated in Fig. 2.3. $\underline{n}$ is the unit vector perpendicular to C, pointing into A : on the 'conductor surfaces' $\underline{n}$ is the outward normal.

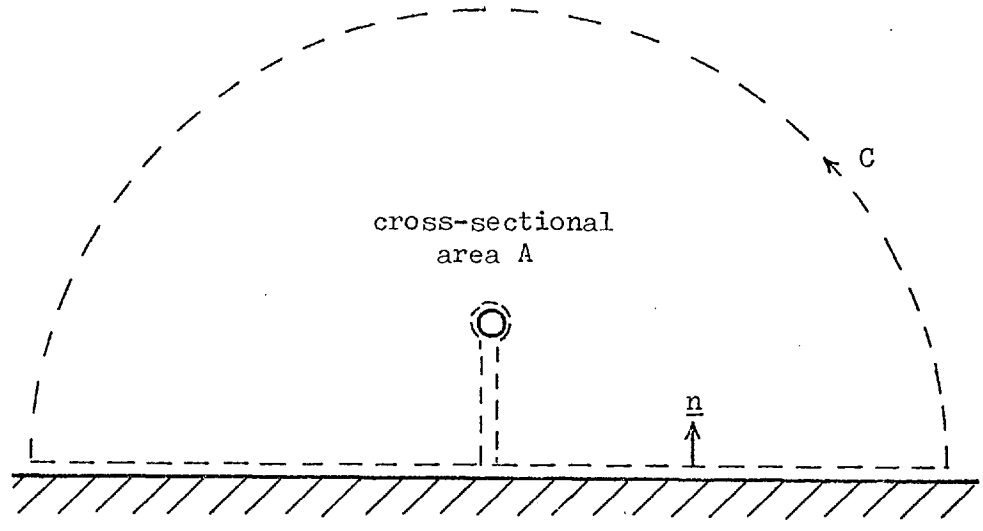


Fig. 2.3 Cross-sectional area A and contour C used in the integrals of equation (2.19). In this example contour C is closed at infinity.

Using (2.10) we can write

$$\int_A \underline{E}_z \cdot \underline{\nabla}_t \wedge \underline{H}_t^* = - j\omega\epsilon \int_A \underline{E}_z \cdot \underline{E}_z^* dA \qquad (2.20)$$

Substitution from (2.19) and (2.20) into (2.18) yields

$$N_1 = - j\omega\epsilon \oint_C (\underline{E}_z \wedge \underline{H}_t^*) \cdot \underline{n}\, d\ell + \omega^2\epsilon^2 \int_A \underline{E}_z \cdot \underline{E}_z^* dA \qquad (2.21)$$

To transform N_2 we make use of another vector identity

$$\underline{\nabla} \cdot (\phi \underline{A}) = \phi(\underline{\nabla} \cdot \underline{A}) + (\underline{\nabla}\phi) \cdot \underline{A} \qquad (2.22)$$

whence

$$N_2 = - \gamma \int_A \underline{H}_t^* \cdot \underline{\nabla}_t H_z \, dA$$

$$= - \gamma \int_A [\underline{\nabla}_t \cdot (H_z \underline{H}_t^*) - H_z(\underline{\nabla}_t \cdot \underline{H}_t^*)] dA \qquad (2.23)$$

Two other alternative forms are also possible for expressing N_2:

$$N_2 = \gamma \oint_C \underline{H}_t^* H_z \cdot \underline{n}\, d\ell + \gamma\gamma^* \int_A \underline{H}_z \cdot \underline{H}_z^*\, dA \qquad (2.24)$$

or

$$N_2 = \gamma \oint_C \underline{H}_t^* H_z \cdot \underline{n}\, d\ell + \int_A |\, \underline{\nabla}_t \cdot \underline{H}_t\, |^2\, dA \qquad (2.25)$$

To obtain Eqs. (2.24) and (2.25) we have used the divergence theorem, Eq. (2.19), and also the relation

$$\underline{\nabla} \cdot \underline{H}^* = \underline{\nabla}_t \cdot \underline{H}_t^* - \gamma^* H_z^* = 0 \qquad (2.26)$$

substituting into (2.16), from (2.21) for N_1 and from (2.24) for N_2, we obtain the following expression

$$\gamma^2 + k^2 = \frac{-j\omega\epsilon \oint_C \underline{E}_z \wedge \underline{H}_t^* \cdot \underline{n}\, d\ell + \omega^2\epsilon^2 \int_A \underline{E}_z \cdot \underline{E}_z^*\, dA + \gamma \oint_C H_z \underline{H}_t^* \cdot \underline{n}\, d\ell + \gamma\gamma^* \int_A \underline{H}_z \cdot \underline{H}_z^*\, dA}{\int_A \underline{H}_t^* \cdot \underline{H}_t\, dA} \qquad (2.27)$$

It should be noted that in an open structure, such as in Fig. 2.3, the cross-section A considered above becomes infinite in area and contour C has to be closed at infinity; in such circumstances, expression (2.27) can only be evaluated if the integrals converge. Otherwise a finite area A must be considered such that the contour C can be closed at a convenient, finite distance from the structure.

Expression (2.27) can be applied to any uniform structure to determine its propagation constant γ; the limitations of this expression are only imposed by problems associated with the evaluation of integrals. Furthermore, it is interesting to note, from Eqs. (2.16) and (2.27), that N_1 is associated with TM modes and N_2 with TE modes.

The configuration of Fig. 2.2 is defined by a plane interface at $x = 0$ and a perfectly conducting wire at $(b,0,z)$. In order to apply expression (2.23) to this configuration, we specify the boundary condition at the interface in terms of a longitudinal surface impedance $Z_s = R_s + jX_s$ by the relation

$$\underline{E}_z = Z_s \, \underline{n} \wedge \underline{H}_\ell \tag{2.28}$$

where $\underline{H}_\ell$ is the component of $\underline{H}_t$ normal to $\underline{n}$, and $\underline{H}_n$ the component parallel to $\underline{n}$. In fact Eq. (2.28) is an expression of boundary conditions for the TM mode.

$$\underline{E}_z \wedge \underline{H}_t^* = Z_s(\underline{n} \wedge \underline{H}_\ell) \wedge \underline{H}_t^*$$

$$= - Z_s[\underline{n} \, |H_\ell|^2 - \underline{n}.\underline{H}_t^* \underline{H}_\ell]$$

$$\therefore (\underline{E}_z \wedge \underline{H}_t^*) \cdot \underline{n} = - Z_s |H_\ell|^2 \tag{2.29}$$

Thus Eq. (2.27) gives

$$\gamma^2 + k^2 = \frac{j \frac{k}{Z} \oint_C Z_s |H_\ell|^2 d\ell + \frac{k^2}{Z^2} \int_A |E_z|^2 \, dA + \gamma \oint_C H_z H_n^* d\ell + \gamma\gamma^* \int_A |H_z|^2 dA}{\int_A \underline{H}_t^* . \underline{H}_t \, dA} \tag{2.30}$$

where we have written $\frac{k}{Z}$ for $\omega\varepsilon$, Z being the intrinsic impedance of free space.

2.5. Effect of Approximations on the Propagation Constant

In many applications it may be difficult to determine the distribution of fields in the cross-section exactly, or to evaluate the expression for the propagation constant γ using the exact field distribution. Hence it is worthwhile to examine the error in γ due to approximations in the field distribution.

Rewriting the equations for γ^2 from the previous section

$$(\gamma^2 + k^2) \int_A \underline{H}_t \cdot \underline{H}_t^* dA = N_1 + N_2 \tag{2.31}$$

where

$$N_1 = - j \frac{k}{Z} \oint_C \underline{E}_z \wedge \underline{H}_t^* \cdot \underline{n} \, d\ell + \frac{k^2}{Z^2} \int_A \underline{E}_z \cdot \underline{E}_z^* \, dA \tag{2.32}$$

$$N_2 = - \gamma \int_A \underline{H}_t^* \cdot \underline{\nabla}_t H_z \, dA = - \int_A \underline{H}_t^* \cdot \underline{\nabla}_t (\underline{\nabla}_t \cdot \underline{H}_t) dA \tag{2.33}$$

Let the error in γ^2 be $\delta\gamma^2$ due to errors $\delta\underline{H}_t$ and $\delta\underline{E}_z$ in correct field quantities $\underline{H}_t$ and $\underline{E}_z$ respectively. Substituting these approximate field quantities in equations (2.31), (2.32) and (2.33), and neglecting second and higher order error terms

$$\delta\gamma^2 \int_A \underline{H}_t \cdot \underline{H}_t^* \, dA + (\gamma^2 + k^2) \int_A (\underline{H}_t \cdot \delta\underline{H}_t^* + \delta\underline{H}_t \cdot \underline{H}_t^*) dA = \delta N_1 + \delta N_2 \tag{2.34}$$

where

$$\delta N_2 = -\int_A [\delta \underline{H}_t^* \cdot \underline{\nabla}_t (\underline{\nabla}_t \cdot \underline{H}_t) + \underline{H}_t^* \cdot \underline{\nabla}_t (\underline{\nabla}_t \cdot \delta \underline{H}_t)] dA \tag{2.35}$$

$$\delta N_1 = -j \frac{k}{Z} \oint_C (\underline{E}_z \wedge \delta \underline{H}_t^* + \delta \underline{E}_z \wedge \underline{H}_t^*) \cdot \underline{n} \, d\ell$$

$$+ \frac{k^2}{Z^2} \int_A (\underline{E}_z \cdot \delta \underline{E}_z^* + \delta \underline{E}_z \cdot \underline{E}_z^*) dA \tag{2.36}$$

Using Eqs. (2.29) and (2.10), the expression for δN_1 can be transformed to give

$$\delta N_1 = j \frac{k}{Z} \oint_C (Z_s H_\ell \delta H_\ell^* + Z_s \delta H_\ell H_\ell^*) d\ell$$

$$- j \frac{k}{Z} \int_A (\delta E_z^* \cdot \underline{\nabla}_t \wedge \underline{H}_t - \delta \underline{E}_z \cdot \underline{\nabla}_t \wedge \underline{H}_t^*) dA \tag{2.37}$$

Assuming

$$[\gamma^2]^* = \gamma^2 \tag{2.38}$$

then substitution from Eq. (2.15), and its conjugate form, into Eq. (2.34) leads to

$$\delta\gamma^2 \int_A |H_t|^2 dA = -\int_A \delta H_t^* \cdot [j \frac{k}{Z} \underline{\nabla}_t \wedge \underline{E}_z - \underline{\nabla}_t (\underline{\nabla}_t \cdot \underline{H}_t)] dA$$

$$- \int_A \delta \underline{H}_t \cdot [- j \frac{k}{Z} \underline{\nabla}_t \wedge E_z^* - \nabla_t (\nabla_t \cdot \underline{H}_t^*)] dA + \delta N_1 + \delta N_2$$

$$= \delta N_1 + \int_A [\delta \underline{H}_t \cdot \underline{\nabla}_t (\underline{\nabla}_t \cdot \underline{H}_t^*) - \underline{H}_t^* \cdot \nabla_t (\nabla_t \cdot \delta H_t)] dA$$

$$+ j \frac{k}{Z} \int_A (\delta \underline{H}_t \cdot \underline{\nabla}_t \wedge \underline{E}_z^* - \delta \underline{H}_t^* \cdot \underline{\nabla}_t \wedge \underline{E}_z) dA$$

(2.39)

The last integral in Eq. (2.39) can be transformed, using Eqs. (2.17), (2.19) and (2.29); the result is;

$$- j \frac{k}{Z} \oint_C (Z_s H_\ell \delta H_\ell^* - Z_s^* H_\ell^* \delta H_\ell) d\ell + j \frac{k}{Z} \int_A (\underline{E}_z^* \cdot \nabla_t \wedge \delta \underline{H}_t - E_z \cdot \nabla_t \wedge \delta H_t^*) dA \tag{2.40}$$

Substituting from Eqs. (2.37) and (2.40) into Eq. (2.39) and rearranging,

$$\begin{aligned} \delta\gamma^2 \int_A |H_t|^2 dA = \; & j \frac{k}{Z} \oint_C (Z_s^* H_\ell^* \delta H_\ell + Z_s H_\ell^* \delta H_\ell) d\ell \\ & + \int_A [\delta \underline{H}_t \cdot \underline{\nabla}_t (\underline{\nabla}_t \cdot \underline{H}_t^*) - \underline{H}_t^* \cdot \underline{\nabla}_t (\underline{\nabla}_t \cdot \delta \underline{H}_t)] dA \\ & + j \frac{k}{Z} \int_A [\underline{E}_z^* \cdot \underline{\nabla}_t \wedge \delta \underline{H}_t - \delta \underline{E}_z^* \cdot \underline{\nabla}_t \wedge \underline{H}_t] dA \\ & - j \frac{k}{Z} \int_A [E_z \cdot \underline{\nabla}_t \wedge \delta \underline{H}_t^* - \delta \underline{E}_z \cdot \underline{\nabla}_t \wedge \underline{H}_t^*] dA \end{aligned} \tag{2.41}$$

It can be seen that, with the exception of the contour integral, the terms on the right-hand side of Eq. (2.41) tend to cancel each other out; furthermore, their contribution to $\delta\gamma^2$, the error in γ^2, is reduced by the normalization factor $\int_A |H_t|^2 dA$. The contour integral vanishes identically when, R_s, the real part of the surface impedance is zero. This result might be expected, as assumption Eq. (2.38) is strictly valid for a lossless structure only, i.e., for $R_s = 0$.

The expression for the propagation constant is a perturbation formula, and its accuracy depends on the approximations made in the

field distribution. For this reason, we shall develop an iterative process for the application of Eq. (2.30). However, it is interesting to note that expression (2.30) for the propagation constant becomes variational when the right-hand side of Eq. (2.41) vanishes identically. Inspection of the last equation indicates that this occurs when the following conditions are fulfulled:

(1) On the conducting boundaries, the longitudinal electric field is linearly related to the tangential component of the transverse magnetic field, i.e., relation (2.38) is valid.

(2) The surface impedance Z_s is purely reactive, i.e., $R_s = 0$ where $Z_s = R_s + jX_s$: then the contour integral in Eq. (2.41) vanishes.

(3) Both the correct and approximate field distributions are transverse magnetic : then the first surface integral in Eq. (2.41) vanishes.

(4) The approximate fields satisfy equation (2.10), i.e. $\underline{\nabla}_t \wedge \delta\underline{H}_t = j\frac{k}{Z}\delta\underline{E}_z$: then the last two surface integrals in Eq. (2.41) vanish.

In the summary above, assumption (1) is tantamount to accepting the surface impedance concept. Condition (2) implies that the expression for the propagation constant will probably be more accurate for a lossless structure: we cannot be more definite on this point as we arrived at the above conditions by the ab initio assumption that $[\gamma^2]^* = \gamma^2$. Approximation (3) requires that the TE mode transports much less power then the TM mode. The significance of condition (4) is that independent approximations should not be used for the distribution of $\underline{H}_t$ and $\underline{E}_z$: <u>either</u> $\underline{H}_t$ <u>or</u> $\underline{E}_z$ is approximated by an assumed distribution, and the other is derived using Eq. (2.10).

In the previous section if equation (2.15) had been multiplied by $\underline{H}_t$ instead of $\underline{H}_t^*$, we would have obtained the following expression:

$$\gamma^2 + k^2 = \frac{+ j\frac{k}{Z}\oint_C Z_s H_\ell^2 d\ell - \frac{k^2}{Z^2}\int_A E_z^2 dA + \gamma\oint_C H_z H_n d\ell + \gamma^2\int_A H_z^2 dA}{\int_A H_t^2\, dA} \qquad (2.42)$$

The above expression is very similar to Eq. (2.30), the only difference being the absence of complex conjugates. For this alternative expression, a relation can be derived for the error terms, analogous to that presented earlier in this section. In this case assumptions $[\gamma^2]^* = \gamma^2$ and $R_s = 0$ are not necessary in order to show that Eq. (2.42) is a variational expression. However, expression (2.30), involving conjugate terms, is more convenient for our purposes as the denominator $D = \int_A \underline{H}_t \cdot \underline{H}_t^* dA$ can be related to the power flow more easily than $\int_A \underline{H}_t \cdot \underline{H}_t\, dA$.

REFERENCES

2.1 Beverage H.H., Rice, C.W., Kellog, E.W.; 'The Wave Antenna : a New Type of Highly Directive Antenna', A.I.E.E., Vol. 42, pp 215-266, February, 1923.

2.2 Beverage, op. cit., p. 242.

2.3 Carson, J.R.; 'Wave Propagation in Overhead Wires with Ground Return', Bell System Technical Journal, Vol. 5, pp 539-554, Oct. 1926.

2.4 Wise, W.H.; 'Propagation of High-frequency Currents in Ground Return Circuits', Proc. I.R.E., Vol. 22, No. 4, pp 522-527, April 1934.

2.5 Jenssen, M.; 'On Radiation From Overhead Transmission Lines', Proc. I.E.E., Vol. 97, Part III, pp 166-178, 1950.

2.6 Belousov, S.P., Yampolskii, V.G.; 'Single-Wire Medium-Wave Travelling-Wave Receiver Antennas', Radiolekhnika, Vol. 15, pp 16-25, 1960.

2.7 Seeley, E.W.; 'Optimum Reception Pattern of the Beverage Wave Antenna at Very Low Frequencies', Journal of Research of National Bureau of Standards, Vol. 67D, No. 4, pp 387-395, July-August, 1963.

2.8 Kikuchi, H.; 'Wave Propagation Along an Infinite Wire Above Ground', Electrotechnical Journal of Japan, Vol. 2, pp 73-78, December 1956.

2.9 Kikuchi, H.; 'On Transition From a Ground Return Circuit to a Surface Waveguide', Onde Electrique, Special Supplement : Proc. of the International Congress on Ultra High Frequency Circuits and Antennas, Vol. 1, pp 39-45, Paris, Oct. 1957.

2.10 Kikuchi, H.; 'Propagation coefficient of the Beverage Aerial', Proc. I.E.E., Vol. 120, No. 6, pp 637-638, June, 1973.

2.11 Kikuchi, H.; 'Investigations of Electromagnetic Noise and Interference

Due to Power Lines in Japan and Some Results from the Aspect of Electromagnetic Theory', Proceedings of Symposium on Electromagnetic Hazards, Pollution and Environmental Quality, pp 147-162, Purdue University, May 8-9, 1972.

2.12 dos Santos A.F.; 'Electromagnetic-Wave Propagation Along a Horizontal Wire Above Ground', Proc. I.E.E., Vol. 119, No. 8, pp 1103-1109, August, 1972.

2.13 Wait, J.R.; 'Theory of Propagation Along a Thin Wire Parallel to an Interface', Radio Science, Vol. 7, No. 6, pp 675-679, June 1972.

2.14 Knight, P.; 'The Propagation Constant of the Beverage Aerial', Proc. I.E.E., Vol. 119, No. 7, pp 821-826, July 1972.

2.15 Monteath, G.D.; 'Application of Compensation Theorem to Certain Radiation and Propagation Problems', Proc. I.E.E., Vol. 98, Part IV, pp 23-30, 1951.

2.16 Miller, E.K., Poggio, A.J., Burke, G.J., Selden, E.S.; 'Analysis of Wire Antennas in the Presence of Conducting Half-Space : Part II; The Horizontal Antenna in Free-Space', Canadian Journal of Physics, Vol. 50, No. 21, pp 2614-2627, November 1972.

2.17 Barlow, H.M., Brown, J.; 'Radio Surface Waves', Oxford Clarendon Press 1962, pp 15-17.

2.18 Hessel, A.; 'General Characteristics of Travelling Wave Antennas', published as chapter 19 of "Antenna Theory", Part II, edited by Collin, R.E. and Zucker, F.J., McGraw-Hill, 1969, pp 163-165.

2.19 Schelkunoff, S.A.; 'The Impedance Concept and its Applications to Problems of Reflection, Refraction, Shielding and Power Absorption", Bell System Technical Journal, Vol. 17, pp 17-48, January 1938.

2.20 Schelkunoff, S.A.; 'Transmission Theory of Plane Electromagnetic Waves', Proc. I.R.E., Vol. 25, No. 11, pp 1457-1492, November, 1937.

2.21 Feinberg, E.L.; 'Propagation of Radio Waves Along an Inhomogeneous Surface', Supplemento al Nuouo Cimento, serie 10, Vol. 11, pp 60-91, 1959.

2.22 Waldron, R.A.; 'Theory of Waveguides and Cavities', Maclaren and Sons Ltd., London, 1967, pp 63-71.

2.23 Waldron, R.A.; 'Theory of Guided Electromagnetic Waves', Van Nostrand Reinhold, London, 1970, pp 369-370.

2.24 Waldron, R.A.; 'Comments On : Modes of Propagation in a Coaxial Waveguide with Lossless guiding Surfaces', I.E.E.E. Transactions on Microwave Theory and Techniques, Vol. MTT-21, p.61, January, 1973.

2.25 Barlow, H.M., Brown, J.; op. cit., pp 60-69.

2.26 Walter, C.H.; 'Travelling Wave Antennas', McGraw-Hill, 1965, pp 172-183.

2.27 Goldstone, L.O., Oliner, A.A.; 'Anote on Surface Waves Along Corrugated Structures', I.R.E. Transactions on Antennas and Propagation, Vol. AP-7, pp 274-276, July 1959.

2.28 Senior, T.B.A.; 'Impedance Boundary Conditions for Imperfectly Conducting Surfaces', Applied Scientific Research, Vol. B8, pp 418-436, The Hague 1960.

2.29 Sharma, K.P.; 'The Estimation of Reactance of a Loss-Free Surface Supporting Surface Waves', Proc. I.E.E., Vol. 106B, pp 427-430, July 1959.

2.30 Johnson, C.C.; 'Field and Wave Electrodynamics', McGraw-Hill, 1965, p. 150.

CHAPTER III

PROPAGATION CONSTANTS OF THE BEVERAGE ANTENNA AND THE IPA

3.1. Introduction

In the previous chapter a general expression was derived for propagation constant of electromagnetic waves travelling along a structure of uniform cross-section. In this chapter we shall evaluate the expression for propagation constant for two particular structures : the Beverage antenna, and the Inductive Plane Antenna (IPA). Both these antennas share the same geometric configuration, their difference being in the nature of the plane interface (see Fig. 2.1). For this reason there are some considerations which are common to both antennas, leading to common field equations and approximations in both boundary--value problems. This part of the analysis, which is identical in both problems, is described in Section 3.2.

The necessary relations for the propagation constant of the Beverage antenna are derived in Section 3.3, where a comparison is also made with other theoretical results.

Propagation constant of the IPA is considered in Section 3.4. An experimental study of the propagation constant (of the IPA) was also undertaken : this is described in Section 3.5. Finally, Section 3.6 is devoted to a comparison between theoretical and experimental results obtained for the propagation constant (of the IPA).

3.2. Evaluation of Integrals in the Expression for Propagation Constant

3.2.1. A Priori Assumptions

In order to evaluate expressions (2.30) for the uniform transmission system depicted in Fig. 2.2, we require the distribution of field components in the cross-section. The wire at $x = b$ will be regarded

as perfectly conducting. When the interface at x = 0 represents a perfectly-conducting plane, the problem reduces to an ideal two--conductor transmission line : in this case the dominant mode of propagation is TEM, for which the wave equation reduces to Laplace's equation [Ref. 3.1], and the field distribution can be derived from a single potential function. We are only concerned with configurations for which $b < \lambda_o/2$ and $a \ll b$, where a is the wire radius. Hence the potential function can be obtained from image theory, in terms of a line current I_z at (b, 0, z) and its image I'_z at (-b, 0, z).

When the interface represents an impedance plane, power is stored or absorbed in the conducting region $x < 0$, and there must be a component of Poynting vector directed into the interface. This implies at least a longitudinal component of electric field. In general, a longitudinal component of magnetic field will also exist, and will have associated with it transverse currents on the plane, and possibly on the wire.

In the analysis presented in this section, we shall assume, ab initio, that even if a longitudinal component of magnetic field exists and transverse currents are present, their contribution to integrals in Eq. (2.30) can be neglected. This approximation is partly justified by the considerations given in Section 2.4, but the primary basis for our assumption is heuristic considerations, supported qualitatively by the conclusions of Kikuchi on the Beverage antenna [Refs. 2.8, 2.9], and by Stratton's analysis for propagation along a wire in free-space [Ref. 3.2].

Kikuchi was the first person to realize the significance of the hybrid magnetic (HM) mode in determining the propagation characteristics of the Beverage structure. Kikuchi's analysis indicated that for a Beverage configuration, as in Fig. 2.2, with typical parameters, the

mode of propagation is essentially TEM at low frequencies ($f < 10$ MHz), and TM at very high frequencies ($f > 100$ MHz) : the transformation occurs in a 'transition region', 10 - 100 MHz approximately, when the field distribution becomes hybrid magnetic. One particularly significant result which has emerged from Kikuchi's analysis is that the transverse component of magnetic vector potential parallel to the interface is identically zero, i.e., $A_y \equiv 0$. As a corollary, we can conclude that $J_y \equiv 0$, where J_y is the y component of conduction current density : therefore power stored or dissipated in the conducting regions is only associated with current density components J_x and J_z. Furthermore, it appears that the longitudinal component of magnetic field, H_z, is not excited by conduction currents, but arises from the perturbation of the TEM mode into a TM mode : this situation is in contrast to hollow waveguides where TE modes are supported by transverse surface currents on the guide walls.

As a result of these observations, we expect that the magnitude of H_z will be small relative to the magnitudes of transverse components of magnetic field. In particular, considerations of symmetry show that $H_z \equiv 0$ on the plane $y = 0$: this conclusion is also supported by Kikuchi's analysis. Also Sommerfield's radiation condition requires that $H_z \rightarrow 0$ as $y \rightarrow \infty$. Thus it is reasonable to assume that, in Eq. (2.30), the contribution from integrals involving H_z can generally be neglected.

We are interested in configurations for which $b \gg a$. Hence we can assume that the current distribution in the wire is essentially the same as for a wire in free space (this assumption has also been made by Kikuchi and others). It follows that the field distribution in close proximity to the wire must also be nearly the same as for a wire in free-space. Stratton [Ref. 3.2] has concluded that although

there are an infinite number of modes of propagation along a solid conducting cylinder, in free-space, there is only one predominant mode which has a low attenuation : the symmetric transverse magnetic mode. All other modes are damped out within a couple of centimetres from the source.

Stratton's analysis brings out two points which are particularly relevant to the present study. Firstly, for the symmetric TM mode the wire current is only axial. Similarly, we shall consider only axial currents in the wire. Secondly, in the vicinity of a thin wire, the magnetic field distribution corresponds closely to the electrostatic distribution. This approximation is only valid for $|hr| \ll |$, where $h = (k^2 + \gamma^2)^{\frac{1}{2}}$ and r is the radial distance from the wire axis. On this basis, we shall continue to derive the distribution of the transverse component of magnetic field from image theory, even when the surface impedance at the interface has a non-zero value. However, we shall use a weighting function for the image line current in order to take into account the surface impedance effect on the distribution of magnetic field, and to ensure the continuity of tangential field components across the interface.

3.2.2. Approximations in the Distribution of Magnetic Field

Neglecting the contributions from H_z, the longitudinal component of magnetic field, Eq. (2.30) reduces to

$$\frac{\gamma^2}{k^2} + 1 = \frac{\frac{1}{k^2}\left[j\frac{k}{Z_1}\oint_C Z_s|H_\ell|^2 d\ell + \frac{k^2}{Z_1^2}\int_A |E_z|^2 dA \right]}{\int_A |H_t|^2 dA} \qquad (3.1)$$

We shall consider a line current $I_z = -I$ at $x = b$, and an effective image current $I'_z = I(1 + q_2)$ at $x = -b$. A variation $\exp(+ j\omega t - \gamma z)$ is

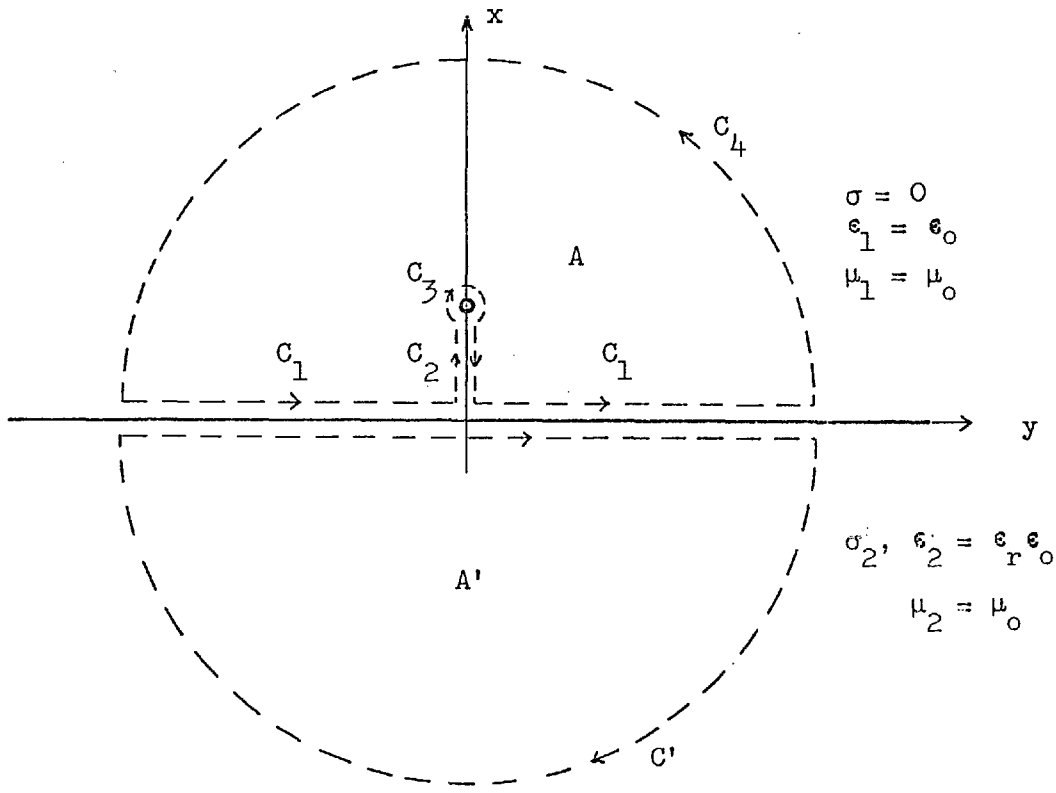


Fig. 3.1

assumed, but for convenience this factor is omitted from equations in the following analysis.

Let the y component of magnetic field at the interface be denoted by H_{oy}. Assuming that H_{oy} is approximately given by the electrostatic distribution, i.e.

$$H_{oy} = \frac{I(2 + q_2)}{2\pi} \frac{b}{b^2 + y^2} \tag{3.2}$$

$$|H_{oy}|^2 = \frac{I^2}{4\pi^2} (2 + q_2)(2 + q_2^*) \frac{b^2}{(b^2+y^2)^2} \tag{3.3}$$

where I has been taken as real, without loss of generality. The contour integral in Eq. (3.1) is evaluated along $C = C_1 + C_2 + C_3 + C_4$, as depicted in Fig. 3.1. Contributions from opposite banks of C_2 cancel

out; the integral along C_3 is zero as we consider a perfectly conducting wire, for which $Z_s = 0$; and the contribution from C_4 is taken as negligible, which follows from the radiation condition. Thus, from Eq. (3.3)

$$N_c = j\frac{k}{Z_1}\oint_C Z_s|H_\ell|^2 d\ell = j\frac{k}{Z_1}\int_{-\infty}^{\infty} Z_s|H_{oy}|^2 dy$$

$$= j\frac{k}{Z_1}\frac{Z_s I^2}{2\pi b}(1 + q_2/2)(1 + q_2^*/2) \qquad (3.4)$$

3.2.3. Approximations in the Distribution of E_z

The value of E_z at the interface is determined by the boundary condition relation (2.28), which can be written

$$E_z\Big|_{x=0+} = E'_z\Big|_{x=0-} = E_s = Z_s H_{oy} \qquad (3.5)$$

In order to evaluate the surface integral involving E_z, in Eq. (3.1), we can make the following approximations

(i) E_z has a 'separable' field distribution, i.e.

$$E_z = E_s(y)f(x) \qquad (3.6)$$

(ii) for $x > 0$, E_z has an x-variation given by

$$f(x) = e^{-jhx} \qquad (3.7)$$

$$\text{where } h = h_r - jh_i = (k^2 + \gamma^2)^{\frac{1}{2}} \qquad (3.8)$$

The first approximation is suggested by boundary condition Eq. (3.5); furthermore, it is consistent with an a priori assumption of neglecting the longitudinal component of magnetic field [Ref. 3.3]. The second approximation follows from the separability Eq. (3.8) in which the y-variation of E_z has been neglected. Further discussion of Eq. (3.8) is given in Appendix 3B. It can be seen from Eqs. (3.5) and (3.2) that this is a valid assumption at the interface for small values of y, i.e., the range which makes the most significant contribution to the surface integral $\int_A |E_z|^2 dA$.

Alternatively, we can represent E_z as an angular spectrum of plane waves in the x - y plane:

$$E_z(x,y) = \frac{k}{2\pi} \int_{-\infty}^{\infty} P(s) e^{-jk(cx + sy)} ds \cdot \frac{Z_s I_w}{2\pi} (2 + q_2) \tag{3.9}$$

where $$c^2 + s^2 = h^2/k^2 \tag{3.10}$$

Using Eqs. (3.5) and (3.2), inversion of the above integral yields, for $y > 0$

$$P(s) = \pi e^{-kb|s|} \tag{3.11}$$

$$E_z(x,y) = Z_s I_w (2 + q_2) k \int_0^{\infty} e^{-kbs - jkcx} \cos(ksy) ds \tag{3.12}$$

Again, inspection of the integrand in Eq. (3.12) indicates that the most significant contribution to E_z comes from that part of the spectrum which has the least variation with y, i.e. from the range when s is small.

A consequence of approximation Eq. (3.7) is that E_z does not satisfy the boundary conditions at the wire. We shall take this effect into account in two distinct ways: firstly, we shall assume that $|E_z|^2$ is negligible above the wire, i.e., for $x > b$, when we evaluate $\int_A |E_z|^2 dA$. Secondly, we shall resort to transmission-line equations by representing the effect of finite E_z at the wire as inducing a change in the wire current, and therefore equivalent to a change in the characteristic impedance.

The effect of wire scattering is considered in Appendix 3A. The scattered electric field is given by Eq. (3A.12). This leads to the following expression for the total electric field E_z for $0 < x < b$:

$$E_z = E_s(e^{-jhx} - e^{-jhb}) \tag{3.13}$$

The second term in the numerator of Eq. (3.1) can now be evaluated

$$N_A = \frac{k^2}{Z_1^2} \int_A |E_z|^2 dA$$

$$= \frac{k^2}{Z_1^2} |Z_s|^2 \int_{-\infty}^{\infty} H_{oy} H_{oy}^* dy \int_0^b (e^{-jhx} - e^{-jhb})(e^{jh^*x} - e^{jh^*b}) dx$$

(3.14)

$$N_A = k Z_{sn} Z_{sn}^* I^2 (1 + q_2/2)(1 + q_2^*/2)$$

$$\frac{1 - e^{-2h_i b}}{2h_i/k} - kbe^{-2h_i b} \left[\frac{e^{jhb} - 1}{(jhb)} + \frac{e^{-jh^*h}}{(-jh^*b)} - 1 \right]$$

(3.15)

where $$Z_{sn} = \frac{Z_s}{Z_1} \tag{3.16}$$

3.2.4. Evaluation of Denominator D

To evaluate the denominator D on the right-hand-side of Eq. (3.1), we define a characteristic impedance Z_c in terms of the total power flow, P_z, in the z-direction:

$$P_z = P_1 + P_2 = Z_c I^2 \tag{3.17}$$

where P_1 is the power flowing in the region $x > 0$, and P_2 the power flow in the region $x < 0$. From the definition of complex Poynting vector [Ref. 3.4],

$$P_1 = \int_A \underline{E} \wedge \underline{H}^* \cdot \underline{dA}$$

$$= \int_A (E_x H_y^* - E_y H_x^*) dA \tag{3.18}$$

From Maxwell's equation $\underline{\nabla} \wedge \underline{H} = j \frac{k}{Z} \underline{E}$ we obtain

$$j \frac{k}{Z_1} E_x = \frac{\partial H_z}{\partial y} - \frac{\partial H_y}{\partial z} \tag{3.19a}$$

$$- j \frac{k}{Z_1} E_y = \frac{\partial H_z}{\partial x} - \frac{\partial H_x}{\partial z} \tag{3.19b}$$

Neglecting the terms containing H_z, the above equations yield

$$E_x \simeq \frac{\gamma}{jk} Z_1 H_y \tag{3.20}$$

$$- E_y \simeq \frac{\gamma}{jk} Z_1 H_x \tag{3.21}$$

Substitution in Eq. (3.18) for E_x and E_y gives

$$P_1 \simeq \frac{\gamma}{jk} Z_1 \int_A (H_y H_y^* + H_x H_x^*) dA$$

$$= \frac{\gamma}{jk} Z_1 \int_A \underline{H}_t \cdot \underline{H}_t^* \, dA \qquad (3.22)$$

Evaluation of P_2, power flow in the z-direction in the region $x < 0$, depends on the nature of the interface : this will be dealt with in later sections.

From Eqs. (3.17) and (3.22) we obtain

$$D = \int_A |H_t|^2 dA = \frac{jk}{\gamma} \frac{Z_c}{Z_1} I^2 \left(1 - \frac{P_2}{Z_c I^2}\right) \qquad (3.23)$$

3.2.5. Determination of the Weighting Function q_2

The integral form of (2.10) is given by

$$\oint_C \underline{H}_\ell \cdot d\ell = j \frac{k}{Z} \int_A E_z dA \qquad (3.24)$$

Applying the above equation to the dielectric region $x > 0$, for which the contour C and the area A are shown in Fig. 3.1, page 46 , we obtain

$$\int_{-\infty}^{\infty} H_{oy} dy = - j \frac{k}{Z_1} \int_A E_z dA + I \qquad (3.25)$$

For region $x < 0$, (3.24) gives

$$\int_{-\infty}^{\infty} H_{oy} dy = j \frac{k}{Z_2} \int_{A'} E'_z dA' + I(1 + q_2) \qquad (3.26)$$

where $$I(1 + q_2) = \sigma_2 \int_{A'} E'_z \, dA' \tag{3.27}$$

and the primed quantities refer to the region $x < 0$, and σ_2 is the conductivity for $x < 0$.

Combining Eqs. (3.25) and (3.26) we obtain

$$q_2 = - j \frac{k}{Z_1} [F_1 + \epsilon_r F_2] \tag{3.28}$$

where

$$F_1 = \frac{1}{I} \int_A E_z dA \tag{3.29}$$

$$F_2 = \frac{1}{I} \int_{A'} E'_z \, dA' \tag{3.30}$$

F_1 can be evaluated with the same approximations as were used in the derivation of Eq. (3.15), but neglecting the effect of scattering by the wire; the result is given by:

$$F_1 = Z_s(1 + q_2/2) \frac{(1 - e^{-jhb})}{jh} \tag{3.31}$$

Evaluation of F_2 depends on the nature of the interface, and will be dealt with in later sections.

3.2.6. Characteristic Impedance Z_c

When the interface $x = 0$, Fig. 2.2, page 28 , represents a perfectly conducting plane, we obtain the standard open-wire transmission line ; in this case the characteristic impedance is given by [Ref. 3.5],

$$Z_{co} = \frac{Z_1}{2\pi} \cosh^{-1}\left(\frac{b}{a}\right) \tag{3.32}$$

For $b/a > 10$, for a line in free-space we obtain

$$Z_{co} \simeq 138 \log_{10}\left(\frac{2b}{a}\right) \tag{3.33}$$

In the more general case, the non-zero value of surface impedance, Z_s, at the interface gives rise to a finite component of electric field parallel to the wire. This can be regarded as an 'incident field' which will induce a current in the wire. This effect is equivalent to a change in the characteristic impedance of the line, which we shall determine in this section.

Let the induced current, i.e. the change in the original current I_o, be ΔI, and the equivalent change in the characteristic impedance ΔZ_c:

$$I = I_o\left(1 + \frac{\Delta I}{I_o}\right) \tag{3.34}$$

$$Z_c = Z_{co}\left(1 + \frac{\Delta Z_c}{Z_{co}}\right) \tag{3.35}$$

Then for a constant voltage excitation, we can write

$$\frac{1}{1 + \frac{\Delta Z_c}{Z_{co}}} = 1 + \frac{\Delta I}{I_o} \tag{3.36}$$

$$\frac{\Delta Z_c}{Z_{co}} = \frac{-(\Delta I/I_o)}{(1 + \Delta I/I_o)} \tag{3.37}$$

In terms of I_o (the wire current in the negative z-direction), the longitudinal component of electric field is obtained from expressions (3.5) to (3.8); namely

$$E_z(x,y) = Z_s \frac{I_o(2 + q_2)}{2\pi} \frac{b}{b^2 + y^2} e^{-jhx} \qquad (3.38)$$

From Eq. (3.8) it can be seen that at x = b, y = 0 the predominant component of the above field corresponds to a plane wave propagating in the x - z plane; the amplitude of this wave at the wire is given by

$$E_o = E_z(b,0) = Z_s \frac{I_o(2 + q_2)}{2\pi b} e^{-jhb} \qquad (3.39)$$

The three-dimensional problem of scattering by a perfectly-conducting wire is considered in Appendix 3A; the induced current in the wire is given by Eq. (3A.22), which is repeated below, in the present notation;

$$\Delta I = - j \frac{2\pi E_o}{kZ_1 \ell n(\frac{1}{ha})} \qquad (3.40)$$

$$\Delta I = - j \frac{Z_s I_o}{Z_1 kb} \frac{(2 + q_2)}{2\pi} \frac{e^{-jhb}}{\ell n(\frac{1}{ha})} \qquad (3.41)$$

Substitution from Eq. (3.41) into Eq. (3.37) yields

$$\Delta Z_{cn} = \frac{\Delta Z_c}{Z_{co}} = \frac{+ j(Z_s/Z_1)(2 + q_2)e^{-jhb}}{2\pi kb \ell n(\frac{1}{ha}) - j(Z_s/Z_1)(2 + q_2)e^{-jhb}} \qquad (3.42)$$

3.3. Calculations for a Transition-Boundary Interface

We shall now consider the particular case when the plane interface at $x = 0$ represents a transition boundary between two homogeneous isotropic media. In Fig. 2.2, the region $x > 0$, outside the perfectly-conducting wire, represents a dielectric medium with zero conductivity; subscript 1 is used to refer to this region, which we shall take as free-space for computational purposes. The region $x < 0$ represents a dielectric medium with finite, non-zero conductivity σ_2. Subscript 2 is used to refer to this region. For computation of parameters, it will be assumed that both regions have a permeability equal to that of free space, i.e.

$$\mu_1 = \mu_2 = \mu_o \tag{3.43}$$

Also

$$\epsilon_2 = \epsilon_r \epsilon_1 \tag{3.44}$$

$$\epsilon_2' = \epsilon_1 (\epsilon_r - j \frac{\sigma_2}{\omega \epsilon_1}) = \epsilon_1 K_r \tag{3.45}$$

We shall now proceed to evaluate the surface impedance Z_s, and quantities F_2 and P_2 in Eqs. (3.30) and (3.17).

3.3.1. Approximations Related to Transition-Boundary Parameters

We shall start from the proposition that the field in the region $x < 0$ can be represented in terms of a predominant plane wave component travelling in the x - z plane, away from the interface $x = 0$. In other words, the variation of field components in the y direction is negligible compared with variations in the x and z directions; hence we can assume a separation of variables solution for an approximate evaluation of

integrals. The extent of the approximation can be appreciated by inspection of a representation in terms of angular spectrum of plane waves; $x < 0$

$$E_z(x,y) = \frac{k}{2\pi} \int_{-\infty}^{\infty} P(s) e^{(+\gamma_x x - jksy)} ds \frac{Z_s I_w}{2\pi} (2 + q_2) \tag{3.46}$$

where

$$(ks)^2 - \gamma_x^2 = h_2^2 = -\gamma_2^2 + \gamma^2 \tag{3.47}$$

$$\gamma_2 = jk K_r^{\frac{1}{2}} \tag{3.48}$$

from Eq. (3.11) $P(s) = \pi e^{-kb|s|}$

$$E_z(x,y) = Z_s I_w (2 + q_2) k \int_0^{\infty} e^{-kbs} e^{\gamma_x x} \cos(ksy) ds \tag{3.49}$$

from Eq. (3.47)

$$\gamma_x = k[(\frac{\gamma}{jk})^2 - K_r + s^2]^{\frac{1}{2}} \tag{3.50}$$

The choice of branch cuts, associated with the square root in Eq. (3.50), is determined by the radiation condition, which requires that γ_x have a positive real part. From Eq. (3.49) it can be seen that the most significant contribution to the integral comes from the range when s is small, i.e., from the bundle of waves travelling almost parallel to the plane y = 0. For this group of plane waves, Eq. (3.50) reduces to

$$\gamma_x \simeq k[(\frac{\gamma}{jk})^2 - K_r]^{\frac{1}{2}} \tag{3.51}$$

Evidently, the above approximation becomes better as $|K_r|$ increases.

Henceforth we shall assume the following approximation

$$E_z(x,y) = E_s(y)e^{\gamma_x x}, \qquad x < 0 \tag{3.52}$$

where from Eq. (3.51),

$$\gamma_x = [\gamma_2^2 - \gamma^2]^{\frac{1}{2}} = \gamma_2 q_3 \tag{3.53}$$

$$q_3 = [1 - (\frac{\gamma}{\gamma_2})^2]^{\frac{1}{2}} = [1 - \frac{1}{K_r}(\frac{\gamma}{jk})^2]^{\frac{1}{2}} \tag{3.54}$$

From Maxwell's Eq. (2.6), for $x < 0$

$$j\omega\epsilon_2' E_z = \frac{\partial H_y}{\partial x} - \frac{\partial H_x}{\partial y} \tag{3.55}$$

$$= \gamma_x H_y - \frac{\partial H_x}{\partial y}$$

$$E_z = \frac{\gamma_x}{\gamma_2} Z_2 H_y [1 - \frac{1}{\gamma_x H_y} \frac{\partial H_x}{\partial y}]$$

therefore $$E_z \simeq q_3 Z_2 H_y \tag{3.56}$$

From the definition of surface impedance Z_s, in Section 2.3, it follows that

$$Z_s = q_3 Z_2 \tag{3.57}$$

From Maxwell's Eq. (2.5), for $x < 0$

$$j\omega\mu H_y = \frac{\partial E_z}{\partial x} - \frac{\partial E_x}{\partial z} \tag{3.58}$$

$$H_y = \frac{\gamma}{\gamma_z Z_2} E_x + \frac{\gamma_x}{\gamma_2 Z_2} E_z$$

$$E_x = \frac{\gamma_2}{\gamma} (Z_2 H_y - q_3 E_z)$$

Substituting from Eq. (3.56) for E_z,

$$E_x = \frac{\gamma_2}{\gamma} Z_2 H_y (1 - q_3^2) \tag{3.59}$$

Power P_2 flowing in the z direction in the region $x < 0$ is given by

$$P_2 = \int_{A'} \underline{E} \wedge \underline{H}^* \cdot \underline{dA'} \tag{3.60}$$

$$= \int_{A'} (E_x H_y^* - E_y H_x^*) dA'$$

Since $|E_y| \ll |E_x|$ and $|H_x| \ll |H_y|$ to the same order of accuracy as the plane wave approximation,

$$P_2 \simeq \int_{A'} E_x H_y^* \, dA'$$

therefore

$$P_2 = \frac{\gamma_2}{\gamma} Z_2 (1 - q_3^2) \int_{A'} H_y H_y^* \, dA' \tag{3.61}$$

By plane wave approximation, for $x < 0$

$$H_y(x,y) = H_{oy}(y)e^{\gamma_x x} \tag{3.62}$$

where $H_{oy}(y)$ is given by Eq. (3.2).

Direct evaluation of Eq. (3.61) yields

$$P_2 = \frac{\gamma_2}{\gamma} Z_2(1 - q_3^2)\frac{I^2}{2\pi b} \frac{(1 + q_2/2)(1 + q_2^*/2)}{(\gamma_x + \gamma_x^*)} \tag{3.63}$$

Evaluation of F_2, Eq. (3.30), is also straightforward, and we obtain

$$F_2 = \frac{1}{I}\int_{A'} E_z' dA'$$

$$= Z_s \frac{(1 + q_2/2)}{\gamma_x} = \frac{Z_2(1 + q_2/2)}{\gamma_2} \tag{3.64}$$

3.3.2. Summary of Equations

For completeness, all the equations used in computations are given below in their final form. New variables defined below were only introduced to simplify the process of computation: square-bracketted numbers indicate the source of equations

$$\frac{\gamma}{jk} = (1 + \delta)^{\frac{1}{2}} \tag{3.65}$$

[3.1]

$$\delta = |\delta| e^{j\phi_\delta} = -1 - \left(\frac{\gamma}{k}\right)^2 = -\frac{N}{D}\ ; \quad -\frac{\pi}{4} < \phi_\delta < \frac{3\pi}{4} \tag{3.66}$$

[3.8, 3B.8]

$$u = |u|e^{j\phi_u} = jh = k\sqrt{\delta} \quad ; \quad -\frac{\pi}{2} < \phi_u < 0 \tag{3.67}$$

$$\text{or} \quad \frac{\pi}{2} < \phi_u < \pi$$

$$V_1 = ub \tag{3.68}$$

$$V_2 = (u + u^*)b \tag{3.69}$$

$$W_1 = 1 - e^{-V_1} \tag{3.70}$$

$$W_2 = 1 - e^{-V_2} \tag{3.71}$$

$$W_3 = \frac{W_2}{0.5(u + u^*)/k} - 2kbe^{-V_2}\left[\frac{e^{V_1} - 1}{V_1} + \frac{e^{V_1^*} - 1}{V_1^*} - 1\right] \tag{3.72}$$

[3.54]

$$q_3 = (1 - \frac{1 + \delta}{K_r})^{\frac{1}{2}} \tag{3.73}$$

[2.33]

$$Z_{cn} = \frac{Z_{co}}{Z_1} = \frac{138}{120\pi} \log_{10} (\frac{2b}{a}) \tag{3.74}$$

[3.16, 3.57]

$$Z_{sn} = \frac{Z_2}{Z_1} q_3 \tag{3.75}$$

$$q_1 = -j \frac{Z_{sn}}{\sqrt{\delta}} \tag{3.76}$$

[3.28, 3.31, 3.64]

$$q_2 = \frac{q_1[W_1 - j(\frac{\epsilon_r}{q_3}) \frac{\sqrt{\delta}}{\sqrt{K_r}}]}{1 - 0.5\, q_1[W_1 - j(\frac{\epsilon_r}{q_3}) \frac{\sqrt{\delta}}{\sqrt{K_r}}]} \tag{3.77}$$

[3.1, 3.4, 3.15]

$$N = j\frac{Z_{zn}}{2\pi kb}(1 + \frac{q_2}{2})(1 + \frac{q_2^*}{2})(1 - jZ_{sn}^* W_3) \tag{3.78}$$

[3.42]

$$\Delta Z_{cn} = \frac{\Delta Z_c}{Z_{co}}$$

$$= \frac{j2Z_{sn}(1 + \frac{q_2}{2})e^{-V_1}}{kb[\ell n\left|\frac{1}{ua}\right| + j(\frac{\pi}{2} - \phi_u)] - j2Z_{sn}(1 + \frac{q_2}{2})e^{-V_1}} \tag{3.79}$$

[3.53]

$$\gamma_x = q_3\gamma_2 \tag{3.80}$$

[3.63]

$$q_5 = \frac{(1 - q_3^2)(1 + \frac{q_2}{2})(1 + \frac{q_2^*}{2})}{Z_{cn}\sqrt{(1 + \delta)}2\pi(\gamma_x + \gamma_x^*)b} \tag{3.81}$$

[3.23, 3.42, 3.63]

$$D = \frac{Z_{cn}}{\sqrt{(1 + \delta)}}(1 + \Delta Z_{cn} - q_5) \tag{3.82}$$

The above system of equations can be solved for δ by an iterative process. The starting point for the iterative process is

$$N = N_o = j\frac{Z_2/Z_1}{2\pi kb} \tag{3.83}$$

$$D = D_o = Z_{cn} \tag{3.84}$$

$$\delta = \delta_o = -\frac{N_o}{D_o} \qquad (3.85)$$

3.3.3. Propagation Constant of the Beverage Structure : Comparison With Other Theories

From a pragmatic point of view, the usefulness and limitations of any theoretical model depend on the accuracy with which physical behaviour can be predicted. To this end, two possible avenues exist for testing a particular model : theoretical results can be compared with other analytical results, particularly if the other analyses are known to be more rigorous ; alternatively, theoretical results can be correlated with experimental data.

For the Beverage structure, analytical results have been given by Knight [Ref. 2.14], Kikuchi [Refs. 2.9, 2.11], and dos Santos [Ref. 2.12]. Measured data is also available from many sources (see Section 2.2), but experiments, reported by the above authors are probably the most reliable available, at least for purposes of comparison with theory.

A computer program was written which solved the system of equations given in Section 3.3.2 by an iterative process. The results of each iteration were written out to check for convergence, and as a safeguard against instability. Numerical data were obtained corresponding to three distinct sets of parameters considered by Kikuchi, dos Santos and Knight. The table in Fig. 3.2 shows a typical set of parameters reported by each author, which we have used for comparison purposes.

Set Number	1	2	3
Source Author	Kikuchi	dos Santos	Knight
Source Reference	Refs. 2.10 2.11	Ref. 2.12	Ref. 2.14
Wire Radius a(cm)	0.25	0.25	0.24
Wire Spacing From Interface b(cm)	750	100	300
Ground Dielectric Constant ε_r	1	15	10
Ground Conductivity σ (S/m)	10^{-2}	10^{-2}	10^{-2}

Fig. 3.2. Summary of line parameters used by authors whose theoretical results are compared with those due to the present theory.

Figures 3.3, 3.4 and 3.5 depict variations of attenuation with frequency : in each graph, the solid line represents the present theory, and the dashed line the corresponding analytical results against which the present theory is being compared; available experimental data has also been indicated (approximately), where ever possible. It can be seen that at HF and lower frequencies all theories lead to similar variations of attenuation with frequency. Only the analyses of dos Santos (proper mode) and Kikuchi give identical results. The present theory yields somewhat higher attenuation values than other theories.

At VHF the attenuation characteristics are no longer similar : Knight's theory indicates that attenuation increases with frequency, tending to a maximum value; other theories, including the present one, all indicate a decrease in attenuation. However, the rate of decrease of attenuation with frequency indicated by the present theory is found to be sensitive to the choice of parameters. The shape of characteristics obtained by Kikuchi and dos Santos is not sensitive to the choice of parameters, and changing the parameters mainly causes a shift in the position of the attenuation curve.

Figs. 3.6 and 3.7a , indicate the variation of velocity ratio ($= v/c$) with frequency, for structures considered by dos Santos and Knight respectively. Kikuchi has not given any quantitative results for the phase velocity v. It can be seen that the present theory yields velocity ratios closer to unity than the other theories. Otherwise, there are only two significant observations to be noted. Firstly, dos Santos' analysis indicates velocity ratios greater than unity above 10 MHz : this is probably due to theoretical or computational errors, unless these results are related to unforeseen higher-order modes sought by dos Santos' algorithm. Secondly,

in Fig. 3.6, the slope of Knight's theoretical curve at lower frequencies suggests that phase velocity becomes zero at some non-zero frequency; on physical considerations this conclusion seems untenable.

To our knowledge, the only published data on the characteristic impedance of the Beverage structure is due to Knight [Ref. 2.14]. Figure 3.8 provides a comparison between the corrected version of this data (see Section 2.2) and results based on our analysis; real and imaginary parts of characteristic impedance, R_c and X_c respectively, are given by

$$R_c = Z_{co}(1 + \Delta R_{cn}) \tag{3.88}$$

$$X_c = Z_{co}\Delta X_{cn} \tag{3.89}$$

where Z_{co} is the nominal characteristic impedance for the corresponding perfectly-conducting transmission line, given by Eq. (3.74).

Neither Kikuchi nor dos Santos has published computed values for characteristic impedance. However, approximate calculations indicate that Kikuchi's analysis leads to negative values of ΔX_{cn}; $|\Delta X_{cn}| \sim 1\%$ at 2 MHz and increases with decreasing frequency. ΔR_{cn} is positive below 8 MHz, and increases with decreasing frequency ($\Delta R_{cn} \sim 1\%$ at 2 MHz). Above 8 MHz ΔR_{cn} is negative and reaches a minimum value $\sim 0.1\%$ at approximately 20 MHz; at higher frequencies ΔR_{cn} tends to zero through negative values. Computations, for Kikuchi's line, based on the equations of Section 3.3.2. yield very different results: magnitudes of ΔR_{cn} and ΔX_{cn} obtained are about four times the corresponding values based on Kikuchi's analysis; furthermore, in contrast to Kikuchi's analysis, the present theory gives positive values of ΔX_{cn}, and values for ΔR_{cn} which are negative at lower frequencies and positive at higher frequencies.

The divergence between characteristic impedance results, by the present theory and the other analyses, arises from the difference in the interpretation of field equations. In order to obtain the equivalent-circuit elements, field equations can be expressed in a form analogous to the following transmission-line equations:

$$\frac{\partial V}{\partial z} = - ZI \qquad (3.90)$$

$$\frac{\partial I}{\partial z} = - YV \qquad (3.91)$$

In effect Kikuchi has chosen the former representation, and we have chosen the latter. The choice has not been an arbitrary one: it is believed that Kikuchi's choice was perhaps historical in nature, as Carson [Ref. 2.3] and Wise [Ref. 2.4] originally interpreted the effect of finite longitudinal electric field as equivalent to a series line impedance. Our choice has two justifications : firstly, sources connected to the line are generally 'voltage sources' and not 'current generators', even though both Norton and Thevenin representations are valid (for example, sources generally tolerate open-circuit better than short-circuit). Secondly, in the limit as the frequency tends to zero, we would expect the (instantaneous) energy transferred to the line to become increasingly reactive, and the real (propagating) energy to vanish gradually. This behaviour is indicated by the present theory, whereas the analyses by Kikuchi and Knight suggest that, in the above limit, approximately half the energy in the line remains real - corresponding to real power propagation at zero frequency.

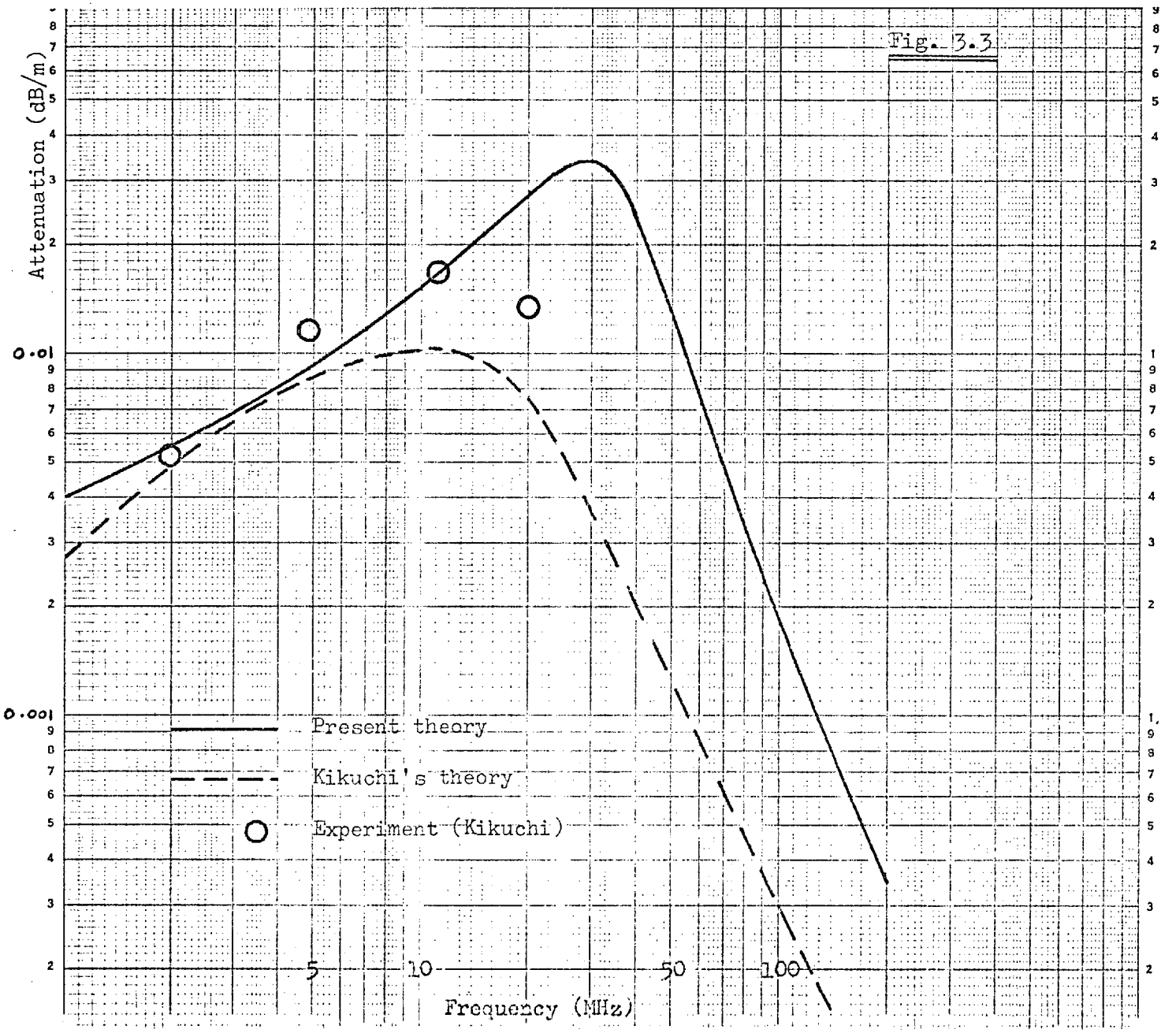

Attenuation (dB/m)
0.01
0.001
Present theory
Kikuchi's theory
Experiment (Kikuchi)
5
10
50
100
Frequency (MHz)

Fig. 3.3

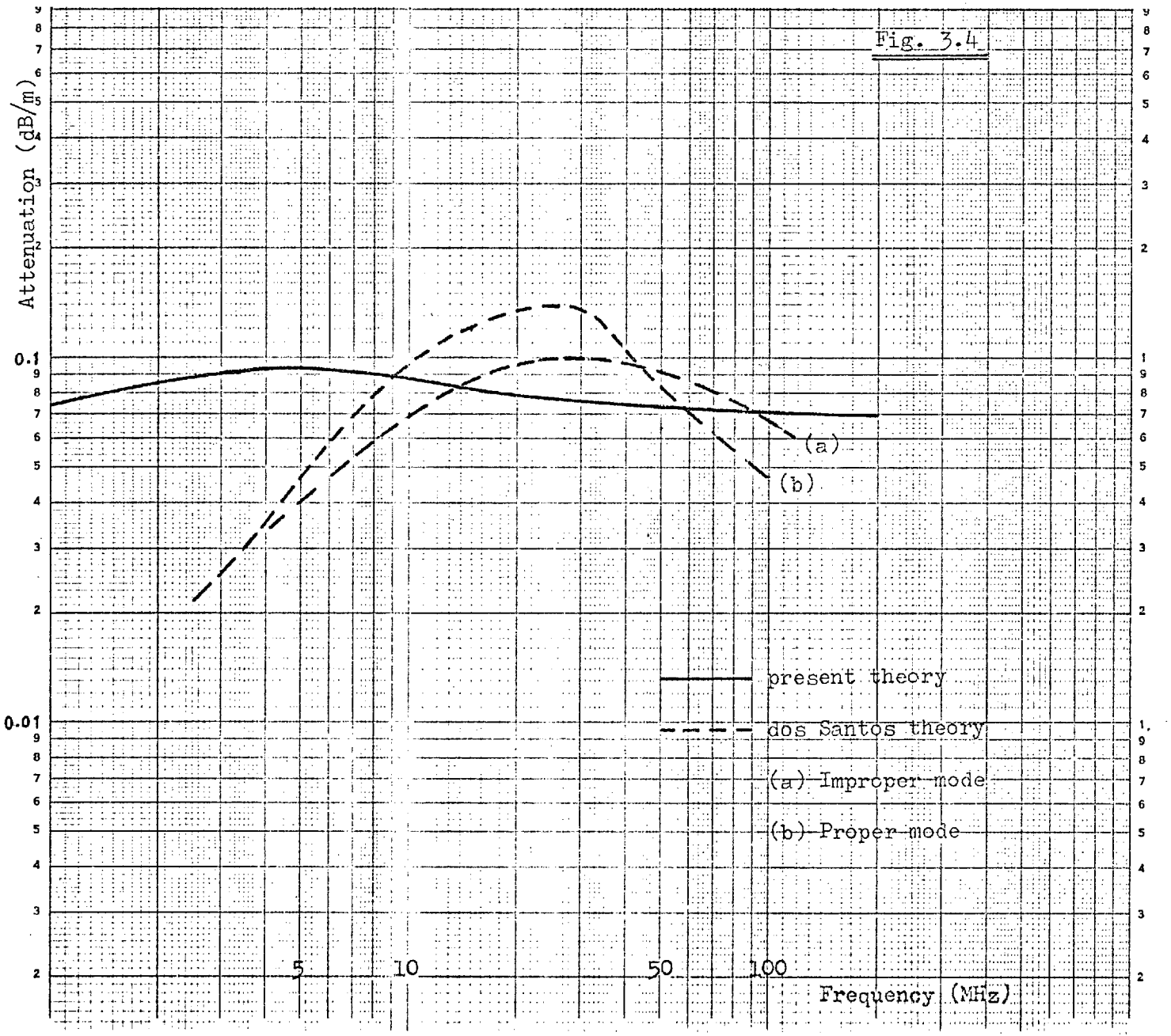
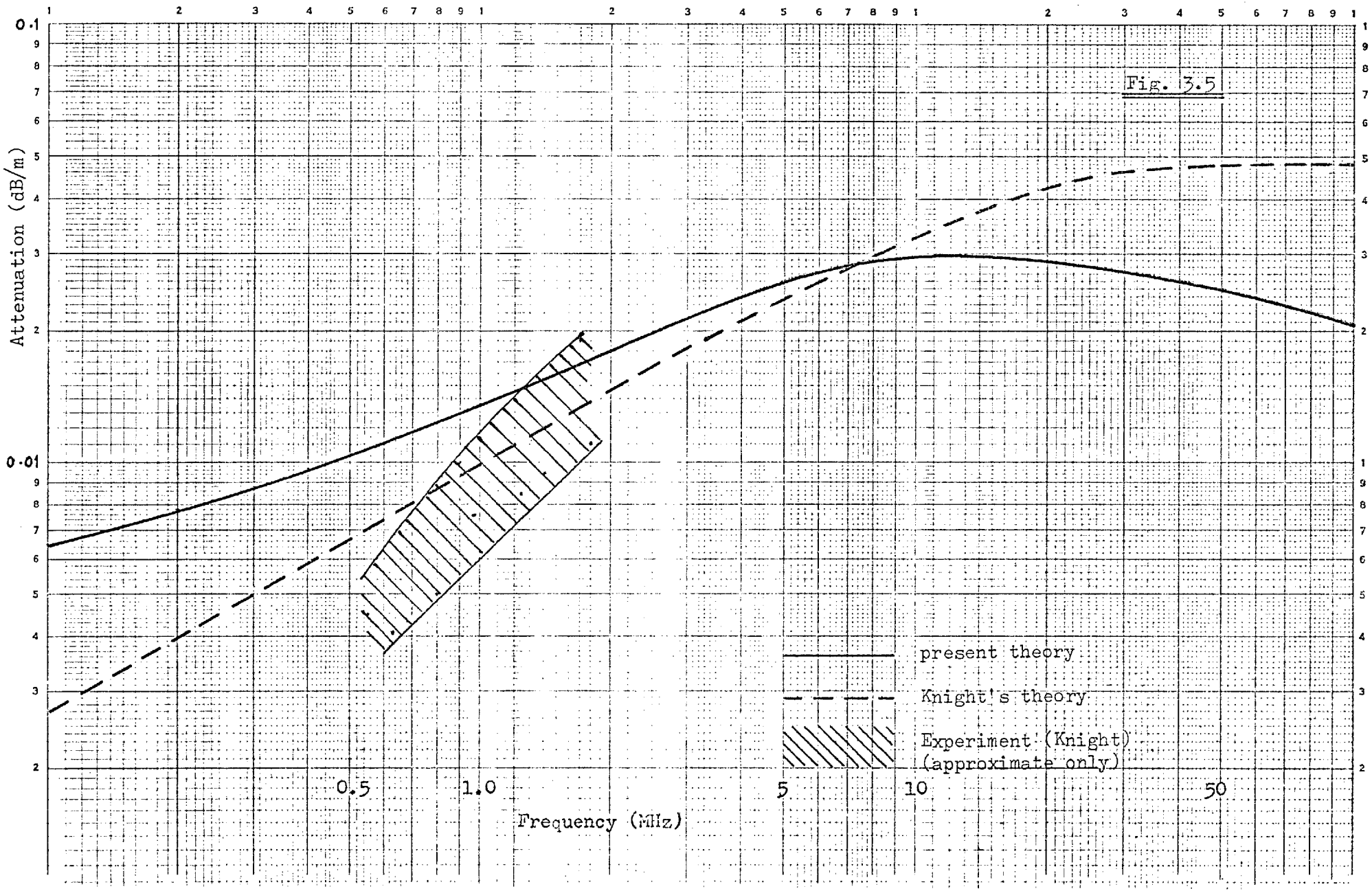
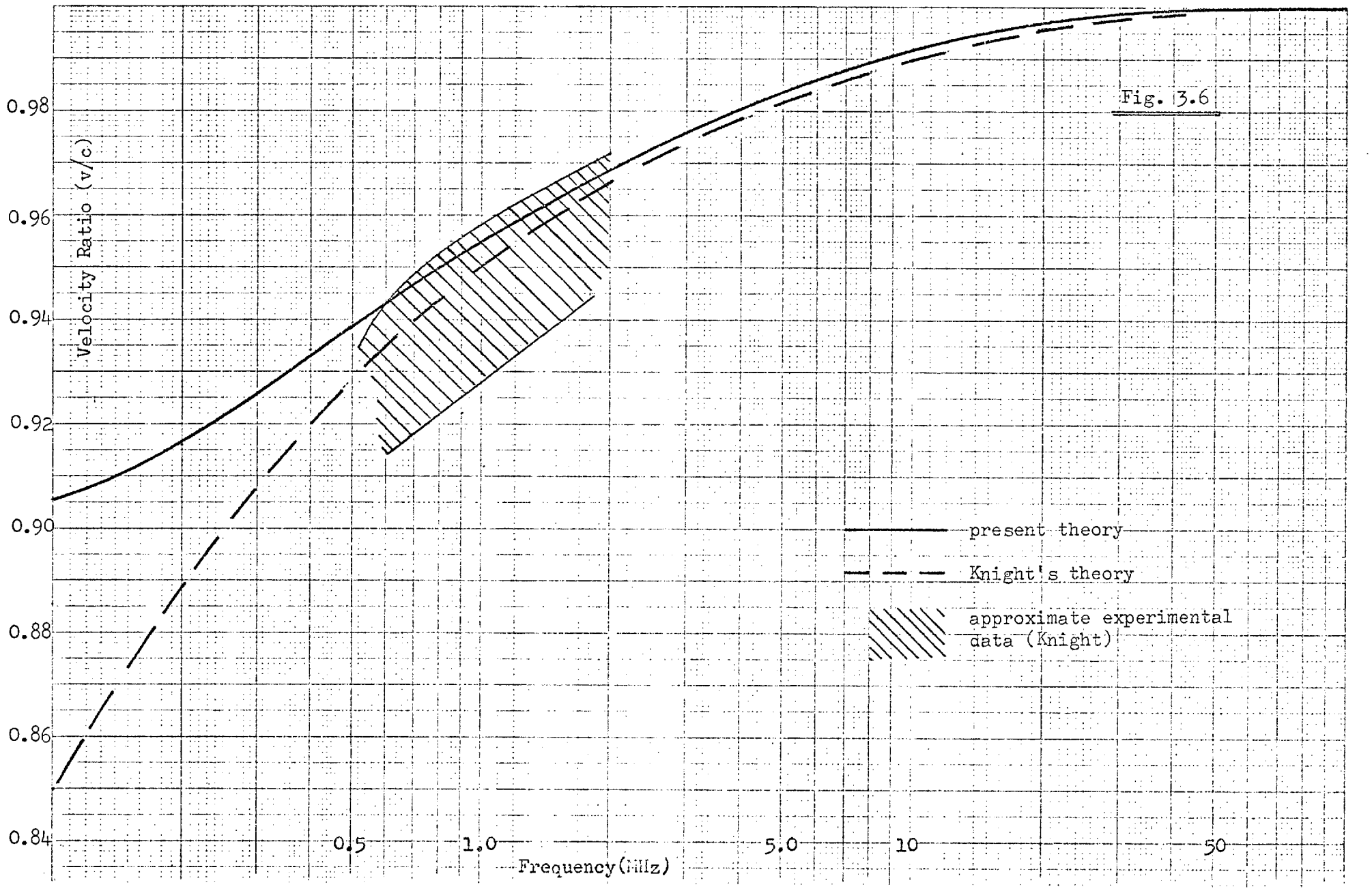

Attenuation (dB/m)
0.1
0.01
5
10
50
100
Frequency (MHz)
(a)
(b)
present theory
dos Santos theory
(a) Improper mode
(b) Proper mode

Fig. 3.4


Fig. 3.5
Attenuation (dB/m)
0.1
0.01
0.5
1.0
5
10
50
Frequency (MHz)
present theory
Knight's theory
Experiment (Knight)
(approximate only)


Fig. 3.6
Velocity Ratio (v/c)
0.98
0.96
0.94
0.92
0.90
0.88
0.86
0.84
0.5
1.0
5.0
10
50
Frequency (MHz)
present theory
Knight's theory
approximate experimental data (Knight)

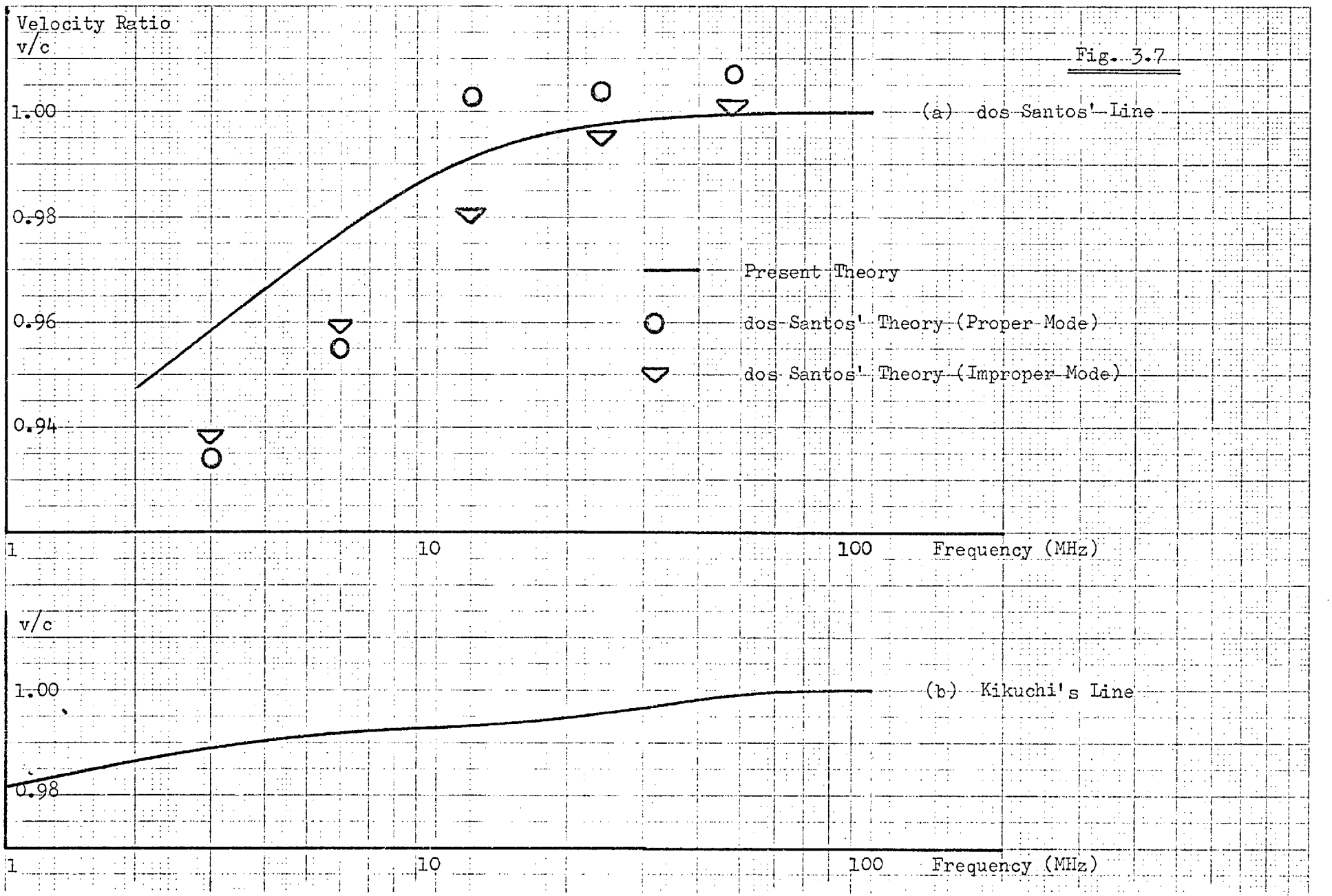
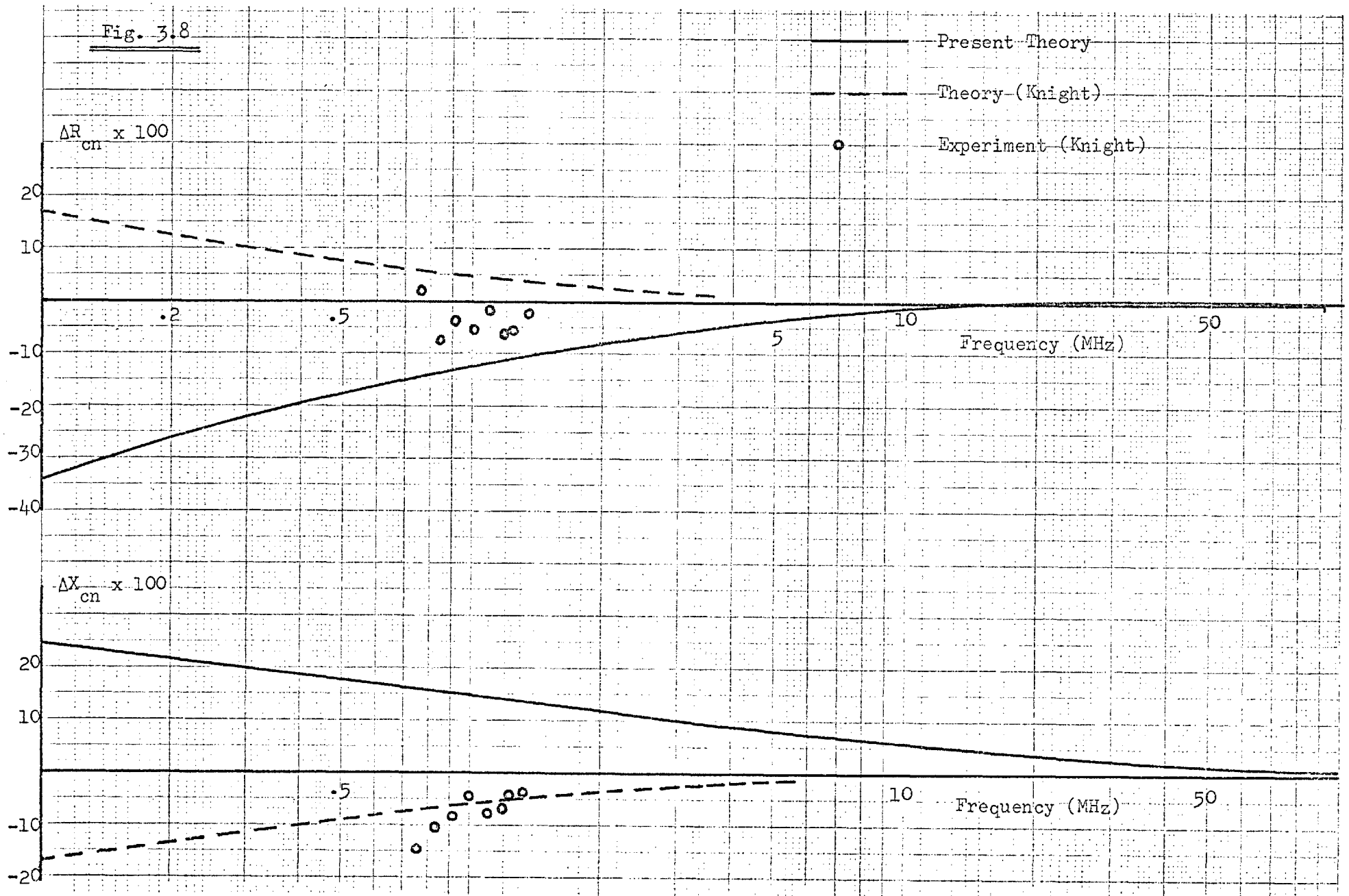

Velocity Ratio
v/c
1.00
0.98
0.96
0.94
1
10
100
Frequency (MHz)
(a) dos Santos' Line
Present Theory
dos Santos' Theory (Proper Mode)
dos Santos' Theory (Improper Mode)
v/c
1.00
0.98
1
10
100
Frequency (MHz)
(b) Kikuchi's Line

Fig. 3.7


Fig. 3.8
Present Theory
Theory (Knight)
Experiment (Knight)
ΔR_cn x 100
20
10
-10
-20
-30
-40
.2
.5
5
10
50
Frequency (MHz)
ΔX_cn x 100
20
10
-10
-20
.5
10
50
Frequency (MHz)

3.4. Calculations for a Corrugated-Plane Interface

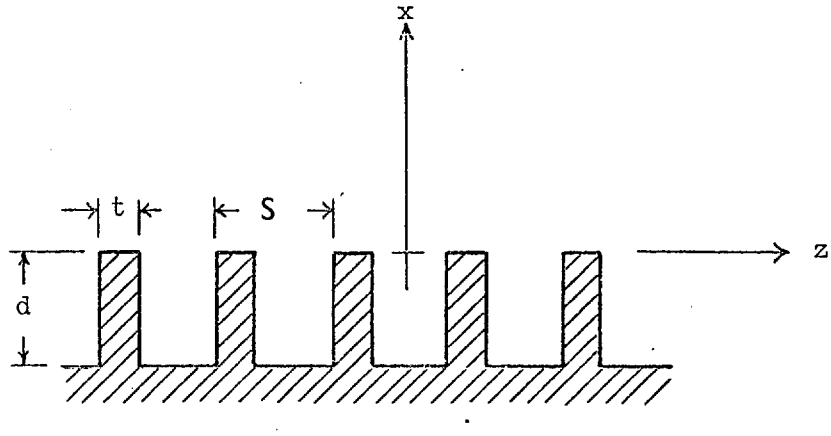


Fig. 3.9. Section of the Corrugated Plane

In this section we shall derive the required relations for the calculation of propagation constant of the IPA. In this case, the interface consists of a corrugated perfectly-conducting plane, as shown in Fig. 3.9 : the periodic spacing is S, wall thickness t, and corrugation depth d; the top of the corrugation walls lie in the plane x = 0.

We wish to evaluate the surface impedance Z_s, and quantities F_2 and P_2 in Eqs. (3.50) and (3.17) respectively. To this end we require the behaviour of fields inside the corrugations. We shall restrict our considerations to configurations for which $S \ll \lambda_1$, $d < \lambda_1/4$ and $S < d$, where $\lambda_1 = \frac{2\pi}{k_1}$ and k_1 is the wave number for the medium in the region $x > 0$, outside the wire, and inside the corrugations (generally the medium is taken as air, with free-space constants ϵ_o, μ_o).

With the above restrictions, the dominant mode of propagation inside the corrugations is TEM, travelling in the x - y plane [Ref. 3.6], with polarization E_z. As mentioned in Section 3.2.2., outside the corrugations, in the region $x > 0$, E_z can be represented as an angular spectrum of plane waves, as in Eq. (3.9). For each elementary component

of this spectrum we can obtain the corresponding field distribution in the corrugated region. This can be done in the manner indicated by Goldstone and Oliner [Ref. 2.27], using existing solutions for the corresponding two dimensional problem, where fields are assumed to be invariant with y [Refs. 3.7, 3.8, 3.9].

Analysis of the corresponding two-dimensional problem [Ref. 3.9] has provided certain conclusions which are pertinent to our considerations. When $S \ll \lambda_1$ the TE modes (with respect to the z-direction) becomes evanescent; therefore we need only consider TM modes. Secondly, in the corrugations only the TEM mode (w.r.t. the x-direction) propagates, the other (TM) modes being evanescent. The requirement $d > S$ ensures that the short-circuit at $x = -d$ does not appreciably interact with the evanescent modes. These evanescent modes give rise to a storage of electric energy at the corrugation edges, and therefore the corrugations are effectively terminated, at $x = 0$, in a capacitive reactance. The equivalent length of transmission line, representing the edge capacitance, can be obtained from the analysis by R.E. Collin [Ref. 3.9], or Marcuvitz [Ref. 3.7]; it is given by

$$\Delta L = -\frac{S}{\pi} \ell n\, 2 \tag{3.92}$$

Taking the above capacitance into account, the surface impedance Z_s for a corrugated plane is given by

$$Z_s = \frac{S - t}{S} Z_1 \tan k_1 (d - \frac{S}{\pi} \ell n\, 2) \tag{3.93}$$

where the factor $\frac{S - t}{S}$ is a correction factor to allow for the wall thickness t [Ref. 3.10]. The above equation is valid for a single TEM mode propagating parallel to the x-axis, in the corrugated region.

These are two justifications for using the above relation. Firstly, in the 'aperture plane' $x = 0$ H_x must be very small, if not zero, as required by boundary conditions at the corrugation edges. It follows that the field inside the corrugations must be a combination of TM (w.r.t. the x-direction) modes; as already stated, for $S \ll \lambda_1$ only the TEM mode propagates. Secondly, in the angular spectrum representation of E_z for $x > 0$, it was seen that the predominant contribution to E_z comes from elementary waves having little or no variation with y; for this predominant range, only modes propagating in the x direction need be considered in the corrugated region.

To evaluate P_2, Eq. (3.17), we recall that

$$P_2 = \int_{A'} (E_x H_y^* - E_y H_x^*) dA' , \qquad x < 0$$

It follows that $P_2 = 0$, since no power can flow through the corrugation walls, and $E_x = E_y = 0$.

To evaluate F_2, we start from (3.30):

$$F_2 = \frac{1}{I} \int_{A'} E_z' dA' = \frac{1}{I} \int_{-\infty}^{\infty} \int_{-d}^{0} E_z' dx dy \qquad (3.94)$$

where

$$E_z' = E_s(y) \frac{\sin[k(d + x)]}{\sin(kd)} \qquad (3.95)$$

and $E_s(y)$ is given by Eq. (3.5). Integration of Eq. (3.94) yields

$$F_2 = Z_s(1 + \frac{q_2}{2}) \frac{1 - \cos(kd)}{k \sin(kd)} \qquad (3.96)$$

To obtain q_2, we substitute from Eqs. (3.31) and (3.96) into Eq. (3.28):

$$q_2 = \frac{\left[- j \frac{Z_s}{Z_1} \right]\left[\frac{1 - \cos kd}{\sin kd} + \frac{1 - e^{-jhb}}{jh/k} \right]}{1 - \frac{1}{2}\left[- j \frac{Z_s}{Z_1} \right]\left[\frac{1 - \cos kd}{\sin kd} + \frac{1 - e^{-jhb}}{jh/k} \right]} \qquad (3.97)$$

Inspection of Eqs. (3.65) to (3.84) shows that when a corrugated--plane interface is considered instead of a transition-boundary interface, only three equations need be replaced : (3.75) by (3.93); (3.77) by (3.97); and (3.81) by the following equation

$$D = \frac{Z_{cn}}{\sqrt{1 + \delta}} (1 + \Delta Z_{cn}) \qquad (3.98)$$

The new system of equations can again be solved for δ by an iterative process as before.

3.5. Near-field Measurements on the Inductive-Plane-Antenna

3.5.1. Preliminary Experiments

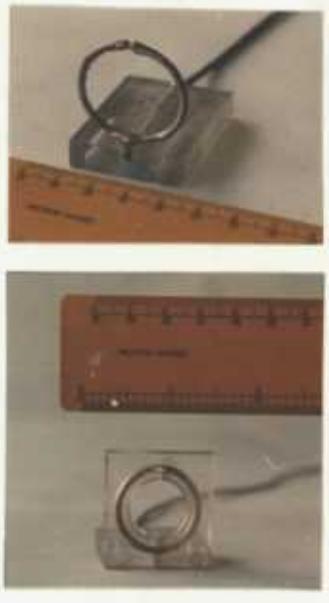


Fig. 3.10. Magnetic Loop Probes

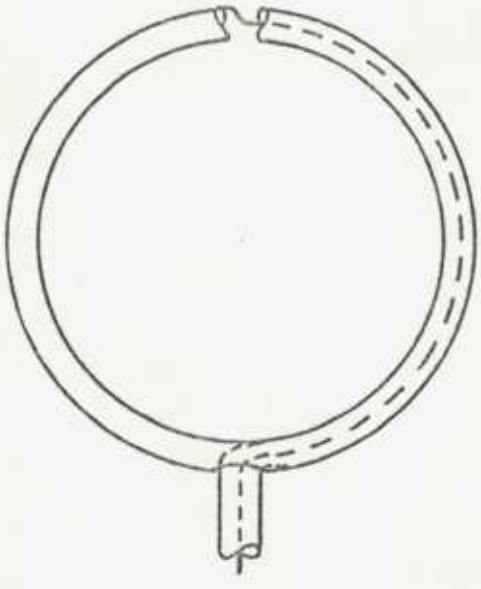


Fig. 3.11. Detail of Loop Construction

Two small loops and one electric probe were constructed for the purpose of carrying out the near-field measurements. The loops are shown in Fig. 3.10; particular attention was paid to the symmetry of construction, as depicted in Fig. 3.11, in order to minimize the dipole mode of response. The electric probe is shown in Fig. 3.12, and was constructed such that the monopole could be removed from its coaxial socket, for test purposes.

A short-circuited transmission-line was also constructed for testing the probes. The test line consisted of a straight length of enamelled copper wire, 0.12 cm in diameter, at a height of 3.2 cm above a copper plane (width greater than 150 cm); the line length was 344 cm. In the tests carried out on each probe, the distance between the probe and the plane of symmetry of the line was 2.5 cm approximately.

Tests were carried out at frequencies 0.710 and 0.995 GHz.

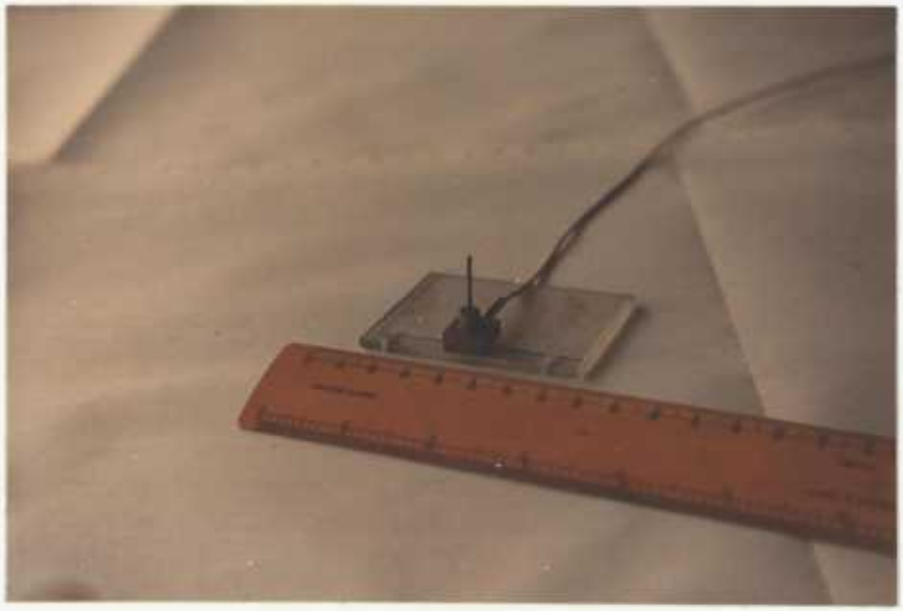


Fig. 3.12. The Electric Probe

Standing-wave-ratios indicated by all three probes exceeded 30 dB (with the line short-circuited). In these tests the plane of the loops were parallel to the plane of symmetry of the line.

Another test consisted of placing the loop in a position of maximum output, and then turning the loop (through 90 degrees) until its plane became parallel to the transmission-line cross-section. Both loops gave output ratios of the order of 40 dB. This was taken as a figure of merit for the loop, indicating a satisfactory discrimination against the dipole mode of response.

The corresponding test for the electric probe consisted of comparing the outputs before and after removing the monopole (2.5 cm long) from its coaxial socket : again a satisfactory output ratio of 40 dB was obtained.

Finally the velocity ratio of the test transmission line was measured at frequencies 0.715 GHz and 0.910 GHz, using all three probes. Velocity ratios obtained were in the range 0.993 to 0.998

(corresponding to β/k values from 1.007 to 1.002 approximately); at the lower frequency consistently higher velocity ratios were measured with each probe. A variational analysis indicated that the measured reduction in phase velocity could be due to the thin layer of enamel on the copper wire : assuming a dielectric coating of dielectric constant $\epsilon_r = 3$, and thickness $t \simeq 0.25 \times 10^{-2}$ cm (i.e. 10^{-3} inches), the velocity ratio obtained was 0.997 approximately.

3.5.2. Experimental Determination of the Propagation Constant

In Section 1.2, a brief description was given of the considerations leading to the choice of short-circuited corrugations for the purpose of realizing an inductive ground-plane. In this section, firstly, we shall describe the technique employed for near-field measurements; secondly we shall outline some constructional details for the structure used in these measurements.

In general, there are two possible methods for determining the propagation characteristics of a travelling-wave structure by experiment. If the structure can be terminated in a matched load, i.e., for standing wave ratios close to unity, the amplitude and phase variations along the structure can be measured directly to yield the attenuation and phase constants of the line. This technique was not used in the present study (except as a final check on the scaled antenna, prior to far field measurements) for two reasons : it was found that reflections from the line termination could not be reduced to acceptable levels required for accurate phase measurements; this was due to a lack of suitable resistors which could be used as matched loads over a wide band in the frequency range of interest (above 300 MHz). Secondly, at the time, an elaborate set-up would

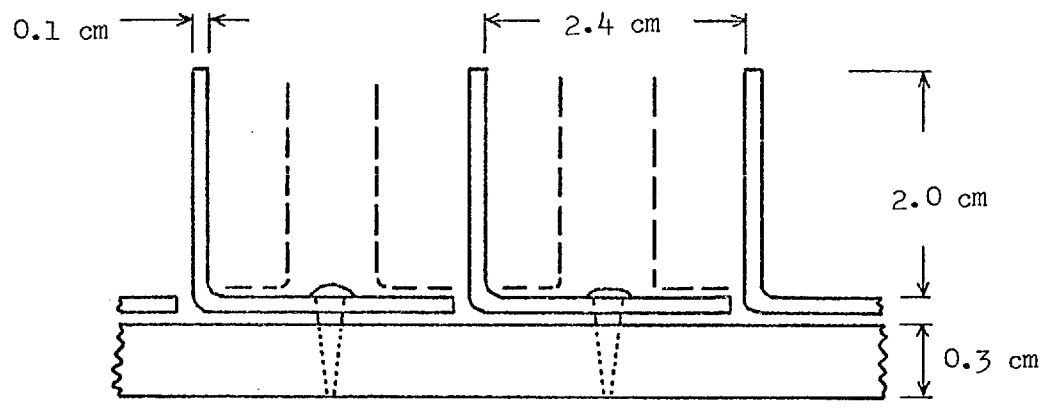


Fig. 3.13. Detail of Construction of Corrugations.

Dashed-lines indicate the positioning of additional spacers used to reduce the corrugation spacing.

have been required for accurate phase measurements, as there was no apparatus available capable of direct phase measurements.

The second method, outlined below, was adopted for the determination of the propagation constant. The line was terminated in a short-circuit and the depths and distribution of the minima were observed in the resulting standing wave pattern. This technique is only suitable for uniform structures which exhibit relatively small attenuations. However, the accuracy of phase measurements can often be increased by constructing a longer line so that a greater number of minima can be observed, (since the distance between successive minima corresponds to one-half the guided wavelength).

The corrugated plane was made in two sections, each constructed by screwing L-shaped strips of aluminium (length 45.7 cm, section 2.0 x 2.4 x 0.1 cm) onto a sheet of Dural (183 x 45.7 cm, thickness 0.3 cm), as depicted in Fig. 3.13. The two sections were placed end to end, thus making a corrugated plane 45.7 x 353 cm (approx.) : proper electrical connection between the two sections was ensured by screwing one of the

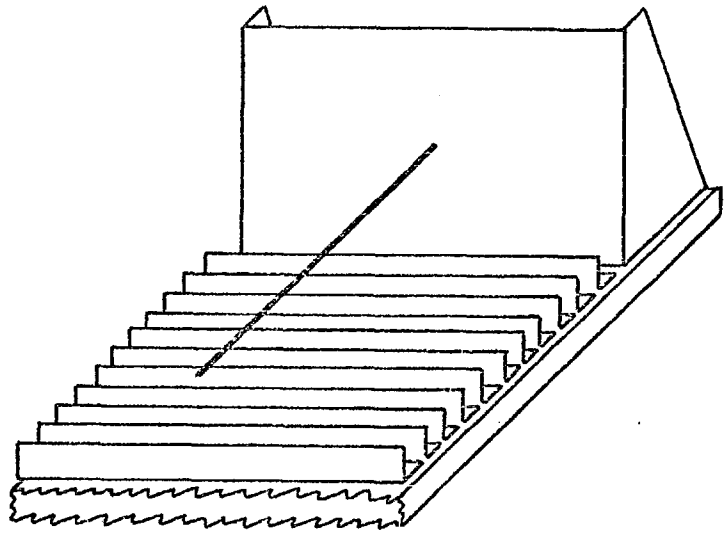
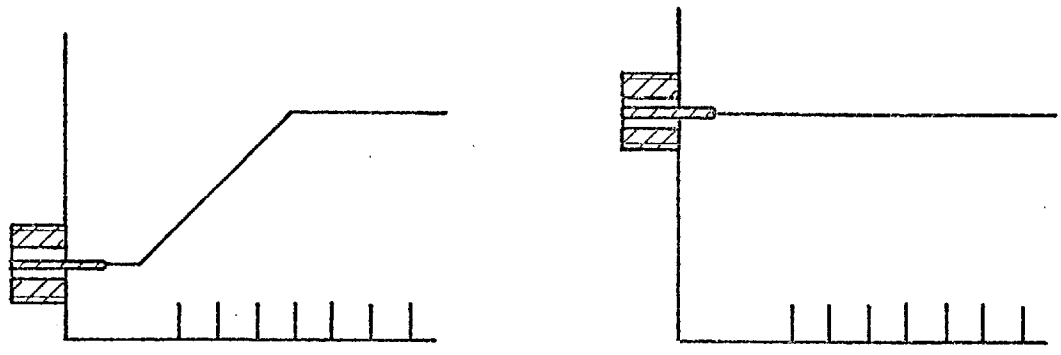


Fig. 3.14. Schematic Representation of the Short-Circuit Line Termination

L-shaped strips onto both Dural sheets.

At a later stage it was decided to reduce the corrugation spacing S, from 2.5 cm to 0.8 cm. This was accomplished by placing L-shaped strips of aluminium (1.9 x 0.7 x 0.1 cm) inside the corrugations, forming conducting planes parallel to the original corrugation walls. Expanded polyethylene spacers were used to hold these additional strips in position.

A copper sheet (width 45 cm, height 20 cm) was used as short--circuit termination for the line, as depicted in Fig. 3.14. The line was excited from a coaxial feed-point, as shown in Fig. 3.15. In the first part of the experiment the feed-point was between the wire and the corrugated plane ; and in the second part, at the wire height, such that the wire formed a straight-line extention to the centre--conductor of the coaxial feed-point.



(a) LD1 (Launching Device 1) (b) LD2

Fig. 3.15. Different Methods of Line Excitation Used in Near-Field Measurements

3.6. Comparison Between Theory and Experiment

A digital computer was used to obtain analytical results corresponding to the parameters of the experimental model, which is represented in Fig. 3.16. The value of these parameters are given below (all dimensions are in centimetres):

wire radius, a	=	0.06
wire height above corrugation tips, b	=	variable: 6.45, 5.5, 4.5 and 3.5
depth of corrugations, d	=	2.0
corrugation spacing, S	=	variable: 2.5 and 0.8
wall thickness, t	=	0.1
width of corrugated plane, w	=	45.7
length of structure from feed-point to short-circuit, L	=	353

Figs 3.17 through 3.23 provide graphical comparisons between theoretical and experimental results. It should be noted that Fig. 3.22 is related to a structure of different cross-section : in this structure, the single wire was replaced by a pair of parallel wires, of the same

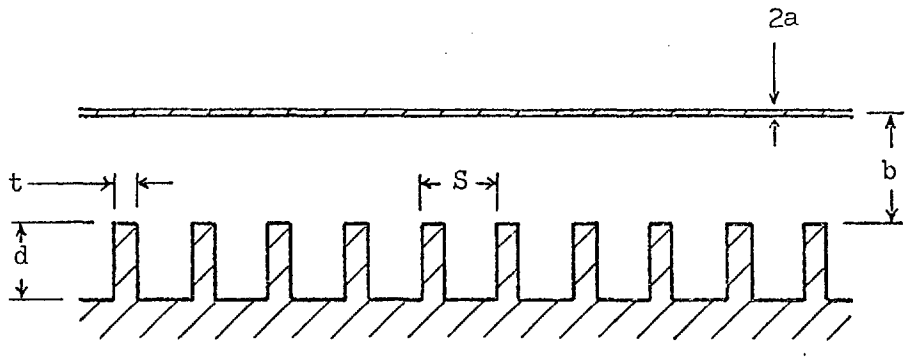


Fig. 3.16 Longitudinal Section of the IPA

diameter, equidistant from the corrugated plane. Theoretical results shown in Fig. 3.22 were obtained by extending the analysis given earlier in this chapter to the double-wire system. The additional analysis required for the double-wire system is given in Appendix 3C; this part of the analysis is based on classical coupled-line theory.

In the presentation of graphical results, the phase constant β has been represented in normalized form β/k, where k is the phase constant in free-space. It should be remembered that in our analysis we have assumed the wire to be perfectly-conducting; but in the experimental set-up an enamelled wire was used. The reduced phase velocities measured on the test line were associated with this enamelled coating. This factor should be taken into account in the interpretation of the graphical results.

Inspection of graphical results reveal two points which are of particular interest. Firstly, better agreement is generally obtained between theory and experiment at lower frequencies. It is believed that this phenomenon is associated with the approximation in Eq. (3.2), where it was assumed that the magnetic field in the cross-section can be derived from electrostatics. As explained in Section 3.1, this approximation is only valid for small values of hr, where h is the

transverse wave number and r the radial distance from the wire axis. Magnitude of hr at the interface decreases as the wire height b becomes smaller, or as the frequency decreases. A better approximation could be obtained by assuming the following magnetic field distribution due to the wire current

$$H_{\phi} = I \frac{jh}{4} H_1^{(1)}(hr) \qquad (3.100)$$

where $H_1^{(1)}$ is the Hankel function of first kind and first order. In this case the electrostatic distribution $H_{\phi} = I/(2\pi r)$ would be obtained only in the limit as hr approaches zero. However, it was felt that the additional accuracy did not justify the increased mathematical complexity associated with the use of Eq. (3.100).

The second observation is that, within experimental error, theoretical values of β/k, the normalized phase constant, are always lower than corresponding experimental results - <u>except</u> in Fig. 3.21 which corresponds to the lowest wire-height used. The reason for this anomoly (in Fig. 3.21) is not entirely clear, but a likely explanation is the following : in the present analysis, the interface has been treated as a uniform surface. A more exact analysis should take into account the periodic nature of the currugated interface. It is known that higher order (evanescent) modes in the corrugated region give rise to a storage of electric energy in the vicinity of corrugation tips [Ref. 3.9]; this stored energy is associated with the periodicity of the structure. When the wire is not too near the corrugated surface, the interface 'appears' uniform. On the other hand, if the wire-interface separation is small there will be an interaction between the wire and the stored electric energy. This interaction gives rise to an increase in the phase velocity, analogous

to a series capacitive loading of the wire.

In one set of measurements, two types of launching device were used to investigate the possibility of exciting different propagating modes along the structure considered. The two launching devices, LD1 and LD2, are depicted in Fig. 3.15. The results of this investigation [Fig. 3.20] indicated that the mode of propagation is independent of the type of feed-point used to energize the structure.

Fig. 3.23 shows the results of measurements carried out on a 3:1 scaled antenna which was constructed for far field studies. These near-field measurements were only made as a final check, while standing waves along the antenna were being minimized by making adjustments to the antenna termination. A (Hewllet-Packard) Network-Analyser was used in these measurements.

In conclusion, the comparsion between theory and experiment yield a satisfactory degree of correlation. Although the analysis presented in this chapter could be made more accurate, the necessary premium would be greater mathematical complexity leading to increases in computer time required for the numerical solutions. For the present study, the analysis was found to yield sufficient accuracy, as supported by the experimental results.

The analysis and the associated computer program can now be used as a basis for further study, and also for design purposes. However, we would point out that the computer program was written for purposes of research and analysis. Naturally, such a program would be inefficient, in terms of cost, for engineering design applications. For this reason, we have refrained from including a listing of the above-mentioned computer program, although such a program could easily be compiled from the results given earlier in this chapter.

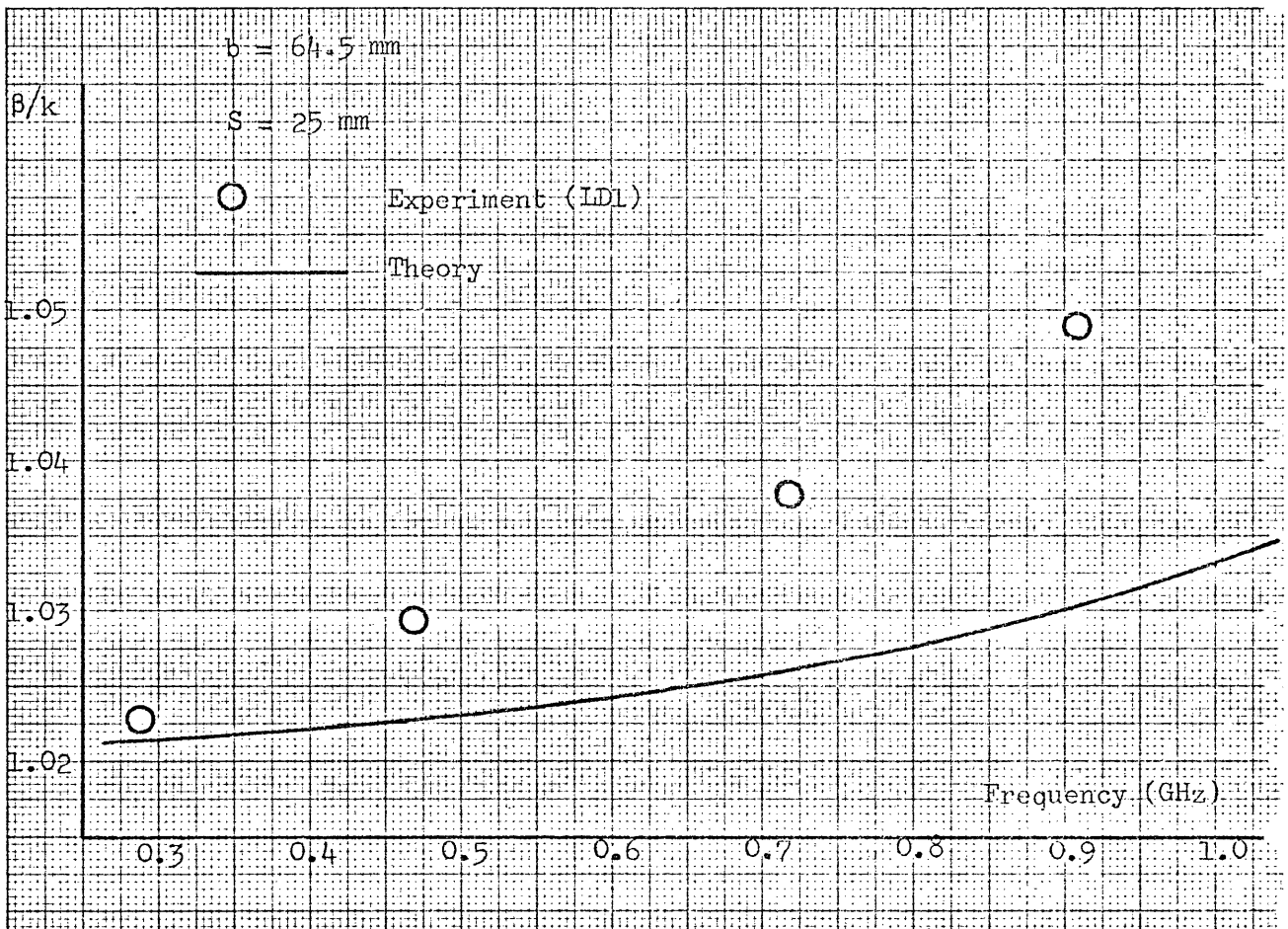


Fig. 3.17

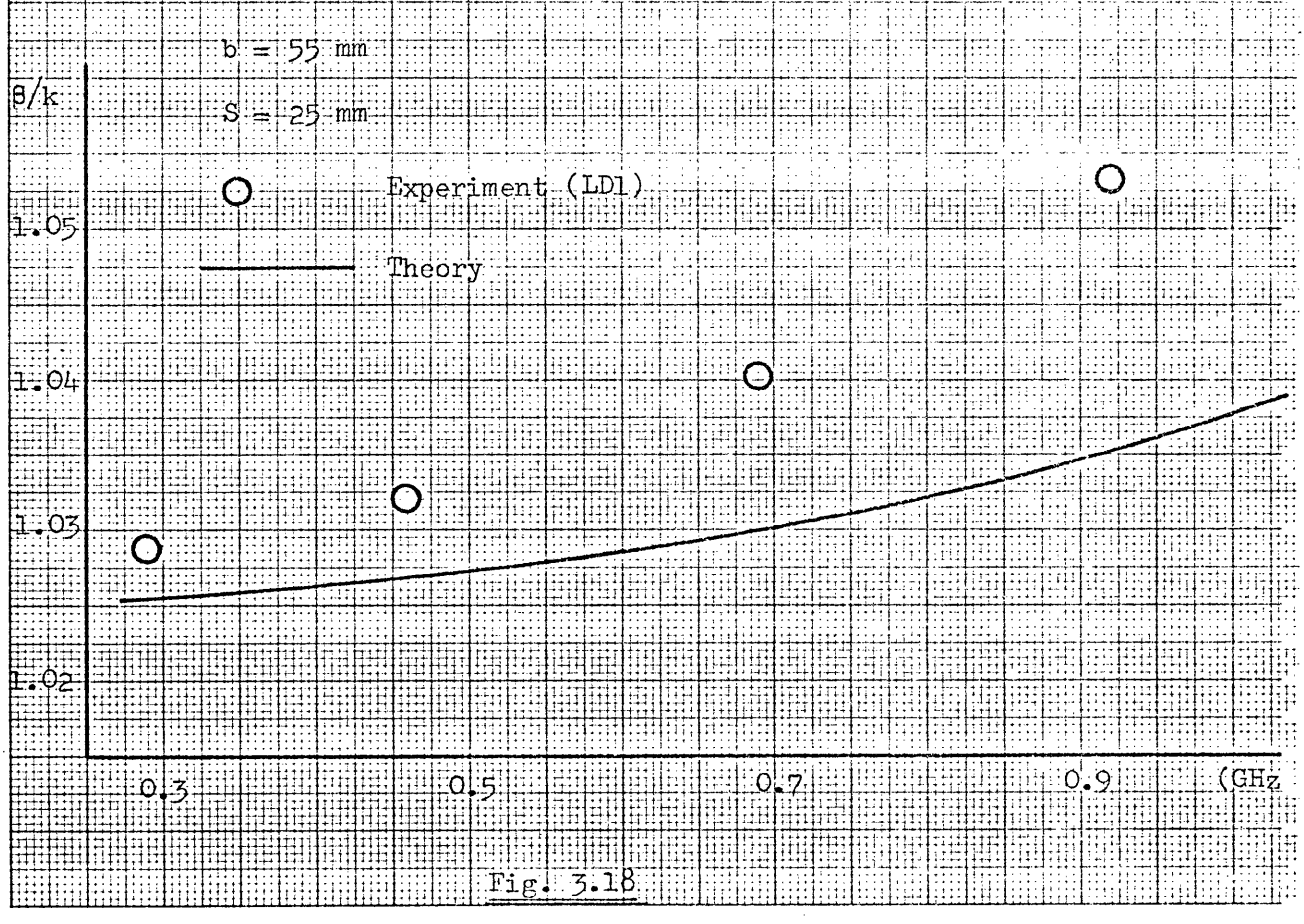


Fig. 3.18

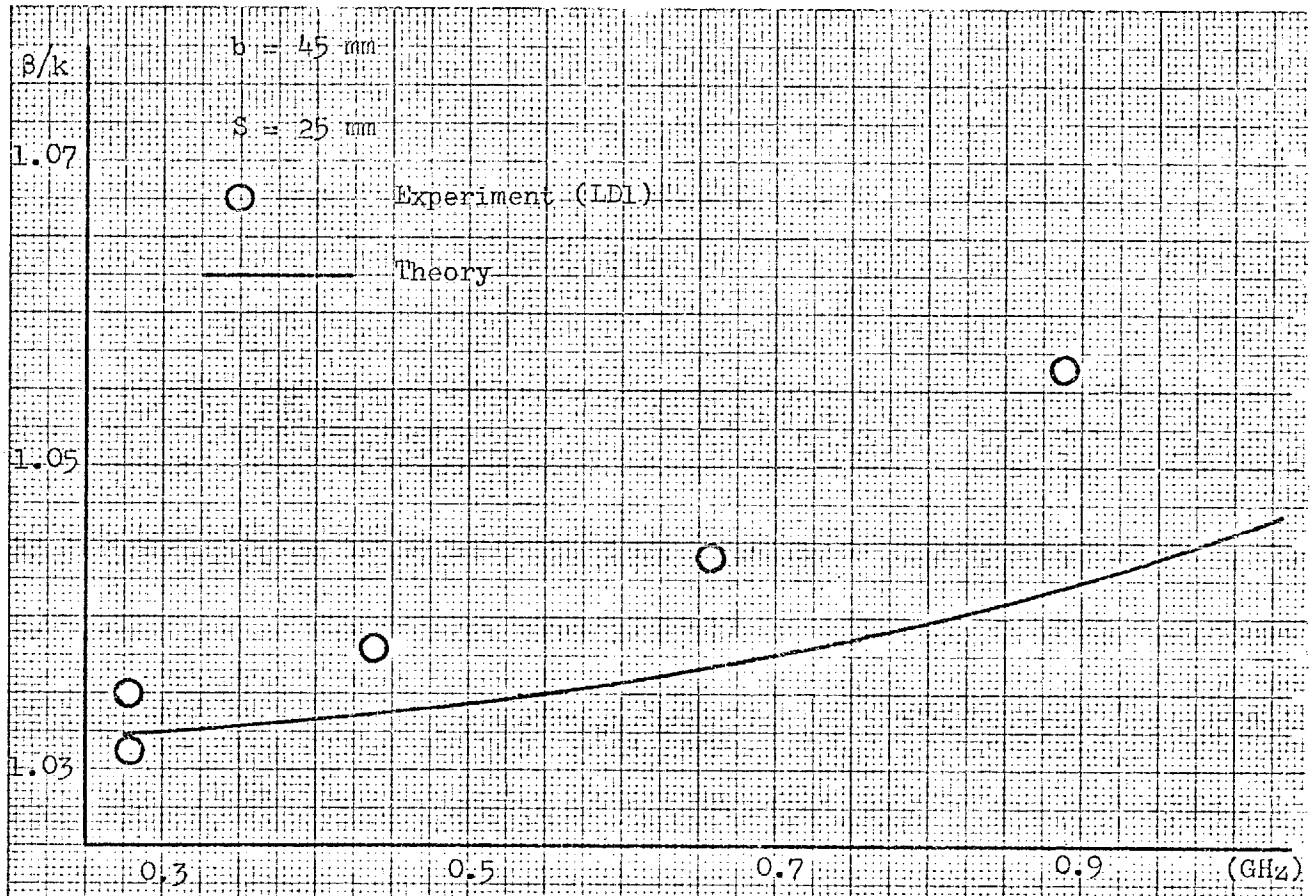


Fig. 3.19

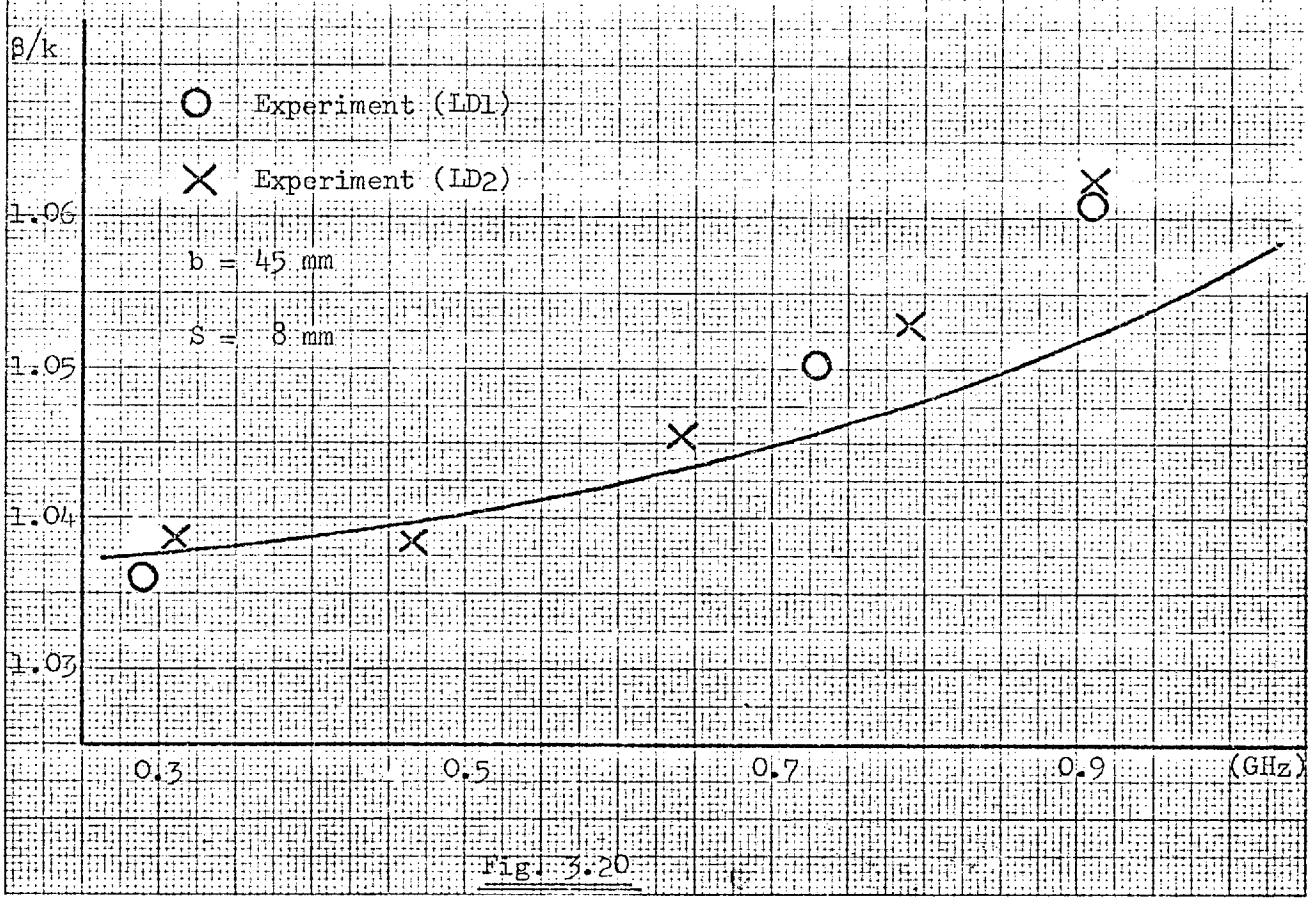


Fig. 3.20

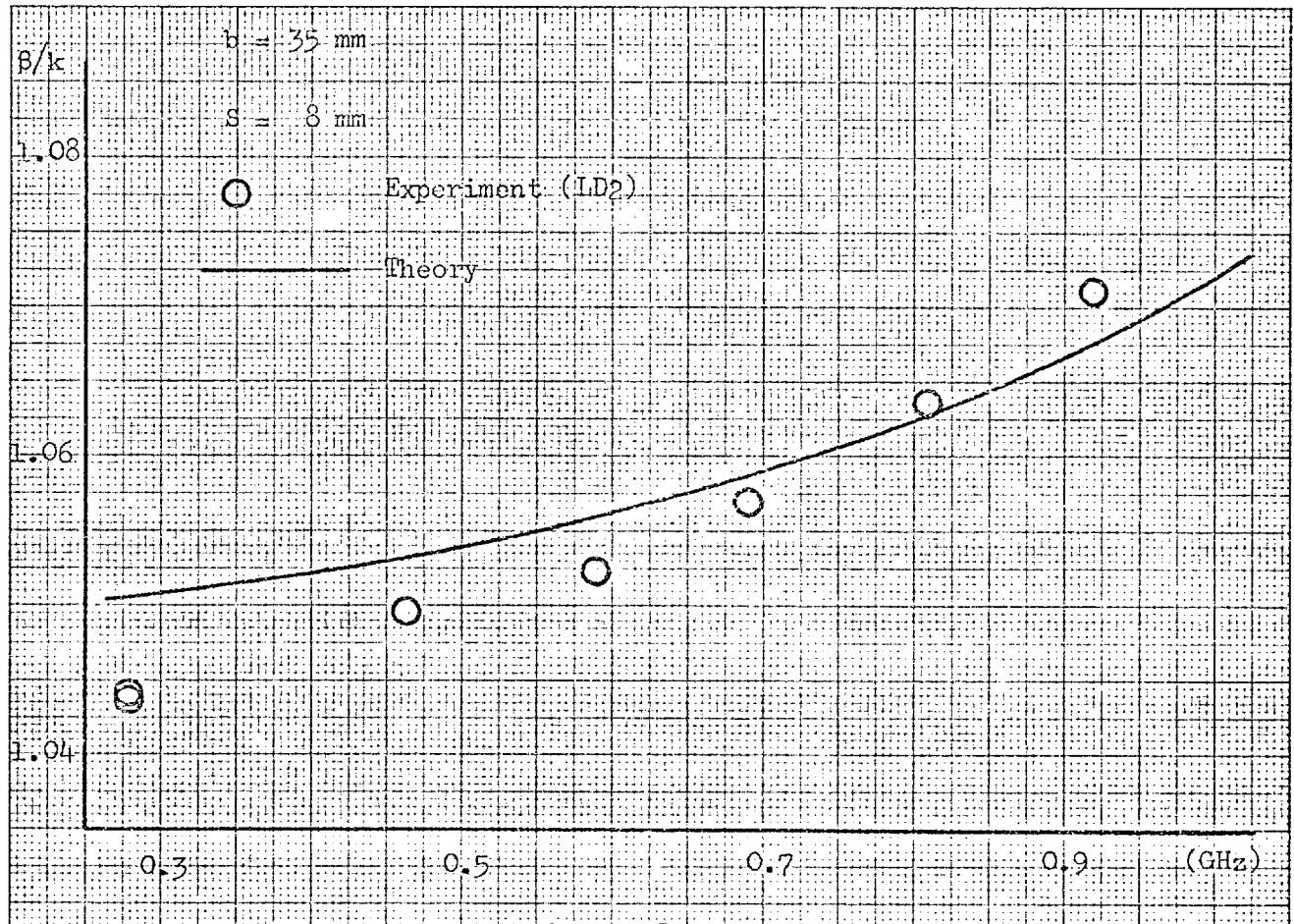

β/k
b = 35 mm
S = 8 mm
1.08
Experiment (LD2)
Theory
1.06
1.04
0.3
0.5
0.7
0.9
(GHz)

Fig. 3.21

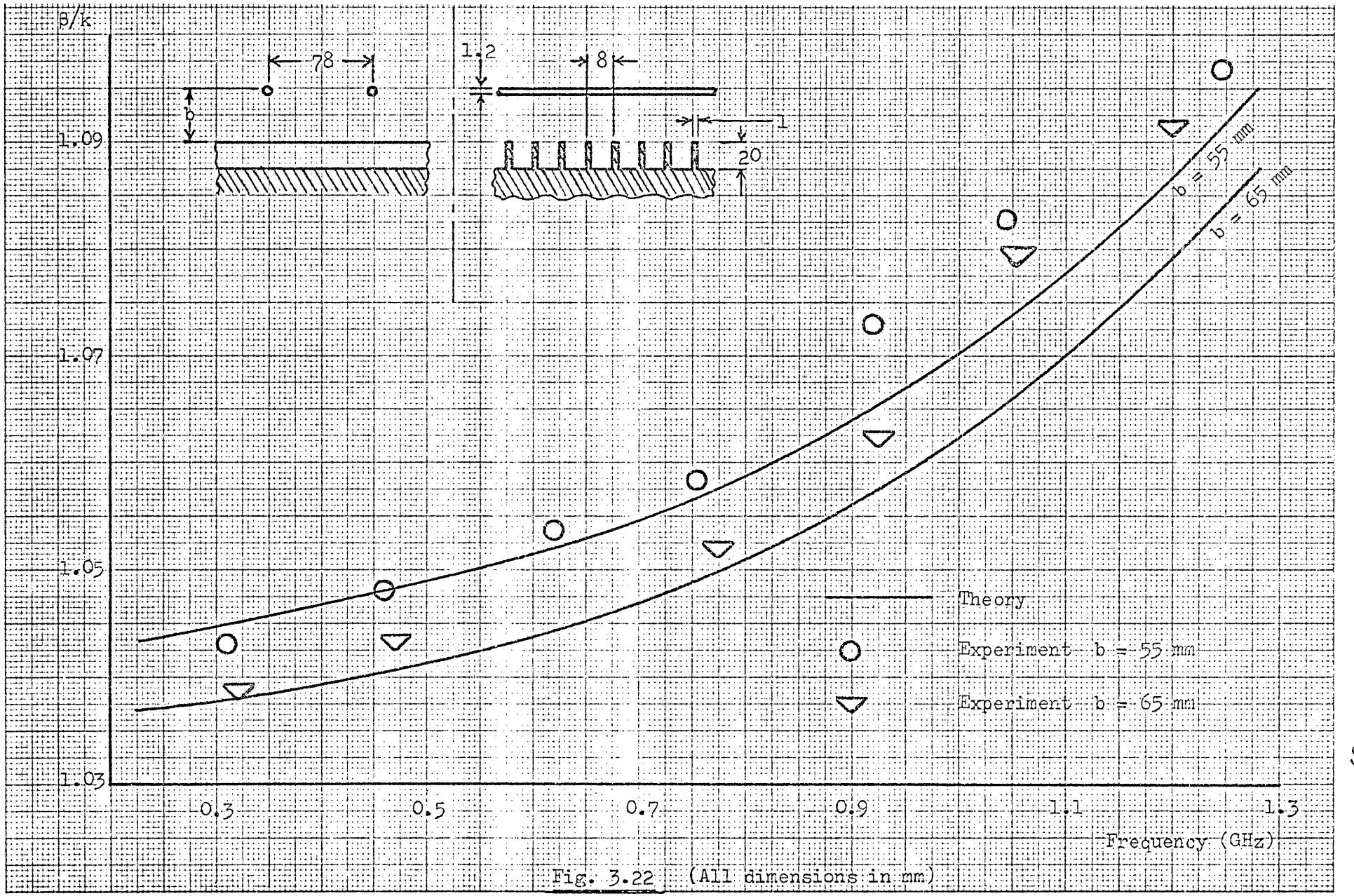


Fig. 3.22 (All dimensions in mm)

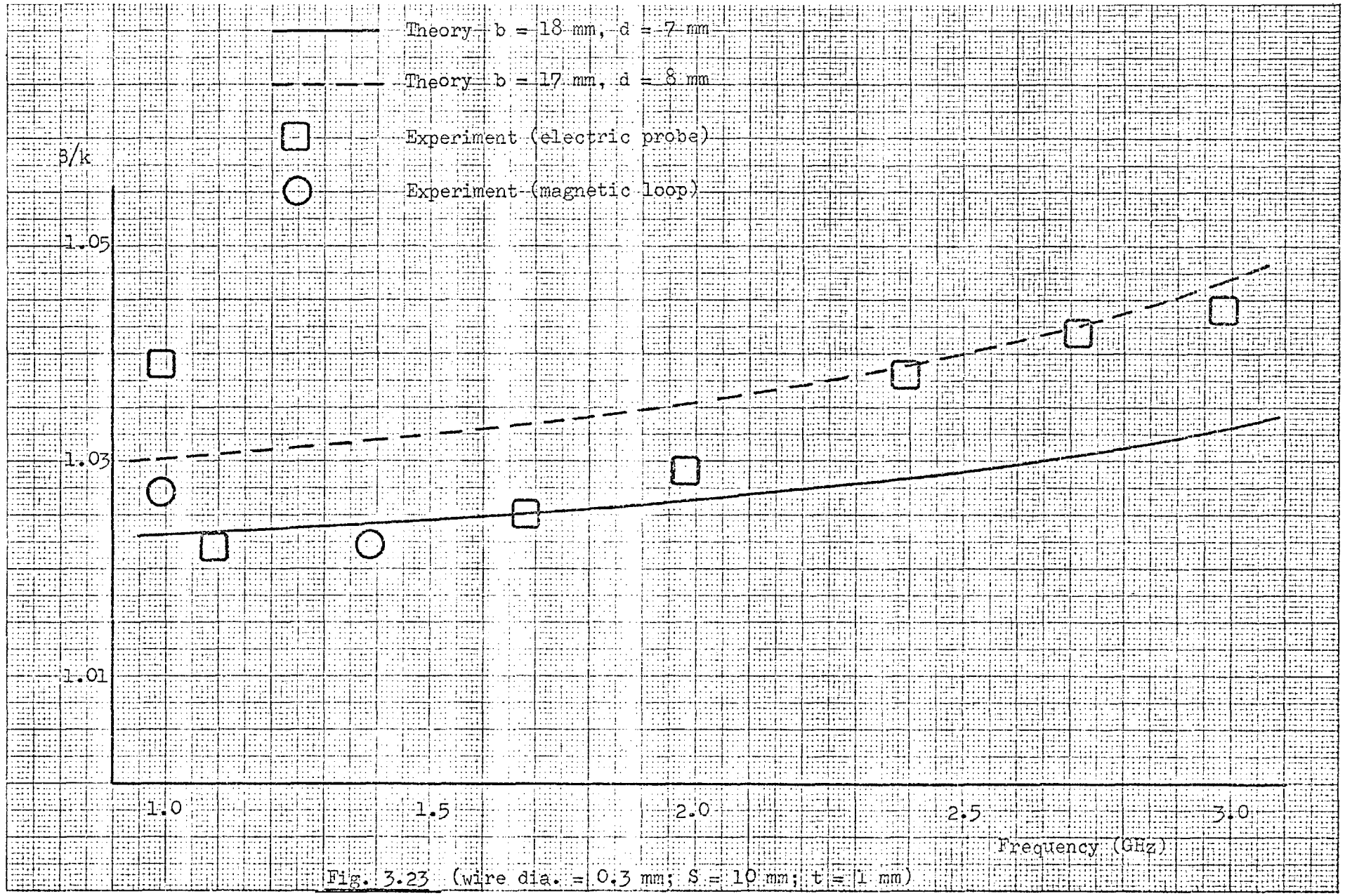


Fig. 3.23 (wire dia. = 0.3 mm; S = 10 mm; t = 1 mm)

APPENDIX 3A

DIFFRACTION BY AN INFINITELY LONG, PERFECTLY-CONDUCTING CYLINDER

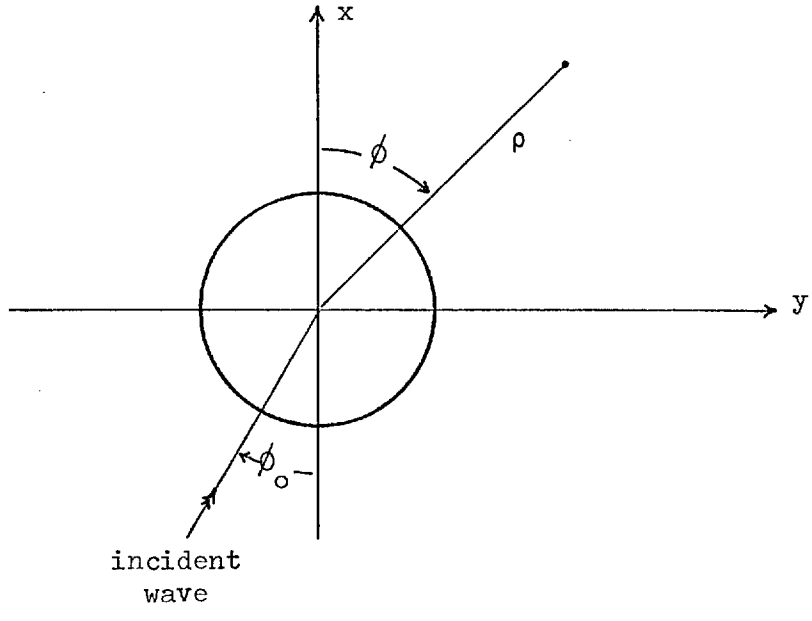


Fig. 3A.1

3A.1. Field Scattered by the Cylinder

The two-dimensional problem of scattering by a perfectly-conducting cylinder of infinite length, due to uniform plane wave incidence, has been solved. We shall base our results on the solution given by R.F. Harrington [Ref. 3.11], and we shall begin by giving a brief description of his solution. We shall assume an implicit time variation $e^{j\omega t}$.

Harrington considers a uniform plane wave, with (electric) polarization parallel to the axis of the cylinder, incident in the positive x-direction, i.e.,

$$E_z^i = E_o e^{-jkx} = E_o e^{-jk\rho \cos \phi} \qquad (3A.1)$$

The configuration considered and the coordinate system are shown in

Fig. 3A.1. The cylinder radius is a; the region $\rho > a$ is free-space, or a dielectric region, for which the wave number is k.

The total field E_z can be written as the sum of the incident field E_z^i and the scattered field E_z^s, i.e.,

$$E_z = E_z^i + E_z^s \tag{3A.2}$$

The incident field can be represented in terms of cylindrical waves:

$$E_z^i = E_o e^{-jk\rho \cos \phi} = E_o \sum_{n=-\infty}^{\infty} j^{-n} J_n(k\rho) e^{jn\phi} \tag{3A.3}$$

where J_n represents Bessel function of the first kind of order n.

The scattered field must represent outward travelling waves, and must have the form

$$E_z^s = \sum_{n=-\infty}^{\infty} j^{-n} a_n H_n^{(2)}(k\rho) e^{jn\phi} \tag{3A.4}$$

where $H_n^{(2)}$ represents Hankel function of second kind of order n.

Boundary condition $E_z = 0$ at $\rho = a$ leads to the result:

$$a_n = - \frac{J_n(ka)}{H_n^{(2)}(ka)} \tag{3A.5}$$

We are interested in the three dimensional scattering problem when the uniform plane wave of Eq. (3A.1) is replaced by an inhomogeneous plane wave with a z-variation $e^{-\gamma z}$, and variation in the x-y plane of the form $e^{-jh\rho\cos(\phi-\phi_o)}$, where $\phi = \phi_o$ defines the plane of propagation, and the value of the transverse wave-number h is determined from the separability relation,

$$h^2 = k^2 + \gamma^2 \qquad (3A.6)$$

The choice of branch cuts associated with the square root of Eq. (3A.6) is made according to the nature and location of plane boundary supporting the 'incident' plane wave. This question is disucssed in Appendix 3B. For convenience we shall omit the factor $e^{-\gamma z}$ in the following equations.

The required solution is easily obtained by replacing k by h and ϕ by $\phi' = \phi - \phi_o$, in Eqs. (3A.4) and (3A.5) : the resulting expression for the scattered field is

$$E_z^s = - E_o \sum_{n=-\infty}^{\infty} j^{-n} \frac{J_n(ha)}{H_n^{(2)}(ha)} H_n^{(2)}(h\rho) e^{jn\phi'} \qquad (3A.7)$$

where E_o is the amplitude of the 'incident' wave at the origin.

For a thin wire, $| ha | \ll 1$, and we can use the small argument approximations:

$$\begin{aligned} J_n(ha) &\simeq \frac{(ha/2)^n}{\Gamma(n+1)} \quad , \quad n \geqslant 0 \\ H_n^{(2)}(ha) &\simeq j \frac{(n)}{\pi(ha/2)^n} \quad , \quad n > 0 \\ H_o^{(2)}(ha) &\simeq - j \frac{2}{\pi} \ell n(ha) \end{aligned} \qquad (3A.8)$$

where Γ denotes the Gamma function. Noting that for $n > 0$

$$J_{-n} = (-1)^n J_n \qquad (3A.9)$$

$$H_{-n}^{(2)} = e^{-jn\pi} H_n^{(2)}$$

$$E_z^s \simeq E_o \frac{j\pi}{2\ell n(ha)} H_o^{(2)}(h\rho)$$

$$- E_o \sum_{n=1}^{\infty} j \frac{\pi(ha/2)^{2n}}{\Gamma(n+1)\Gamma(n)} H_n^{(2)}(h\rho)[j^{-n} e^{jn\phi'} - j^{n} e^{-jn\phi'}]$$

(3A.10)

For $|h\rho| < 2/3$ we obtain the following approximate expression for the scattered field:

$$E_z^s = - E_o \left\{ \frac{\ell n(h\rho) - 0.1059 - (h\rho)^2/4 + j \frac{\pi}{2}[1 - (h\rho)^2/4]}{\ell n(ha)} \right\}$$

$$E_z^s = - E_o \left\{ 1 - \frac{\ell n(\rho/a) - 0.1059 - (h\rho)^2/4 - j \frac{\pi}{2}[1 - (h\rho)^2/4]}{\ell n(\frac{1}{ha})} \right\}$$

(3A.11)

It can be seen that, for small values of $|ha|$, the total field is nearly zero in the proximity of the wire, i.e.,

$$E_z^s \doteq - E_o \qquad (3A.12)$$

For example, for $|ha| < 10^{-3}$ and $\rho/a < 5$ the error in the above approximation is about 20%. Furthermore, the smaller the value of h, the transverse wave number, the greater is the area around the wire where approximation Eq. (3A.12) is valid.

3A.2. Current Induced in the Wire

The surface current density (amperes per unit length of wire circumference) is given by

$$J_z = H_\phi \Big|_{\rho=a} = \frac{1}{j\omega\mu_1} \frac{\partial E_z}{\partial \rho} \Big|_{\rho=a} \tag{3A.13}$$

Replacing k by h in the expansion of Eq. (3A.3) and using Eq. (3A.7) leads to the following expression for the total field;

$$E_z = E_o \sum_{n=-\infty}^{\infty} j^{-n}[J_n(h\rho) + a_n H_n^{(2)}(h\rho)]e^{jn\phi'} \tag{3A.14}$$

where

$$a_n = -\frac{J_n(ha)}{H_n^{(2)}(ha)}$$

For an arbitrary solution to Bessel's equation, $B_n(v)$, the following relation holds:

$$B_n(v)' = -B_{n+1}(v) + \frac{n}{v} B_n(v) \tag{3A.15}$$

where the prime denotes differentiation with respect to the argument.

Using the above relation, from (3A.14) we obtain

$$\frac{\partial E_z}{\partial \rho} \Big|_{\rho=a} = E_o \sum_{n=-\infty}^{\infty} j^{-n} \frac{h}{H_n^{(2)}} [J_n H_{n+1}^{(2)} - J_{n+1} H_n^{(2)}]e^{jn\phi'}$$

(3A.16)

where J_n and $H_n^{(2)}$ denote $J_n(ha)$ and $H_n^{(2)}(ha)$ respectively.

$$J_n H_{n+1}^{(2)} - J_{n+1} H_n^{(2)} = j(J_n Y_{n+1} - J_{n+1} Y_n)$$

$$= j \frac{2}{\pi ha} \tag{3A.17}$$

where $Y_n [\equiv Y_n(ha)]$ denotes Bessel function of the second kind of order n.

In the derivation of the last relationship we have used Eq. (3A.14) and the Wronskian of Bessel's equation:

$$J_n(v)Y_n'(v) - Y_n(v)J_n'(v) = \frac{2}{\pi v} \tag{3A.18}$$

$$\left.\frac{\partial E_z}{\partial \rho}\right|_{\rho=a} = - j \frac{2E_o}{\pi a} \sum_{n=-\infty}^{\infty} j^{-n} \frac{e^{jn\phi'}}{H_n^{(2)}(ha)} \tag{3A.19}$$

Substituting from Eq. (3A.19) into Eq. (3A.13) we obtain

$$J_z = - \frac{2E_o}{\omega \mu_1 \pi a} \sum_{n=-\infty}^{\infty} j^{-n} \frac{e^{jn\phi'}}{H_n^{(2)}(ha)} \tag{3A.20}$$

For $|ha|$ very small, the n = 0 term is dominant, and the small-argument approximation of $H_n^{(2)}$ yields

$$J_z \simeq - \frac{2E_o}{\omega \mu_1 \pi a} \frac{1}{- j \frac{2}{\pi} \ell n(ha)} \tag{3A.21}$$

Hence the total induced current is given by

$$I_z = \int_0^{2\pi} J_z a d\phi = + j \frac{2\pi E_o}{kZ_1 \ell n(\frac{1}{ha})} \qquad (3A.22)$$

where we have used the relation $\omega\mu_1 = kZ_1$, Z_1 being the intrinsic impedance of the region outside the wire.

APPENDIX 3B

BRANCH CUTS ASSOCIATED WITH THE TRANSVERSE WAVE NUMBER h

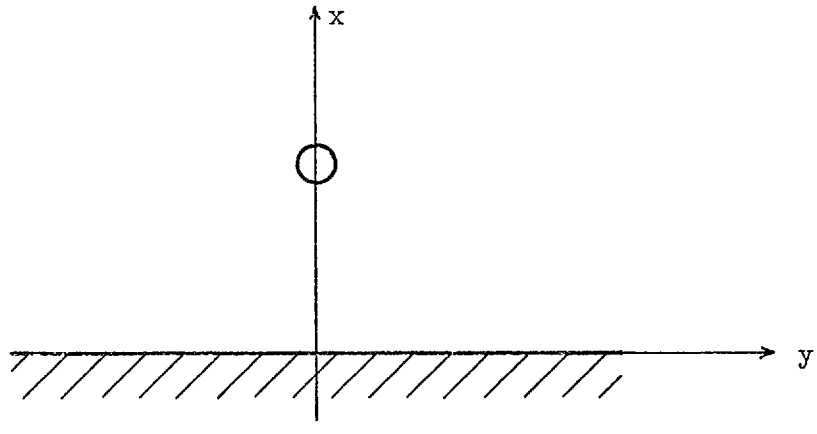


Fig. 3B.1

In Section 3.2.2., the distribution of E_z in the region $x > 0$ was approximated by

$$E_z = E_s(y)e^{-jhx} \tag{3B.1}$$

where E_s was given by Eqs. (3.5) and (3.3):

$$E_s = Z_s H_{oy} = Z_s I \frac{(1 + q_2/2)}{\pi} \frac{b}{b^2 + y^2} \tag{3B.2}$$

and h, the transverse wave number, was given by Eq.(3.8):

$$h = (k^2 + \gamma^2)^{\frac{1}{2}} \tag{3B.3}$$

Eq. (3B.1) does not take into account the effect of scattering by the wire. This effect was considered in Appendix 3A, where again the transverse wave number h was frequently used in the analysis.

In this section we shall devote our attention to Eq. (3B.3), and consider the behaviour of h as a function of $(k^2 + \gamma^2)$.

h is a multivalued function due to the presence of square-root function in Eq. (3B.3). Therefore branch cuts must be defined in the complex h^2-plane in order to make h single-valued. The choice of branch-cuts is determined by the behaviour of E_z, Eq. (3B.1), as $x \to +\infty$.

We define

$$\gamma = \alpha + j\beta \tag{3B.4}$$

where $\alpha > 0$, $\beta > 0$ for a single wave travelling in the positive z-direction. From Eq. (3B.3)

$$h^2 = k^2 + \alpha^2 - \beta^2 + 2j\alpha\beta \tag{3B.5}$$

For $\alpha = 0$, radiation and ohmic losses must both be zero along the structure, which requires that $\beta/k > 1$; then

$$h = \pm j(\beta^2 - k^2)^{\frac{1}{2}} \tag{3B.6}$$

In this case, the negative sign must be chosen so that E_z satisfies the radiation condition as $x \to \infty$ [Ref. 3.12]. Denoting phase angles of complex quantities h and h^2 by ψ_1 and ψ_2 respectively, the above choice of the square-root sign corresponds to the requirement

$$\psi_o - 2\pi < \psi_2 < \psi_o \tag{3B.7}$$

where ψ_o is a positive angle not greater than π. Solution (3B.6) is analogous to a two-dimensional surface wave (no variation with y) supported by a lossless surface.

When there is a small loss present, $\alpha > 0$ and $\mathrm{Im}(h^2) > 0$. However, the physical situation has hardly changed, and therefore h must have nearly the same value as given by Eq. (3B.6). This consideration precludes us from choosing $\psi_o = \pi$. Inspection of Eq. (3B.5) leads to the

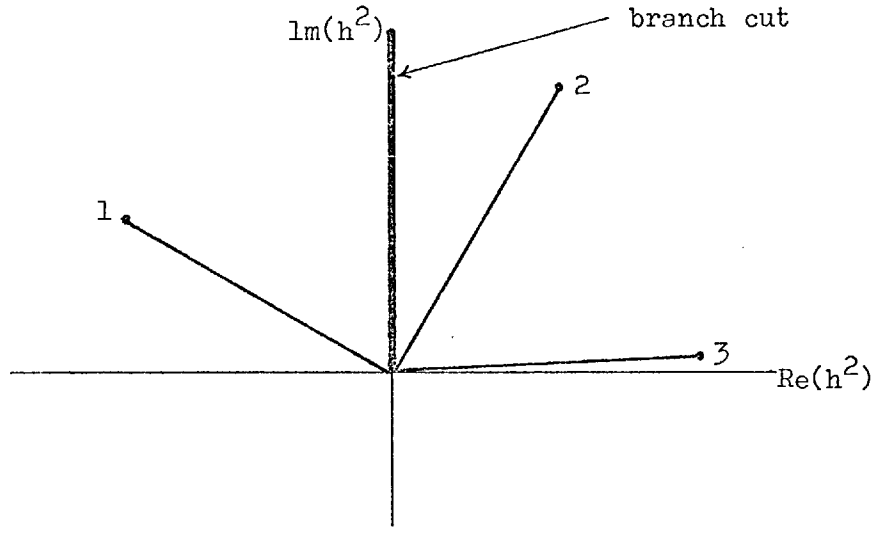


Fig. 3B.2 Complex h^2 Plane

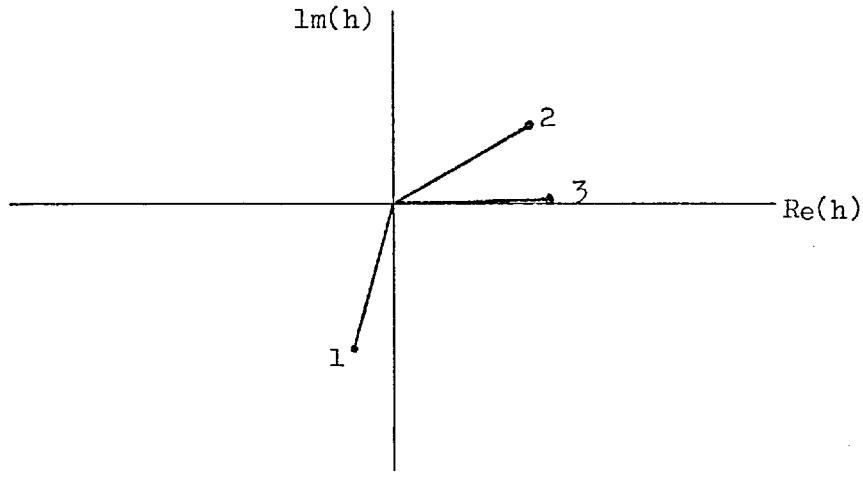


Fig. 3B.3 Complex h Plane

choice $\psi_o = \pi/2$, corresponding to a branch cut along the positive imaginary axis in the complex h^2-plane, as depicted in Fig. 3B.2. Consideration of a few examples will justify the above choice.

Points marked, 1, 2 and 3 in Fig. 3B.2 indicate three possible examples for values of h^2; corresponding values of h are indicated in Fig. 3B.3. From Eq. (3B.5) it can be seen that $\mathrm{Im}(h^2) > 0$. The case $\mathrm{Re}(h^2) < 0$, example 1, corresponds to a proper mode, satisfying the

radiation condition, analogous to a surface-wave mode.

In example 2, $\mathrm{Re}(h^2) > 0$, corresponding to an improper mode; this value of h represents an outgoing wave in the cross-section, with an amplitude which grows exponentially in the positive x direction. For an infinitely long structure, the radiation condition is not satisfied; however, the solution has a physical significance for finite structures, as in leaky-wave antennas [Ref. 3.13].

Example 3 in Figs. 3B.2 and 3B.3 corresponds to an evanescent wave along the structure, analogous to the situation in a linear array with broadside radiation.

In the boundary-value problem considered in chapter 3, values of h^2 obtained generally correspond to example 1 given above. Writing

$$h = h_r - jh_i \tag{3B.8}$$

from Fig. 3B.3 we find that, for example 1 above,

$$h_r \leqslant 0$$

$$h_i \geqslant 0$$

APPENDIX 3C

PROPAGATION ALONG PARALLEL WIRES EQUIDISTANT FROM A PLANE INTERFACE

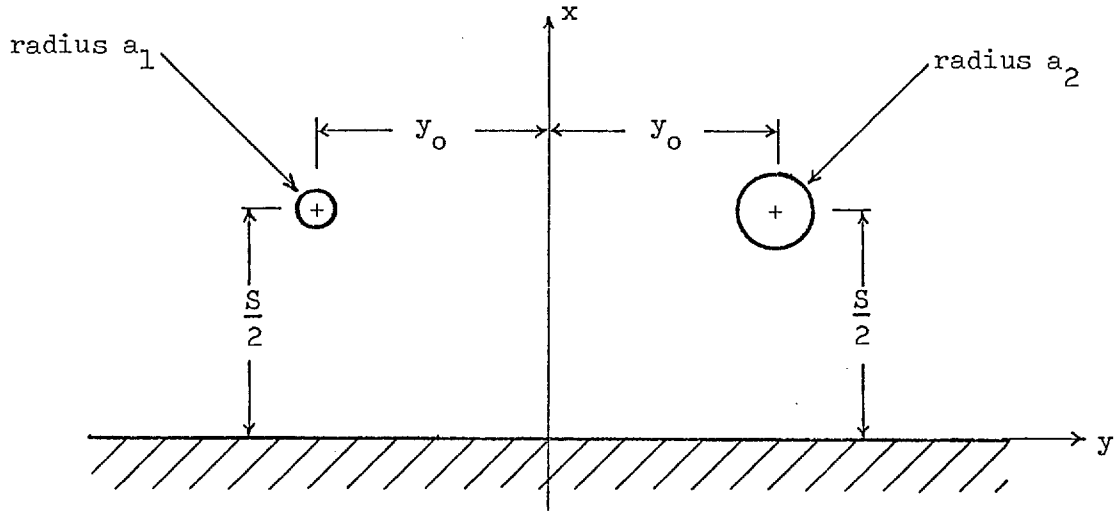


Fig. 3C.1 Cross-Section of the Double-Wire System

Inspection of equations derived for the iterative determination of propagation constant γ along a single wire parallel to an interface (Sections 3.2, 3.3 and 3.4) indicates that the quantities which are significantly affected by the addition of a second wire are: Z_c, the characteristic impedance of the line, Eqs. (3.33) and (3.35); and the integral $G = \int_{-\infty}^{\infty} |H_{oy}|^2 dy$ appearing in Eqs. (3.4) and (3.14). Furthermore, computation results have shown that a non-zero value of surface impedance generally has only a small effect on the characteristic impedance of the line. Therefore, it is a reasonable approximation to consider the interface as perfectly conducting in order to compute the change in Z_c due to parallel coupling between the wires. This approximation will be particularly justified if the change in Z_c due to parallel coupling proves to be greater than the change due to $Z_s \neq 0$. The change in G, due to parallel coupling, will be evaluated, as before, by employing image-theory approximations.

3C.1. Characteristic Impedance of the Coupled Line

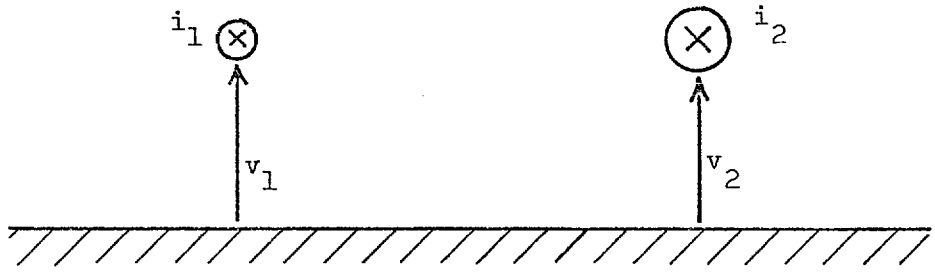


Fig. 3C.2 Definition of Currents and Voltages

The analysis given here corresponds to that given by R.E. Matick [Ref. 3.14]. Referring to Fig. 3C.2, the differential equations for coupled lines 1 and 2 are

$$\frac{dv_1}{dz} = - Z_{11}i_1 - Z_{12}i_2 \qquad (3C.1)$$

$$\frac{di_1}{dz} = - Y_{11}v_1 - Y_{12}v_2 \qquad (3C.2)$$

$$\frac{dv_2}{dz} = - Z_{22}i_2 - Z_{21}i_1 \qquad (3C.3)$$

$$\frac{di_2}{dz} = - Y_{22}v_2 - Y_{21}v_1 \qquad (3C.4)$$

Differentiation of the above equations and substitution lead to the following equations:

$$\frac{d^2v_1}{dz^2} = J_1v_1 + K_1v_2 \qquad (3C.5)$$

$$\frac{d^2v_2}{dz^2} = J_2v_2 + K_2v_1 \qquad (3C.6)$$

$$\frac{d^2 i_1}{dz^2} = J_2 i_1 + K_3 i_2 \qquad (3C.7)$$

$$\frac{d^2 i_2}{dz^2} = J_4 i_2 + K_4 i_1 \qquad (3C.8)$$

where

$$J_1 = Z_{11}Y_{11} - Z_{21}Y_{21} \qquad (3C.9)$$

$$J_2 = Z_{22}Y_{22} - Z_{21}Y_{12} \qquad (3C.10)$$

$$J_3 = Z_{11}Y_{11} - Z_{21}Y_{12} \qquad (3C.11)$$

$$J_4 = Z_{22}Y_{22} - Z_{12}Y_{21} \qquad (3C.12)$$

$$K_1 = Z_{12}Y_{22} - Z_{11}Y_{12} \qquad (3C.13)$$

$$K_2 = Z_{21}Y_{11} - Z_{22}Y_{21} \qquad (3C.14)$$

$$K_3 = Z_{12}Y_{11} - Z_{22}Y_{12} \qquad (3C.15)$$

$$K_4 = Z_{21}Y_{22} - Z_{11}Y_{21} \qquad (3C.16)$$

If the lines are located in a linear isotropic medium, or if the lines are symmetrical,

$$Z_{12} = Z_{21} \quad , \quad Y_{12} = Y_{21} \qquad (3C.17)$$

Therefore

$$J_3 = J_1 \quad , \quad J_4 = J_2 \qquad (3C.18)$$

$$K_3 = K_2 \quad , \quad K_4 = K_1 \qquad (3C.19)$$

Furthermore, it can be shown that for symmetrical lines

$$J_1 = J_2 = J \qquad (3C.22)$$

$$K_1 = K_2 = 0 \tag{3C.23}$$

Assuming relations (3C.20) and (3C.21), Eqs. (3C.5) and (3C.6) reduce to

$$\frac{d^2v_1}{dz^2} = Jv_1 + Kv_2 \tag{3C.24}$$

$$\frac{d^2v_2}{dz^2} = Jv_2 + Kv_1 \tag{3C.25}$$

For a general solution, it can be assumed that

$$v_1(z,t) = (V_1e^{-\gamma_1 z} + V_1'e^{\gamma_1 z})e^{j\omega t} \tag{3C.26}$$

$$v_2(z,t) = (V_2e^{-\gamma_2 z} + V_2'e^{\gamma_2 z})e^{j\omega t} \tag{3C.27}$$

When lines 1 and 2 are in the same medium

$$\gamma_1 = \gamma_2 = \gamma \tag{3C.28}$$

With the above assumptions, Eqs. (3C.24) and (3C.25) become

$$\gamma^2v_1 = Jv_1 + Kv_2 \tag{3C.29}$$

$$\gamma^2v_2 = Kv_1 + Jv_2 \tag{3C.30}$$

Adding the above equations, we obtain

$$\gamma^2(v_1 + v_2) = (J + K)(v_1 + v_2) \tag{3C.31}$$

This represents the "sum" mode of propagation, with propagation constant

$$\gamma_s^2 = J + K \tag{3C.32}$$

Substracting Eq. (3C.30) from Eq. (3C.29) yields

$$\gamma^2(v_1 - v_2) = (J - K)(v_1 - v_2) \tag{3C.33}$$

which corresponds to the "difference" mode of propagation with propagation constant

$$\gamma_d^2 = J - K \tag{3C.34}$$

Thus we obtain the general solutions

$$v_s = v_1 + v_2 = (V_s e^{-\gamma_s z} + V'_s e^{\gamma_s z}) e^{j\omega t} \tag{3C.35}$$

$$v_d = v_1 - v_2 = (V_d e^{-\gamma_d z} + V'_d e^{\gamma_d z}) e^{j\omega t} \tag{3C.36}$$

Similarly the currents are found to be

$$i_s = i_1 + i_2 = \frac{1}{Z_s}(V_s e^{-\gamma_s z} - V'_s e^{\gamma_s z}) e^{j\omega t} \tag{3C.37}$$

$$i_d = i_1 - i_2 = \frac{1}{Z_d}(V_d e^{-\gamma_d z} - V'_d e^{\gamma_d z}) e^{j\omega t} \tag{3C.40}$$

where Z_s and Z_d are characteristic impedances which, for symmetrical lines, are given by

$$Z_s = \frac{v_1 + v_2}{i_1 + i_2} = \frac{Z_{11} + Z_{12}}{\gamma_s} \tag{3C.41}$$

$$Z_d = \frac{v_1 - v_2}{i_1 - i_2} = \frac{Z_{11} - Z_{12}}{\gamma_d} \tag{3C.42}$$

For perfectly-conducting lines in a linear isotropic medium $K = 0$ and therefore

$$\gamma_s^2 = \gamma_d^2 = J = \gamma^2 \tag{3C.43}$$

Substituting for J from Eq. (3C.9).

$$\gamma^2 = Z_{11}Y_{11} - Z_{12}Y_{12} \tag{3C.44}$$

Defining coupling coefficients

$$k_i = \frac{Z_{12}}{\sqrt{Z_{11}Z_{22}}} \tag{3C.45}$$

$$k_c = \frac{Y_{12}}{\sqrt{Y_{11}Y_{22}}} \tag{3C.46}$$

It can be shown that for TEM modes

$$k_i = k_c = k \tag{3C.47}$$

Whence Eq. (3C.44) can be written

$$\gamma^2 = Z_{11}Y_{11}(1 - k^2)$$

Substitution in Eqs. (3C.41) and (3C.42) yields

$$Z_s = \left[\frac{Z_{11}}{Y_{11}} \frac{(1 + k)}{(1 - k)} \right]^{\frac{1}{2}} \tag{3C.48}$$

$$Z_d = \left[\frac{Z_{11}}{Y_{11}} \frac{(1 - k)}{(1 + k)} \right]^{\frac{1}{2}} \tag{3C.49}$$

k is calculated by considering the self and mutual inductances of the lines. With reference to Fig. 3C.1, the result is

$$k = \frac{\ell n[1 + (\frac{S}{2y_o})^2]^{\frac{1}{2}}}{[\ell n(\frac{S}{a_1})\ell n(\frac{S}{a_2})]^{\frac{1}{2}}} \qquad (3C.50)$$

where it has been assumed that the radii a_1 and a_2 are small compared to distances S and $2y_o$. If Z_c is the characteristic impedance of line 1 in the absence of line 2, we can use the approximation,

$$Z_c = \sqrt{\frac{Z_{11}}{Y_{11}}} \qquad (3C.51)$$

to rewrite Eqs. (3C.48) and (3C.49):

$$Z_s = Z_c \left[\frac{1 + k}{1 - k} \right]^{\frac{1}{2}} \qquad (3C.52)$$

$$Z_d = Z_c \left[\frac{1 - k}{1 + k} \right]^{\frac{1}{2}} \qquad (3C.53)$$

For equal radii $a_1 = a_2 = a$

$$Z_s = Z_c \left\{ \frac{\ell n(S/a) + \ell n[1 + (S/2y_o)^2]^{\frac{1}{2}}}{\ell n(S/a) - \ell n[1 + (S/2y_o)^2]^{\frac{1}{2}}} \right\}^{\frac{1}{2}} \qquad (3C.54)$$

$$Z_d = Z_c \left\{ \frac{\ell n(S/a) - \ell n[1 + (S/2y_o)^2]^{\frac{1}{2}}}{\ell n(S/a) + \ell n[1 + (S/2y_o)^2]^{\frac{1}{2}}} \right\} \qquad (3C.55)$$

It should be noted that if the lines are excited with symmetrical (even) voltages relative to ground, the actual characteristic impedance <u>measured</u> between the wires and ground, Z_{sm}, is given by

$$Z_{sm} = \frac{v_1}{i_1 + i_2} = \frac{Z_s}{2} \qquad (3C.56)$$

Similarly if the lines are excited with antisymmetric (odd) voltages relative to ground, i.e. in the "balanced mode", the actual characteristic impedance measured between the two wires, Z_{dm}, is given by

$$Z_{dm} = \frac{v_1 - v_2}{\frac{1}{2}(i_1 - i_2)} = 2Z_d \qquad (3C.57)$$

3C.2. Evaluation of $G = \int_{-\infty}^{\infty} |H_{oy}|^2 dy$ for the Coupled Line

Assuming that H_{oy}, in the tangential component of transverse magnetic field at ground, can be derived approximately from image theory, we consider values for the image currents, as depicted in Fig. 3C.3, given by

$$I_1' = I_1(1 + q_{21}) \qquad (3C.58)$$

$$I_2' = I_2(1 + q_{22}) \qquad (3C.59)$$

Application of the principle of superposition yields the following result for the y-component of magnetic field at point P on the ground

$$H_{oy} = \frac{b}{\pi}\left\{\frac{I_1(1 + q_{12}/2)}{b^2 + (y + y_o)^2} + \frac{I_2(1 + q_{22}/2)}{b^2 + (y - y_o)^2}\right\} \qquad (3C.60)$$

The integral G can be written as

$$G = \int_{-\infty}^{\infty} |H_{oy}|^2 dy$$

$$= G_1 + G_2 + G_3 \qquad (3C.61)$$

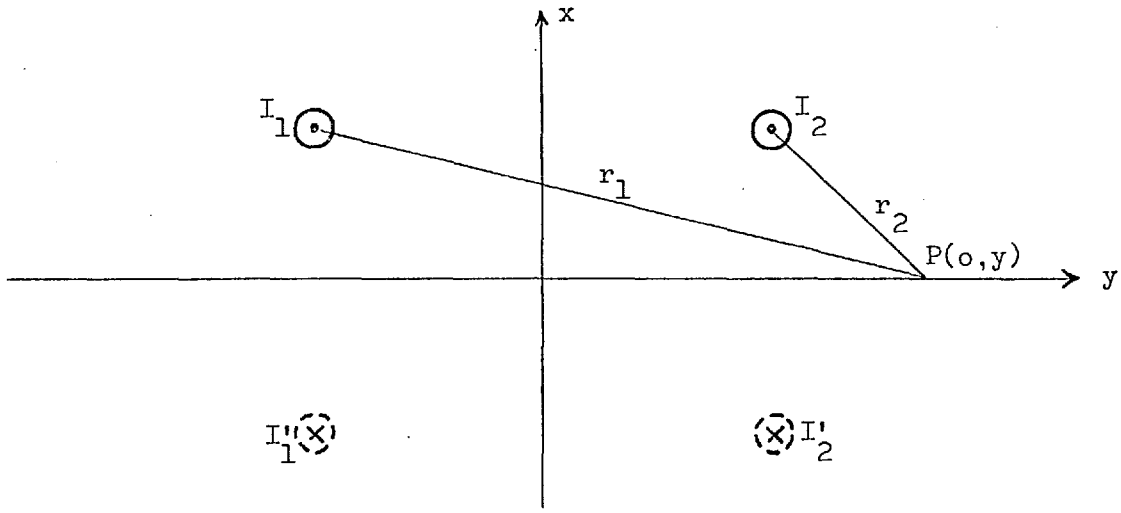


Fig. 3C.3 Definition of Line Currents and Their Images

where

$$G_1 = A_1 \int_{-\infty}^{\infty} \frac{b^2}{[b^2 + (y + y_o)^2]^2}\, dy \qquad (3C.62)$$

$$A_1 = \frac{I_1^2}{\pi^2}(1 + \tfrac{1}{2}q_{12})(1 + \tfrac{1}{2}q_{12}^*) \qquad (3C.63)$$

$$G_2 = A_2 \int_{-\infty}^{\infty} \frac{b^2}{[b^2 + (y - y_o)^2]^2}\, dy \qquad (3C.64)$$

$$A_2 = \frac{I_2^2}{\pi^2}(1 + \tfrac{1}{2}q_{22})(1 + \tfrac{1}{2}q_{22}^*) \qquad (3C.65)$$

$$G_3 = A_3 \int_{-\infty}^{\infty} \frac{b^2}{[b^2 + (y + y_o)^2][b^2 + (y - y_o)^2]}\, dy \qquad (3C.66)$$

$$A_3 = \frac{I_1 I_2}{\pi^2}[(1 + \tfrac{1}{2}q_{12})(1 + \tfrac{1}{2}q_{22}^*) + (1 + \tfrac{1}{2}q_{12}^*)(1 + \tfrac{1}{2}q_{22})] \qquad (3C.67)$$

Evaluation of G_1 and G_2 is straightforward, and we obtain

$$G_1 = \frac{I_1^2}{2\pi b}(1 + \tfrac{1}{2}q_{12})(1 + \tfrac{1}{2}q_{12}^*) \qquad (3C.68)$$

$$G_2 = \frac{I_2^2}{2\pi b}(1 + \tfrac{1}{2}q_{22})(1 + \tfrac{1}{2}q_{22}^*) \qquad (3C.69)$$

G_3 is also a standard integral and can be written as

$$G_3 = \lim_{y \to \infty} G_3^1$$

where

$$G_3^1 = A_3 b^2 \int_{-y}^{+y} \frac{dy}{p_o y^4 + p_1 y^2 + p_2} \qquad (3C.70)$$

$$p_o = 1$$

$$p_1 = 2(b^2 - y_o^2)$$

$$p_2 = (b^2 + y_o^2)$$

G_3^1 has been evaluated elsewhere [Ref. 3.15], and is given by

$$G_3^1 = \frac{A_3 b^2}{4 p_o m^3} \left\{ \frac{1}{2\cos\frac{\alpha}{2}} \ell n \left[\frac{y^2 + 2my\cos\frac{\alpha}{2} + m^2}{y^2 - 2my\cos\frac{\alpha}{2} + m^2} \right] + \frac{1}{\sin\frac{\alpha}{2}} \tan^{-1}\left[\frac{2my\sin\frac{\alpha}{2}}{m^2 - y^2} \right] \right\}_{-y}^{+y} \qquad (3C.71)$$

where

$$\cos\alpha = \frac{y_o^2 - b^2}{y_o^2 + b^2}, \qquad 0 < \alpha < \pi$$

$$m = (y_o^2 + b^2)^{\frac{1}{2}}$$

whence

$$G_3 = \frac{\pi A_3}{2b} \frac{b^2}{b^2 + y_o^2} \qquad (3C.72)$$

For symmetrical lines with symmetrical excitation,

$$I_1 = I_2 = \frac{I}{2} \quad ; \qquad q_{12} = q_{22} = q_2 \ ,$$

which lead to the simple result

$$G = \frac{I^2}{2\pi b} (1 + \tfrac{1}{2}q_2)(1 + \tfrac{1}{2}q_2^*)[\tfrac{1}{4} + \tfrac{1}{4} + \tfrac{1}{2} \frac{b^2}{b^2 + y_o^2}] \qquad (3C.73)$$

REFERENCES

3.1 Collin, R.E.; 'Field Theory of Guided Waves', McGraw-Hill,1960, pp 67-70.

3.2 Stratton, J.A.; 'Electromagnetic Theory', McGraw-Hill 1941, pp 527-537.

3.3 Stratton, J.A.; op. cit., p. 349.

3.4 Stratton, J.A.; op. cit., p. 137.

3.5 Stuart, J.L.; 'Circuit Analysis of Transmission Lines', John Wiley & Sons, 1958, p. 178.

3.6 Collin, R.E.; op. cit., p. 466.

3.7 Marcuvitz, N. (editor); 'Waveguide Handbook', McGraw-Hill 1951, pp 289-290.

3.8 Hurd, R.A.; 'The Propagation of an Electromagnetic Wave Along An Infinite Corrugated Surface', Canadian Journal of Physics, Vol. 32, No. 12, pp 727-734, December 1954.

3.9 Collin, R.E.; op. cit., pp 465-468.

3.10 Walter, C.H.; op. cit., p. 259.

3.11 Harrington, R.F.; 'Time-Harmonic Electromagnetic Fields', McGraw-Hill 1961, pp 232-234.

3.12 Stratton, J.A.; op. cit., pp 485-6.

3.13 Tamir, T.; 'Leaky Wave Antennas', Published as chapter 20 of "Antenna Theory", Part II, edited by Collin, R.E. and Zucker, F.J., McGraw-Hill, 1969.

3.14 Matick, R.E.; 'Transmission Lines for Digital and Communication Networks', McGraw-Hill 1969, Chapter 7.

3.15 Ryshik, I.M. and Gradstein, I.S.; 'Tables of Series Products and Integrals', Academic Press 1965, p. 64.

CHAPTER IV

ANALYSIS OF RADIATION CHARACTERISTICS

4.1. Introduction

It was pointed out in Section 1.3 that, although certain aspects of the Beverage antenna have remained as subjects of debate till the present, there has been general agreement concerning the far field characteristics of this antenna. For this reason, a detailed treatment of the Beverage antenna in this chapter would be superfluous; instead, in the next section, we shall briefly mention some of the more significant papers on the subject, in an historical context. Section 4.3 will be devoted to the controversial problem of the mode of action of the Beverage antenna. The remainder of this chapter will be concerned solely with the performance of the Inductive Plane Antenna (IPA).

As mentioned in Section 1.1, the present study is concerned, in particular, with two arrangements of the Inductive Plane Antenna : IPA_1 and IPA2 shown in Figs. 1.2 and 1.3 (Chapter I) respectively. In Section 4.4, we shall demonstrate that the responses of these two configurations are directly related to each other. This result has been used in the evaluation of far-field characteristics of the antennas considered, both theoretically and experimentally.

To evaluate by analysis the radiation characteristics of the IPA, it is more convenient to consider the antenna as receiving than transmitting. In the absence of nonlinear and active elements in an antenna, its radiation characteristics are the same for both transmission and reception, in linear isotropic media; this is a corollary of the reciprocity theorem [Ref. 4.1]. Thus treatment of the receiving problem is merely a choice of convenience : for the IPA, it

is easier to determine the open-circuit voltage at the antenna terminals, on reception, than to determine the far-field from an equivalent current or field distribution on transmission. This is partly associated with the fact that the IPA geometry can not be defined by a simple equation in any one coordinate-system (rectangular, cylindrical or spherical), and partly because the end-discontinuities in the antenna have significant effects on the radiation characteristics.

In contrast to the above situation, a few well-known examples might serve as illustration : the radiation-field of the dipole antenna is usually determined by considering the transmitting problem. In this case the far-field is easily obtained in terms of an equivalent line-current distribution coincident with one of the axes in rectangular coordinates. Furthermore, the effect of the end-discontinuity is taken into account, with sufficient accuracy, by requiring the current to be continuous at all points [Ref. 4.2].

To cite another pertinent example, the dielectric-rod antenna has been analysed in cylindrical coordinates. This is natural, as the antenna surface is specified by a single generator parallel to the z-axis. The end discontinuity, in this case, defines the location of antenna aperture from which radiation occurs [Ref. 4.3]. There is also some radiation from the launching device, used to energize the antenna, although most of the power is transferred to the surface wave which illuminates the aperture. The role played by the end discontinuity is two-fold. Firstly, its location determines how the feed-point radiation interacts with radiation from the aperture; secondly the nature of the discontinuity determines the mechanism of the radiation from the surface wave, and therefore the shape of the radiation pattern. For example, if the dielectric rod is terminated

by a taper, radiation will occur continuously along the taper; but if the rod has a uniform cross-section along all its length, radiation occurs only from the end discontinuity. However, an important consideration is that, irrespective of the nature of the discontinuity, very little power is reflected towards the antenna input [Ref. 4.4]. This knowledge further simplifies design problems associated with the dielectric-rod antenna.

In the case of IPA_1 , the antenna geometry is more complicated than in either example mentioned above. This leads to two problems : firstly, we have no a priori knowledge of the effect of end discontinuities in the antenna. Consequently, in the transmission problem, there would be the additional complication of evaluating the change in the antenna currents due to the end discontinuities . Secondly, evaluation of the far-field in terms of an equivalent current distribution would be cumbersome - again in contrast to the examples cites above. Hence it was decided to evaluate the radiation characteristics of IPA_1 and IPA_2 by considering the receiving problem.

The problem can be resolved into two parts : firstly, the component of electric field along the wire must be determined due to uniform plane wave incidence : this is the field that would exist in the absence of the wire, and is predominantly due to the non-zero value of surface impedance. This is a mixed boundary-value problem which can be approached in a number of ways. One formulation of a similar problem has been in terms of angular spectrum of plane waves, and involves Wiener-Hopf techniques with successive approximations [Ref. 4.5]. However, we have chosen an alternative approach, which is simpler, though less direct, in the particular case considered. This formulation is given in sub-section 4.5.2.: a perturbation relation is derived for the electric field along the wire, based on Monteath's application of

the reciprocity theorem [Ref. 4.6]. The expression for the electric field distribution involves a surface integral of fields : numerical techniques were employed to evaluate the field distribution in a number of particular examples. Graphical results are presented in Sub-section 4.5.3., which clearly demonstrates the influence of discontinuities, in the surface impedance, on the near-field distribution.

The second part of the radiation problem consists of calculating the open-circuit voltage V_{OC} at the antenna terminals, due to an incoming plane wave; starting from the reciprocity theorem, the required expressions are derived in Section 4.6. The question of gain and directivity of both antennas (IPA_1 and IPA_2) are considered in Sections 4.7 and 4.8 respectively. Presentation of theoretical results is postponed to Chapter V, in order to facilitate comparison between theory and experiment.

4.2. Radiation Characteristics of the Beverage Antenna : An Historical Survey

The Beverage antenna was originally developed in the early nineteen-twenties, for the reception of European transmitting stations on the Atlantic coast of America [Ref. 4.7]. The antenna was designed to operate in the band 40 - 130 KHz, and consisted of a pair of wires, connected in parallel, suspended at a height of 7m. (approx.) above ground, and extending a distance of 13 Km (approx.). Its success was primarily due to two factors : first, the directive pattern of the Beverage antenna marked a distinct advance on the reduction of interference and atmospheric noise; second, its wide-band characteristics made possible simultaneous operation of a single

antenna on a large number of channels. An additional attraction of the Beverage antenna was its relatively low cost due to its simple construction.

In 1931, a report was published on the development of directive antennas for transmission in the HF band [Ref. 4.8]; the Beverage antenna was considered for transmission, but experiments were discontinued in favour of other directive types of antenna. The reason for the failure of the Beverage antenna was its low gain, in spite of having satisfactory values of directivity.

In 1951, the Beverage antenna was again considered as a transmitting antenna, this time by Professor Jenssen [Ref. 4.9]; the application envisaged was for broadcasting at low and medium frequencies in countries, like Norway, which are populated in narrow strips through valleys. As a figure of merit, Professor Jenssen uses the 'equivalent height' of the Beverage antenna, h_{eq} : this is defined as the effective height h_{eff} of a monopole which produces the same field, at ground level, as the Beverage antenna when both antennas have identical input currents. Graphical results presented indicate values for h_{eq} of the order of 200 m. at frequencies above 1 MHz; h_{eq} has values exceeding 400 m. at frequencies below 100 KHz, and its value increases with decreasing ground conductivity.

Professor Jenssen has also noted that a better figure of merit would be obtained by comparing input power requirements of the two antennas to produce the same field; i.e. actual antenna gains should be compared. For example, Carter has reported that the measured gain of a Beverage antenna, three wavelengths long, was one quarter the gain of a "plain antenna" (presumably a short monopole) at 182 KHz [Ref. 4.8]. Other factors which would influence the choice of the

Beverage antenna for broadcasting are : relative construction costs; cost of transmitter equipment; and the number of broadcast channels required.

Professor Jenssen has also mentioned two other applications of the Beverage antenna, both of which make use of the near field of the antenna. In a project to construct a power-line, the carrier system (wire-to-ground excitation) was employed for transmitting messages to working parties along the line; reception was by means of hand-held receivers [Ref. 4.10]. In another experiment in Sweden, broadcast programmes were transmitted along power-lines to compensate for the high noise level in the vicinity of high-voltage lines.

The only questionable conclusion in Professor Jenssen's paper is his statement that the conditions justifying the use of the Beverage antenna for transmission "are the same conditions under which it has proved useful for reception". This conclusion would be valid only if external noise were negligible compared with receiver noise (see Section 1.3, or [Ref. 4.14] for a more detailed discussion)

In 1960, S.P. Belousov and V.G. Yampolskii provided an excellent reference for the application of the Beverage antenna for reception in the broadcast band 150 - 1500 KHz [Ref. 4.11]. Extensive graphical data are presented in this reference. One important conclusion in this paper is that antenna lengths exceeding 3 Km are not advantageous, due to serious deterioration of the horizontal directivity near the top of the band.

Design considerations at VLF for the receiving characteristics of the Beverage antenna can be found in a paper published in 1963 [Ref. 4.13]. The starting premise is that the most important criterion is the directivity of the antenna, and that the front-to-back power ratio

R_b is a measure of this directivity. As the antenna length is increased R_b goes through a series of maxima and minima; for a lossless antenna, optimum lengths corresponding to maxima of R_b are given by

$$L = \frac{M r_v}{r_v + 1} \lambda_o \quad ; \qquad M = 1, 2, 3, \ldots\ldots$$

where $r_v = v/c$, the velocity ratio, and λ_o is the free space wavelength. The above equation is also a good approximation for a lossy line. The remainder of this paper is concerned with antennas having the first (i.e. shortest) optimum length - which is of the order of $\lambda_o/3$. Expressions and graphs are given for R_b, positions and levels of lobe nulls and peaks, and the 3 dB beam width.

The principal conclusions are : (1) the antenna is <u>not</u> broadband and the first optimum length varies approximately with inverse of the frequency; (2) the lobe pattern is sensitive to changes in the soil moisture content; (3) at the first optimum length, the beam-width is practically independent of the attenuation, and only a slowly--varying function of the velocity ratio; (4) with increasing moisture content in the soil, the attenuation increases and the velocity ratio decreases.

Among the above conclusions only item (3) seems correct. Item (4) contradicts all other published results, as explained in Section 2.2. As regards item (2), the change in the lobe structure is relatively unimportant as far as the signal-to-noise ratio is concerned - unless there is a strong interference from a particular direction. Item (1) is also misleading : because it seems possible to design a Beverage antenna such that it has a front-to-back ratio exceeding a specified

value (say 12 dB), and a specified bandwidth (say 1.5 to 1) at VLF.

A comprehensive evaluation of the Beverage antenna for reception in the HF band was presented by A.F. dos Santos in 1970 [Ref. 4.14]. In this thesis, it was proposed to employ the Beverage antenna as the element of a circular array designed for multi-beam reception : this proposal was an alternative to another (existing) system based on the Luneberg lens. Both systems have similar characteristics, but the Beverage circular-array has the advantage that its realization is easily practicable and much more economical.

An important parameter of the Beverage antenna is its efficiency η (= ratio of gain to directivity). Dos Santos appears to be the first person to have presented quantitative results for this parameter. For an antenna 300 m. long, η ranges from 2% at 3MHz to 25% at 30 MHz (the corresponding range for directivity is from 14 dB to 21 dB). These results were computed for : wire height b = 3m.; wire radius a = 2.5×10^{-3}m.; ground conductivity $\sigma = 10^{-2}$ S/m.; and relative permittivity of ground $\epsilon_r = 15$.

In 1972, Kikuchi reported an unusual application of the Beverage structure [Ref. 4.15]: in Japan it has been used as a transmission line for community television systems. This successful innovation was possible because the line attenuation goes through a minimum value (approximately 5dB/km) in the vicinity of 100 MHz. Kikuchi omits any reference to the type of launching device employed for the above application; but the mode of propogation might have been the cylindrical surface-wave mode supported by the polyethylene-coated wire (wire radius 1.15×10^{-3}m; outer radius of dielectric 4.2×10^{-3} m; relative permittivity of dielectric 2.3; wire height 5 m).

A modified form of the Beverage antenna, known as the Sanguine type, has been considered for ELF transmitting systems [Ref. 4.16]. This can

be regarded as a multiple Beverage antenna in which the Beverage elements are grounded at both ends, and usually excited at the centre. Since the gain of such a system varies inversely as the ground conductivity, site evaluation and selection become important factors in system design.

Often there are local variations of ground conductivity within the volume of earth affecting the gain of an ELF antenna. In 1972, a simple method was reported for the evaluation of prospective sites [Ref. 4.16], which constitutes another application of the Beverage antenna. This method has the advantage that the 'effective ground conductivity' σ_e of the site can be determined from a single test which allows for the effect of inhomogeneities. The test procedure is the following : an insulated wire about 2 km long is grounded at both ends and energized at the frequency of interest. The transverse component of the horizontal magnetic field, H_t, is measured at a point about 20 km off the end of the wire. Then σ_e can be determined from the theoretical magnetic field for homogeneous earth of conductivity σ_e.

In 1973, a doctoral thesis was presented to the University of London which evaluated a proposal for a new transmitting antenna at HF [Ref. 4.17]. This antenna consisted of a Beverage antenna with series capacitive loading along the horizontal wire. Since this modification yields antenna characteristics significantly different from the characteristics of the classical Beverage antenna, the discussion of this proposal will be postponed until Chapter VI.

4.3. Mode of Action of the Beverage Antenna

The Beverage Antenna was conceived over fifty years ago. In spite of this fact, there still remains one controversial question concerning

the radiation mechanism from this antenna : does radiation occur continuously along the length of the Beverage antenna, or from the end aperture analogous to radiation from a surface wave antenna? The end aperture is defined by the plane, at the load termination, perpendicular to the horizontal wire.

The analysis of the Beverage structure due to A.F. dos Santos [Ref. 4.18] provides a basis for the evaluation of the above problem. Dos Santos found that the field distribution above the wire can be represented in terms of a complex line integral : however he discovered that two radically different integration paths existed for which convergence occured. Along one path of integration (along the real axis) the integrand represents a superposition of incoming plane waves which satisfy the radiation condition. This solution was termed the 'proper mode'; there is an analogy between this mode and a superposition of surface-wave modes above a corrugated plane with a positive surface reactance [Ref. 4.19]. It can be argued that the proper mode represents a non-radiating solution of the Beverage boundary-value problem; the conclusion is that such a mode would only radiate at the aperture defined by the antenna termination, similar to the mode of action of a surface-wave antenna.

The alternative path of integration yields a solution which corresponds to a superposition of outgoing plane waves which do not satisfy the radiation condition. This is the 'improper mode' solution; it is analogous to leaky-wave modes which exist outside a slotted-waveguide array [Ref. 4.20]. It should be noted that violation of the radiation condition only occurs when the uniform structure considered is infinitely long. It is evident that the improper mode tends to radiate along the antenna, in contrast to the proper mode.

Dos Santos has suggested that the choice between the two solutions is determined by boundary conditions at the antenna input : when the launching device corresponds to a discrete source connected between the horizontal wire and ground, then the correct solution is the improper mode; because outgoing waves must be excited above the wire. This argument is inconclusive, to say the least, for the following reason : the same argument can be applied to a plane surface-wave antenna. The false conclusion would be that the mode propagating along the surface-wave antenna must correspond to outgoing waves above the antenna.

There is evidence that the Beverage antenna radiates both along the length and at the aperture defined by the antenna termination - irrespective of the nature of the propagating mode. In this respect, the mode of action of the Beverage antenna is analogous to a lossy surface-wave antenna. This behaviour is due to the intrinsic losses present in the Beverage antenna. The evidence supporting the above proposition is presented in the following paragraphs.

A comparison between theoretical and experimental results reported by Kikuchi [Ref. 4.15] suggests that there is radiation along the length of the Beverage structure : as indicated in Fig. 3.3, the experimental values of attenuation constant are consistently higher than Kikuchi's theoretical results. As Kikuchi's analysis does not seem to take into account radiation effects, it is plausible to attribute the above discrepancy to radiation effects.

Another argument supporting radiation along the length is based on a simple theoretical consideration. It can be shown that the open-circuit voltage V_{OC} at the input terminal of a Beverage antenna of infinite length, due to plane wave incidence, is given by the expression

$$V_{OC} = -\tfrac{1}{2}\frac{E_o}{jkC - \gamma}$$

where E_o is the electric field along the horizontal wire at the terminal; γ, the propagation constant of the Beverage antenna; k, the free-space wave number; and C is the direction cosine referred to the wire direction (see Eq. 4.36 and Fig. 4.9).

The above result indicates that radiation occurs along the length, because radiation from the end aperture must be zero due to antenna losses and the infinite length.

To determine whether or not there is radiation from the end aperture, we shall start by considering the ideal transmission-line corresponding to the Beverage structure : i.e., the line consisting of a horizontal wire above perfectly-conducting ground. In this case, it has been established that radiation along the line is negligible provided $b \ll \lambda_o$ (where b is the wire height, and λ_o the free-space wavelength), particularly if the line is very long [Ref. 4.21]. Also, if the line is open-circuited, there is no radiation from the termination; but if the horizontal wire is grounded through a vertical conductor, then there is radiation, associated with the vertical electric current.

When the ground is <u>not</u> perfectly conducting, it is evident that the vertical current still radiates - a fact which is not disputed. However, there is another component of radiation associated with the end discontinuity, because the far field contribution due to the wire current I_w does not cancel the contribution due to ground surface currents J_s. It is possible to regard J_s as the sum of two components:

$$J_s = J_s^o + J_s^p$$

where J_s^o corresponds to the transverse distribution of surface currents when the ground is perfectly-conducting; and J_s^p is a perturbation term required to satisfy boundary conditions when the ground has finite conductivity. (In the above equation the longitudinal variation has been omitted).

In the far field, contributions of I_w and J_s^o cancel, particularly for $b \ll \lambda_o$. Whether or not there is a radiation term associated with J_s^p depends on the longitudinal variation. However, there must be radiation from the end discontinuity in J_s^p - even if the latter corresponds to a surface-wave distribution.

There is only indirect experimental evidence to suppose that the Beverage radiates from its termination. In Section 3.5, we reported near-field measurements carried out to determine the propagation constant of the IPA; in these measurements, no significant attenuation was noted along the structure. Far-field measurements carried out on the IPA (see Section 5.6) indicate substantial radiation which can only be associated with the end aperture. There is a high degree of similarity between the Beverage antenna and the IPA, the major difference being that the latter exhibits a negligible attenuation constant. Provided the analogy between the antennas is valid, it can be concluded that the Beverage antenna also radiates from its end aperture. Whether or not this is an important factor for design purposes depends on the length and attenuation constant of the antenna.

4.4. Considerations of Symmetry

There is a relationship between the responses of IPA_1 and IPA_2 (shown in Figs. 1.2 and 1.3, Chapter I, respectively) analogous to the relationship that exists between a vertical monopole of length L above

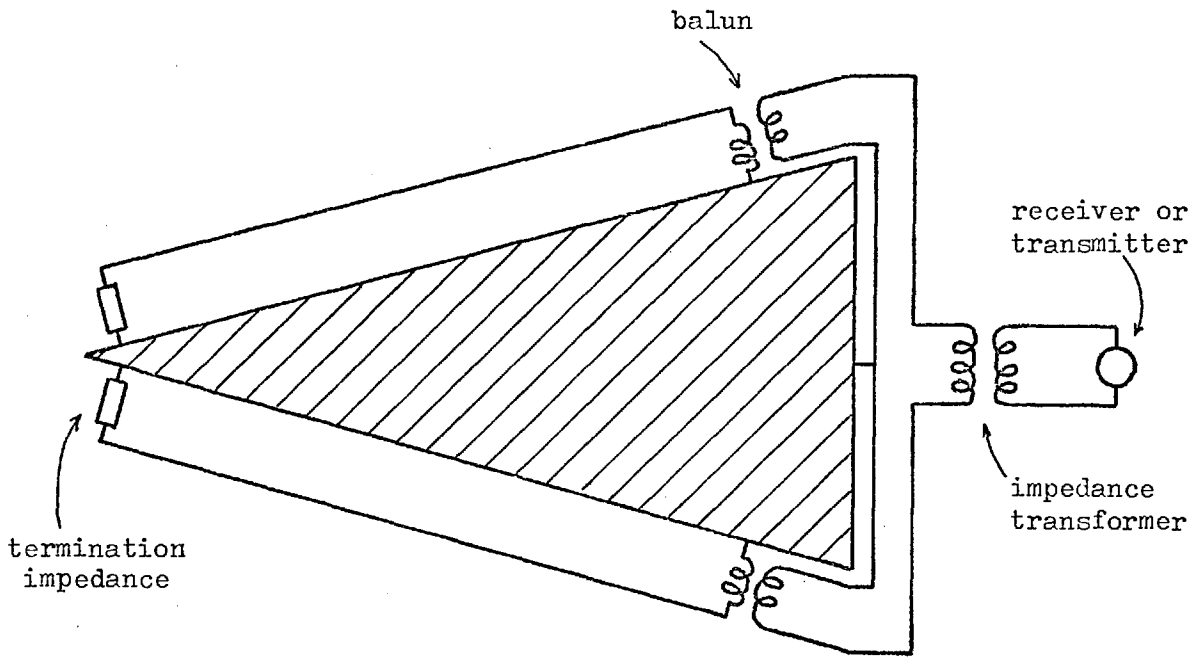


Fig. 4.3. Schematic Representation of the 'Wedge Antenna' (WA_2), With Antisymmetric Excitation

perfectly-conducting (plane) ground and a dipole of (total) length 2L in free-space. However, this relationship is valid for a larger class of antennas, to which the IPA also belongs:
wire antennas based on the wedge configuration and excited antisymmetrically. In this section,we shall demonatrate this relationship for the general class of 'Wedge Antennas' (WA), since the IPA might also be used in the wedge configuration (Fig. 1.5, Chapter I) and because consideration of this more general case does not require any additional effort or space.

The Wedge Antenna is shown schematically in Fig. 4.3. Obviously, there are many possible variations, but for the present, we shall consider the simplest form only. The wedge cross-section has the form of an isosceles triangle, and therefore can be defined by

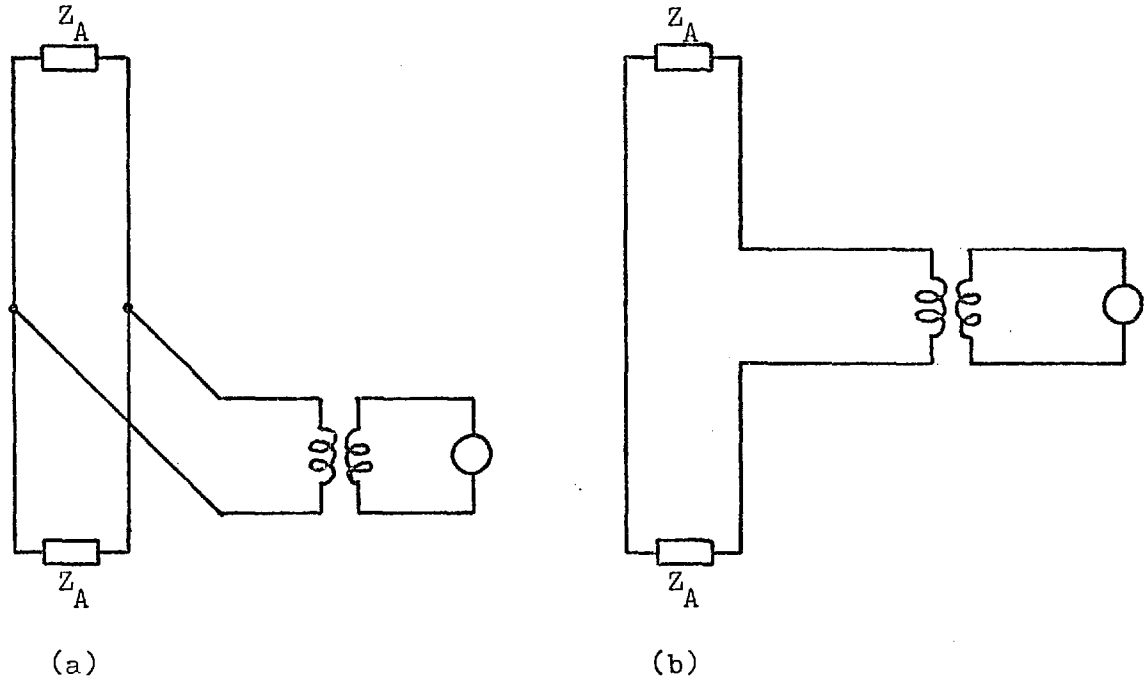


Fig. 4.4. Circuit Representation of Possible Modes of Exciting The 'Wedge Antenna': (a) Symmetric Excitation; (b) Antisymmetric Excitation.

specifying one length and one angle only : for example, the length of one of the symmetrical sides (L) and the included angle (2Δ). The antenna consists of two lengths of straight wire, one parallel to each symmetrical face of the wedge. Both wires are connected to the wedge surface: near the apex through identical impedances; and near the base, through an impedance transformer or balun.

In Figure 4.3., these transformers are connected in series with the receiver (or transmitter) via another transformer. Figure 4.4(b) indicates the circuit diagram for the same mode of excitation, where the antenna input impedance due to each wire is represented as Z_A. However, an alternative mode of excitation would be obtained by connecting the antenna wires in parallel with the receiver (or transmitter), as

indicated in Figure 4.4(a). The former arrangement is termed antisymmetric, series or odd mode of excitation, as in Figure 4.4(b). The latter arrangement is called symmetric, even or parallel mode of excitation, as in Figure 4.4(a). In this section only the antisymmetric mode of excitation (or response) will be considered. Consequently, for the sake of simplicity, in some diagrams the wedge antenna WA_2 (Figure 4.3) will be represented by a simple triangle only - the antisymmetric mode of response always being implicit.

To obtain the radiation pattern and gain of the antenna WA_2, we consider a general case, as shown in Figure 4.5: the wedge-antenna is symmetrical about the $x = 0$ plane, with the wedge apex at the origin of the coordinate system. We shall consider the receiving problem, where we wish to find the current in the receiver, connected to WA_2, due to a current element $I\delta h$ at (R, θ, ϕ); the current element is, of course, in the far field of the antenna, i.e., $R \gg L$, where L is the length of the identical sides of the wedge-antenna.

Throughout this chapter, both spherical coordinates (r, θ, ϕ) and rectangular coordinates (x, y, z) will be used. θ is measured from the positive x-direction; but ϕ is measured from the negative z-direction, in the y-z plane. This slightly unusual convention was adopted, early in the research programme, when a preliminary analysis of the wedge antenna was carried out : this convention yields more convenient transformation equations for the rotation of rectangular axes about the y-axis.

The orientation of the current element determines the polarization of (locally) uniform plane wave incident on the receiving wedge-antenna. We shall consider the current element at (r, θ, ϕ) to be directed parallel but opposite to the unit vector $\underline{a}_\theta$, as indicated in Figure 4.5; the

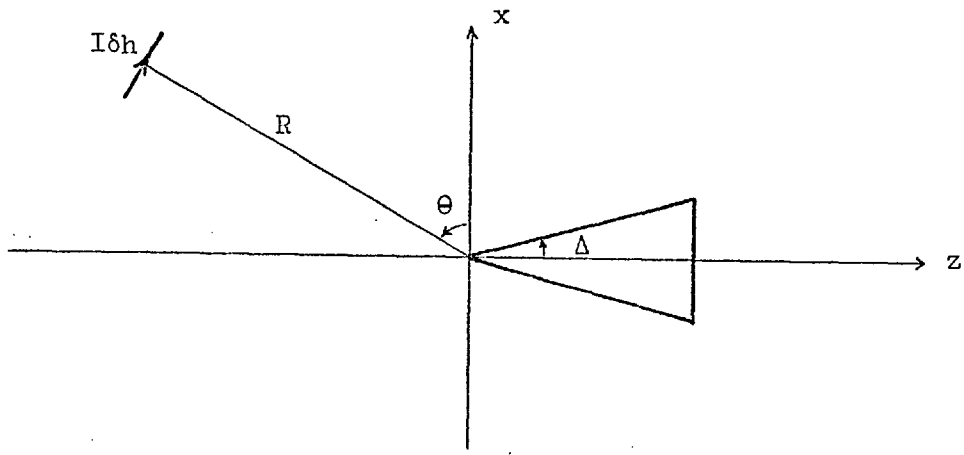


Fig. 4.5 Asymmetric dipole excitation

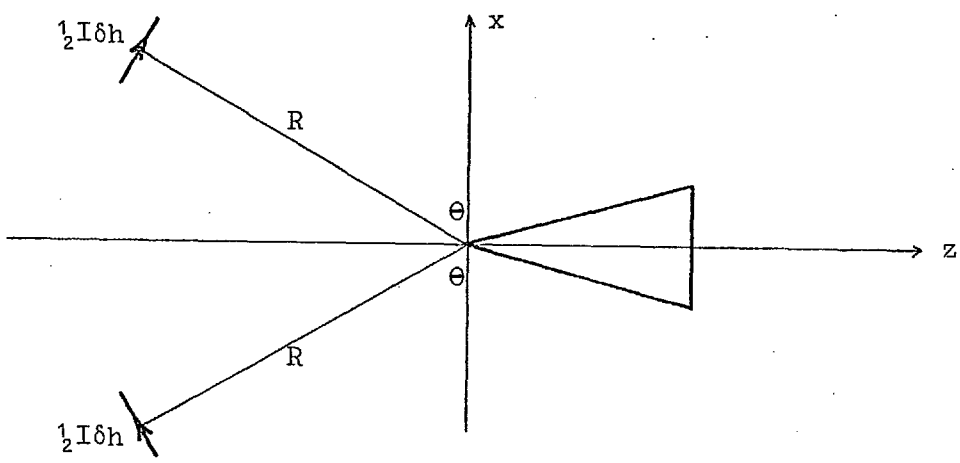


Fig. 4.6 Antisymmetric dipole excitation

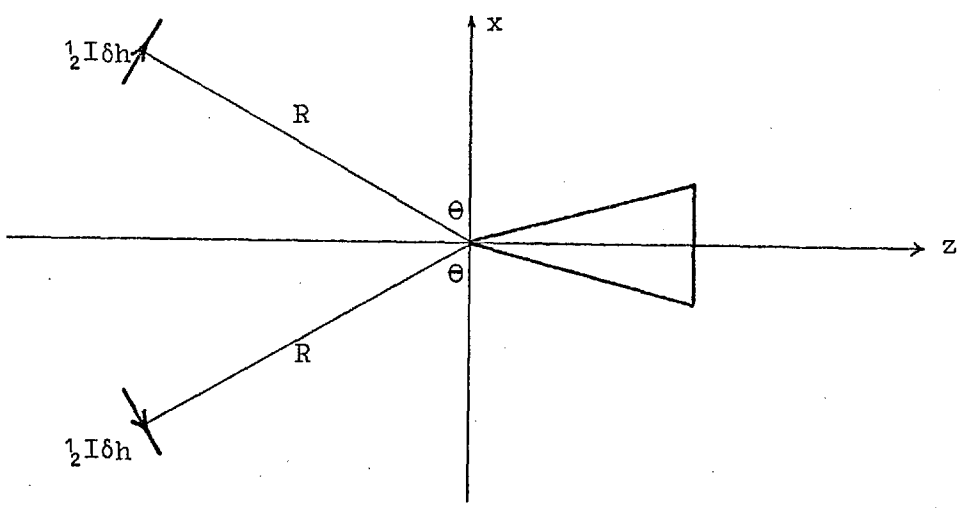


Fig. 4.7 Symmetric dipole excitation

associated incident wave at the wedge-antenna will be referred to as 'parallel polarized'. Similarly, a current element parallel to the unit vector $\underline{a}_\phi$ will give rise to an incident wave, at the wedge--antenna, which will be 'perpendicular polarized'. The terms parallel and perpendicular refer to the polarization of the electric field, in the incident wave, relative to the plane of incidence.

The current element in Figure 4.5 can be replaced by two pairs of current elements of moment $\frac{1}{2}$ Iδh : one pair placed antisymmetrically with respect to the y - z plane, as in Figure 4.6, and the other pair placed symmetrically, as in Figure 4.7. According to the principle of superposition, the response of the wedge-antenna to the original asymmetric dipole excitation (Fig. 4.5) can be obtained by adding the responses of the wedge-antenna to the antisymmetric and symmetric dipole excitations of Figures 4.6 and 4.7 respectively.

Since the two wires of the wedge-antenna are connected in series (circuit of Figure 4.4(b)), it is evident that the symmetric dipole excitation of Figure 4.7 will induce zero current in the receiver. Hence we need only consider the antisymmetric dipole excitation of Figure 4.6. In the latter case, from considerations of symmetry, the tangential component of electric field must be zero on the plane x = 0. Hence we can consider the plane x = 0 to consist of an infinite perfectly conducting sheet, of infinitesimal thickness. The original problem has now been transformed to one in which we require to find the current in the receiver of a half-wedge-antenna placed on an infinite perfectly-conducting plane, due to a distant current element. It should be noted that the receiver impedance has been halved in the above transformation : instead of <u>two</u> antenna wires originally connected in series with the receiver, now there is only

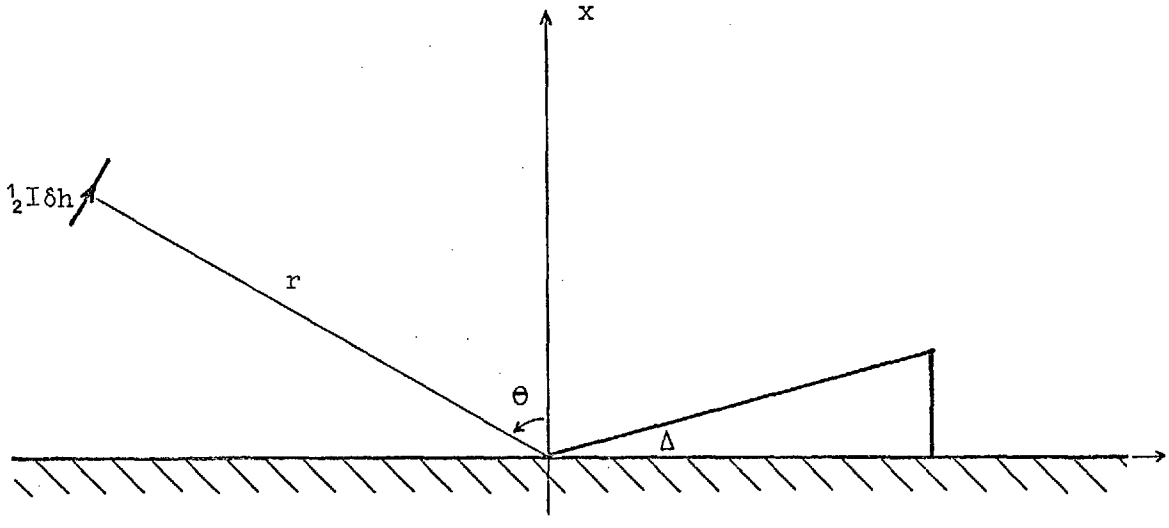


Fig. 4.8. The Transformed Problem of the Half-Wedge-Antenna

one antenna wire connected to the receiver; hence, for maximum power transfer, the receiver impedance must be halved. The transformed problem is depicted in Figure 4.8.

So far we have considered the transformation problem for parallel polarization only. However, for perpendicular polarization, the transformation is identical, and therefore does not require further consideration.

In Section 4.1, it was pointed out that the electric field distribution along the antenna wire(s) was required in order to calculate the receiver current. This distribution can be obtained more easily in the transformed problem (half-wedge on an infinite conducting plane) than in the original problem of scattering by a wedge in free--space. In the next section a first-order solution will be presented for the field distribution near a strip of non-zero surface impedance on perfect ground. This corresponds to scattering by a wedge of zero angle and finite surface impedance.

4.5. Near-Field Scattering By An Impedance-Strip on Perfect Ground

4.5.1. General Considerations

In scattering problems, there are a number of general considerations which influence the choice of analytical technique for problem formulation and evaluation of solution. In all but the simplest problems, it is necessary to resort to approximate techniques [Ref. 4.22], the nature of which depends on the particular problem considered.

Generally, the shape of the scattering body determines the coordinate system most suitable for problem formulation. For example, cylindrical coordinate system is chosen for analysis of the scattering problem by a conducting cylinder [Ref. 4.23]. This is for two reasons : firstly, choice of a 'natural' coordinate system always simplifies the formulation of the problem, and sometimes even leads to a 'separation of variables' solution. Secondly, the solution can be represented as a superposition of characteristic wave functions [Ref. 4.24], and proper choice of the natural coordinate system leads to the simplest formulation of boundary conditions [Ref. 4.25].

Size of the scattering body, relative to the wavelength considered, defines the nature and limitations of approximations used in analysis and evaluation of results. For example, when a large scattering body is illuminated by a point source, the geometrical optics approximation yields accurate results, as least in the far field, for the slaient features of the scattered field [Ref. 4.26]. On the other hand, when the scattering geometry is small compared with wavelength, quasi-static approximations can be used [Ref. 4.27]: this technique has been particularly useful in the derivation of equivalent circuit representations for wave-guide discontinuities.

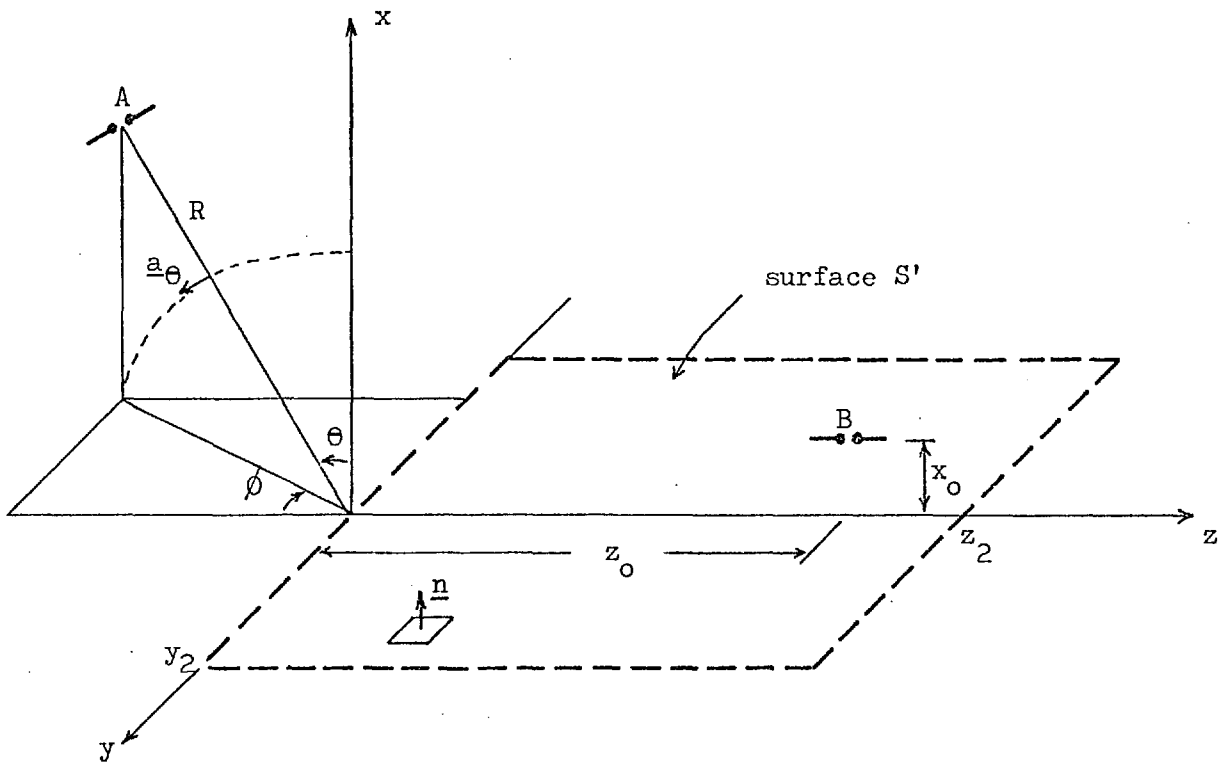


Fig. 4.9. The Scattering Impedance Surface S' In Relation To The Coordinate System

In this section we are concerned with scattering from a plane boundary which contains surface discontinuities represented by changes in the surface impedance.

4.5.2. Distribution of E_z Along the Position of the Wire

The problem to be examined in this section is represented in Figure 4.9. We wish to obtain the z-component of the electric field at an observation point (x_o, y_o, z_o), $x_o > 0$, due to a uniform plane wave incident from the direction (θ, ϕ). As indicated in Figure 4.9, θ is measured from the positive x-direction, and ϕ from the negative z-direction on the y-z plane. The plane surface $x = 0$ is perfectly-conducting except for a region S' where the boundary conditions are defined in terms of Z_{sz} and Z_{sy}, the surface impedances in the positive

z- and y- directions respectively:

$$\left.\frac{E_z}{H_y}\right|_{x=0_+} = Z_{sz} \qquad (4.1)$$

$$\left.\frac{E_y}{H_z}\right|_{x=0_+} = -Z_{sy} \qquad (4.2)$$

That is to say, the impedance normal to the surface is defined for both rectangular components of the tangential electric field.

The analysis to be presented in this section is based on G.D. Monteath's application of the compensation theorem [Ref. 4.6]. The required field distribution can be obtained by calculating the mutual impedance Z'_{AB} between a doublet A, at spherical coordinates (R, θ, ϕ), and another doublet B, at the observation point with rectangular coordinates (x_o, y_o, z_o), as indicated in Figure 4.9. Both doublets are of length $\delta h \ll \lambda_o$. R is assumed large enough so that the incident wave due to doublet A is locally plane in the vicinity of region S'. Doublet A is orientated parallel to the unit vector $\underline{a}_\theta$ for parallel polarisation, and parallel to the unit vector $\underline{a}_\phi$ for perpendicular polarisation : the terms 'parallel' and 'perpendicular' refer to the polarisation of the incident electric field relative to the plane of incidence. Since we are only interested in the z-component of electric field, the orientation of doublet B will be assumed to be parallel to the unit vector $\underline{a}_z$.

The electric field component E_z at (x_o, y_o, z_o), in the absence of doublet B, due to radiation from doublet A, is given by

$$E_z = -\frac{Z'_{AB} I}{\delta h} \qquad (4.3)$$

where I is the current flowing in the terminals of doublet A. An expression for Z'_{AB} is given by Monteath [Ref. 4.6], based on Ballantine's formulation of the reciprocity theorem:

let

$$\Delta Z'_{AB} = Z'_{AB} - Z_{AB} \tag{4.4}$$

then

$$\Delta Z'_{AB} = \frac{1}{I^2}\iint_S (\underline{E}_A \wedge \underline{H}'_B - \underline{E}'_B \wedge \underline{H}_A) \cdot \underline{n}\, ds \tag{4.5}$$

or

$$\Delta Z'_{AB} = \frac{1}{I^2}\iint_S (\underline{E}_B \wedge \underline{H}'_A - \underline{E}'_A \wedge \underline{H}_B) \cdot \underline{n}\, ds \tag{4.6}$$

Essentially the above equations enable us to calculate the change $\Delta Z'_{AB}$ in the mutual impedance between two antennas A and B, radiating in the presence of a closed scattering surface S, when some perturbation is made to the surface S. Subscript A denotes field quantities due to current I flowing in terminals of (doublet) antenna A, with terminals of doublet B open-circuited. Similarly, subscript B has a corresponding meaning. The unprimed and primed quantities denote values before and after the surface S is perturbed respectively. The surface integral in the above equations is evaluated over all S; $\underline{n}$ is the unit vector normal to S, and is directed out of the scattering volume (i.e. into the space containing the antennas). It should be noted that Eqs. (4.5) and (4.6) are exact.

In the present context, S consists of the infinite plane surface $x = 0$, which can be considered 'closed' as infinity. In Figure 4.9, $\underline{n} \equiv \underline{a}_x$. Before perturbation all S is regarded as perfectly-conducting;

after perturbation, the surface impedance becomes non-zero over a region S' only.

The choice between Eq. (4.5) and Eq. (4.6) is a matter of convenience only : we shall use Eq. (4.6) because this choice will enable us to make better approximations. Eq. (4.5) can be reduced to

$$\Delta Z'_{AB} = \frac{1}{I^2} \iint_S (\underline{E}_{Bt} \wedge \underline{H}'_{At} - \underline{E}'_{At} \wedge \underline{H}_{Bt}) \cdot \underline{a}_x \, ds \qquad (4.7)$$

where subscript t denotes components tangential to the surface x = 0. Noting that $\underline{E}_{Bt} = 0$ at all points on the surface, and that $\underline{E}'_{At}$ is zero outside the region S', Eq. (4.7) can further be simplified to the following equation:

$$\Delta Z'_{AB} = -\frac{1}{I^2} \iint_{S'} (\underline{E}'_{At} \wedge \underline{H}_{Bt}) \cdot \underline{a}_x \, ds \qquad (4.8)$$

$$= \frac{1}{I^2} \iint_{S'} (E'_{Ay} H_{Bz} - E'_{Az} H_{By}) \, dydz \qquad (4.9)$$

where subscript y and z denote respective components of tangential fields.

In the present application we are interested in the effect of a rectangular strip of finite surface impedance. Hence we define S' as follows (see Figure 4.9):

$$\begin{aligned} 0 \leqslant z \leqslant z_2 \\ -y_2 \leqslant y \leqslant y_2 \end{aligned} \qquad (4.10)$$

Also, boundary conditions over S', Eqs. (4.1) and (4.2), yield

$$E_{Az}' = Z_{sz} H_{Ay}' \tag{4.11}$$

$$E_{Ay}' = - Z_{sy} H_{Az}' \tag{4.12}$$

Substituting from the above equations into Eq. (4.9), we obtain

$$\Delta Z_{AB}' = \frac{1}{I^2} \int_0^{z_2} \int_{-y_2}^{y_2} (Z_{sy} H_{Az}' H_{Bz} + Z_{sz} H_{Ay}' H_{By}) dy dz \tag{4.13}$$

At this stage we make the assumption that H_{At}', the tangential component of the magnetic field due to current I flowing in terminals of doublet A, remains constant at least to the first order when surface S is perturbed. This leads to a variational expression based on Monteath's application of the compensation theorem [Ref. 4.6].

For parallel polarisation, we shall consider an incident (locally) uniform plane wave given by

$$\underline{H}_A^{inc} = H_o(\cos \phi \, \underline{a}_y - \sin \phi \, \underline{a}_z) \exp[- jk (-S_1 x + S_2 y + Cz)] \tag{4.14}$$

where k is the free-space wave number; S_1, S_2 and C are direction cosines given by

$$S_1 = \cos \theta \tag{4.15}$$

$$S_2 = \sin \theta \sin \phi \tag{4.16}$$

$$C = \sin \theta \cos \phi \tag{4.17}$$

The quantity H_o is the amplitude of the incident wave at the origin, and

is related to the moment of the radiating doublet A by the relation [Ref. 4.28]

$$H_o = I\delta h \frac{jk}{4\pi R} \tag{4.18}$$

Accordingly, the approximation for the total magnetic field is given by

$$\begin{aligned} \underline{H}'_{At} &\simeq \underline{H}_{At} \\ &= 2H_o(\cos\phi\, \underline{a}_y - \sin\phi\, \underline{a}_z) \exp[-jk(S_2 y + C_z)] \end{aligned} \tag{4.19}$$

The field distribution of a horizontal doublet above perfect ground can be derived from classical image theory : the relevant equations are given in Appendix 4A. For doublet B parallel to the z-axis, positioned at $(x_o, 0, z_o)$, the tangential magnetic field components at a point (x, y, z) are given by

$$H_{Bz} = 0 \tag{4.20}$$

$$H_{By} = -\frac{I\delta h}{2\pi} \frac{kx_o}{r^2} \left(j + \frac{1}{kr}\right) \exp(-jkr) \tag{4.21}$$

where

$$r = [x_o^2 + y^2 + (z - z_o)^2]^{\frac{1}{2}} \tag{4.22}$$

Substitution from Eqs. (4.19), (4.20) and (4.21) leads to

$$\Delta Z'_{AB} = -\frac{H_o \delta h}{I} Z_{sz} \cos\phi \exp(-jkCz_o) G_z \tag{4.23}$$

where

$$G_z = \int_{-kz_o}^{kz_2'} \int_{-ky_2}^{ky_2} \frac{kx_o}{\pi} \left[\frac{1}{(kr')^3} + \frac{j}{(kr')^2} \right] \times$$

$$\exp[-jk(S_2 y + Cz' + r')]d(ky)d(kz') \qquad (4.24)$$

$$kr' = [(kx_o)^2 + (ky)^2 + (kz')^2]^{\frac{1}{2}} \qquad (4.25)$$

$$z' = z - z_o \quad ; \qquad z_2' = z_2 - z_o \qquad (4.26)$$

In general, the quantity of interest is the total electric field component in the z-direction. This can be obtained from Eq. (4.3) and the following expression for mutual impedance after the perturbation:

$$Z'_{AB} = -Z_o \frac{H_o \delta h}{I} \cos \phi \exp(-jkCz_o)$$

$$\left\{ \cos \theta [\exp(jkx_o S_1) - \exp(-jkx_o S_1)] + Z_{zn} G_z \right\} \qquad (4.27)$$

where

Z_o = free-space impedance

$$Z_{zn} = \frac{Z_{sz}}{Z_o} \qquad (4.28)$$

The resulting expression for the electric field is given by:

$$E_z = Z_o H_o \cos \phi \exp(-jkCz_o)$$

$$\left\{ \cos \theta [\exp(jkx_o S_1) - \exp(-jkx_o S_1)] + Z_{zn} G_z \right\} \qquad (4.29)$$

The above equation is in the form:

$$E_z = (E_z^o + E_z^s)\exp(-jkCz_o) \qquad (4.30)$$

where $E_z^o \exp(-jkCz_o)$ is the original field distribution in the presence of perfect ground, and $E_z^{S'}$ is a perturbation term associated with scattering due to the impedance strip.

It should be noted that, in the derivation of Eq. (4.29), there have only been two sources of approximation : replacement of $\underline{H}'_{At}$ by $\underline{H}_{At}$, and the implicit assumption that surface impedance over S' is independent of position and independent of direction of incidence. The question of surface impedance has already been considered, in Section 2.3, and suffice it to say that the assumption of constant surface impedance over a uniform region S' is least accurate near the perimeter of S' : however the effect of this error is reduced by the averaging process represented by the integral G_z in Eq. (4.23).

As for the error in the magnetic field, we note that this is a variational approximation. For example, if the region S' represents an aperture in a perfectly conducting screen, the error in $\underline{H}'_{At}$ becomes of the order of 50% only, for normal incidence. However, in this case the 'equivalent' surface impedance would have the value of free-space impedance, and it would be more appropriate to regard the electric field as variational, corresponding to Kirchhoff's approximation [Ref. 4.29]. The present approximation is believed to yield sufficiently accurate results, for the present application, for normalized surface impedance values $|Z_s/Z_o| \lesssim 0.3$.

4.5.3. Evaluation of Results for Near-Field Scattering

A computer program was written in order to compute values of G_z, Eq. (4.24), by numerical integration. A selection of results is presented in graphical form, Figs. 4.10 through 4.14.

Two integration routines were used initially : trapezoidal and Simpson's rule. This was performed as a self-checking process, and to

determine an optimum integration step. It was found that a step of one-half of the height of the observation point gave sufficiently accurate results : i.e., the error due to numerical integration was less than 5% in every integration result. All graphical results presented in this section were obtained with the aid of Simpson's rule.

Figure 4.10 indicates the variation of magnitude and phase of $G_z = |G_z| \exp(j\Psi)$, as a function of position z_o, for normal incidence. There is an increasing ripple in both the magnitude and phase of G_z as the point of observation approaches the surface discontinuity at $z_2 = 10\lambda$, λ being the free-space wavelength. However, in both cases the ripple is less than 5% of the mean value.

Figure 4.11 corresponds to plane wave incidence in the direction of the positive z-axis, analogous to end-fire radiation; as before, the impedance strip considered has a length $z_2 = 10\lambda$ and total width $2y_2 = 2\lambda$, with the point of observation being at a height $x_o = 0.1\lambda$. Again, a small ripple is in evidence near the surface discontinuity. However, in this case there is also a non-linear phase variation along the strip; the total phase change is about 20^o over a distance of ten wavelengths. It should be noted, from Eq. (4.29), that this corresponds to a phase variation in the electric field <u>in addition</u> to the free space value.

The remainder of the graphs are all related to the particular case of end-fire radiation, since this is the region of greatest interest. Figure 4.12 indicates the effect of changing the length z_2 of the impedance strip. It is interesting to note that beyond the discontinuity, i.e., for $z_o > z_2$, the horizontal electric field has an exponential decay with a phase variation approaching k, the value for free space. There is an analogy here with the behaviour of surface

waves at a discontinuity : the small ripple before the discontinuity can be compared with the generally small reflection coefficient for the surface wave; and the exponential decay beyond the discontinuity is analogous to the radiation of a surface wave at a discontinuity.

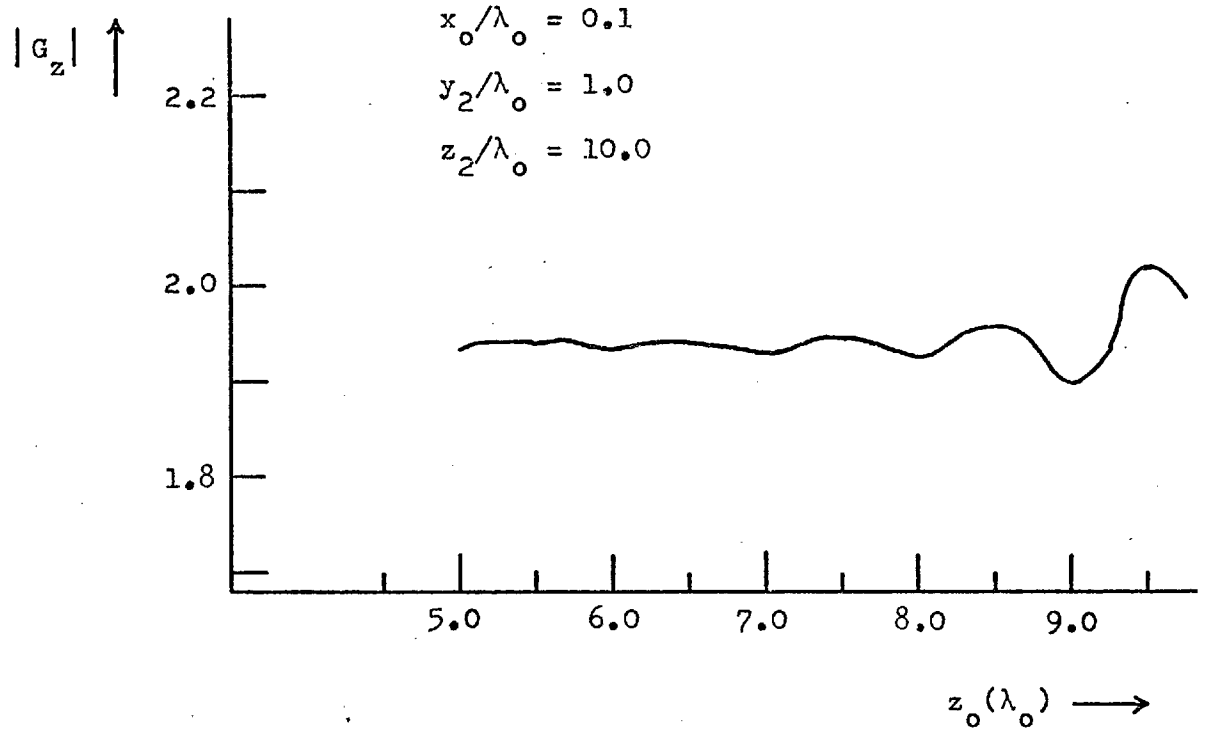
Figure 4.13 shows that the width of the impedance strip has a relatively small effect on the value of the horizontal electric field : but it appears that the narrower the strip the shorter is the distance required for the field to reach its maximum (mean) value.

Variation of G_z with height x_o is depicted in Figure 4.14 : the magnitude of G_z decays exponentially above the surface, whereas Ψ, the phase of G_z, becomes more negative at a slow rate. For the parameters chosen ($z_2 = 10\lambda$, $y_2 = 1.0\lambda$; $z_o = 5\lambda$), the equivalent attenuation was found to be 6.4 dB per wavelength, and the phase change - 30^o per wavelength approximately.

In the above investigations, each dimension was varied in turn keeping the other dimensions constant, the unit of measurement being the wavelength - for obvious reasons! In addition, numerical results were obtained, at different frequencies, for a particular physical size of the impedance strip (frequency 0.25 - 1.0 GHz; observation point at height $x_o = 0.05$m above the centre of a strip 0.46 m x 3.0 m): only the particular case of end-fire radiation was considered. The conclusion was that G_z remained sensibly constant, independent of frequency.

In another series of dimensional analyses, the variation of G_z with the zenith angle of incidence, θ, was also found to be negligible (for $x_o/\lambda = 0.1$: variation of magnitude of G_z was less than 10%; phase variation was less than 20^o).

In conclusion, we note that for the range of parameters of interest



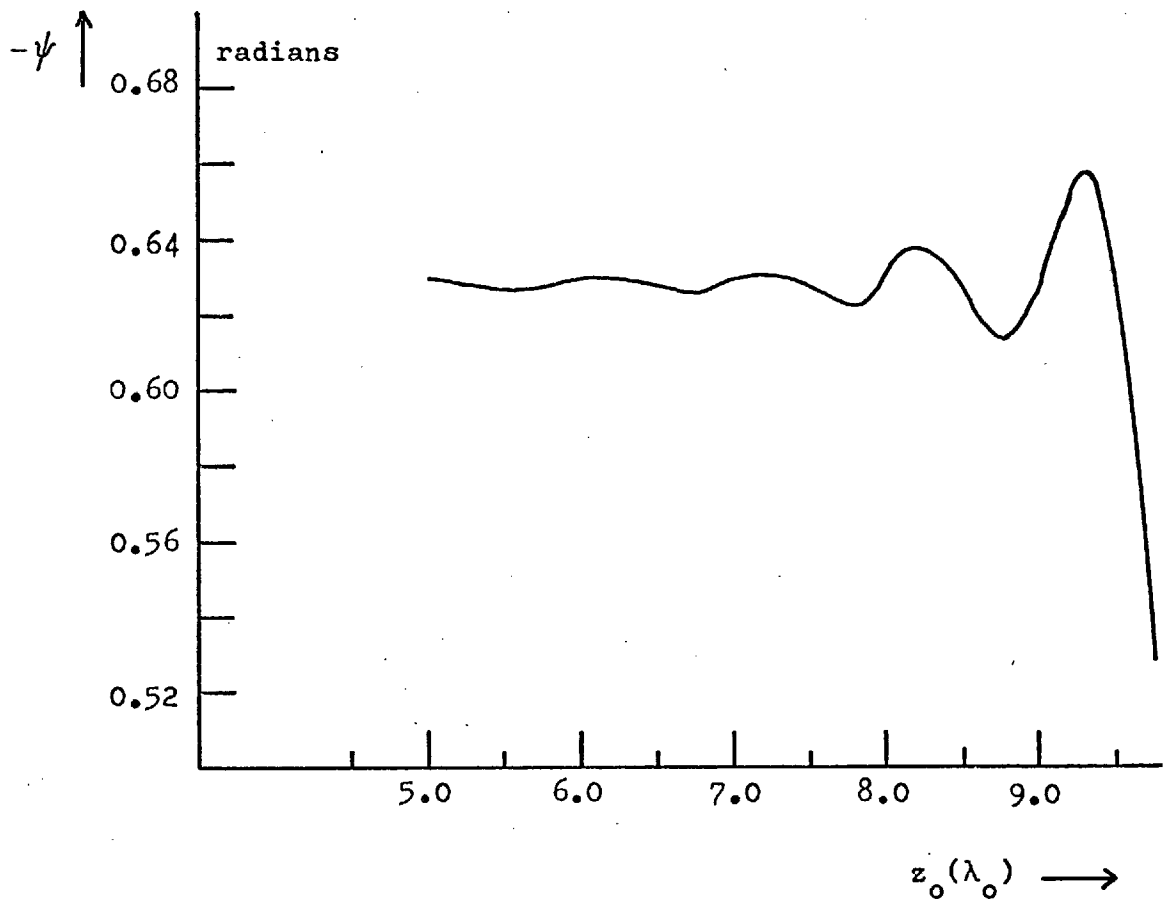


Fig. 4.10 Variation of G_z along the impedance strip for normal incidence

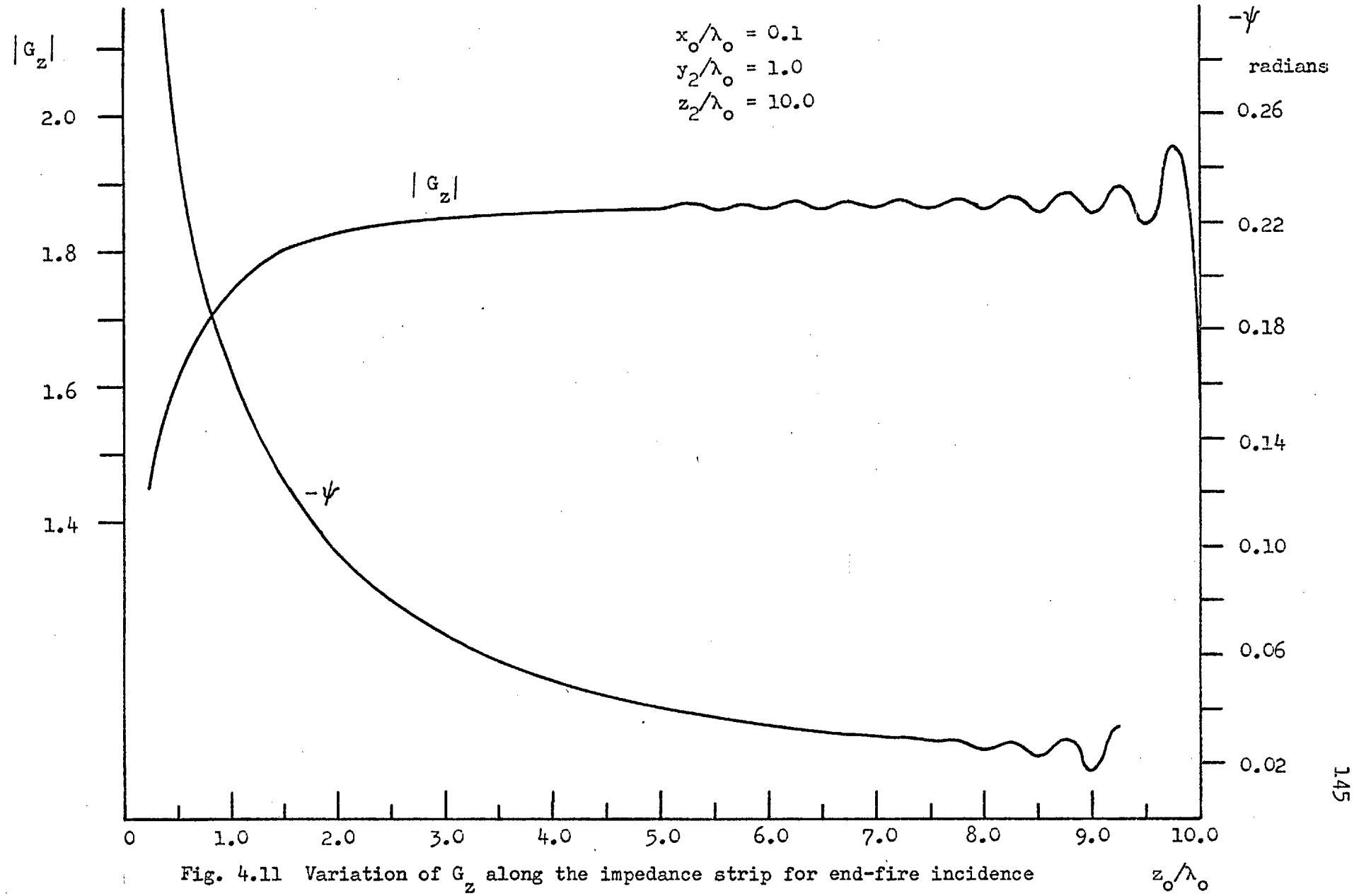


Fig. 4.11 Variation of G_z along the impedance strip for end-fire incidence

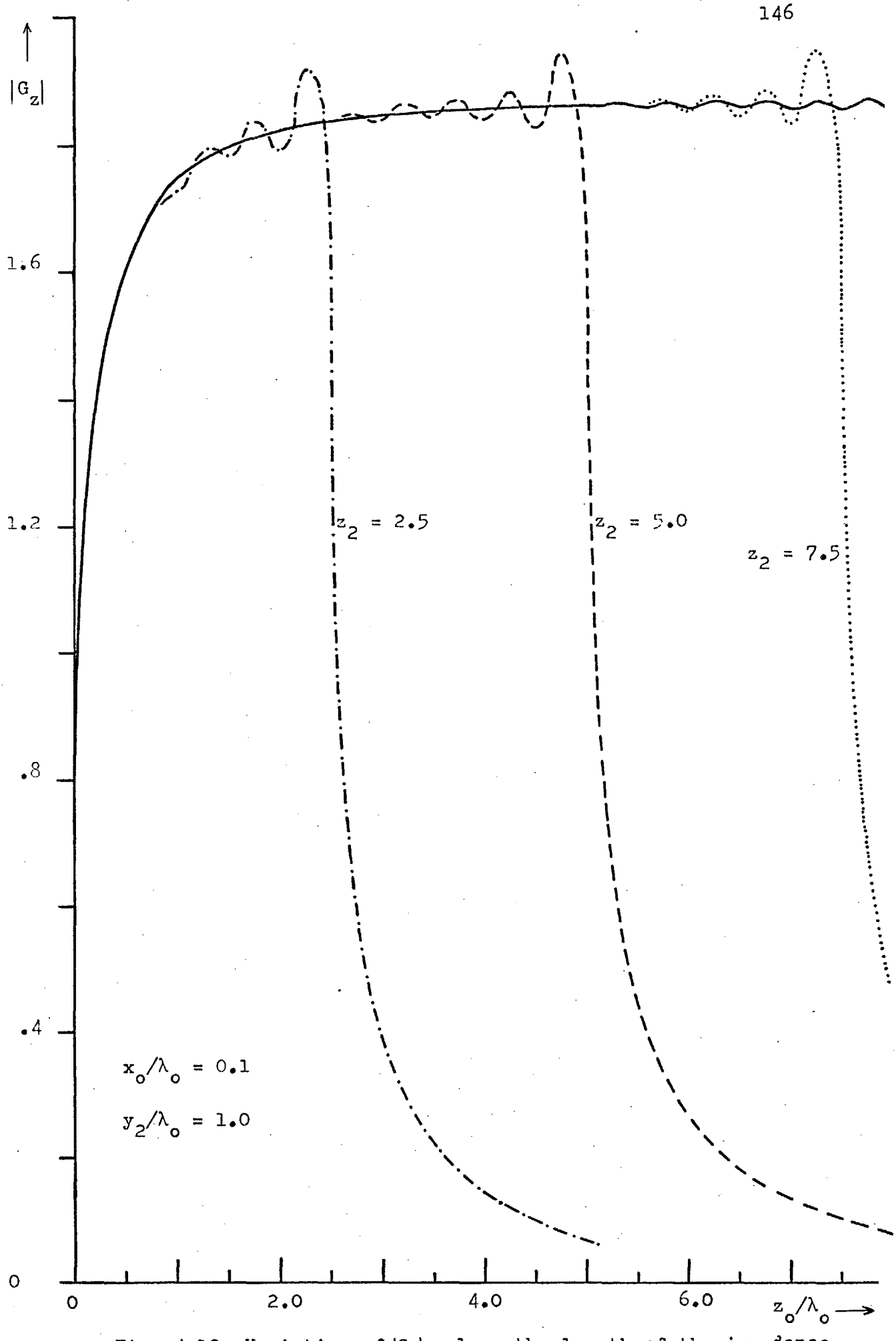


Fig. 4.12 Variation of $|G_z|$ along the length of the impedance strip for end-fire incidence : for different lengths of the strip

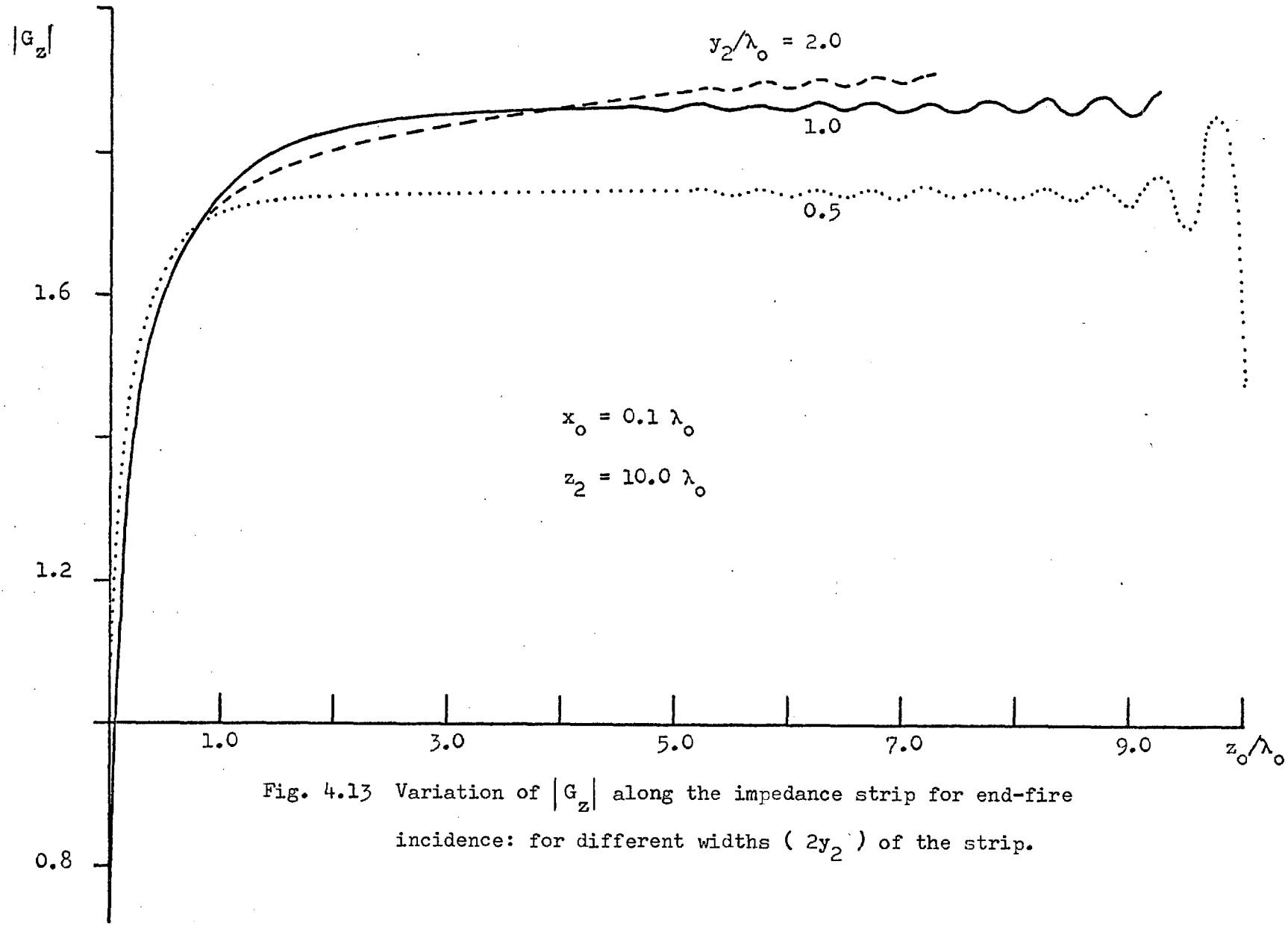


Fig. 4.13 Variation of $|G_z|$ along the impedance strip for end-fire incidence: for different widths ($2y_2$) of the strip.

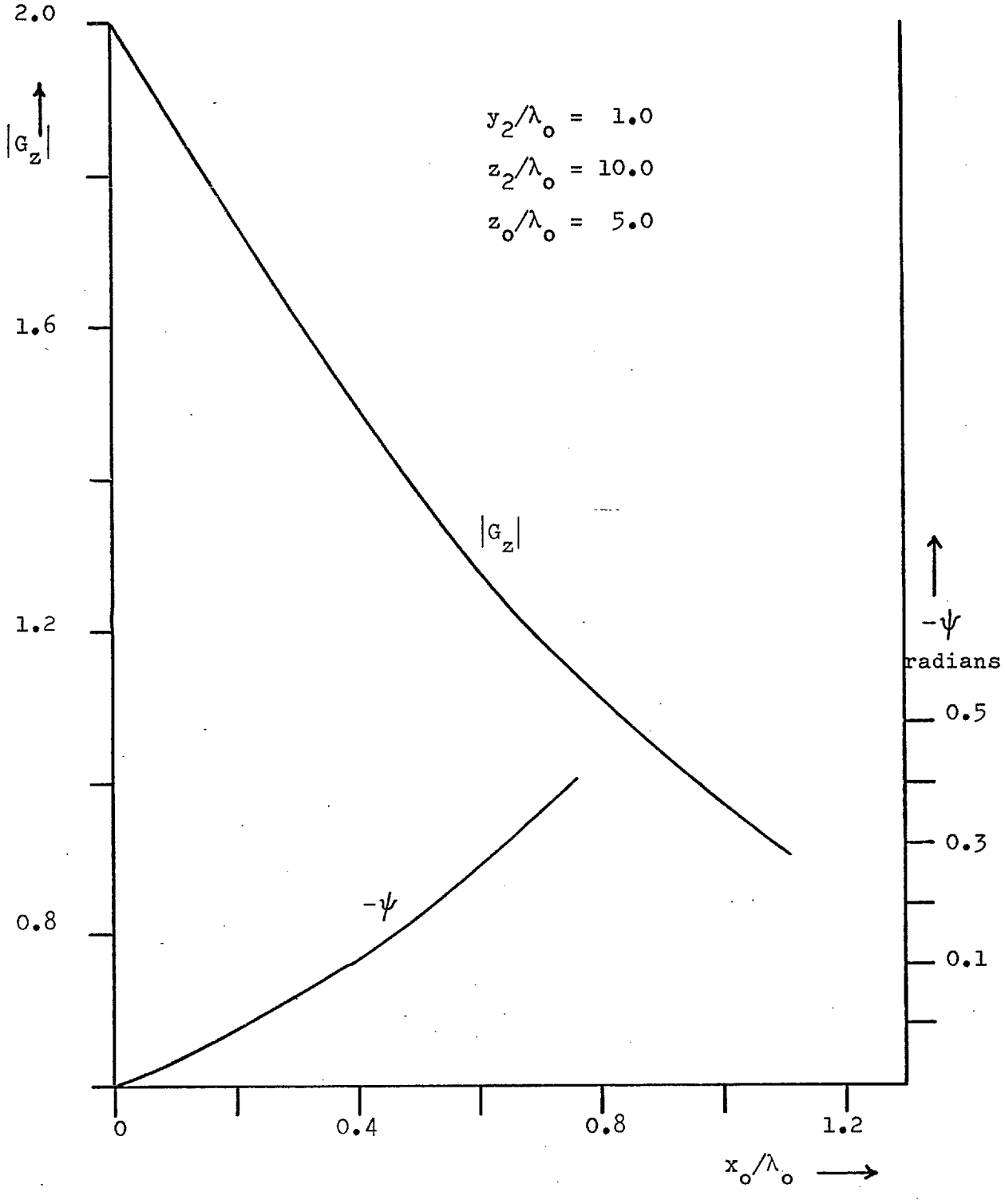


Fig. 4.14 Variation of G_z with height x_o above the impedance strip for end-fire incidence.

it was found that $G_z \simeq 2.0$ along the position of the wire : the magnitude of G_z started from zero at the leading edge of the impedance strip (at $z = 0$), rising exponentially to the mean value in a distance of the order of a wavelength. The particular value $G_z \simeq 2.0$ is related to the approximation $H_{At}' \simeq H_{At}$. Based on physical considerations - such as geometric optics and Fresnel reflection zones - this approximation is expected to yield better results for plane wave incidence near directions corresponding to end-fire ($\theta = 90^\circ$, $\phi = 0^\circ$), than for incidence near the broad-side direction ($\theta = 0^\circ$). In other words, the above approximation is believed to yield reasonably accurate results in the main beam of the antenna; however, more significant errors would be expected in the side lobe region but for the fact that the side-lobes are greatly influenced by radiation from the antenna terminations.

4.5.4. Distribution of E_x Near the Impedance-Strip

In order to estimate the normal component of the electric field, E_x, near the impedance strip, it would be necessary to carry out an analysis analogous to that presented in Sub-section 4.5.2.: to obtain a solution for E_x, the z-orientated doublet at the observation point would be replaced by an x-orientated doublet (Fig. 4.9). It is evident that, as before, the result could be expressed as the sum of two terms : the original field E_x^o in the presence of perfect ground; and a perturbation term E_x^s associated with scattering by the impedance strip:

$$E_x = E_x^o + E_x^s \qquad (4.31)$$

In Sub-section 4.5.2. it was shown that E_z^s, the perturbation term in E_z, was proportional to a surface integral G_z. Similarly, it

could be shown that E_x^s is proportional to another surface integral G_x. Hereafter, 'horizontal' and 'vertical' will be used, for convenience, to refer to directions parallel and normal to the interface respectively.

For the present application, we shall avoid such an analysis as outlined above, for the determination of E_x, by neglecting the contribution of E_x^s to E_x. There are two justifications for this simplification. Firstly it is found that $|E_x^s| \ll |E_z^s|$; in other words, the impedance strip influences the horizontal component E_z of the electric field must more than the vertical component E_x. This is because G_x tends to have a much smaller magnitude than G_z, for reasons explained in the following paragraph.

The magnetic field distribution on perfect ground due to radiation from a vertical doublet has circular symmetry about the position of the doublet (i.e., about the observation point in Figure 4.9); furthermore the magnetic field on perfect ground is zero directly below the vertical doublet, provided $x_o > 0$, where x_o is the height of the doublet above ground (see Appendix 4B). Consequently, it is found that the region, on the surface of integration, in the immediate vicinity of the observation point does <u>not</u> make a significant contribution to the value of the surface integral G_x. In this respect there is a direct contrast between G_x and G_z : inspection and evaluation of Eq. (4.24) indicate that the value of G_z <u>is</u> principally determined by contributions to the surface integral from the area directly below the observation point (i.e., the position of the horizontal doublet).

The second justification for neglecting E_x^s is associated with the relative importance of different parts of the antenna. We are concerned with antennas for which the radiation is principally associated with

wire(s) parallel to the interface. In the present problem, the open-circuit voltage V_{OC} at the terminal of the receiving antenna can be expressed as the sum of two terms : V_z, associated with currents induced in the (horizontal) wire parallel to the z-axis; and V_x, associated with currents induced in the (vertical) wires parallel to the x-axis:

$$V_{OC} = V_z + V_x \tag{4.32}$$

Now the second justification can be stated explicitly : it can be assumed that V_x is much less important than V_z in determining the radiation characteristics.

The last assumption requires certain qualifications for which it is necessary to anticipate some results, both theoretical and experimental, which will be presented in the next chapter. In the main beam of the antenna, radiation characteristics are largely determined by V_z (associated with the horizontal wire); V_x (associated with the vertical wires) has a small influence on the antenna gain, and a marginal effect on the beam-width. Consequently, the <u>overall</u> error in the main beam, due to approximations in the value of E_x, tends to be negligible. On the other hand, the side-lobe levels of the antenna are greatly influenced by V_x; but we are primarily interested in the level and not the detailed structure of the side-lobes. Thus an approximate knowledge of E_x is sufficient for our purposes.

4.6. Radiation Pattern of IPA

4.6.1. Problem Definition

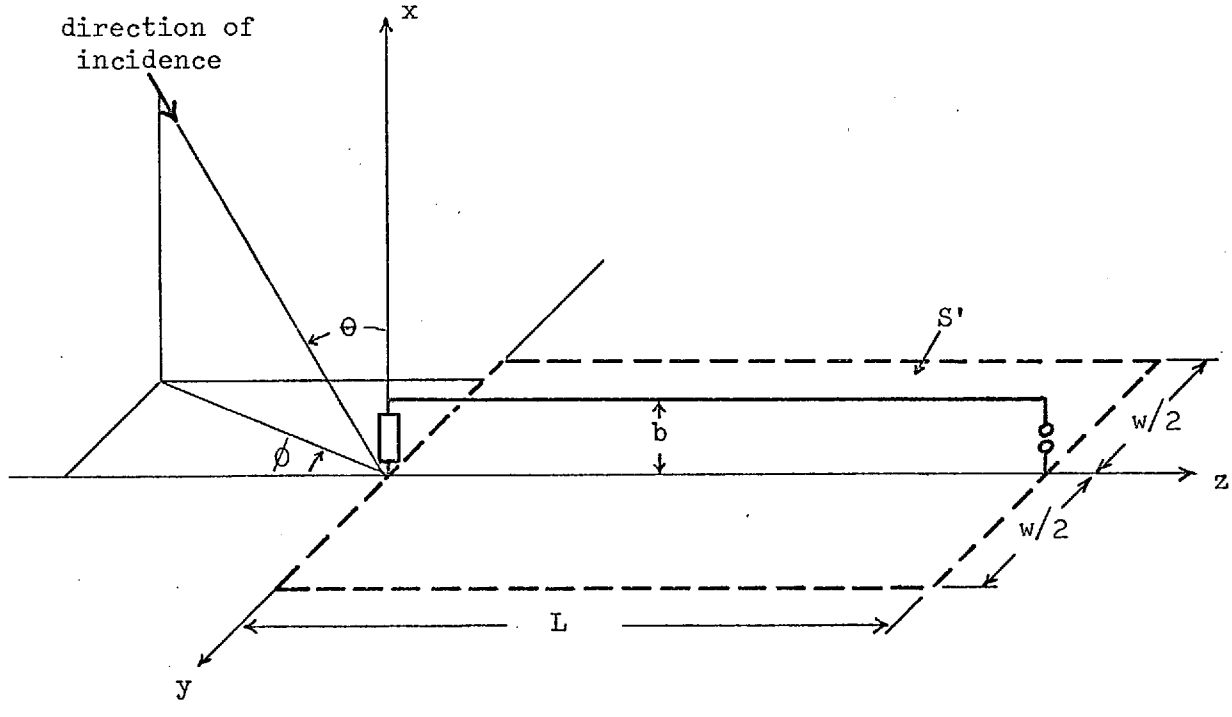


Fig. 4.15 IPA_1 Configuration for (Receiving) Pattern Calculations

The antenna configuration considered in this section is IPA_1, as depicted in Fig. 4.15. The plane surface $x = 0$ is perfectly conducting except over the rectangular region S' defined by: $-\frac{w}{2} < y < \frac{w}{2}$; $0 < z < L$. For convenience, directions parallel and normal to the plane $x = 0$ will be referred to as horizontal and vertical respectively. The antenna wires lie in the vertical plane $y = 0$: the antenna terminal is located at $z = L$; and a load impedance Z_L is connected between the horizontal wire and the conducting plane at $z = 0$. It will be assumed that $Z_L = Z_c$, where Z_c is the characteristic impedance of the antenna, determined by Eqs. (3.35) and (3.80): this condition ensures that there will be no reflected wave along the antenna due to a mismatch at $z = 0$, whether the antenna is transmitting

or receiving.

The radiation pattern can be obtained by deriving an expression for open-circuit voltage V_{OC}, at the antenna terminal, due to a uniform plane wave incident from the direction (θ, ϕ); such an incident wave can be represented by specifying the magnetic field $\underline{H}^i$:

$$\underline{H}^i = \underline{H}_o \exp[- jk(- S_1 x + S_2 y + Cz)] \tag{4.33}$$

where S_1, S_2 and C are the direction cosines:

$$S_1 = \cos \theta \tag{4.34}$$

$$S_2 = \sin \theta \sin \phi \tag{4.35}$$

$$C = \sin \theta \cos \phi \tag{4.36}$$

The direction of incidence is defined by the unit vector $\underline{i}$ where

$$\underline{i} = - S_1 \underline{a}_x + S_2 \underline{a}_y + C \underline{a}_z \tag{4.37}$$

In a uniform plane wave, the field vectors must be transverse to the direction of propagation [Ref. 4.30]. Consequently $\underline{H}_o$ must lie in the $\theta - \phi$ plane, i.e.

$$\underline{H}_o = \underline{H}_\theta + \underline{H}_\phi \tag{4.38}$$

where $\underline{H}_\theta$ can be identified as the perpendicular polarized component of the incident wave, and $\underline{H}_\phi$ as the parallel polarized component. It can be shown that the rectangular components for each polarization are given by:

$$\underline{H}_\theta = - qH_o(- \sin \theta \, \underline{a}_x - \cos \theta \sin \phi \, \underline{a}_y - \cos \theta \cos \phi \, \underline{a}_z) \tag{4.39}$$

$$\underline{H}_{\phi} = - pH_o(- \cos \phi \, \underline{a}_y + \sin \phi \, \underline{a}_z) \qquad (4.40)$$

where H_o is the amplitude of the incident magnetic field. It should be noted that a negative sign has been introduced in the above equations; this was for convenience only : so that H_y and E_z have positive values when the direction cosines are all positive. p and q are polarization factors related by the following equation:

$$p^2 + q^2 = 1 \qquad (4.41)$$

A polarization angle τ can be defined, corresponding to the above equation, such that

$$p = \cos \tau; \qquad q = \sin \tau \qquad (4.42)$$

The above treatment of polarization components is in accordance with standard practice [Refs. 4.31, 4.32], but more restrictive because we shall only consider linearly polarized radiation: for instance, quantities p and q are directly related to the vector effective height of a linearly polarized antenna which could be considered as the 'source' of the incident wave [Ref. 4.31].

In the present application, p is associated with the principal component of polarization, and q with the cross-polarized component; the same letters will be used as subscripts to emphasize either one or the other polarization.

4.6.2. Application of the Reciprocity Theorem

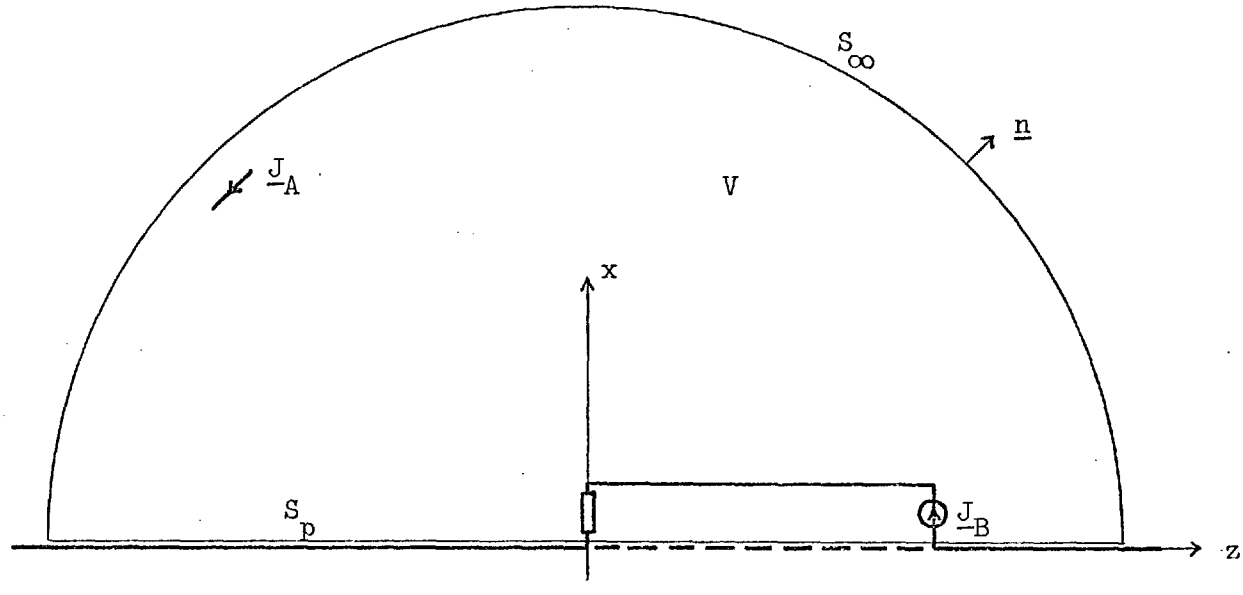


Fig. 4.16 Antenna Configuration for Application of the Reciprocity Theorem

The reciprocity theorem can be stated by the following equation [Ref. 4.33]:

$$\int_S (\underline{E}_A \wedge \underline{H}_B - \underline{E}_B \wedge \underline{H}_A) \cdot \underline{n}\, ds$$

$$= \int_V [(\underline{E}_A \cdot \underline{J}_B - \underline{H}_A \cdot \underline{K}_B) - (\underline{E}_B \cdot \underline{J}_A - \underline{H}_B \cdot \underline{K}_A)]dv \qquad (4.43)$$

where $\underline{E}_A$ and $\underline{H}_A$ are the fields due to a distribution of electric and magnetic current densities $\underline{J}_A$ and $\underline{K}_A$; and we are considering the interaction between two sets of sources $(\underline{J}_A, \underline{K}_A)$ and $(\underline{J}_B, \underline{K}_B)$ within a volume V defined by a closed surface S. The constitutive parameters, permeability and permittivity, of the medium in V are isotropic.

In the present application, we shall consider sources consisting of (a) $\underline{J}_A$ only, corresponding to a current element in the far field of the antenna IPA_1; and (b) $\underline{J}_B$ only, corresponding to a constant current generator connected between the terminals of IPA_1. Surface S consists of a hemispherical surface S_∞ at infinity and a plane surface S_p coincident with the plane interface x = 0, as depicted in Figure 4.16.

Since volume V contains all the sources, the surface integral in Eq. (4.43) vanishes [Ref. 4.33], and we obtain

$$\int_V (\underline{E}_A \cdot \underline{J}_B)dv = \int_V (\underline{E}_B \cdot \underline{J}_A)dv \qquad (4.44)$$

It should be noted that all the field quantities must be evaluated in the presence of the antenna structure and the plane conductor.

Since $\underline{J}_B$ represents a current generator, we can write,

$$\underline{J}_B = \underline{a}_x I_g \delta(y)\delta(z-L)u(x)u(h-x) \qquad (4.45)$$

where $\delta(y)$ is the Dirac-delta function and u(x) the unit step function; h is the length of the small gap between the antenna terminals.

Evaluating the left-hand side of Eq. (4.44),

$$\int_V (\underline{E}_A \cdot \underline{J}_B)dv = + I_g \int_0^h E_{Ax}(x, 0, L)dx$$

therefore

$$\int_V (\underline{E}_B \cdot \underline{J}_A)dv = - IgV_{OC} \qquad (4.46)$$

where V_{OC} is the open-circuit voltage at the terminals of the receiving

antenna due to radiation from $\underline{J}_A$.

According to Love's equivalence principle [Ref. 4.34], if the antenna wire is replaced by a source distribution in space identical to the surface currents ($\underline{J}_w$, $\underline{K}_w$) on the wire, then the field ($\underline{E}_B$, $\underline{H}_B$) will remain the same outside the wires. Applying the reciprocity theorem to the proposed source distribution in space,

$$\int_V [\underline{E}'_A \cdot (\underline{J}_w + \underline{J}_B) - \underline{H}'_A \cdot \underline{K}_w]dv = \int_V \underline{E}_B \cdot \underline{J}_A \, dv \qquad (4.47)$$

where $\underline{E}'_A$ and $\underline{H}'_A$ are the radiation fields of $\underline{J}_A$ <u>in the absence</u> of the antenna wire, but taking into account scattering by the interface [Ref. 4.35]. $\underline{K}_w$ is zero for a perfectly-conducting wire; in the present problem $\underline{K}_w$ is non-zero only on the surface of the load impedance Z_L. However, provided the physical diameter and length of Z_L are small fractions of wavelength, $\underline{H}'_A \cdot \underline{K}_w$ can be neglected in Eq. (4.47).

We shall now assume that the wire diameter is small enough so that $\underline{J}_w$ can be represented as a line current. Then the wire currents can be written as

$$I_z(b, 0, z) = -I_o e^{-\gamma(L-z)} \quad ; \quad 0 \leq z \leq L \qquad (4.48)$$

$$I_x(x, 0, 0) = -I_o e^{-\gamma(L-z)} e^{-jk(b-x)} \quad ; \quad 0 \leq x \leq b \qquad (4.49)$$

$$I_x(x, 0, L) = I_o e^{jk(b-x)} \quad ; \quad h \leq x \leq b \qquad (4.50)$$

Allowing the terminal gap h to become infinitesimally small, we obtain the following expression for the generator current Ig, from the continuity of current:

$$I_g = I_o e^{+jkb} \tag{4.51}$$

In the above equations we have assumed that the current in the vertical wires has a propagation constant equal to that for free-space; for vertical wires short compared with wavelength, the effect of any error in this assumption is negligible.

Combining Eqs. (4.46) and (4.47) we obtain

$$V_{OC} = -\frac{1}{I_g} \int_V \underline{E}'_A \cdot (\underline{J}_w + \underline{J}_B) dv \tag{4.52}$$

Substitution in the above from Eqs. (4.48) through (4.51) leads to

$$V_{OC} = e^{-jkb}[V_z(b, 0, L) + e^{-jkb} e^{-\gamma L} V_x(0, 0, 0) - e^{jkb} V_x(0, 0, L)] \tag{4.53}$$

where

$$V_z(b, 0, L) = \int_0^L E'_{Az}(b, 0, z) e^{-\gamma(L-z)} dz \tag{4.54}$$

$$V_x(0, 0, 0) = \int_0^b E'_{Ax}(x, 0, 0) e^{jkx} dx \tag{4.55}$$

$$V_x(0, 0, L) = \int_0^b E'_{Ax}(x, 0, L) e^{-jkx} dx \tag{4.56}$$

The response of the receiving antenna is related to its far field when transmitting by Eq. (4.46); the latter can be written

$$(E_\theta I_{A\theta} + E_\phi I_{A\phi})\delta h = - V_{OC} I_o e^{jkb} \tag{4.57}$$

where it has been assumed that $\underline{J}_A$ consists of two short current elements of moments $I_{A\theta}\delta h$ and $I_{A\phi}\delta h$ in directions $\underline{a}_\theta$ and $\underline{a}_\phi$ respectively. Substitution from Eqs. (4.18), (4.39) and (4.40) for the current moments yields

$$(E_\theta p - E_\phi q) = \frac{jk}{4\pi R} \frac{I_o e^{jkb}}{H_o} (V_p + V_q) \tag{4.58}$$

where V_p and V_q are open-circuit voltages due to incoming waves which are parallel-polarized and perpendicular-polarized respectively; the amplitude of the incident magnetic field is pH_o for parallel--polarization, and qH_o for perpendicular polarization.

In the above equation, the principal-polarization component is obtained by considering $p = 1$ and $q = 0$;

$$E_\theta = \frac{jk}{4\pi R} \frac{I_o e^{jkb}}{H_o} V_p \tag{4.59}$$

Similarly, to obtain the cross-polarization component we set $p = 0$, $q = 1$;

$$E_\phi = - \frac{jk}{4\pi R} \frac{I_o e^{jkb}}{H_o} V_q \tag{4.60}$$

A quantity of interest is the polarization ratio r_p of the cross--polarization component of the field to the principal-polarization component:

$$r_p = \left| \frac{E_\phi}{E_\theta} \right| = \left| \frac{V_q}{V_p} \right| \tag{4.61}$$

4.6.3. Principal-Polarization Radiation Pattern; Evaluation of V_p

Only the parallel-polarized component of the incident wave is associated with the primary pattern of the antenna; this corresponds to the magnetic field component $\underline{H}_\phi$ in Eq. (4.38).

To evaluate Eq. (4.54), we require the value of E'_{Az} : from Eqs. (4.29) and (4.40)

$$E'_{Az}(b, 0, z) = E^o_z(b, 0, 0)\exp(-jkCz) + E^s_z \exp(- jkCz) \tag{4.62}$$

where

$$E^o_z(b, 0, 0) = pH_o Z_o \cos\phi \cos\theta(e^{jkS_1 b} - e^{-jkS_1 b}) \tag{4.63}$$

and

$$E^s_z = pH_o Z_o \cos\phi \, Z_{zn} G_z \tag{4.64}$$

G_z is given by Eq. (4.24), but the latter equation can only be evaluated by numerical integration. Instead, we shall use the following approximation for G_z, based on graphical results for G_z presented in Sub-section 4.5.3.:

$$G_z = 2.0\, e^{-\alpha_1 \frac{kb}{2\pi}} f(w)[1 - e^{-\alpha_3 \frac{kz}{2\pi}}] \quad \text{for } C \geq 0 \tag{4.65}$$

and

$$G_z = 2.0\, e^{-\alpha_1 \frac{kb}{2\pi}} f(w) \quad \text{when } C < 0 \tag{4.66}$$

where

$$\alpha_1 = 0.74 \tag{4.67}$$

$$f(w) = 1 - \frac{1}{8.58 \frac{w}{\lambda_o} (1 - 0.072 \frac{w}{\lambda_o})} \tag{4.68}$$

$$\alpha_3 = \frac{2.38}{f^2} \tag{4.69}$$

Integration of Eq. (4.54) leads to the following result:

$$V_{zp}(b, 0, L) = pH_o Z_o \cos \phi \, L \, e^{-\gamma L}[A_1 + A_2] \tag{4.70}$$

where

$$A_1 = \cos \theta[e^{jkS_1 b} - e^{-jkS_1 b}] + 2.0 \, Z_{zn} e^{\frac{\alpha_1}{2\pi} kb} f(w) \quad F_s(\psi_1) \tag{4.71}$$

$$A_2 = -2.0 \, Z_{zn} e^{-\frac{\alpha_1}{2\pi} kb} f(w) F_s(\psi_2) \tag{4.72}$$

$$F_s(\psi) = \frac{e^{2j\psi} - 1}{2j\psi} = e^{j\psi} \frac{\sin \psi}{\psi} \tag{4.73}$$

$$\psi_1 = \frac{kL}{2}(\frac{\gamma}{jk} - C) \tag{4.74}$$

$$\psi_2 = \frac{kL}{2}(\frac{\gamma - \frac{k}{2\pi} \alpha_3}{jk} - C) \tag{4.75}$$

To evaluate Eqs. (4.55) and (4.56), we require the value of $E_{Ax}'(x, 0, z)$. As explained in Sub-section 4.5.4., we shall use the approximation $E_{Ax}' \simeq E_x^o$, where E_x^o is the corresponding plane wave solution when the ground is perfectly-conducting. Consequently,

$$E_{Ax}'(x, 0, z) = pH_o Z_o \sin \theta \exp(-jkCz)[\exp(jkS_1 x) + \exp(-jkS_1 x)] \tag{4.76}$$

Substitution from the above equation into Eqs. (4.55) and (4.56) leads to the following expressions respectively

$$V_{xp}(0, 0, 0) = pH_o Z_o b \sin\theta[F_s(\psi_3^+) + F_s(\psi_3^-)] \qquad (4.77)$$

$$V_{xp}(0, 0, L) = pH_o Z_o b \sin\theta[F_s(-\psi_3^+) + F_s(-\psi_3^-)]e^{-jkCL}$$

$$= e^{-jkCL} V_{xp}(0, 0, 0) \qquad (4.78)$$

where

$$\psi_3^+ = \frac{kb}{2}(1 + S_1) \qquad (4.79)$$

$$\psi_3^- = \frac{kb}{2}(1 - S_1) \qquad (4.80)$$

and $F_s(\psi)$ is given by Eq. (4.73). The open-circuit voltage V_p is given by Eq. (4.53) which yields

$$V_p = e^{-jkb}[V_{zp}(b, 0, L) + e^{-jkb-\gamma L} V_{xp}(0, 0, 0)$$

$$- e^{+jkb-jkCL} V_{xp}(0, 0, 0)] \qquad (4.81)$$

When the antenna terminal is placed at a distance L' beyond the edge of the impedance-strip, i.e., at $z = L + L'$ (as in Fig. 5.7 or Fig. 5.8, Chapter V), then it can be shown that instead of Eq. (4.81) we obtain

$$V_p = e^{-jkb-\gamma L'} V_{zp}(b, 0, L)$$

$$+ V_{xp}(0, 0, 0)[e^{-jkb-\gamma L} - e^{jkb-jkC(L+L')+\gamma L'}] \qquad (4.82)$$

The above equation is subject to the following approximations : (I) the mismatch due to the discontinuity at $z = L$ is negligible; (II) the phase change along the section $L < z < L+L'$ is adequately approximated by the factor $e^{-\gamma L'}$; and (III) the contribution to $V_z(b, 0, L)$ due to the section $L < z < L + L'$ is negligible. All these approximations are valid provided $L' \ll L$.

4.6.4. Cross-Polarization Radiation Pattern : Evaluation of V_q

The cross-polarized component of radiation is obtained by considering a perpendicular-polarized incident wave; the corresponding magnetic field component is $\underline{H}_\theta$, Eq. (4.38).

The analysis leading to an expression for the open-circuit voltage V_q is similar to that presented in the last section. The approximation $E_{Ax}' \simeq E_x^o$ this time has the effect that V_{xq} becomes zero. To obtain V_{zq}, the value of E_{Az}' is required : let

$$E_{Az}'(b, 0, z) = E_z^o(b, 0, 0)\exp(-jkCz) + E_z^s\exp(-jkCz)$$

In the above equation, the first term on the right-hand-side is the field when the ground is perfectly-conducting, and the second term is the perturbation component associated with scattering by the impedance strip. By an analysis analogous to that presented in Sub-section 4.5.2., it can be shown that

$$E_z^o(b, 0, 0) = qH_oZ_o\sin\phi[e^{jkS_1b} - e^{-jkS_1b}] \qquad (4.83)$$

and

$$E_z^s = qH_oZ_o \sin\phi \cos\theta Z_{zn}G_z \qquad (4.84)$$

where G_z is given by Eqs. (4.65) and (4.66).

Substituting for E_{Az}' in Eq. (4.53), the following result is obtained:

$$V_q = e^{-jkb} V_{zq}(b, 0, L) \tag{4.85}$$

$$V_{zq}(b, 0, L) = qH_o Z_o \sin \phi \, L e^{-\gamma L}[B_1 + B_2] \tag{4.86}$$

where

$$B_1 = [e^{jkS_1 b} - e^{-jkS_1 b}] + 2.0 \cos \theta \, Z_{zn} e^{-\frac{\alpha_1}{2\pi} kb} f(w) \quad F_s(\psi_1) \tag{4.87}$$

$$B_2 = -2.0 \cos \theta \, Z_{zn} e^{-\frac{\alpha_1}{2\pi} kb} f(w) F_s(\psi_2) \tag{4.88}$$

$F_s(\psi)$, ψ_1 and ψ_2 are given by Eqs. (4.73) through (4.75).

When the antenna terminal is at $z = L + L'$ (as in Figs. 5.7 and 5.8), it can be shown that instead of Eq. (4.85) we obtain

$$V_q = e^{-jkb - \gamma L'} V_{zq}(b, 0, L) \tag{4.89}$$

subject to the same approximations required for Eq. (4.82).

4.7. Power Gain of the IPA

The absolute power gain of the antenna can be defined as [Ref. 4.36]

$$G(\theta, \phi) = \frac{P_{rec}(\theta, \phi)}{P_{iso}} \tag{4.90}$$

where $P_{rec}(\theta, \phi)$ is the power transferred to a (conjugate matched) receiver by the antenna, when a uniform plane wave is incident on the antenna from the direction (θ, ϕ); the plane wave is assumed to have a particular polarization. P_{iso} represents the power transferred to a (matched) receiver by an isotropic antenna, and is given by [Ref. 4.36]

$$P_{iso} = Z_o H_o^2 \frac{\lambda_o^2}{4\pi} \tag{4.91}$$

where H_o is the (r.m.s.) amplitude of the incident magnetic field.

Generally, the gain is referred to a particular direction (θ_o, ϕ_o): often the direction chosen is that which maximizes $G(\theta, \phi)$. However we shall refer the gain to the end-fire direction, even if the gain is not maximum in this direction, i.e.,

$$G_o = G(\frac{\pi}{2}, 0) \tag{4.92}$$

Similarly the polarization of the incident wave is usually chosen such that the gain is maximized. We shall refer the gain to the particular polarization previously referred to as 'parallel-polarized' (i.e., $\underline{H}_{inc} = \underline{H}_{\phi}$); which in fact maximizes $G(\frac{\pi}{2}, 0)$.

For IPA_1 configuration of Fig. 4.15, application of Thevenin's theorem yields

$$P_{rec}(\frac{\pi}{2}, 0) = \frac{V_{P1}^2}{4R_c} \tag{4.93}$$

where R_c is the real part of the characteristic impedance Z_c; and V_{p1} is the (r.m.s.) open-circuit voltage given by Eq. (4.81) with $p = 1$, $\theta = \frac{\pi}{2}$, and $\phi = 0$. Finally, Eq. (4.90) yields

$$G_{01} = \frac{V_{P1}^2}{R_c} \cdot \frac{\pi}{Z_o H_o^2 \lambda_o^2} \quad : \quad \text{for IPA}_1 \tag{4.94}$$

For IPA_2 configuration corresponding to Fig. 4.3, the open-circuit voltage V_{P2} is equal to V_{P1}. This follows from the symmetry considerations of Section 4.4 : each half of the antenna generates an open-circuit voltage $\frac{1}{2} V_{P1}$, since in the transformed problem, Fig. 4.8, the amplitude of the incident wave is halved; the two voltages appear in series, by virtue of the antisymmetric circuit of Fig. 4.4(b), giving rise to a total open-circuit voltage of V_{P1}. However, the antenna input impedance is now $2Z_c$: consequently the gain of IPA_2 is given by

$$G_{02} = \frac{G_{01}}{2} \tag{4.95}$$

It should be noted that when IPA_1 is considered in free-space, and <u>not</u> flush with a perfectly conducting plane of infinite extent, its gain G_{01}' is given by:

$$G_{01}' = \frac{G_{01}}{4} = \frac{G_{02}}{2} \tag{4.96}$$

The above result is based on the following variational approximation : when the direction of incidence is $(\frac{\pi}{2}, \phi)$, the magnetic field tangential to the impedance strip is equal to the incident magnetic field, for parallel polarization.

4.8. Directivity of the IPA

The ratio of radiation intensity $U(\theta_o, \phi_o)$, in a particular direction (θ_o, ϕ_o), to the average radiation intensity of the transmitting antenna is the directivity D of the antenna. For consistency with our definition of power gain G_o, Eq. (4.92), we shall take the above direction to be $(\frac{\pi}{2}, 0)$. Thus

$$D_o = \frac{4\pi U(\frac{\pi}{2}, 0)}{\int U(\theta,\phi)d\Omega} \tag{4.97}$$

where $d\Omega = \sin\theta \, d\theta \, d\phi$

$$U(\theta, \phi) = \frac{1}{Z_o} \left[|E_\theta(\theta,\phi)|^2 + |E_\phi(\theta,\phi)|^2 \right] \tag{4.98}$$

E_θ and E_ϕ are given bynEqs.(4.59) and (4.60) respectively. Substitution into Eq. (4.97) yields

$$D_o = \frac{4\pi \, |V_p(\frac{\pi}{2}, 0)|^2}{\int_0^{\pi}\int_0^{2\pi} \left(|V_p(\theta, \phi)|^2 + |V_q(\theta, \phi)|^2 \right) \sin\theta \, d\phi d\theta} \tag{4.99}$$

where V_p and V_q are given by Eqs. (4.81) and (4.85) respectively. It is evident that Eq. (4.99) can only be evaluated by numerical integration.

In design and evaluation of communication systems a quantity of interest is η, the ratiation efficiency of the antenna, and is given by

$$\eta = \frac{G_o}{D_o} \tag{4.100}$$

η can also be interpreted as the ratio of the power radiated by the antenna to the total power input, when the antenna is transmitting; thus η is a measure of the antenna losses. In the case of the IPA, the only significant losses arise from ohmic losses in the load impedance $Z_L (= Z_c)$, at z = 0 in Fig. 4.15. Consequently the quantity $(1 - \eta)$ represents the proportion of input power which is dissipated in the matching impedance at the end of the antenna.

It is evident that directivity D_{02} of IPA_2 is one half the directivity D_{01} of IPA_1 : this is because IPA_1 radiates into half-space only, whereas IPA_2 radiates into the whole space. Since $G_{02} = \frac{1}{2} G_{02}$, and $D_{02} = \frac{1}{2} D_{01}$, it follows that $\eta_2 = \eta_1$, where η_1 and η_2 are the radiation efficiencies of IPA_1 and IPA_2 respectively.

APPENDIX 4A

Field of horizontal doublet above perfectly-conducting (plane) ground

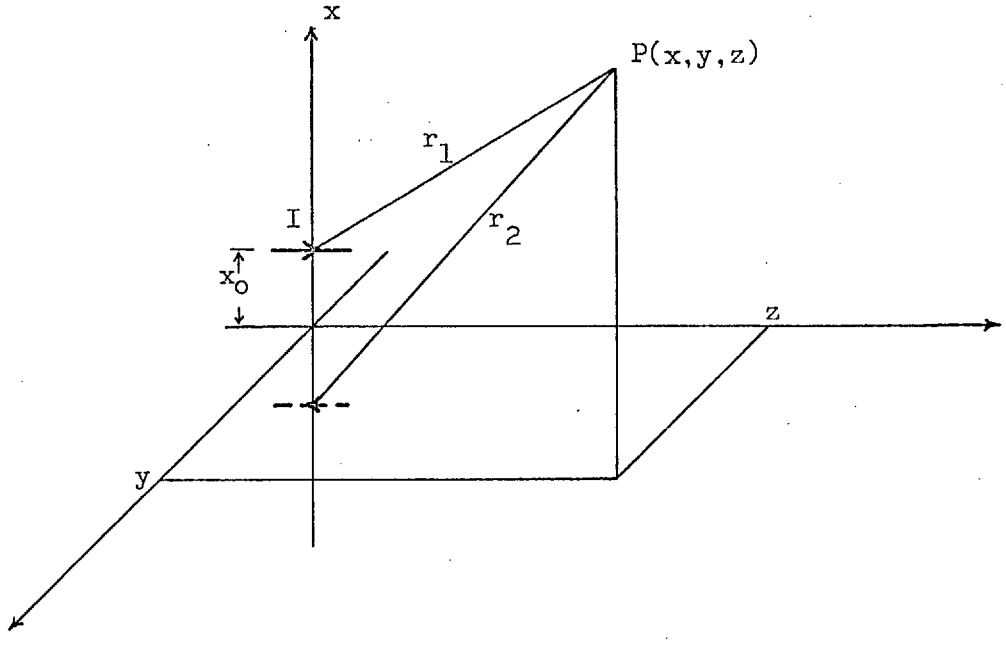


Fig. 4A.1 Doublet Configuration for Field Calculations

For a short current element $I\delta h$ at $(x_o, 0, 0)$, above a perfectly conducting plane $x = 0$, the magnetic vector potential $\underline{A}$, at point $P(x, y, z)$, is given by image theory:

$$\underline{A} = A_z \underline{a}_z = \frac{\mu}{4\pi} I\delta h \left(\frac{e^{-jkr_1}}{r_1} - \frac{e^{-jkr_2}}{r_2}\right)\underline{a}_z \qquad (4A.1)$$

where r_1 and r_2 are distances from the doublet and its image respectively, to the point P. Thus

$$r_1^2 = z^2 + y^2 + (x - x_o^2) \qquad (4A.2)$$

$$r_2^2 = z^2 + y^2 + (x + x_o)^2 \qquad (4A.3)$$

k is the free-space wave-number, and a time variation exp(jωt) has been assumed.

The magnetic field $\underline{H}$ is given by

$$\underline{H} = \frac{1}{\mu} \nabla \wedge \underline{A} \tag{4A.4}$$

$$\underline{H} = \frac{1}{\mu} \left(\frac{\partial A_z}{\partial y} \underline{a}_z - \frac{\partial A_z}{\partial x} \underline{a}_y\right) \tag{4A.5}$$

Noting that

$$\frac{\partial}{\partial x}\left[\frac{1}{r} \exp(-jkr)\right] = (-jk - \frac{1}{r})\frac{e^{-jkr}}{r} \frac{\partial r}{\partial x} \tag{4A.6}$$

$$\frac{\partial r_1}{\partial x} = \frac{(x - x_o)}{r_1} \quad ; \quad \frac{\partial r_1}{\partial y} = \frac{y}{r_1} \tag{4A.7}$$

$$\frac{\partial r_2}{\partial x} = \frac{(x + x_o)}{r_2} \quad ; \quad \frac{\partial r_2}{\partial y} = \frac{y}{r_2} \tag{4A.8}$$

it is evident that on the plane $x = 0$

$$r_1 = r_2 = r \tag{4A.9}$$

$$H_z(0, y, z) \equiv 0 \tag{4A.10}$$

The required result for the component H_y is easily obtained by substitution into Eq. (4A.5):

$$H_y(0, y, z) = -\frac{I\delta h}{2\pi} (j + \frac{1}{kr}) \frac{e^{-jkr}}{r^2} k x_o \tag{4A.11}$$

APPENDIX 4B

Field of a vertical doublet above perfectly-conducting (plane) ground

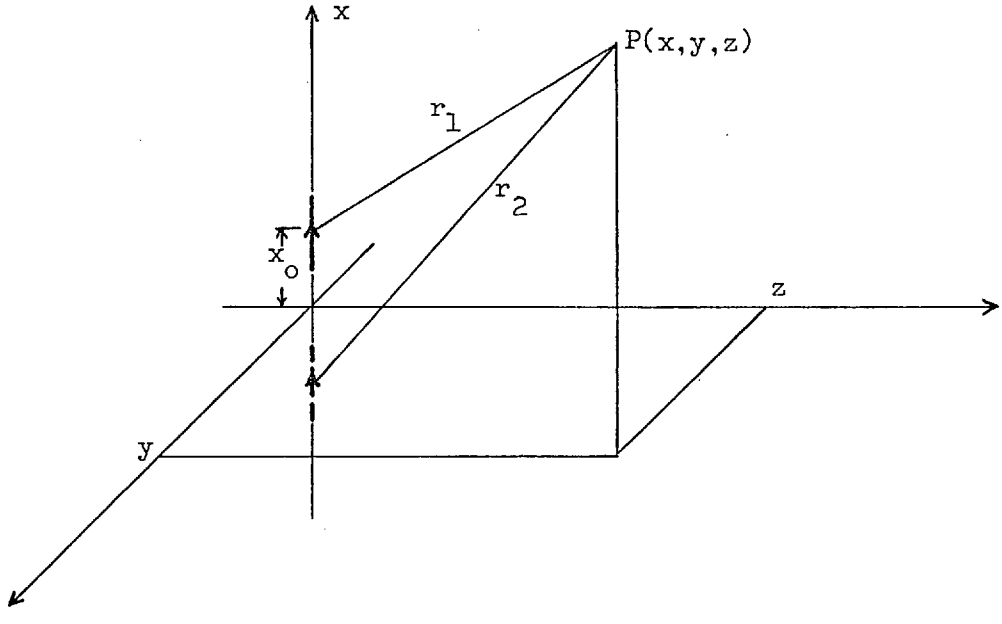


Fig. 4B.1 Doublet Configuration For Field Calculations

Considering a current element $I\delta h$ directed along the x-axis, at height x_o above the perfectly-conducting plane x = 0, the magnetic vector potential $\underline{A}$, at point P(x, y, z), is given by image theory:

$$\underline{A} = A_x \underline{a}_x = \frac{\mu}{4\pi} I\delta h\left(\frac{e^{-jkr_1}}{r_1} + \frac{e^{-jkr_2}}{r_2}\right) \qquad (4B.1)$$

where k is the free-space wave-number, and a time variation exp(jwt) has been assumed. r_1 and r_2 are distances from the doublet and its image respectively, to the point P (Figure 4B.1). Thus

$$r_1^2 = z^2 + y^2 + (x - x_o)^2 \qquad (4B.2)$$

$$r_2^2 = z^2 + y^2 + (x + x_o)^2 \tag{4B.3}$$

The magnetic field $\underline{H}$ is given by

$$\underline{H} = \frac{1}{\mu} \nabla \wedge \underline{A} \tag{4B.4}$$

$$= \frac{1}{\mu} \left(\frac{\partial Ax}{\partial z} \underline{a}_y - \frac{\partial Ax}{\partial y} \underline{a}_z\right) \tag{4B.5}$$

To evaluate $\underline{H}$, the following relations are required:

$$\frac{\partial}{\partial y} \left(\frac{e^{-jkr}}{r}\right) = - \left(jk + \frac{1}{r}\right) \frac{e^{-jkr}}{r} \cdot \frac{y}{r} \tag{4B.6}$$

$$\frac{\partial}{\partial z} \left(\frac{e^{-jkr}}{r}\right) = - \left(jk + \frac{1}{r}\right) \frac{e^{-jkr}}{r} \cdot \frac{z}{r} \tag{4B.7}$$

On the perfectly-conducting plane $x = 0$, $r_1 = r_2 = r$. The required results for components H_y and H_z of the magnetic field, on the plane $x = 0$, are easily obtained by substitution into Eq. (4B.5):

$$H_y(0, y, z) = - \frac{I\delta h}{2\pi} \left(jk + \frac{1}{r}\right) \frac{z}{r^2} e^{-jkr} \tag{4B.8}$$

$$H_z(0, y, z) = - \frac{I\delta h}{2\pi} \left(jk + \frac{1}{r}\right) \frac{y}{r^2} e^{-jkr} \tag{4B.9}$$

REFERENCES

4.1. Collin, R.E.: 'The Receiving Antenna', published as Chapter 4 of "Antenna Theory", Part I (edited by Collin, R.E. and Zucker, F.J.), McGraw-Hill, 1969, pp 94-100.

4.2. Schelkunoff, S.A.: 'Principal and Complementary Waves in Antennas', Proc. I.R.E., Vol. 34, No. 1, pp 23-32, January, 1946.

4.3. Barlow, H.M. and Brown, J.: 'Radio Surface Waves', Oxford Clarendon Press, 1962, p. 156.

4.4. Barlow, H.M. and Brown, J.: Op. cit., p. 141.

4.5. Clemmow, P.C.: 'The Plane Wave Spectrum Representation of Electromagnetic Waves', Pergamon Press, 1966, pp 84-91.

4.6. Monteath, G.D.: 'Application of Compensation Theorem to Certain Radiation and Propagation Problems', Proc. I.E.E., Vol. 98, Part IV, pp 23-30, 1951.

4.7. Beverage, H.H., Rice, C.W. and Kellog, E.W.: 'The Wave Antenna : A New Type of Highly Directive Antenna', Journal of A.I.E.E., Vol. 42, pp 215-266, Feb., 1923.

4.8. Carter, P.S., Hansell, C.W. and Lindenblad, N.E.: 'Development of Directive Transmitting Antennas by R.C.A. Communications, Inc.', Proc. I.R.E., Vol. 19, No. 10, pp 1773-1777, October, 1931.

4.9. Jenssen, M.: 'On Radiation from Overhead Transmission Lines', Proc. I.E.E., Vol. 97, Part III, pp 166-178, 1950.

4.10. Laughlin, J.D.: 'Symposium on Operation of the Boulder Dam Transmission Line, Carrier Current Equipment', Trans. American I.E.E., Vol. 58, p. 147, 1939.

4.11. Belousov, S.P. and Yampolskii, V.G.: 'Single-Wire Medium-Wave Travelling-Wave Receiver Antennas', Radiotekhnika, Vol. 15,

pp 16-25, 1960.

4.12. Waite, J.R.: 'Radiation From a Ground Antenna', Canadian Journal of Technology, Vol. 32, No. 1, pp 1-9, January, 1954.

4.13. Seeley, E.W.: 'Optimum Reception Pattern of the Beverage Wave Antenna at Very Low Frequencies', Journal of Research of National Bureau of Standards, Vol. 67D, No. 4, pp 387-395, July - August, 1963.

4.14. dos Santos, A.F.: 'Multi-Beam Receiving Antenna For the Band 3-30 MHz', Doctoral Thesis, Imperial College, University of London, September 1970.

4.15. Kikuchi, H.: 'Investigation of Electromagnetic Noise and Interference Due to Power Lines in Japan, and Some Results from The Aspect of Electromagnetic Theory', Proc. Symposium on Electromagnetic Hazards, Pollution and Environmental Quality', Purdue University, May 8-9, 1972, pp 147-162.

4.16. Martin, C.A.: 'Ground Conductivity Considerations', Proc. Ocean '72 International Conference on Engineering in the Ocean Environment, 13-15 September, 1972 (published by I.E.E.E.), pp 125-127.

4.17. El-Enein, M.H.: 'A Leaky-Wave Transmitting Antenna for the Band 3-30 MHz', Doctoral Thesis, Imperial College, University of London, May, 1973.

4.18. dos Santos, A.F.: 'Electromagnetic-Wave Propagation along a Horizontal Wire Above Ground', Proc. I.E.E., Vol. 119, No. 8, pp 1103-1109, August 1972.

4.19. Hessel, A.: 'General Characteristics of Travelling-Wave Antennas', Published as Chapter 19 of "Antenna Theory", Part II (edited by Collin, R.E. and Zucker, F.J.), McGraw-Hill, 1969, pp 155-156 and 242-246.

4.20. Tamir, T.: 'Leaky-Wave Antennas', published as Chapter 20 of "Antenna Theory", Part II (edited by Collin, R.E. and Zucker, F.J.), McGraw-Hill, 1969, pp 262-266.

4.21. Weeks, W.L.: 'Antenna Engineering', McGraw-Hill, 1968, pp 31-34.

4.22. Kouyoumjian, R.G.: 'Asymptotic High Frequency Methods', Proc. I.E.E.E., Vol. 53, No. 8, pp 864-876, November, 1965.

4.23. Harrington, R.F.: 'Time-Harmonic Electromagnetic Fields', McGraw-Hill, 1961, pp 232-238.

4.24. Stratton, J.A.: 'Electromagnetic Theory', McGraw-Hill, 1941, p. 482.

4.25. Ramo, S., Whinnery, J.R. and Van Duzer, T.: 'Fields and Waves in Communication Electronics', Wiley, 1965, pp 193-194.

4.26. Silver, S. (editor): 'Microwave Antenna Theory and Design', McGraw-Hill, 1949, pp 138-9.

4.27. Ramo, S., Whinnery, J.R. and Van Duzer, T.: op. cit., pp 442-445, and 597-602.

4.28. Page, H.: 'Principles of Aerial Design', Iliffe, 1966, p.39.

4.29. Stratton, J.A.: Op. cit., pp 460-464.

4.30. Stratton, J.A.: Op. cit., pp 268-273.

4.31. Collin, R.E.: Op. cit., pp 103-109.

4.32. Tai, C.T.: 'On the Definition of the Effective Aperture of Antennas', I.R.E. Transactions on Antennas and Propagation, Vol. AP-9, No. 2, pp 224-225, March 1961.

4.33. Collin, R.E.: 'Electromagnetic Fields', published as Chapter 1 of "Antenna Theory", Part I (edited by Collin, R.E. and Zucker, F.J.), McGraw-Hill, 1969, pp 24-25.

4.34. Collin, R.E.: 'Radiation from Apertures', published as Chapter 3 of "Antenna Theory", Part I (edited by Collin, R.E.

and Zucker, F.J.), McGraw-Hill, 1969, pp 69-71.

4.35. Weeks, W.L.: Op. cit., pp 292-296 and p. 299.

4.36. Weeks, W.L.: Op. cit., p. 297.

CHAPTER V

FAR FIELD MEASUREMENTS

5.1. Introduction

In the best traditions of research, it was decided to complement the theoretical study of the IPA by an experimental evaluation of the far-field characteristics! However, certain limitations of the test--site and available equipment restricted the range and accuracy of measurements which would be carried out. The design of far-field experiments will be outlined later in this section.

In the next section, the choice of the Corner-Reflector-Antenna (CRA) as reference antenna is explained, and its physical parameters are given. Sections 5.3 and 5.4 are devoted to the description of two test-antennas constructed for E-plane and H-plane measurements respectively.

Three sets of preliminary measurements were carried out : to evaluate the test-site; to check the far-field conditions; and to calibrate the refererence antenna, CRA. These experiments are reported in Sub-sections 5.5.1, 5.5.2 and 5.5.3 respectively. Results of the main experiments are given in Section 5.6, together with theoretical results for comparison purposes.

The test-site which was chosen for carrying out antenna field measurements was the roof of the Electrical Engineering Building at Imperial College (Figures 5.1 and 5.2). Inspection of the site indicated that a maximum separation of 10 to 14 metres was feasible between the reference antenna and the test antenna. Consequently it was decided to construct a test antenna such that the Rayleigh range R_R would be 10 metres, where $R_R = L^2/\lambda_o$, and L is the length of the IPA.



Fig. 5.1 Photograph showing a view of the test-site from the turntable



Fig. 5.2 Photograph showing a view of the test-site from the reference-antenna mast

Furthermore, theory indicated that the antenna should be approximately 10 wavelengths in length at the top of the frequency-band; this result was based on the dimensions of the corrugated plane used for near-field measurements. Thus it was determined that the test antenna should be 1.0 metres long (approx.), and that field measurements should be made over a band 1.0 GHz to 3.0 GHz; this represented a scaling factor of 3:1 relative to the model for near-field measurements.

The facilities available for field measurements consisted of : a turntable and its remote-control panel; a mast on which a reference antenna could be mounted; two (Rhode & Schwartz) generators, covering frequency bands of 0.275 - 2.75 GHz and 2.7 - 4.2 GHz; a (Hewlett-Packard) Network-Analyser; a (Hewlett-Packard) X-Y Plotter; two lengths of (Andrews) low-loss semi-rigid coaxial-cable, 10 m. and 15 m. long; and other RF components such as directional couplers and tuners.

As the available facilities permitted measurement of radiation patterns only in the horizontal plane, two antennas were constructed to allow pattern measurements in both orthogonal planes $\theta = 90^{\circ}$ (H-plane) and $\phi = 0^{\circ}$ (E-plane). An IPA_1 was constructed (with a conducting ground-plane of finite extent) for H-plane measurements, and an IPA_2 for E-plane measurements. This procedure, to minimize errors due to ground reflections, was only possible because the performances of the two IPA's are inter-related, as pointed out in Section 4.4.

For any field measurement carried out on a test-site, there are (at least) three physical quantities which are pertinent to analysis and evaluation of data [Ref. 5.1]. These are: height of the (fixed) reference antenna above ground, H_R; height of the test antenna above ground, H_T; and the horizontal distance between the antennas, R. In



Fig. 5.3. CRA : Photograph of Reference Antenna, Mounted On the Mast for Horizontal Polarization

most of the field measurements carried out these parameters have had the following values

H-plane measurements : $R = 11$ m; $H_R = 2.45$ m; $H_T = 1.85$ m

E-plane measurements : $R = 11$ m; $H_R = 2.30$ m; $H_T = 2.20$ m

In later sections, the values of these quantities will be quoted only if the values differ from those given above.

5.2. The Reference Antenna

A necessary requirement for the reference antenna was found to be high directivity for the following reasons : (I) To minimize scattering effects due to other objects, such as other antennas, and due to the perimeter wall on the roof; (II) To minimize the effect of ground reflections, especially as the height of the test antenna was limited



Fig. 5.4. IPA_2 : Photograph of Test Antenna, Mounted on the Turntable for E-Plane Measurements

by the height of the turntable (~ 2 metres); (III) To minimize the transmission loss, and for better discrimination against interference. The antenna eventually chosen was the corner-reflector antenna (CRA): the following parameters were chosen based on a study of published design data [Ref. 5.2]:

corner-reflector angle	=	90°
width and length of each reflector	=	300 x 300 mm
dipole-to-apex spacing	=	55 mm
dipole length	=	110 mm

A photograph of the CRA is given in Fig. 5.2. A double-stub tuner was inserted in the coaxial cable feeding the CRA, to match the antenna to the line. For testing purposes, another (identical) CRA was also constructed.

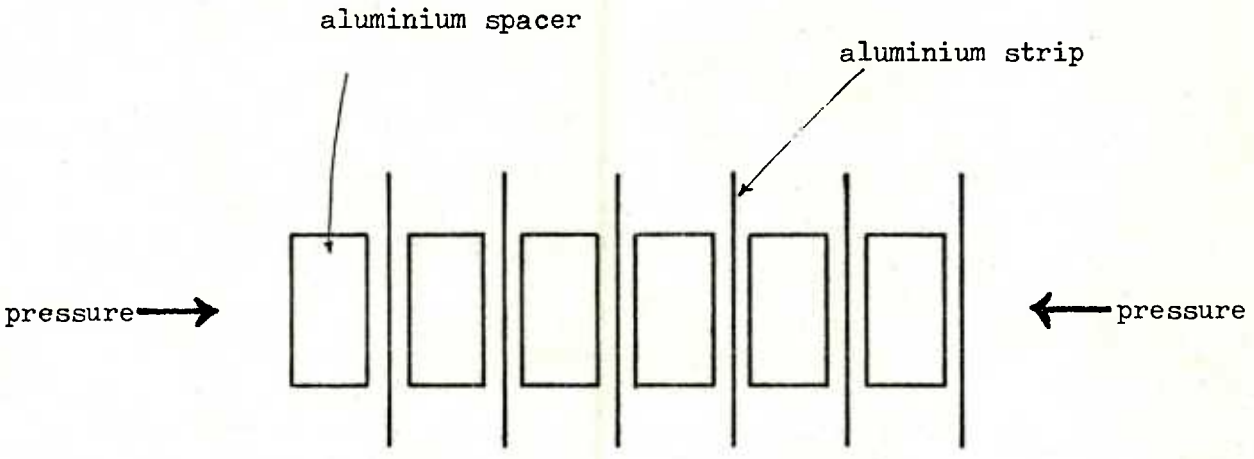


Fig. 5.5. Illustration of Method of Construction of a Double-Sided Corrugated Plane for IPA_2

5.3. Test Antenna for E-Plane Measurements

A photograph of IPA_2 constructed for radiation pattern measurements in the E-plane ($\phi = 0$) is given in Fig. 5.4 : pattern measurements were made in the horizontal plane, with the conducting plane of the antenna mounted in the vertical plane above the turntable. In this section, we shall briefly describe the construction of IPA_2.

The double-sided corrugated plane was constructed from two types of elements : aluminium strips, each 455 mm long and 35 mm x 1 mm in cross-section; and aluminium spacers, each 500 mm long and 20 mm x 9 mm in cross-section. The spacers were made of wooden blocks over which aluminium foil (thickness 0.1 mm) was tightly wrapped and glued-down : this construction had the advantages of low-cost and light weight. Then the spacers were placed in a frame (1.83 m x 0.57 m), and the strips were inserted between the spacers. Mechanical rigidity and electrical contact

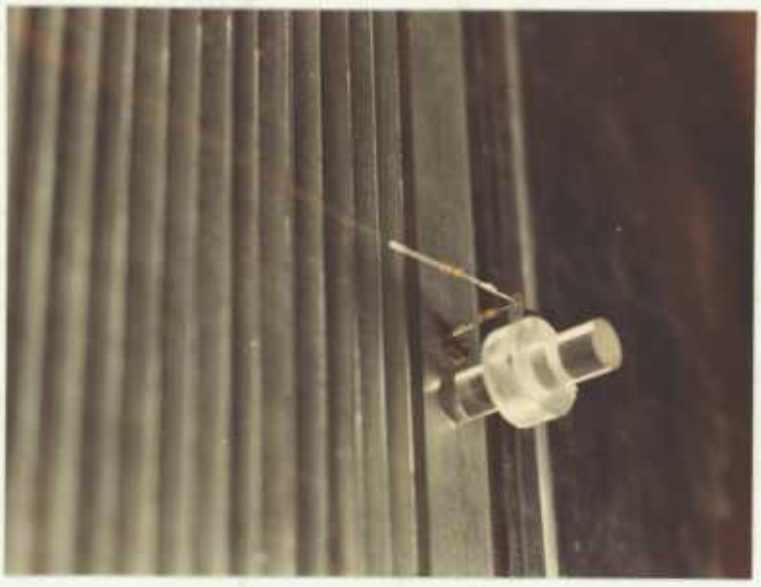


Fig. 5.6. Photograph of the Antenna Termination on Each Side of IPA_2

was ensured (in the resulting corrugated plane) by the application of pressure from both ends of the supporting frame. The construction principle is depicted in Figure 5.5. It should be noted that the excess space in the frame was employed to provide 'ground-plane' extensions on both sides of the corrugated-plane region, as seen in Fig. 5.4. These ground-plane extensions were made of aluminium sheets.

Figure 5.6. shows a photograph of the antenna termination (an identical arrangement was used on the other side of the corrugated plane). The termination consisted of two standard resistors connected in series with the antenna wire : each resistor was of carbon-film type, ¼ watt rating, and had a nominal value of 160 ohms (5% tolerance). The nominal characteristic impedance of the antenna was 328 ohms approximately. Various types and values of termination were tried, and for each arrangement the standing-wave ratio was measured along the antenna : the

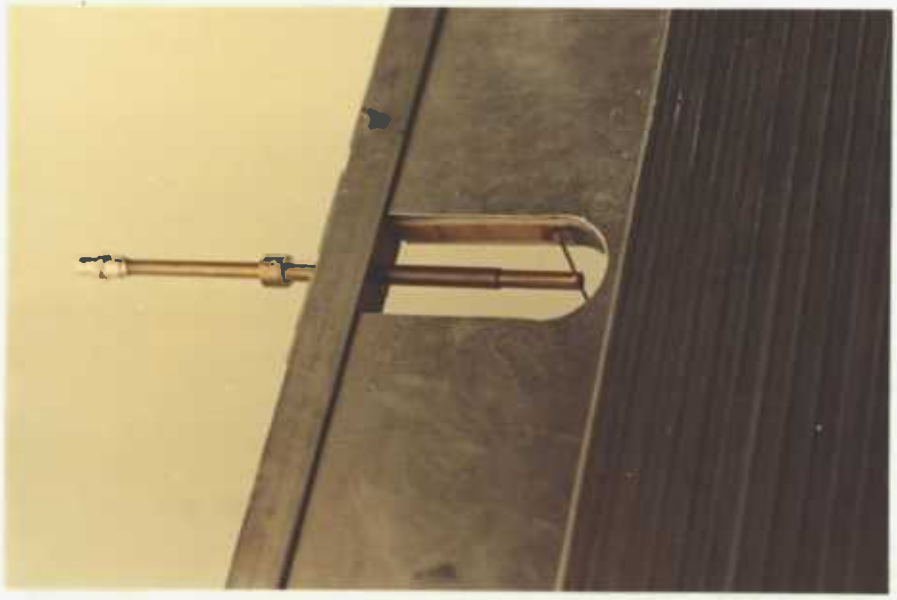


Fig. 5.7. Photograph of the Launching Device Used at the Input to IPA_2

termination chosen was the one for which SWR measurements indicated minimum reflection power over the frequency-band (SWR < 3 dB corresponding to reflection coefficient < - 15 dB).

The feed structure used at the input of IPA_2 is shown in Figure 5.7 : this launching device acts as a balun (with an impedance transformation of 4 to 1), and its construction was almost identical to a slot-fed dipole as described by S. Silver [Ref. 5.3]. In this case, the slot length was made variable by adding a sliding (cylindrical) conductor which fitted tightly over the outer conductor of the coaxial line. Prior to each field measurement, the slot length was adjusted to a quarter of the free-space wave-length. A double-stub tuner, was employed to obtain the impedance transformation required for matching the coaxial cable to the antenna.

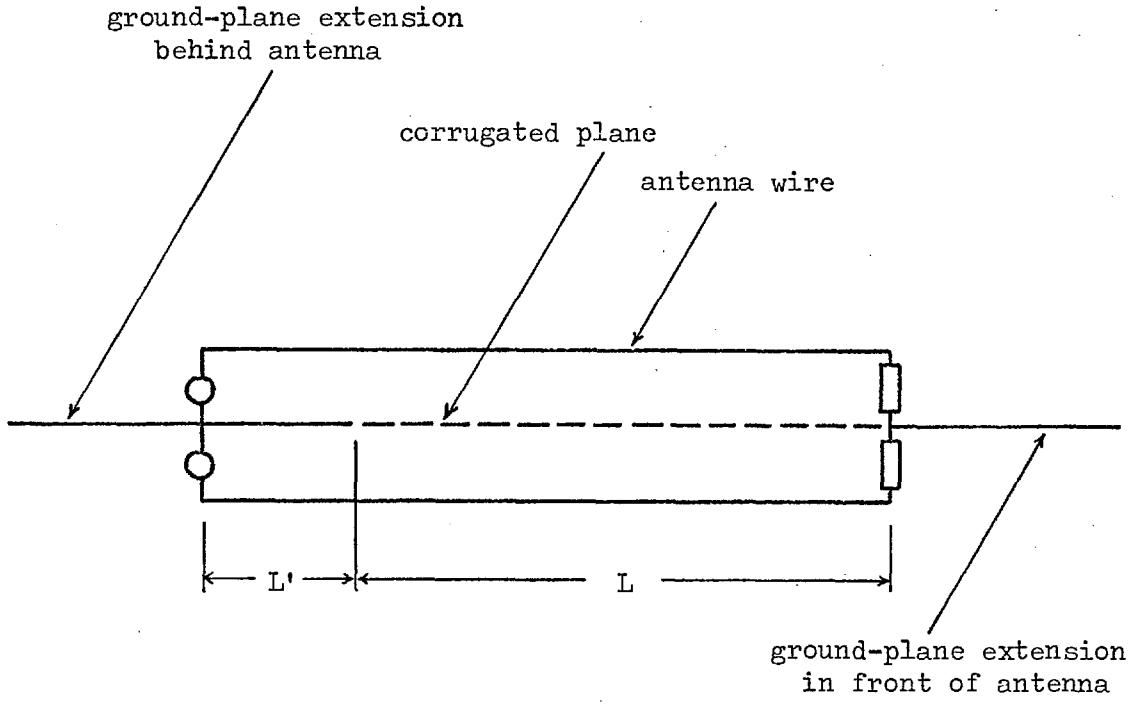


Fig. 5.8. Schematic Representation of Constituent Parts of IPA_2 : the Balun Launching-Device is Represented as Two Series Generators.

The physical parameters of IPA_2 constructed are given below (see Figures 3.16 and 5.8).

length of the corrugated plane, L = 1.08 m

width of the corrugated plane, W = 0.46 m

length and width of the 'ground-plane' extension in front of the antenna = 0.54 m x 0.57 m

length and width of the 'ground-plane' extension behind the antenna = 0.12 m x 0.57 m

extension of the wire beyond the corrugated region L' = 0.03 m

(N.B. The feed-point was located in the 'ground-plane', at distance

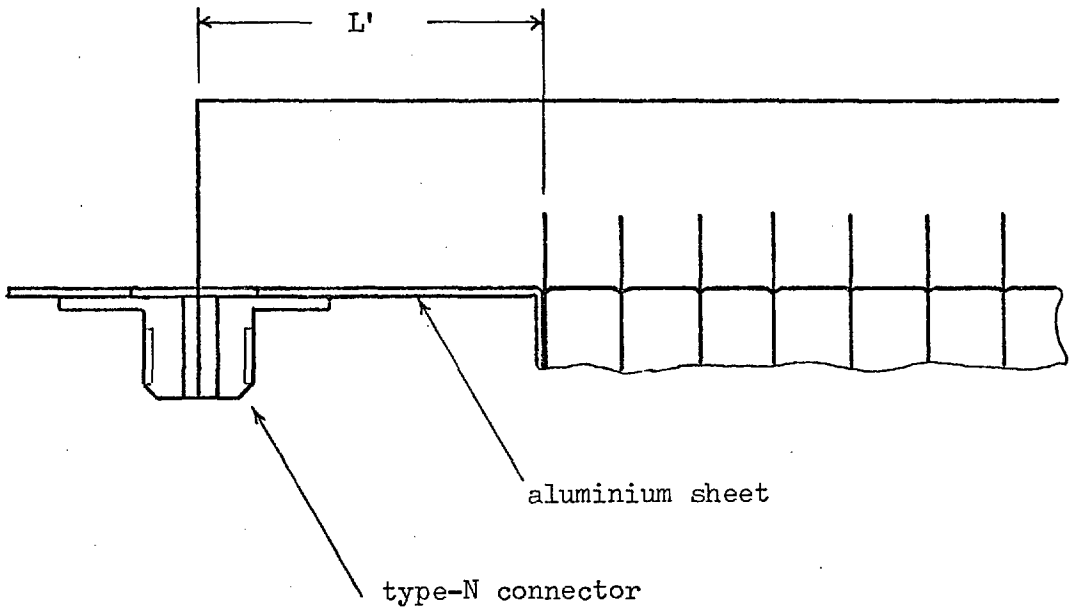


Fig. 5.9. Schematic Representation of the Feed-Structure at Input of IPA_1

L' from the corrugated region).

radius of the copper-wire	a	= 0.15 mm
height of the copper-wire above the corrugation tips	b	= 0.018 m
depth of the corrugations	d	= 0.007 m
corrugation periodic spacing	S	= 0.010 m
thickness of the corrugation walls	t	= 0.001 m

5.4. Test Antenna for H-Plane Measurements

An antenna of type IPA_1 was constructed, with a 'ground-plane' of finite extent, in order to measure the radiation pattern of the proposed antenna in the H-plane (i.e. the plane $\theta = 90^o$). The antenna was mounted on the turntable with its conducting plane horizontal, and pattern measurements were again made in the horizontal plane.

The construction of IPA_1 was almost identical to that of IPA_2 described in the previous section. However, the launching device on IPA_1 was necessarily different from that on IPA_2. As depicted in Fig. 5.9, a type-N coaxial-connector was fixed, from below, to the rear 'ground-plane'; the centre-conductor was extended vertically, above the ground-plane, to the required height of the horizontal wire. The launching device was preceded by a double-stub tuner, to effect the impedance transformation required for matching the antenna to the coaxial cable.

The physical parameters of IPA_1 were identical to those of IPA_2, given in the previous section, except for the parameters given below (see Figs. 5.8 and 5.9)

length of corrugated plane, $L = 1.10$ m

length and width of 'ground-plane' extension behind the antenna $= 0.12$ m x 0.57 m

extension of wire beyond the corrugated region, $L' = 0.07$ m

5.5. Preliminary Measurements

5.5.1. Evaluation of the Test-Site

A series of tests were carried out to estimate possible limitations on the accuracy of antenna field measurements due to test-site imperfections : this exercise was necessary due to lack of any previous evaluation of site performance. In this section we shall report only a selection of measurements carried out for the above purpose.

Fig. 5.10 indicates a plan of the part of the roof of the Electrical Engineering Building, at Imperial College, which was used as the test--site (photographs : Figures 5.1 and 5.2). To evaluate site reflections, a broad-side array of two dipoles with a small reflector was used as reference antenna. This antenna, which we shall designate DA for brevity, was originally designed for optimum performance at 1.5 GHz. The DA was mounted on the mast ($H_R \simeq 2.3$ m), and the CRA on the turntable ($H_T \simeq 2.3$ m). The horizontal spacing between the antennas, R, was approximately 9.5 m; this spacing was dictated by the sensitivity of the receiver (Rhode and Schwartz) which was available for these measurements : sensitivity ~ - 57 dB m, dynamic range ~ 13 dB, output proportional to indicated signal voltage.

With both antennas mounted for vertical polarization, pattern recordings were made in the horizontal plane for three different positions of the turntable (indicated in Fig. 5.10 as A, B and C). The frequency of 2.5 GHz was chosen so that the reference antenna would have a pattern with high sidelobes in order to emphasize the effect of scattering objects and surfaces on the site. The (theoretical) field pattern of the reference antenna DA (at 2.5 GHz) is indicated in Fig. 5.10. The field patterns of CRA, recorded with the antenna in different positions, are shown in Fig. 5.11.

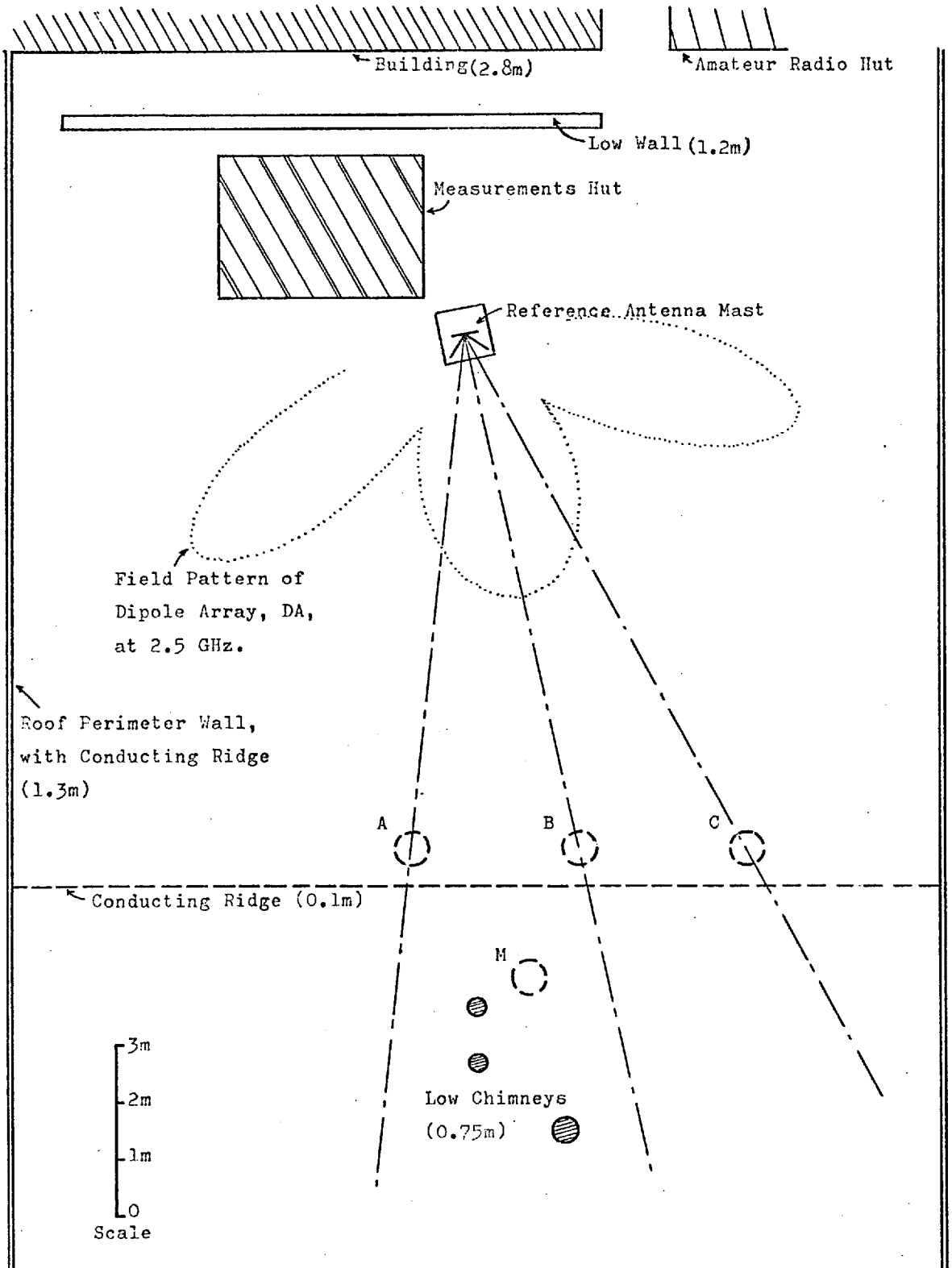
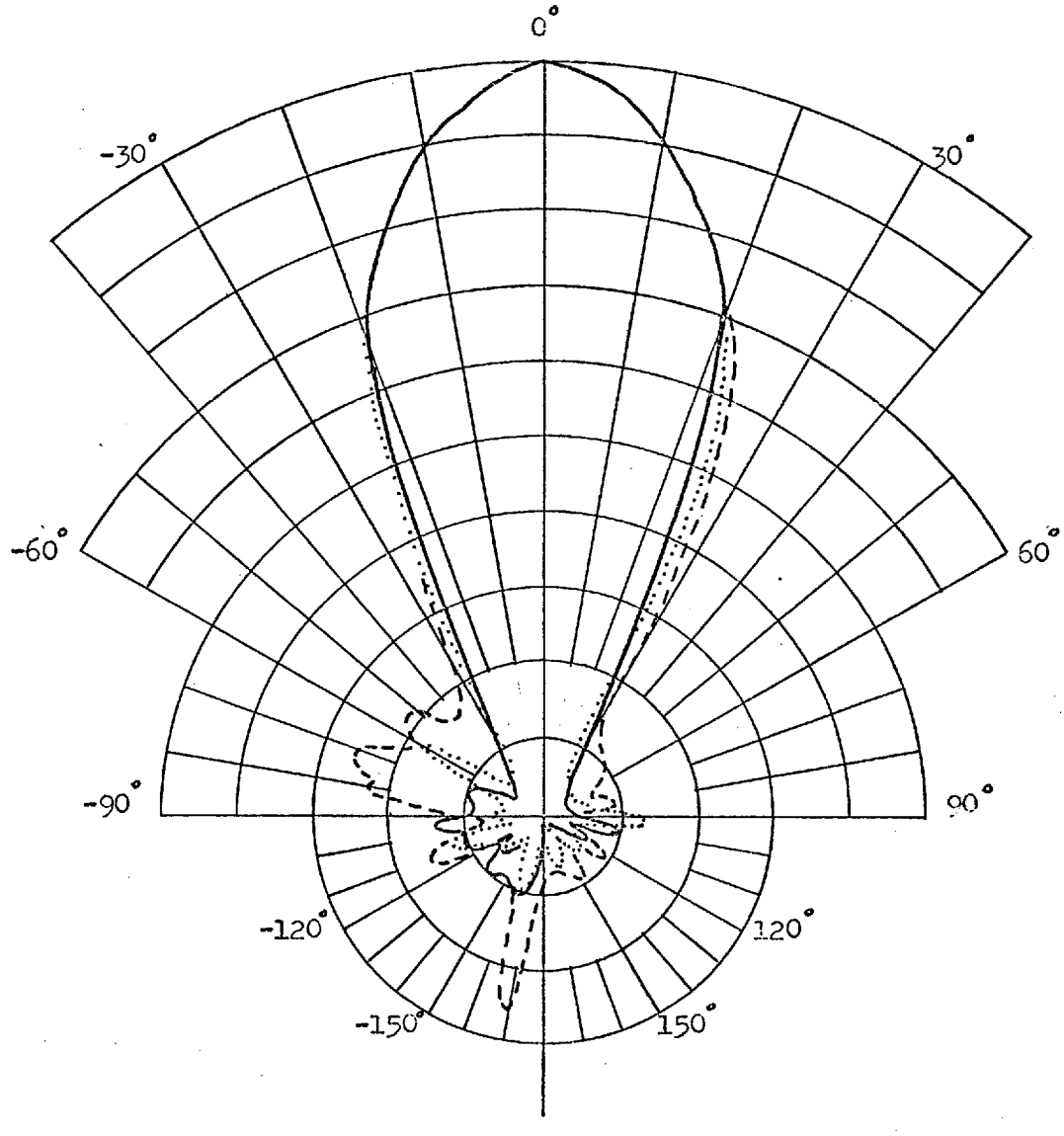


Fig. 5.10 Plan of the test-site: only the main area used for measurements is shown. Dashed circles indicate the turntable positions used. Figures in brackets represent heights above surface of the roof.



-------- Turntable Position A

———— Turntable Position B

..... Turntable Position C

as indicated in Fig. 5.10

Fig. 5.11 CRA: experimental field patterns at 2.5 GHz, for three different turntable positions.

The above test yielded the following observations : first, the main lobe of the recorded pattern was neither sensitive to the location of the antenna under test, nor influenced by site reflections. Second, the position and levels of the measured side-lobes were significantly influenced by site reflections (which were emphasized by the unorthodox pattern of the reference antenna). Third, the range over which the recorded pattern was most sensitive to the position of the turntable (and therefore to site reflections) was the back-lobe region of the antenna under test, and the side-lobe region in the negative-azimuth (i.e., left-half) directions.

In another test to observe the effect of ground reflections, one CRA was used as test antenna (H_T = 1.75 m, turntable position B, Figure 5.10), and another CRA was mounted on the mast; both antennas were mounted for vertical polarization. Two horizontal patterns were recorded with the reference antenna at heights H_R = 1.9 m and H_R = 2.3 m respectively. Comparison of these patterns yielded the following observations : both patterns indicated some degree of asymmetry, particularly with regard to the level of some side-lobe peaks. Increasing the height caused a shift in the position of some of the side-lobes. There was also a change in some of the peak levels : the magnitude of this change was less than 5 dB, and the highest side-lobe recorded was at a level of - 14 dB relative to the main beam. However, the average side-lobe level recorded was the same for both heights of the reference antenna.

The above variations were largely attributed to ground reflections because : (1) both antennas had relatively large beam widths in the vertical plane (Figs. 5.14 and 5.15); and (2) the change of height was not associated with an increase- or decrease- in the side-lobe

levels which was uniform in all directions. Thus ground-reflections could be a source of spurious response in pattern measurements; nevertheless, this is a tolerable limitation - unless detailed information is required regarding the sidelobe distribution of the antenna under test.

5.5.2. Examination of Far-Field Conditions

The test described in this section was carried out to check whether the field radiation by the reference antenna sufficiently approximated a 'locally plane wave' in the vicinity of the test antenna.

A CRA was mounted (for vertical polarization) on the mast at a height $H_R = 2.55$ m. The turntable was placed at a distance $R \simeq 11$ m from the mast. A rectangular sheet of aluminium (0.92 m x 1.83 m) was placed, with its plane horizontal, on the turntable, at a height $H_T = 1.8$ m; the longer sides of the sheet were parallel to the line of sight of the mast.

A short vertical monopole (Fig. 3.12) was used to check the amplitude and phase distribution of the 'incident wave' on the (aluminium) 'ground-plane'. Measurements were carried out at 1.0 GHz and 3.0 GHz.

In the following description, the distance of the probe from the 'leading edge' of the conducting plane will be denoted as x, where the 'leading edge' is the one nearer the transmitting antenna, and the 'trailing edge' the one further away. Thus the x-direction is parallel to the line-of-sight of the mast. The horizontal direction transverse to the line of sight will be denoted as the y-direction; y was measured from the centre-line of the conducting plane.

Along $y = 0$, the phase variation with x was linear and

corresponded to the free-space value, both at 1.0 GHz and at 3.0 GHz. However, there were significant deviations in the signal level. At 1.0 GHz, the mean signal level (dB) decreased uniformly with x, in the forward region of the conducting plane : the signal at x = 1.0 m was - 3.0 dB (approx.) relative to the signal level at x = 0.2 m. There was also a fluctuation of $\pm \frac{3}{4}$ dB (approx.) about the mean signal level. In the rear region of the conducting plane, a higher fluctuation of $\pm 1\frac{1}{4}$ dB was noted, but there was no significant variation of the mean signal level with position. At 3.0 GHz, the mean signal level did not change significantly with x; the fluctuation in the signal level was less than $\pm$ 1 dB.

Measurements in the transverse direction to the line of sight were made along the line x = 0.83 m. The phase variation (across the aperture) was less than $\pm 10^{\circ}$ at 1.0 GHz, and less than $\pm 13^{\circ}$ at 3.0 GHz. The fluctuation in the signal level was less than $\pm$ 1 dB at 1.0 GHz, and less than $\pm$ 2 dB at 3.0 GHz. However, if the measurements made within one wavelength's distance from the edges (parallel to the y direction) are disregarded, then the following figures are obtained for maximum fluctuations in the signal level : $\pm \frac{3}{4}$ dB at 1.0 GHz, and $\pm$ 1 dB at 3.0 GHz.

The above results indicated that the test range was satisfactory for field measurements in the band 1.0 - 3.0 GHz, provided the length of the antenna under test was of the order of 1.0 metres or less. The variation in the mean signal level near the leading edge of the conducting plane indicated significant ground reflections at 1.0 GHz, which could lead to a maximum error of + 3 dB in the measurement of side-lobe levels in the H-plane. At 3.0 GHz, however, probe measurements indicated no significant

errors due to ground reflections.

5.5.3. Reference Antenna Characteristics

One CRA was mounted on the mast ($H_R \simeq 2.55$ m), and the other on the turntable (position M, Fig. 5.10; $H_T \simeq 2.2$ m). With this arrangement, radiation patterns of the CRA were recorded at : 1.0 GHz, 2.5 GHz and 3.0 GHz. H-plane recordings are given in Figs. 5.12 and 5.13; for these measurements both antennas were mounted for vertical polarization, i.e. with their dipole feeds vertical. The dashed-lines in these recordings indicated the response of the CRA to crossed--polarized radiation; the latter response was obtained by mounting the test antenna - i.e. the CRA on the turntable - for horizontal polarization.

Figures 5.14 and 5.15 indicate the E-plane radiation patterns of the CRA, measured at 1.0 GHz and 2.5 GHz respectively. These measurements were carried out with both antennas mounted for horizontal polarization - i.e., with their dipole feeds horizontal. An important observation was that E-plane recordings at 2.5 GHz indicated a significant degree of asymmetry, at levels below - 12 dB relative to the maximum.

Inspection of the above recordings indicates that the choice of a CRA as reference antenna is entirely satisfactory. It might be argued that the reference antenna should always have a narrow beam-width in the vertical plane, in order to provide sufficient discrimination against ground reflection; but, in the E-plane, the CRA has a beam-width - ranging from 60° to 120° over the frequency band - which is too large to allow accurate pattern measurement in the H-plane. To alleviate such anxiety, it should be noted that the test antenna

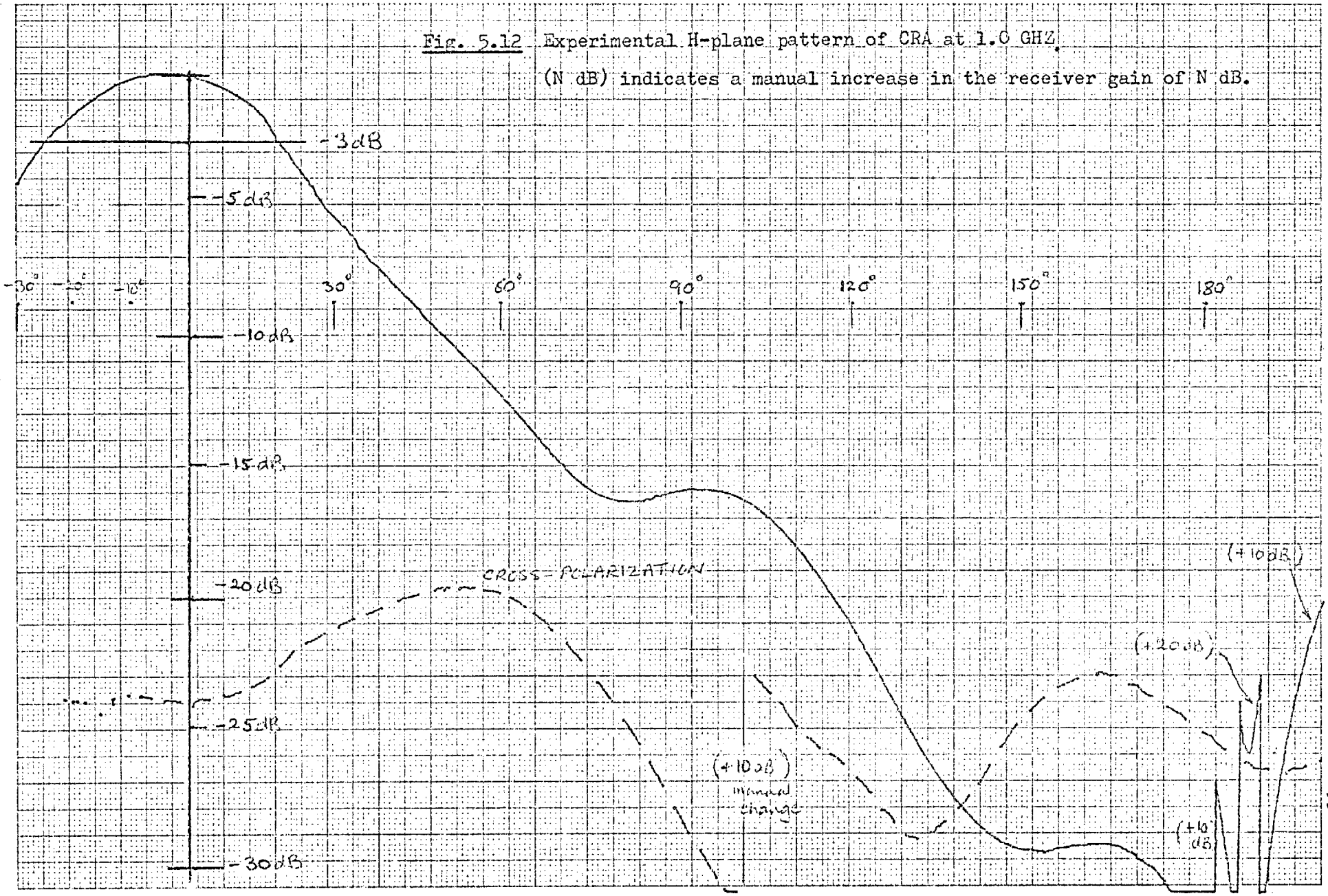


Fig. 5.12 Experimental H-plane pattern of CRA at 1.0 GHz.
(N dB) indicates a manual increase in the receiver gain of N dB.

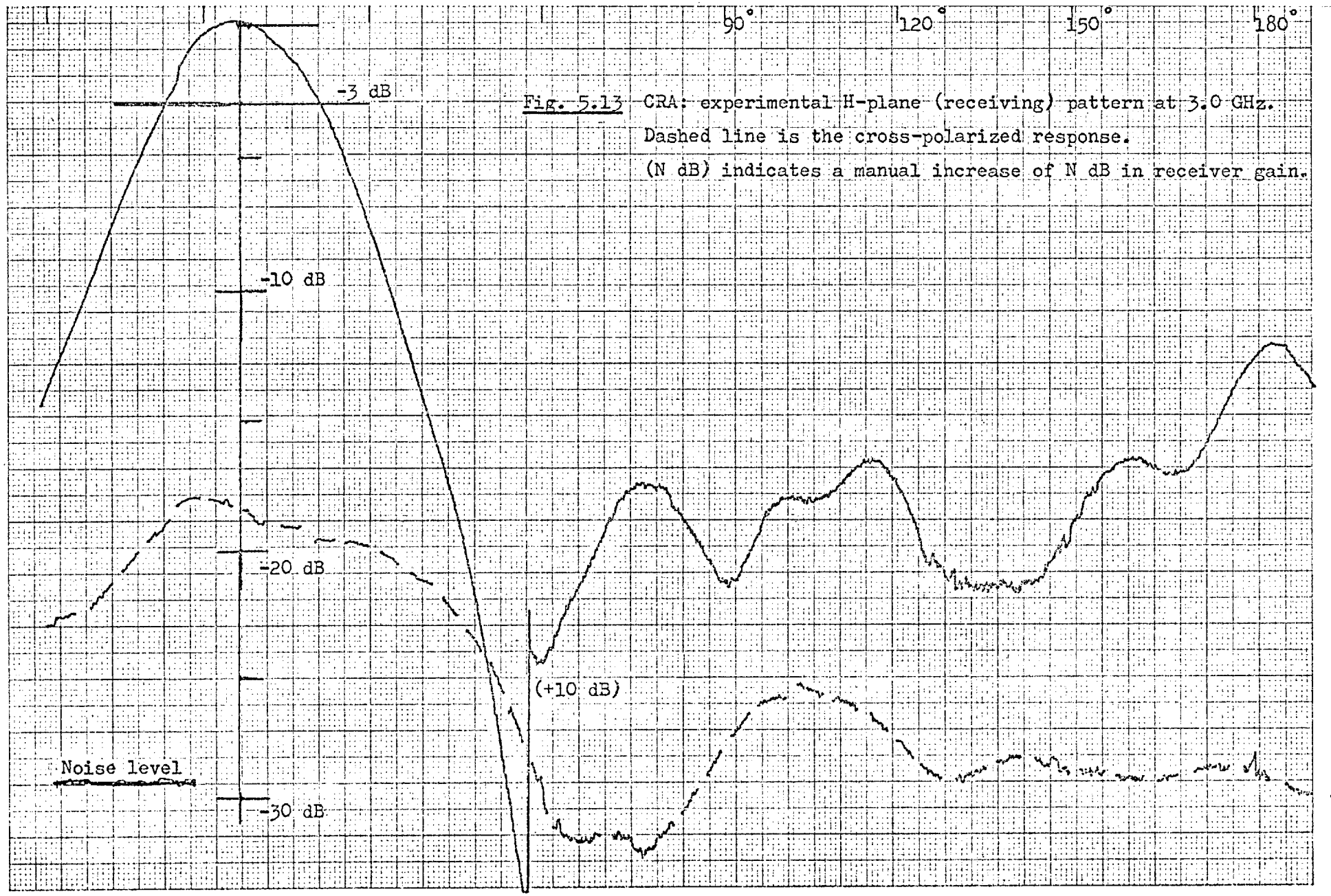


Fig. 5.13 CRA: experimental H-plane (receiving) pattern at 3.0 GHz.
Dashed line is the cross-polarized response.
(N dB) indicates a manual increase of N dB in receiver gain.

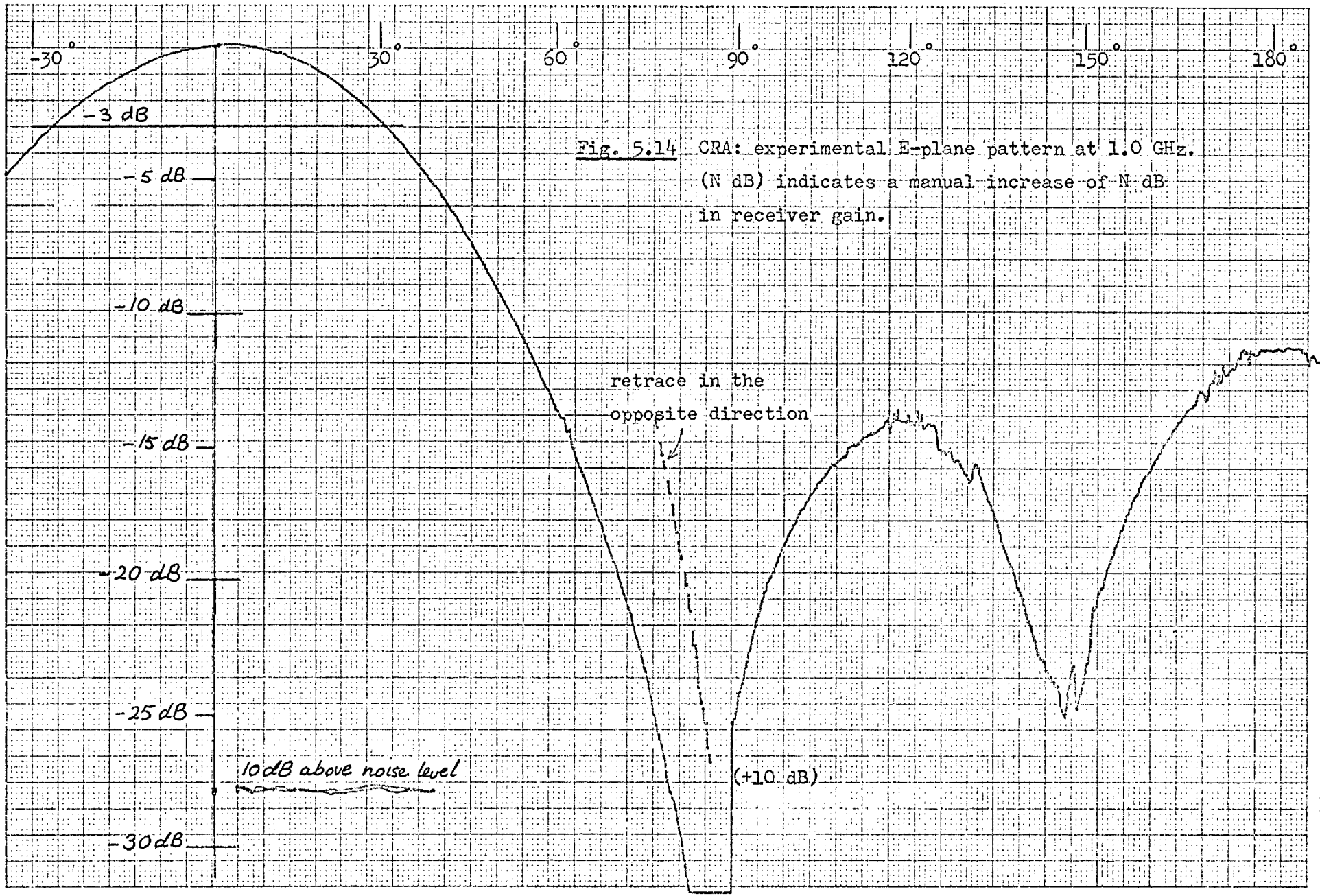


Fig. 5.14 CRA: experimental E-plane pattern at 1.0 GHz. (N dB) indicates a manual increase of N dB in receiver gain.

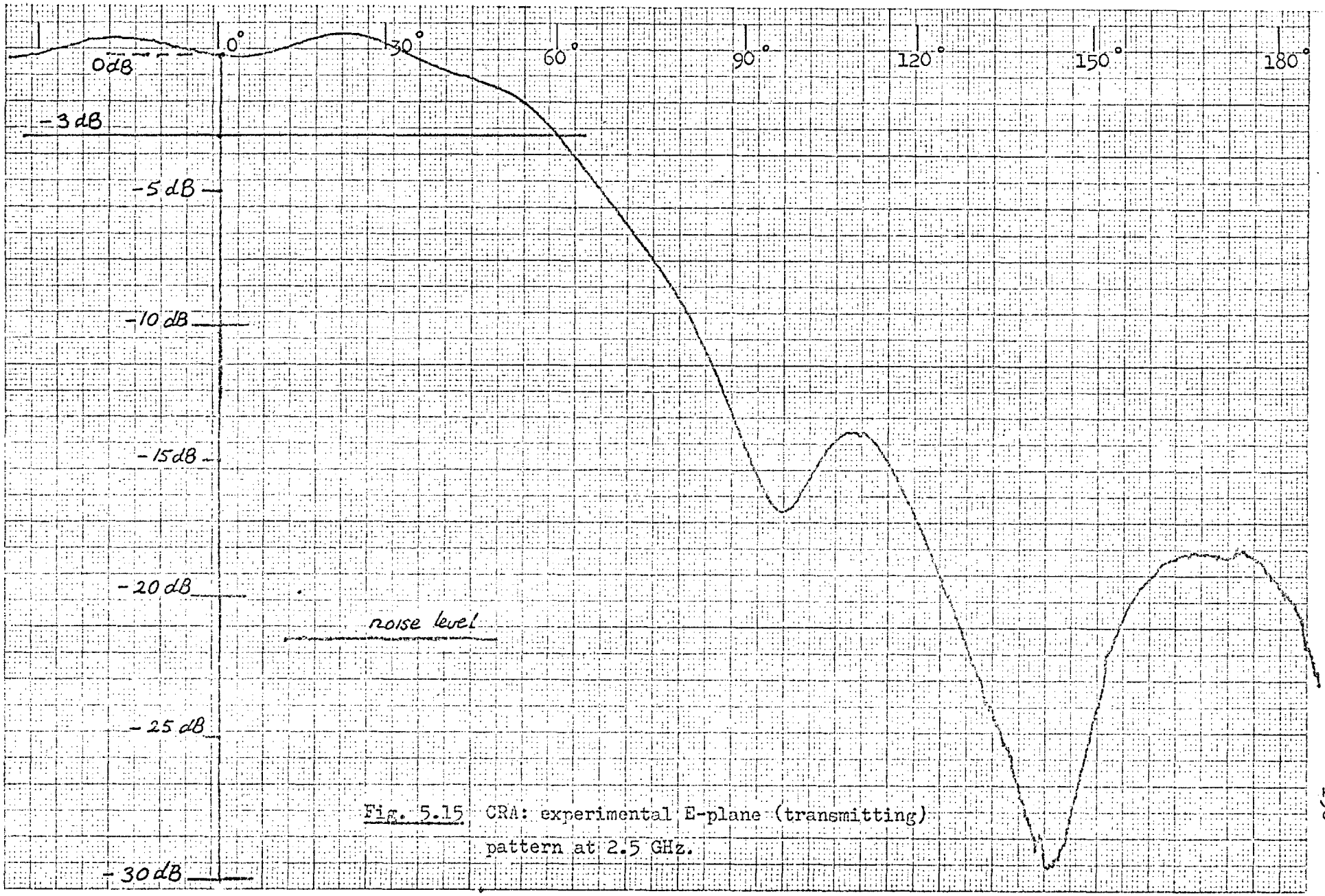


Fig. 5.15 CRA: experimental E-plane (transmitting) pattern at 2.5 GHz.

employed for H-plane measurements was of the type IPA_1 : the 'ground-plane' extensions on this antenna would provide significant discrimination against ground reflections particularly in the main-beam direction; however the width of the conducting plane on IPA_1 was insufficient to provide satisfactory screening against ground reflections at frequencies below 2.0 GHz.

5.6. Comparison of Experimental and Theoretical Results

5.6.1. H-Plane Characteristics

Experimental H-plane patterns are presented at frequencies 3.0, 2.5, 2.0, 1.5 and 1.0 GHz in Figs. 5.17a through 5.21a respectively. Corresponding computed patternsn are presented in Figs. 5.17b through 5.21b. A summary of measured and computed data is given in the table of Figure 5.30. Measured 3 dB beam-widths (b.w.) are accurate within $\pm$ 10% approximately, and computed b.w. within $\pm 2^{\circ}$. Measured average side-lobe levels (s.*l*.*l*.) are within $\pm$ 1 dB approximately, and computed s.*l*.*l*. within $\pm$ 0.5 dB.

At 2.0 GHz and higher frequencies very good agreement is obtained between theory and experiment. It should be noted that computed side-lobe levels (s.*l*.*l*.) represent an upper limit to the actual s.*l*.*l*.. This is because for purposes of analysis (Sub-section 4.6.3.) it was assumed that the current in the load termination of the transmitting antenna is equal to the input current. In general, however, there would be some radiation from the region before the load termination; consequently the load current would actually be less than the assumed value.

At 1.5 GHz and 1.0 GHz, Figures 5.20 and 5.21 respectively, the discrepancies between experimental and computed results (b.w. and

s.ℓ.ℓ.) become significant. It is believed that the above discrepancies are due to experimental error arising from ground reflections. This explanation is strongly supported by results of probe measurements reported in Sub-section 5.5.2, and the observation that the error in measured s.ℓ.ℓ. appears to be + 3 dB approximately. It should be noted that there is excellent correlation between the shapes of corresponding experimental and computed patterns.

The gain of IPA_1 was measured at 1.5 GHz and 3.0 GHz. The technique chosen was the gain comparison method : first the test antenna was connected to the receiver and matched at the input for maximum signal level (using a concentric double-stub tuner); then a half-wave dipole was substituted in the place of the test antenna, at approximately the same height as the fixed CRA, and the same procedure employed to maximize the signal level. The vertical dipole was then manoeuvred into a position of minimum signal variation, and the difference (in dB) between the signal levels was taken as the gain of the test antenna. The fluctuation in the signal level with dipole position was taken as the possible error in the measured gain. The measured gains of IPA_1 (relative to a half-wave dipole) were - 1.5 dB $\pm$ 1.5 dB at 1.5 GHz, and 9 dB $\pm$ 1 dB at 3.0 GHz. These figures yield corresponding absolute gains for IPA_2 of 3.6 $\pm$ 1.5 dB at 1.5 GHz and 14.1 dB $\pm$ 1 dB at 3.0 GHz (see Eq. 4.96). Comparison of these figures with computed absolute gain values (2.5 dB at 1.5 GHz and 15.0 dB at 3.0 GHz) indicates satisfactory correlation between theory and experiment.

Experimental H-plane cross-polarization patterns are presented at 3.0 GHz and 1.0 GHz, Figs. 5.28 and 5.29 respectively. The following experimental procedure was employed. The test antenna, IPA_1, was

connected to the generator and the reference CRA to the receiver. The CRA was mounted on the mast with its dipole feed vertical for principal-polarization measurements (H_R = 2.45 m); and with its dipole feed horizontal for cross-polarization measurements (H_R = 2.65 m). For each polarization the height of the CRA was adjusted for maximum signal level prior to pattern measurements.

The maximum variation of signal level with CRA height was also measured. At 1.0 GHz the SWR (standing-wave-ratio) was 4 dB for vertical polarization and 6 dB for horizontal polarization. At 3.0 GHz the SWR was 1 dB for vertical polarization and 10 dB for horizontal polarization. These observations are an excellent indication of errors due to ground reflections.

It is readily seen that cross-polarization at 3.0 GHz is negligible (Fig. 5.28). At 1.0 GHz, however, measured levels of cross--polarization (Fig. 5.29) were significantly higher than indicated by analysis - even if allowance is made for ground-reflection errors. The only plausible explanation which can be suggested for this discrepancy is that the sizes of 'ground planes' employed in the construction of IPA_1 were too small : consequently significant edge currents were induced, at lower frequencies, which resulted in high levels of measured cross-polarization.

Finally, we note that (at every frequency of measurement) two overlapping H-plane pattern recordings were made, covering the full 360° of azimuth; direct comparison of each pair of recordings indicated a degree of symmetry which was always satisfactory and often excellent.

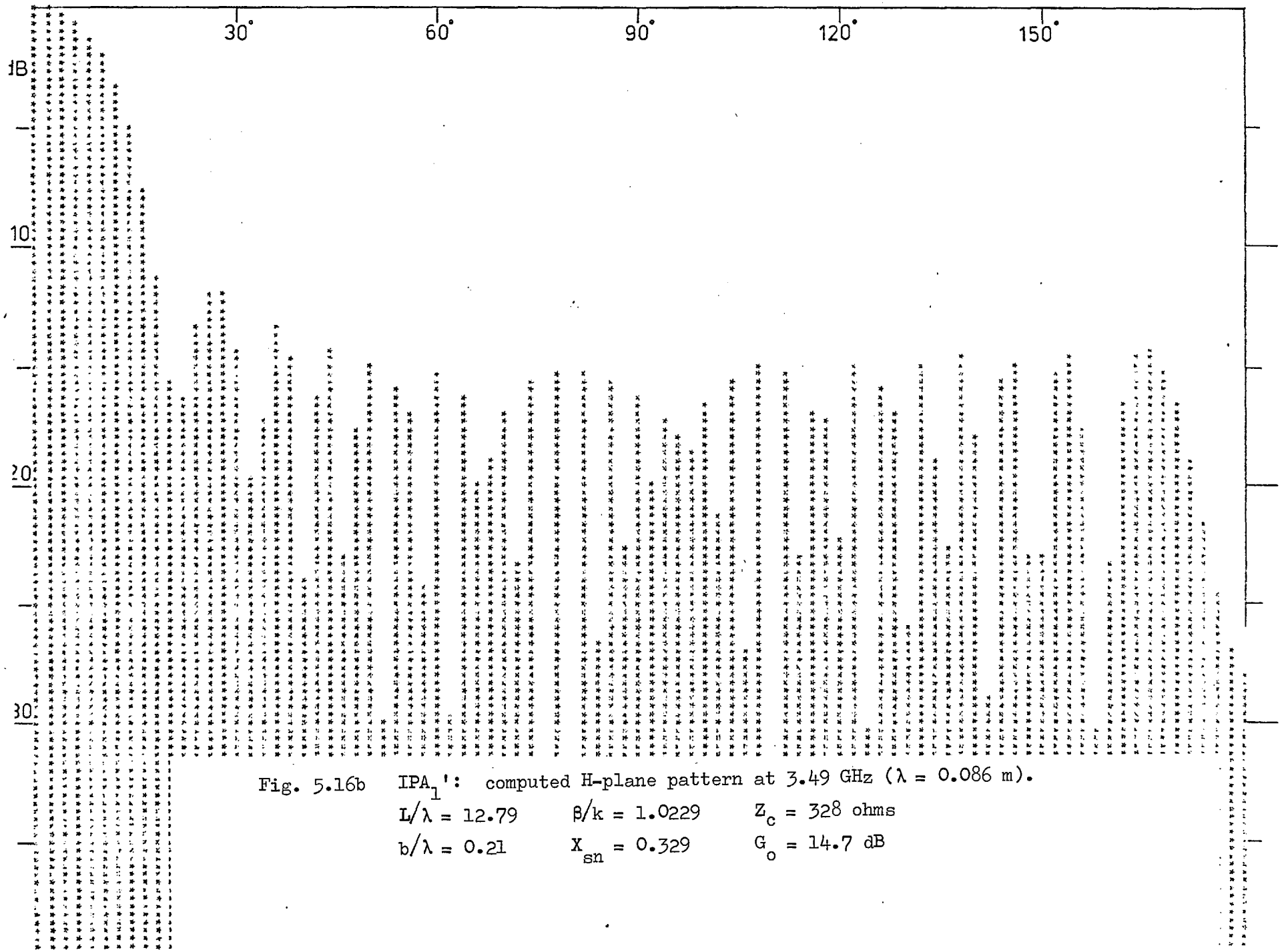


Fig. 5.16b IPA_1': computed H-plane pattern at 3.49 GHz (λ = 0.086 m).

L/λ = 12.79 β/k = 1.0229 Z_c = 328 ohms

b/λ = 0.21 X_{sn} = 0.329 G_o = 14.7 dB

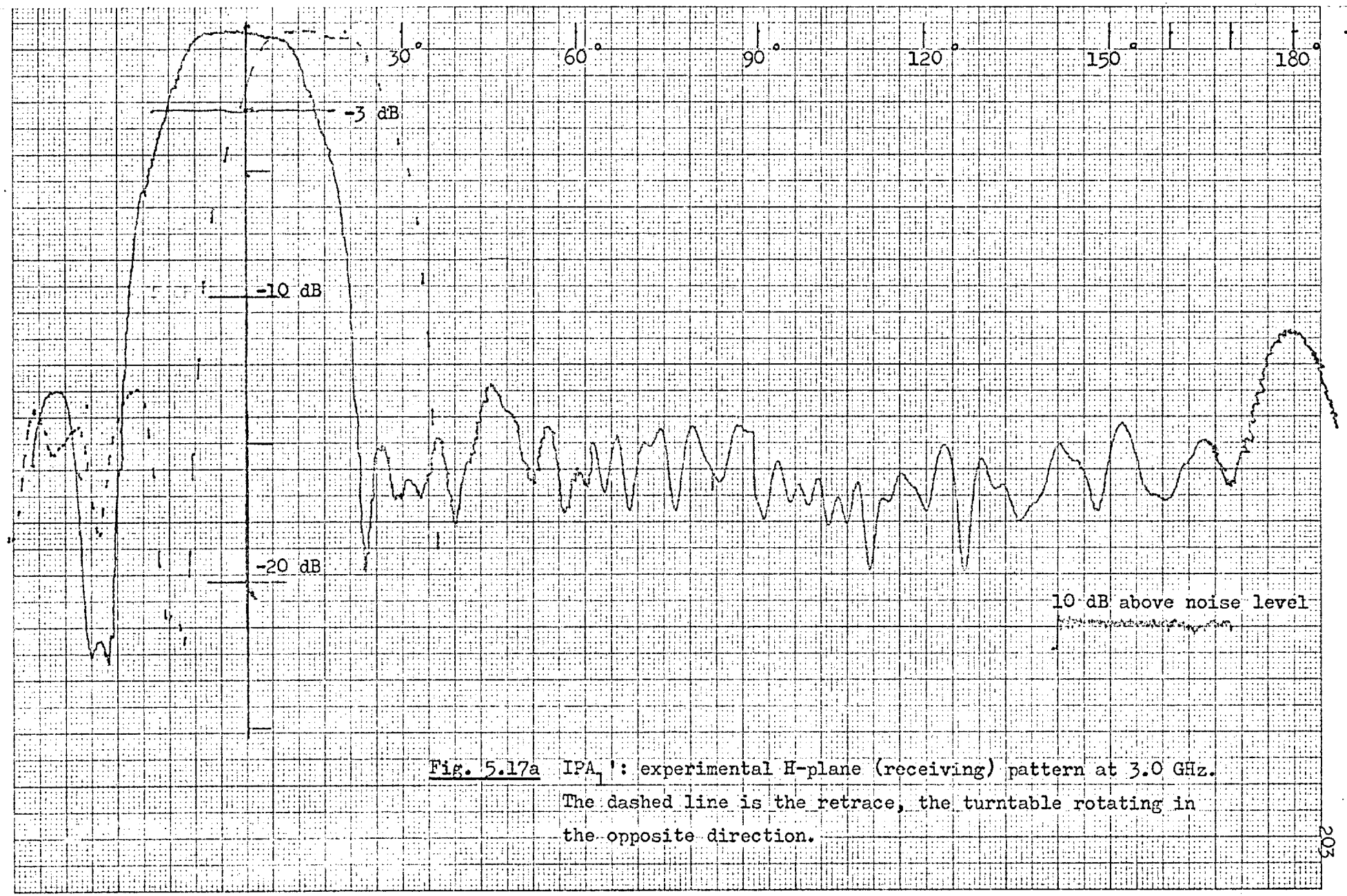


Fig. 5.17a IPA_1': experimental H-plane (receiving) pattern at 3.0 GHz. The dashed line is the retrace, the turntable rotating in the opposite direction.

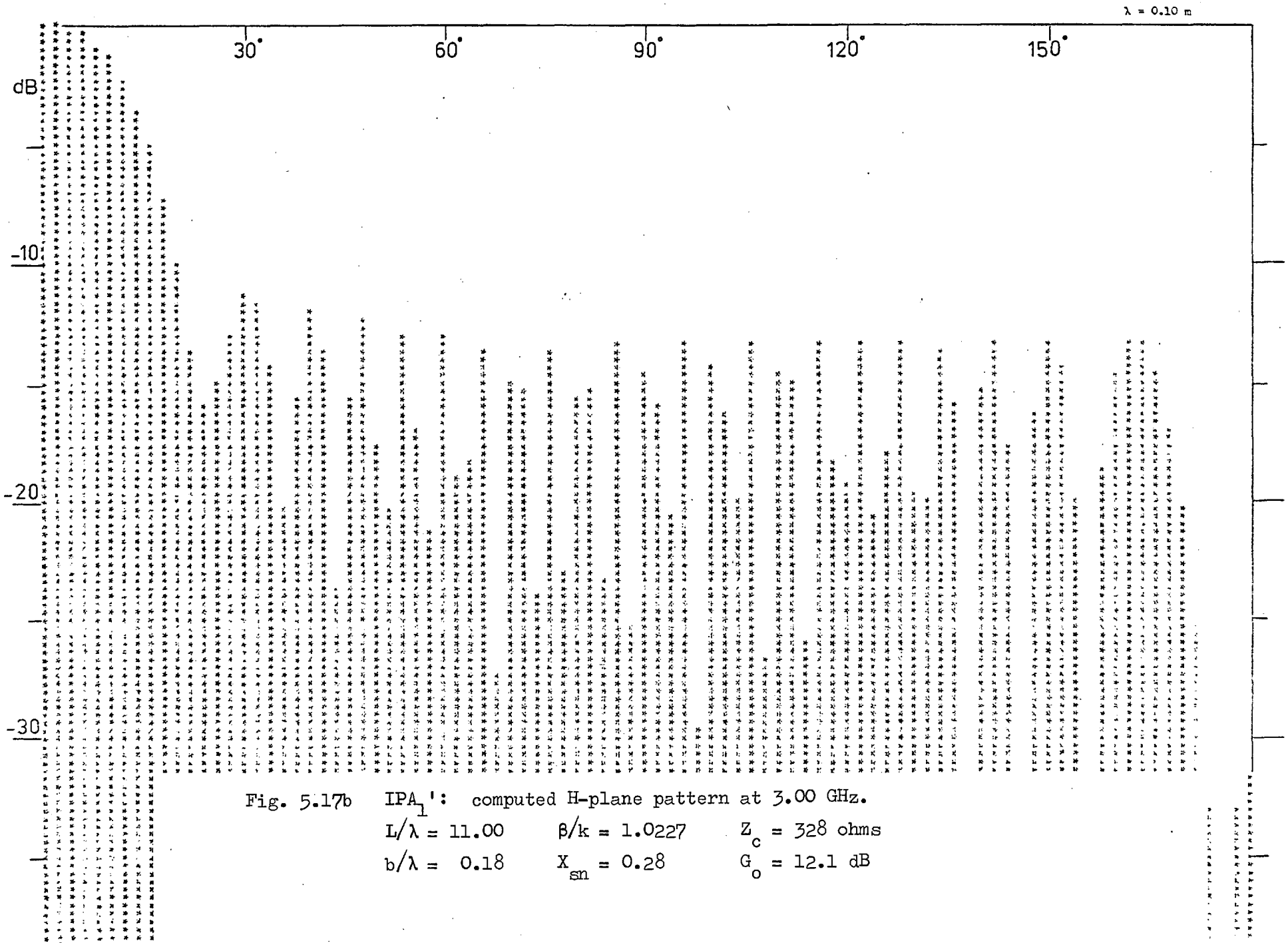


Fig. 5.17b IPA_1': computed H-plane pattern at 3.00 GHz.

L/λ = 11.00 β/k = 1.0227 Z_c = 328 ohms

b/λ = 0.18 X_{sn} = 0.28 G_o = 12.1 dB

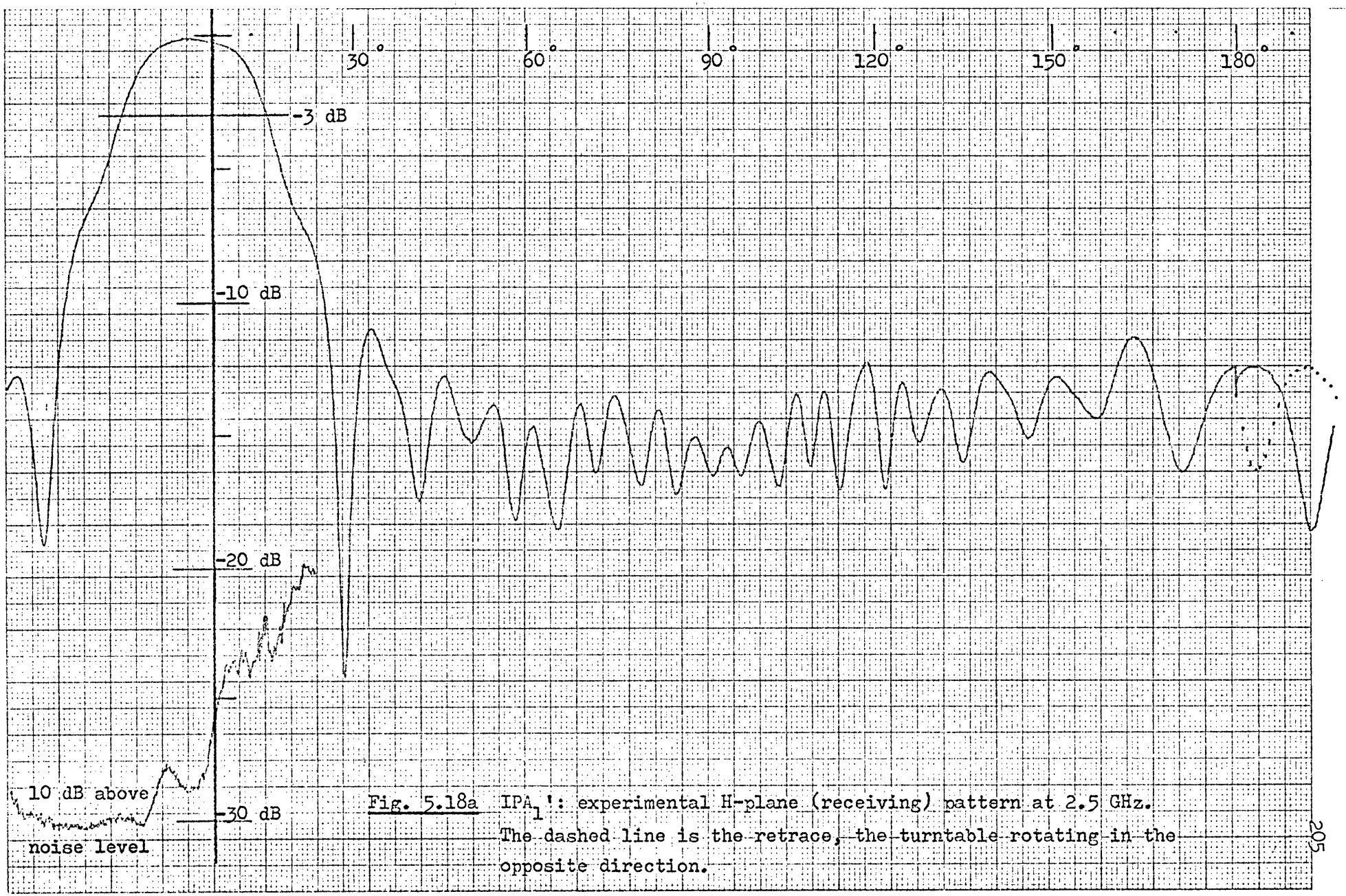


Fig. 5.18a IPA_1': experimental H-plane (receiving) pattern at 2.5 GHz. The dashed line is the retrace, the turntable rotating in the opposite direction.

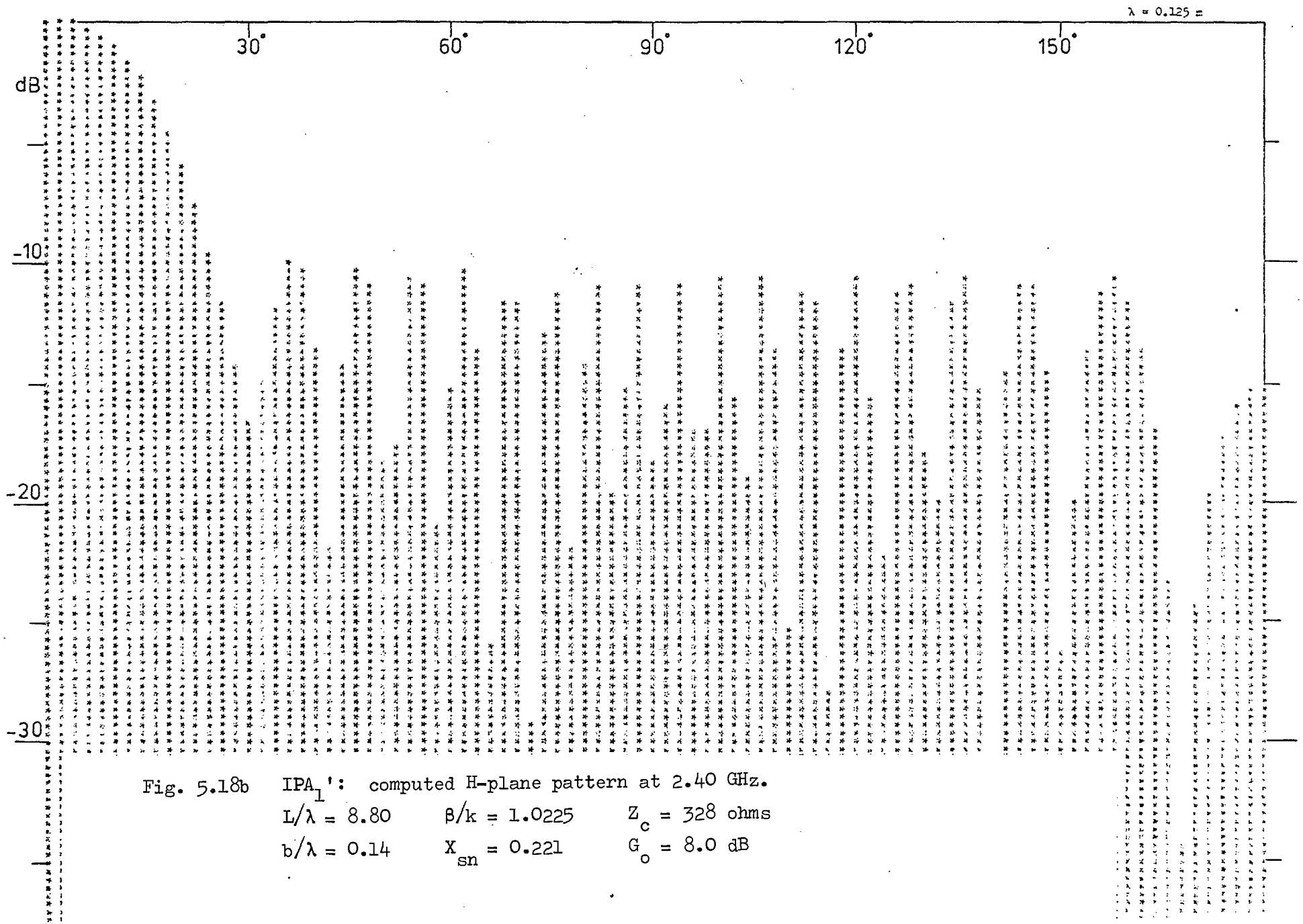


Fig. 5.18b IPA_1': computed H-plane pattern at 2.40 GHz.

$L/\lambda = 8.80$ $\beta/k = 1.0225$ $Z_c = 328$ ohms

$b/\lambda = 0.14$ $X_{sn} = 0.221$ $G_o = 8.0$ dB

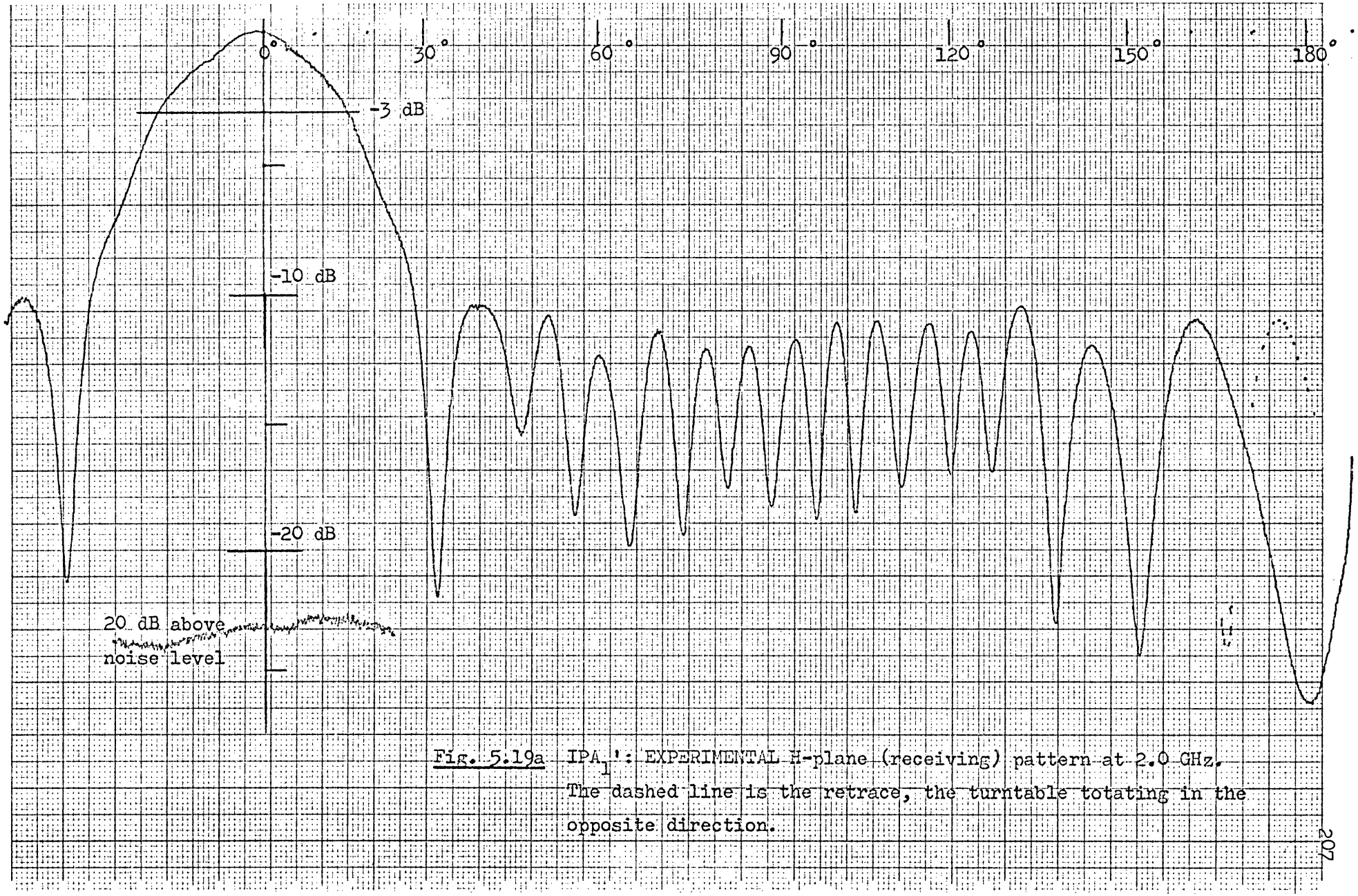


Fig. 5.19a IPA$_1$': EXPERIMENTAL H-plane (receiving) pattern at 2.0 GHz. The dashed line is the retrace, the turntable totating in the opposite direction.

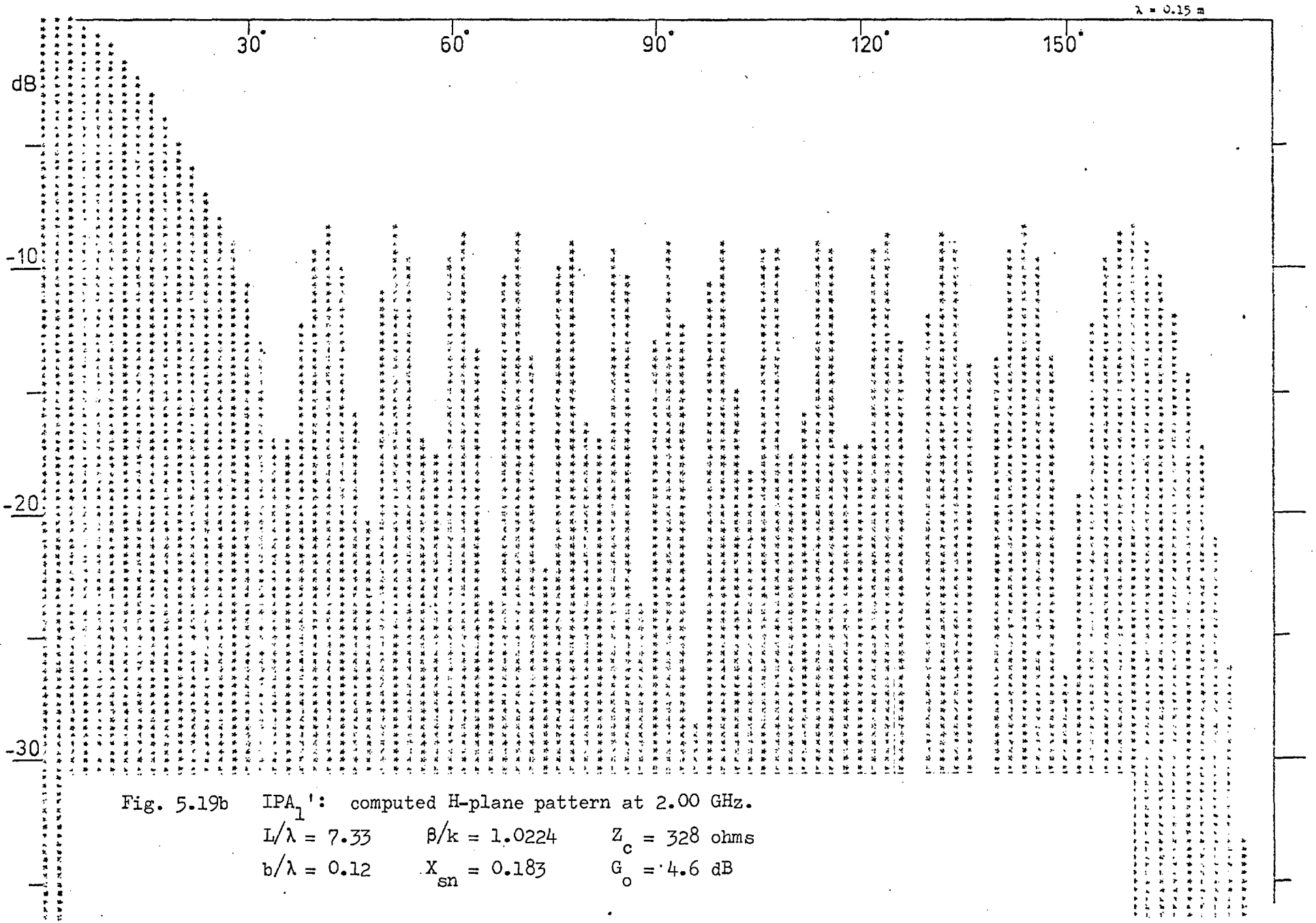


Fig. 5.19b IPA_1': computed H-plane pattern at 2.00 GHz.

$L/\lambda = 7.33$ $\beta/k = 1.0224$ $Z_c = 328$ ohms

$b/\lambda = 0.12$ $X_{sn} = 0.183$ $G_o = 4.6$ dB

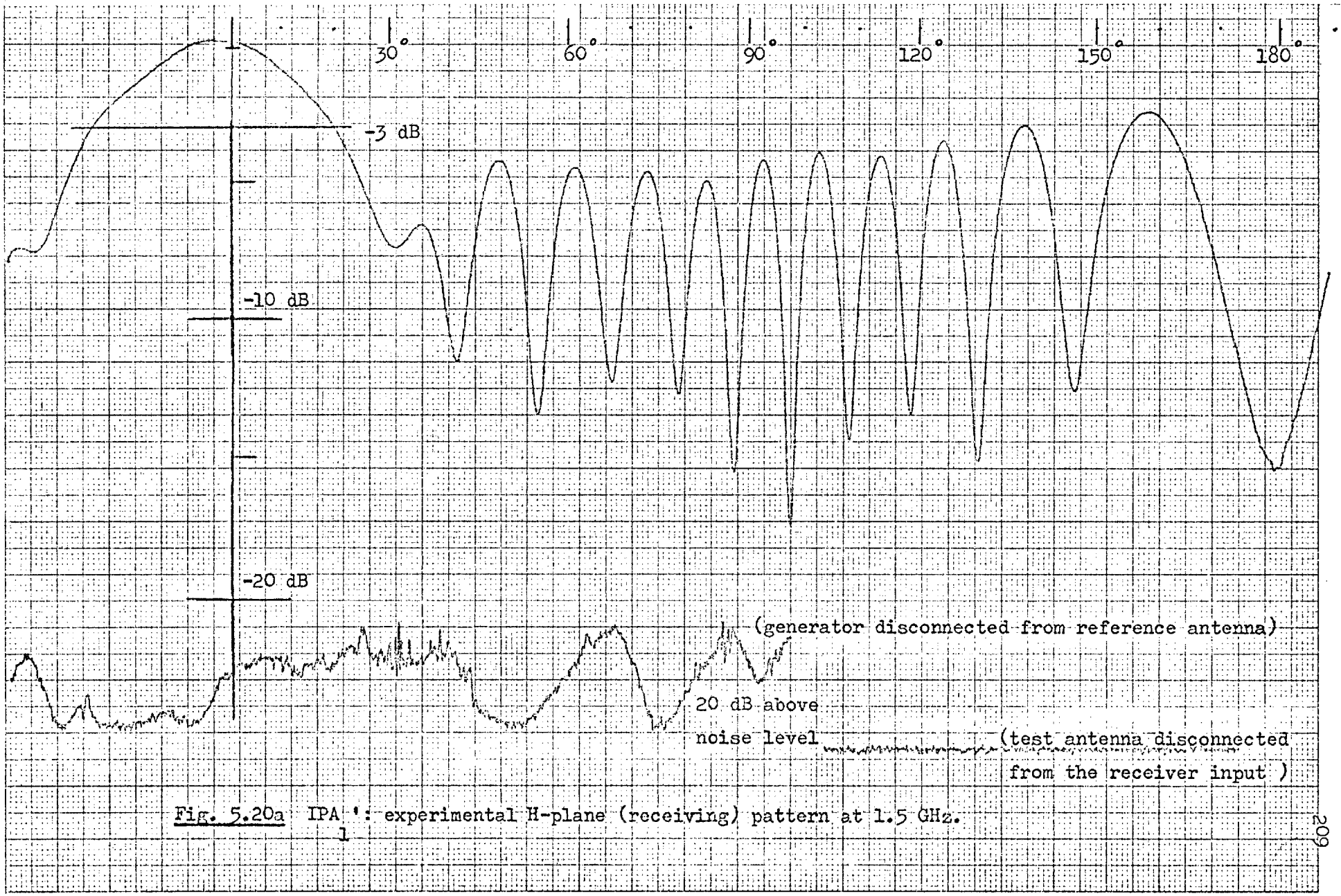


Fig. 5.20a IPA 1: experimental H-plane (receiving) pattern at 1.5 GHz.

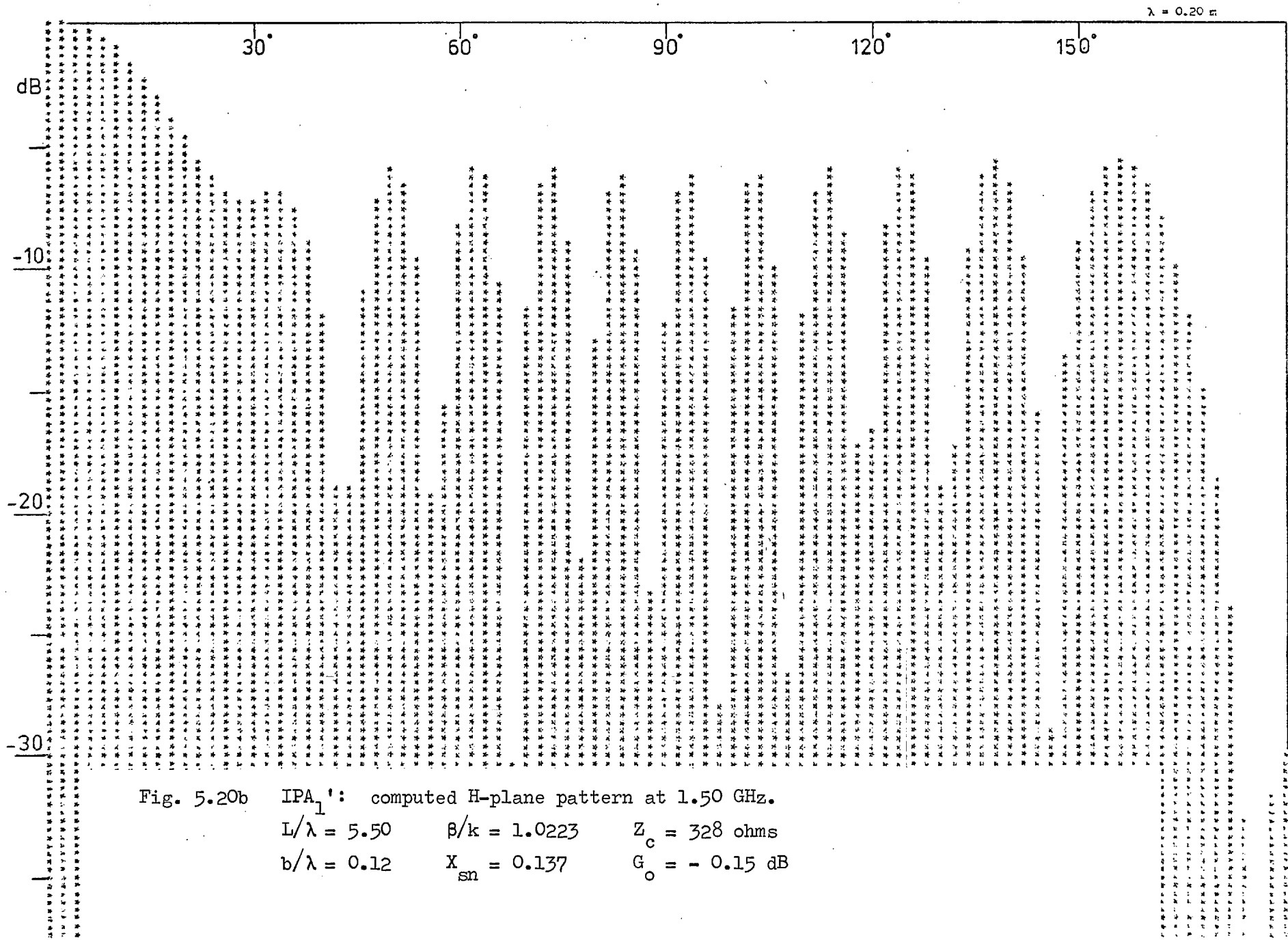


Fig. 5.20b IPA_1': computed H-plane pattern at 1.50 GHz.

$L/\lambda = 5.50$ $\beta/k = 1.0223$ $Z_c = 328$ ohms

$b/\lambda = 0.12$ $X_{sn} = 0.137$ $G_o = -0.15$ dB

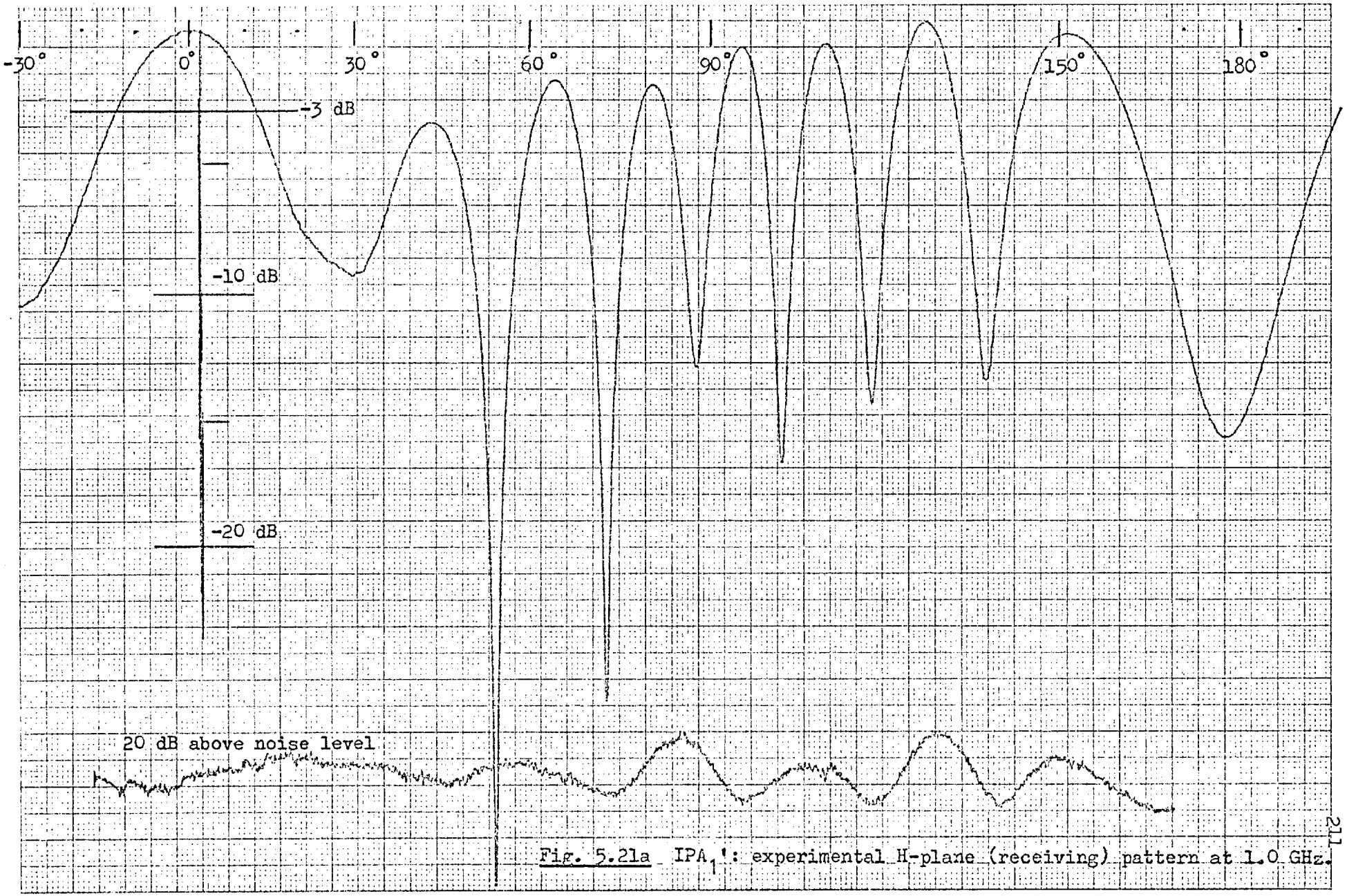


Fig. 5.21a IPA$_1$': experimental H-plane (receiving) pattern at 1.0 GHz.

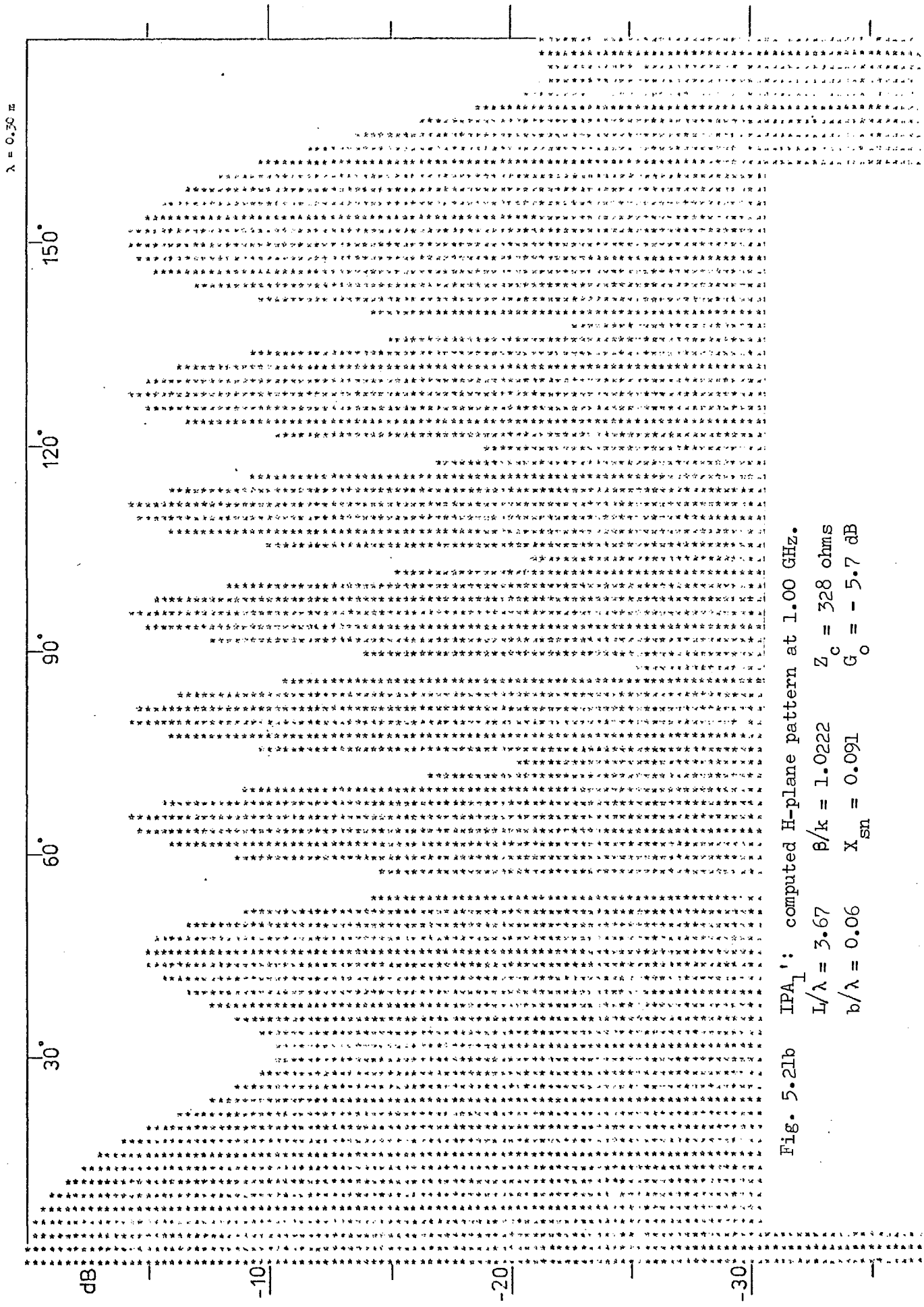


Fig. 5.21b IPA$_1$': computed H-plane pattern at 1.00 GHz.
$L/\lambda = 3.67$ $\beta/k = 1.0222$ $Z_c = 328$ ohms
$b/\lambda = 0.06$ $X_{sn} = 0.091$ $G_o = -5.7$ dB

5.6.2. E-Plane Characteristics

Experimental E-plane patterns are presented at frequencies 3.0, 2.5, 2.0, 1.5 and 1.0 GHz in Figs. 5.23a through 5.27a respectively. Corresponding computed patterns are presented in Figs. 5.23b through 5.27b. It should be noted that the "0°" direction marked on the experimental E-plane patterns corresponds to the direction of IPA_2's long-wire axis (i.e., 0° corresponds to the end-fire direction); however, the "0°" direction marked on the computed E-plane patterns corresponds to the direction normal to IPA_2's long-wire axis, and "90°" corresponds to the end-fire direction.

Mathematically, the above difference can be expressed as:

$$\theta_{experimental} = -\theta_{theoretical} + 90 \text{ degrees}$$

It is recognized that differences in presentation (of experimental and computed E-plane patterns) might unfortunately complicate comparative inspection of results.

A summary of measured and computed data is given in the table of Fig. 5.31 : tolerances and errors are the same as for Fig. 5.30, for which details were given in the previous section.

Compared to H-plane measurements, fewer E-plane measurements were carried out, in less detail and less thoroughly. Also, in many respects the E-plane results are less satisfactory than H-plane results - and certainly less reliable. Qualitatively, there is reasonable correlation between experimental and computed patterns; for example, as regards the shape of radiation patterns, number and position of side-lobes, and variation of the aforesaid characteristics with frequency. Quantitatively, however, the agreement between theory and experiment was not entirely

conclusive. For example, there was a significant lack of symmetry in the experimental E-plane patterns, particularly within the main beam region; experimental 3 dB beam-widths (b.w.) were nearly one-half the computed b.w.; and experimental average side-lobe levels (s.ℓ.ℓ.) were often higher than computed s.ℓ.ℓ. (It should be re-called that computed s.ℓ.ℓ. represent an upper limit to actual s.ℓ.ℓ.).

Fortunately discrepancies between experimental and computed (E-plane) results can be analysed and explained with confidence. There were four sources of error - of which three are experimental - which we shall consider separately.

For purposes of analysis it was assumed that the surface of the reactance plane was flush with the conducting-plane surface (Sections 4.5 and 4.6). This assumption does not strictly apply to the test antenna IPA_2 constructed for E-plane measurements : in the experimental model the effective thickness of the double-sided reactive-plane was 3.5 cm, which corresponds to 0.35 wavelengths at 3.0 GHz. This thickness has the effect of introducing a space-factor in the E-plane pattern, resulting in narrower beam-widths than indicated by computation.

A relatively minor source of error was ground reflections. The reflection coefficient of ground near grazing incidence is higher for horizontal polarization than for vertical polarization. Thus errors due to ground reflections might seem more important in E-plane measurements than in H-plane measurements; however, vertical b.w. of the reference antenna was much narrower for E-plane measurements than for H-plane measurements. At 3.0 GHz, variation in signal level with height of the reference antenna corresponded to a SWR of 5 dB approximately, for E-plane measurements (compared to a SWR of 1 dB for H-plane measurements). The effect of such ground reflections is

that the recorded pattern represents a weighted average of two patterns : one in the plane $\phi = 0$, and the other in the plane $\phi \simeq 22^{\circ}$. Assuming similar patterns in the ϕ = constant planes, the measured pattern can be regarded as the E-plane pattern with a maximum possible error of + 2 dB and - 3 dB.

This type of error generally changes slowly with direction, especially when the test antenna has relatively broad lobes; in the present case, the expected error is less than $\pm$ 2 dB, and it is probable that the sign of the error remains positive in all directions.

Another minor source of error was scattering in the plane of measurements, by perimeter walls on the test-site. (This error was negligible in H-plane measurements due to better directional properties of the reference antenna, CRA, in the horizontal plane when the CRA is mounted for vertical polarization). Approximate calculations based on diffraction theory indicate that the scattered signal level in the receiver would be below - 24 dB relative to maximum level of the direct signal : this would cause maximum errors of + 3 dB and - 4 dB in actual side-lobe levels of - 16 dB. Furthermore, the error would change rapidly with direction of the test antenna; thus this error is detectable as 'amplitude modulation' of the computed pattern. Comparison of experimental and computed patterns (particularly at 3.0 GHz, 2.5 GHz and 2.0 GHz) reveals such modulation effects which indicate some perimeter wall scattering.

The major source of error in E-plane measurements was traced to imperfections and lack of symmetry in the construction of the test antenna, IPA_2. Any mechanical asymmetry about the conducting plane of IPA_2 would be expected to lead to asymmetry in directional characteristics in the E-plane.

It was discovered that the wire-to-corrugation-tip spacings were different on opposite sides of the conducting plane; the spacings were $b_+ = 19$ mm and $b_- = 17$ mm, where subscripts + and - refer to the wire on the right and left sides of the conducting plane respectively (looking from the feed point towards the load termination).

Approximate calculations indicate that the above imperfection would cause errors in the main beam less than 2 dB, and a difference less than 2 dB between s.ℓ.ℓ. on opposite sides of the main beam. Observed experimental asymmetries greatly exceeded estimates due to unequal wire spacings. The degree of asymmetry increased with frequency of measurements : at 3.0 GHz, the maximum main lobe asymmetry was of the order of 6 dB, and the s.ℓ.ℓ. asymmetry 5 dB approximately.

It was concluded that symmetry errors were due to imperfect construction of the feed structure (Fig. 5.7) which resulted in wire currents of unequal amplitude and a phase difference differing from 180°. This conclusion is supported by the following observations:

(a) at 1.0 GHz, there is a difference in the level and direction of maximum intensities due to the two wires (Fig. 5.28a : the differences are 1 dB and 5° respectively); these indicate wire-current amplitude and phase errors respectively.

(b) the s.ℓ.ℓ. on opposite sides of the main beam are different; at 1.0 GHz, the difference is 1 dB, and increases to 5 dB at 3.0 GHz. This indicates wire-current amplitude error.

(c) the pattern symmetry near (experimental) direction 180° deteriorates as the frequency increases.

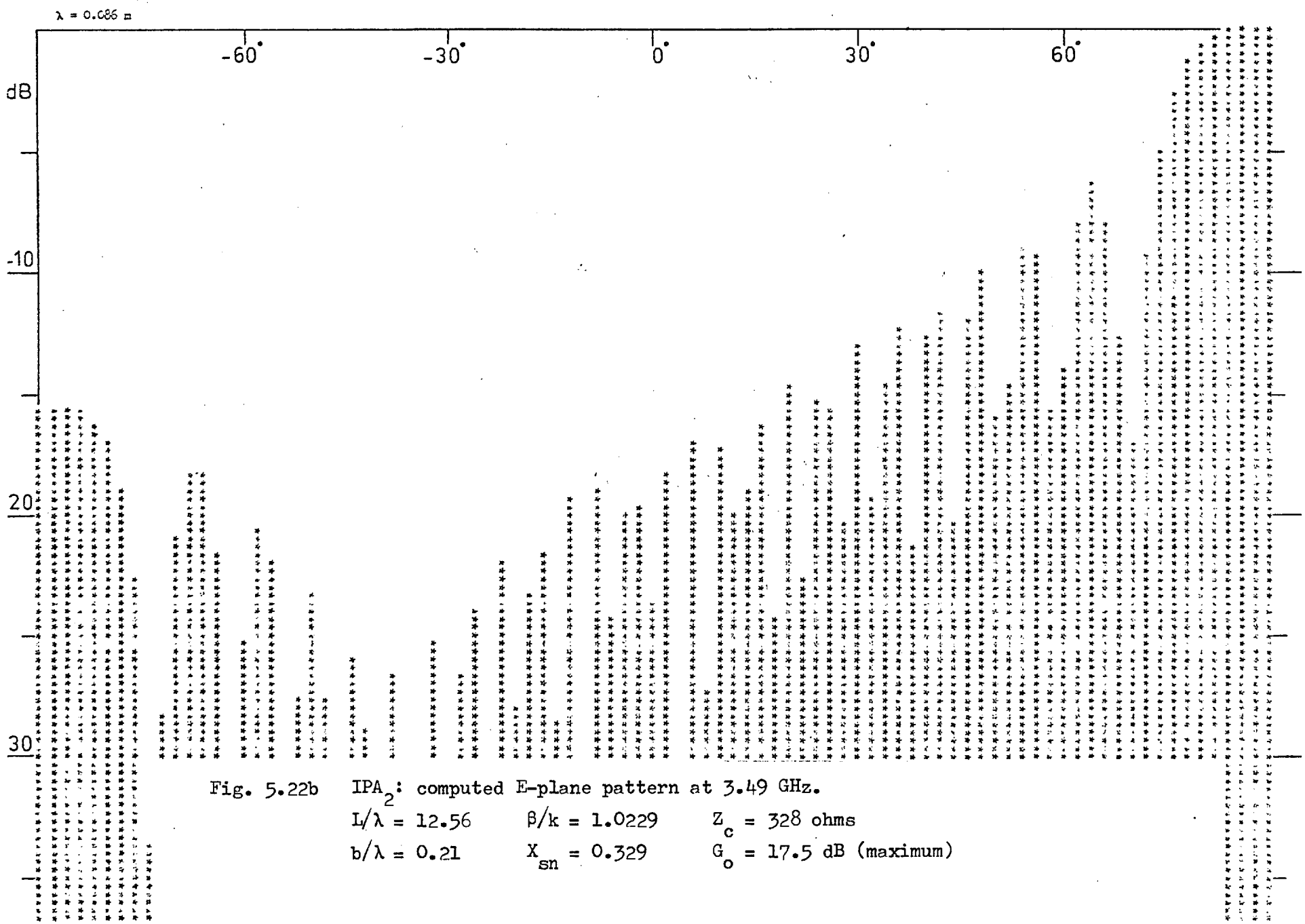


Fig. 5.22b IPA_2: computed E-plane pattern at 3.49 GHz.

$L/\lambda = 12.56$ $\beta/k = 1.0229$ $Z_c = 328$ ohms

$b/\lambda = 0.21$ $X_{sn} = 0.329$ $G_o = 17.5$ dB (maximum)

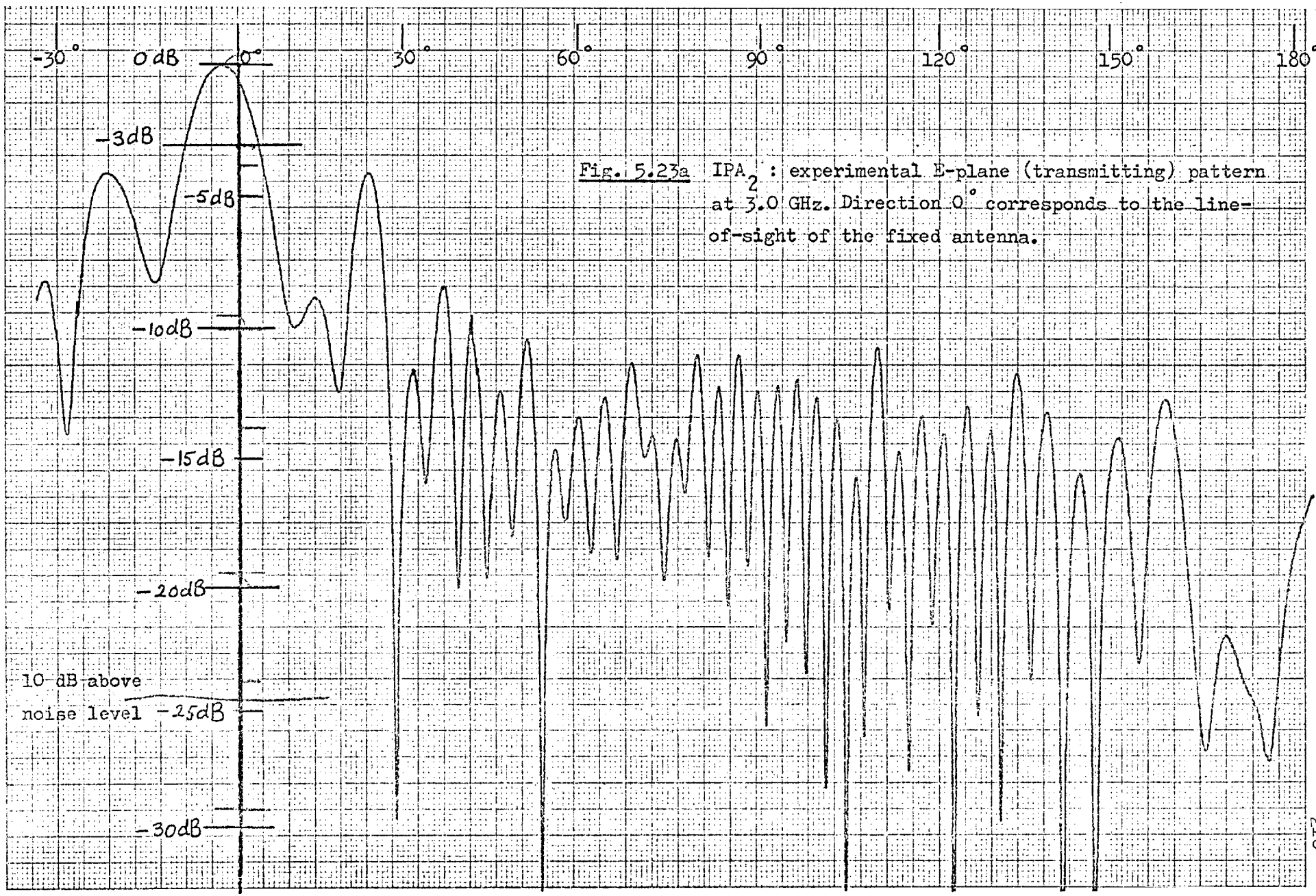


Fig. 5.23a IPA_2 : experimental E-plane (transmitting) pattern at 3.0 GHz. Direction 0° corresponds to the line-of-sight of the fixed antenna.

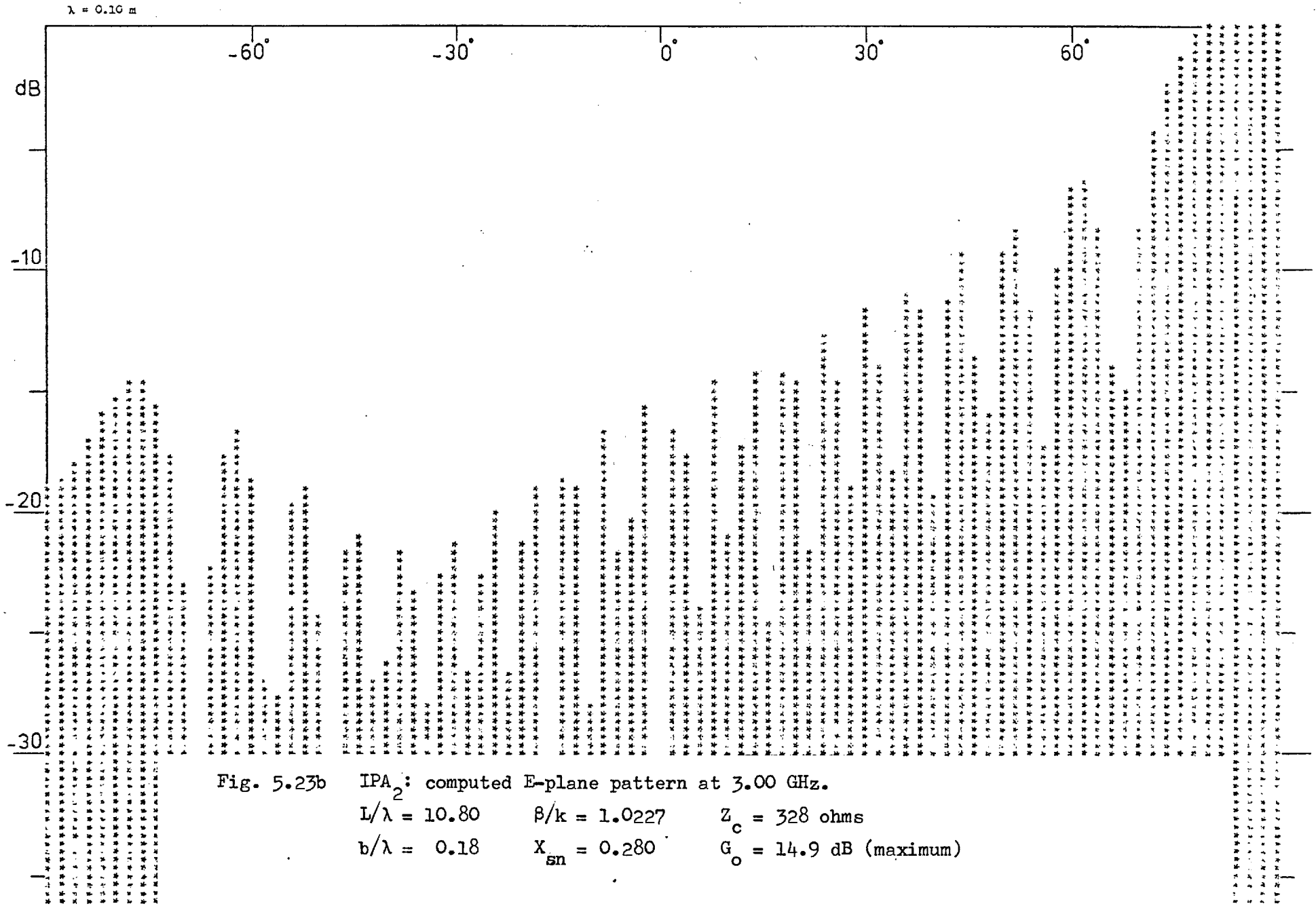


Fig. 5.23b IPA_2: computed E-plane pattern at 3.00 GHz.

$L/\lambda = 10.80$ $\beta/k = 1.0227$ $Z_c = 328$ ohms

$b/\lambda = 0.18$ $X_{sn} = 0.280$ $G_o = 14.9$ dB (maximum)

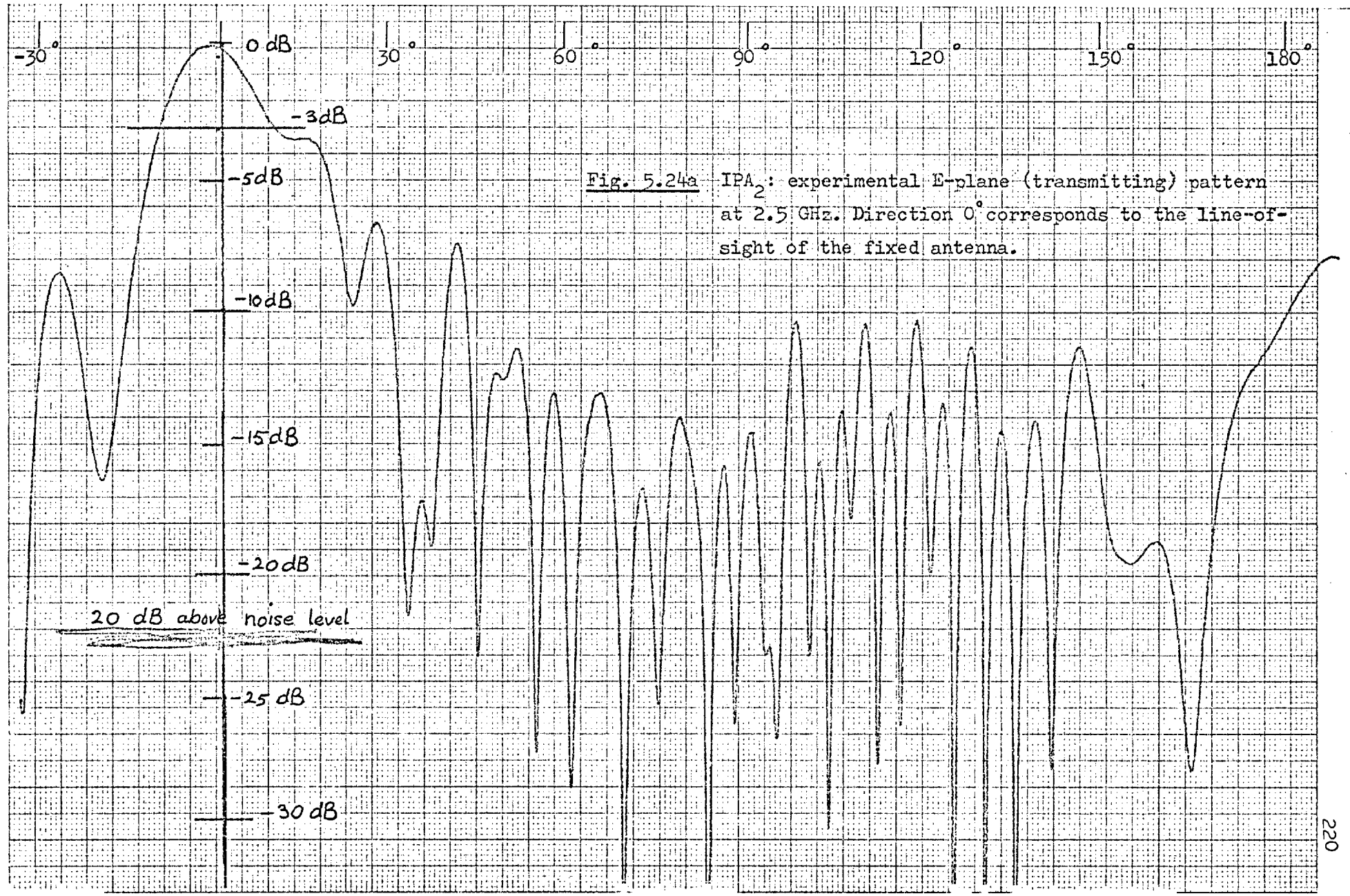


Fig. 5.24a IPA$_2$: experimental E-plane (transmitting) pattern at 2.5 GHz. Direction 0° corresponds to the line-of-sight of the fixed antenna.

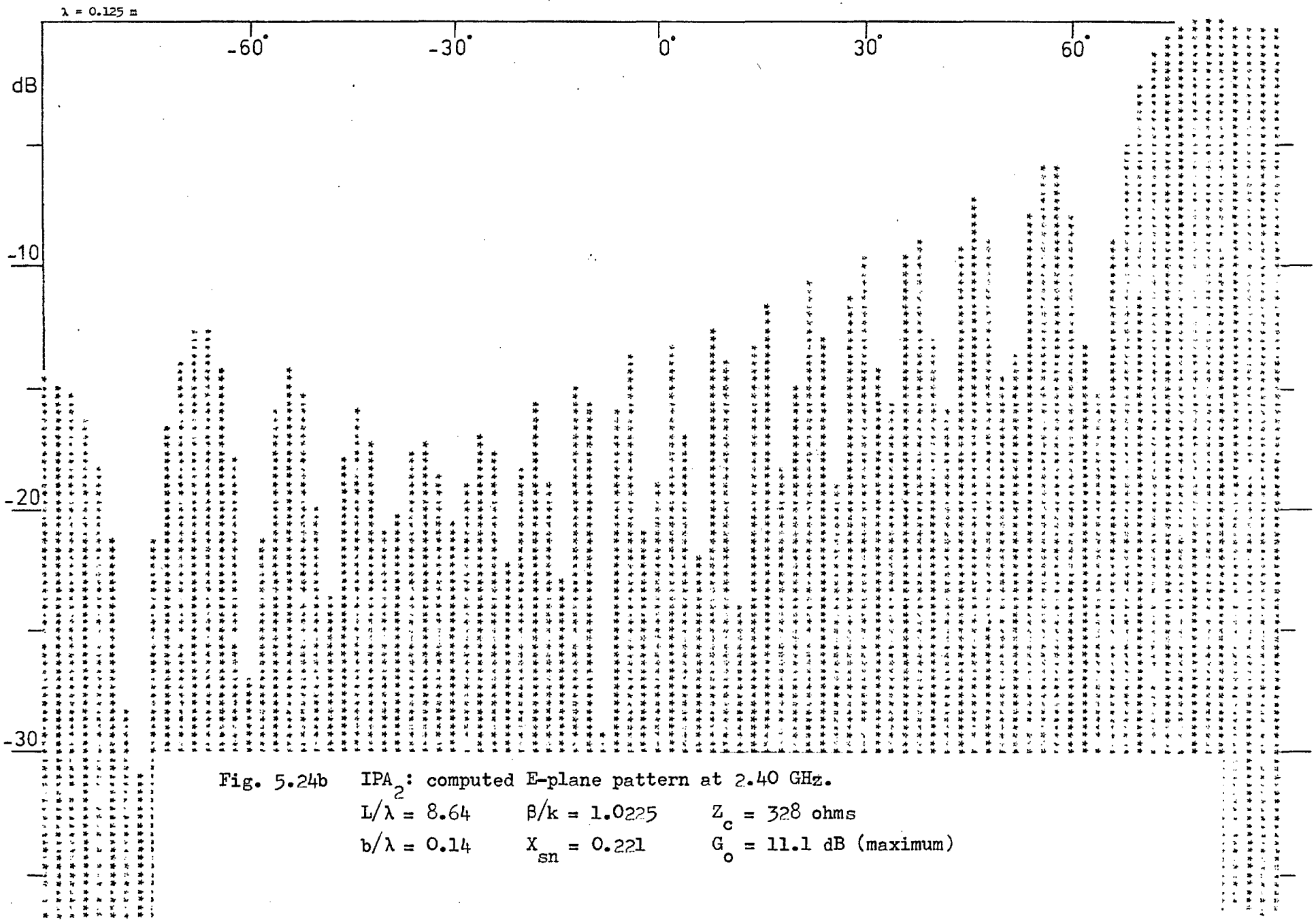


Fig. 5.24b IPA_2: computed E-plane pattern at 2.40 GHz.

$L/\lambda = 8.64$ $\beta/k = 1.0225$ $Z_c = 328$ ohms

$b/\lambda = 0.14$ $X_{sn} = 0.221$ $G_o = 11.1$ dB (maximum)

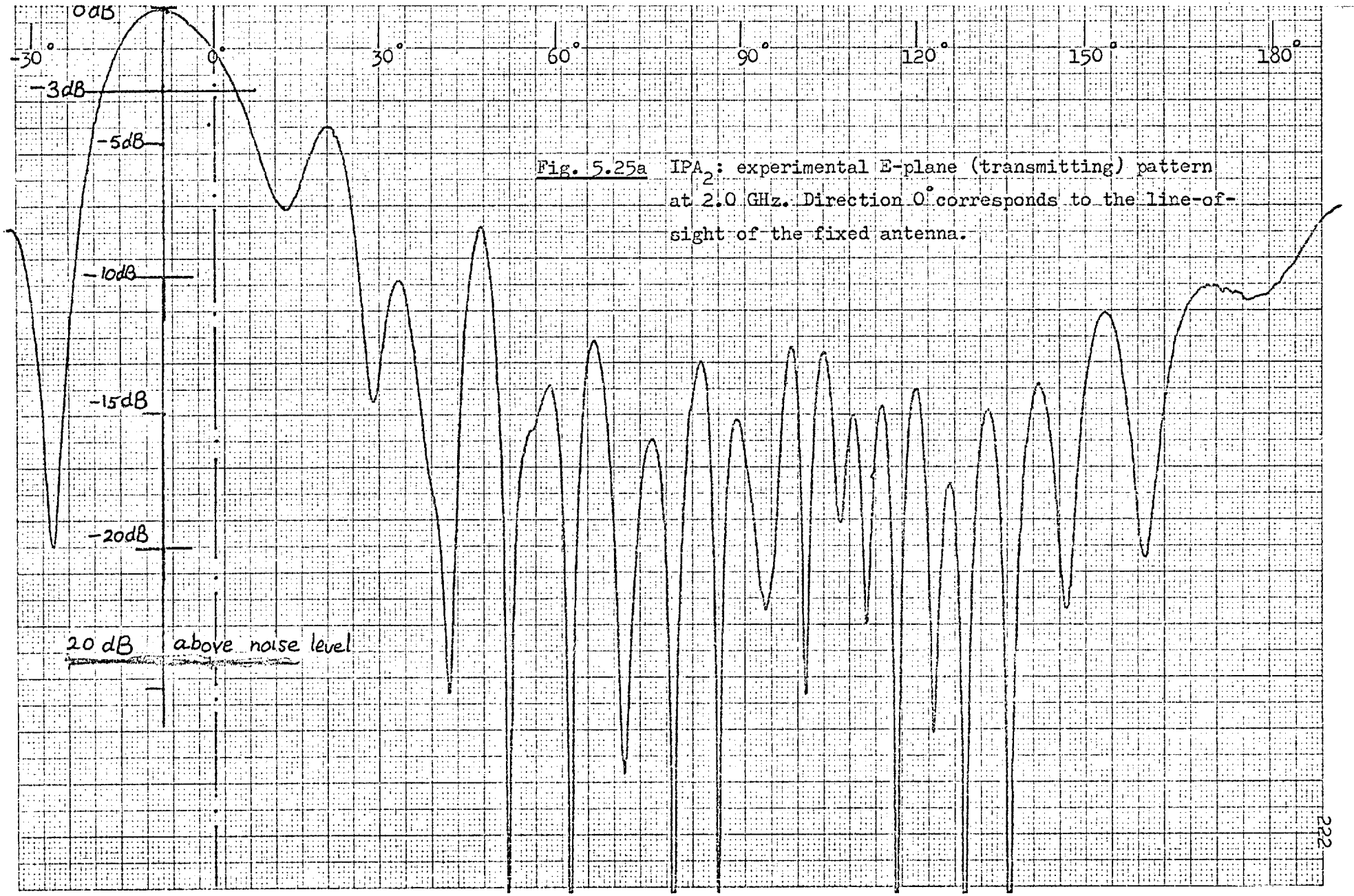


Fig. 5.25a IPA_2: experimental E-plane (transmitting) pattern at 2.0 GHz. Direction 0° corresponds to the line-of-sight of the fixed antenna.

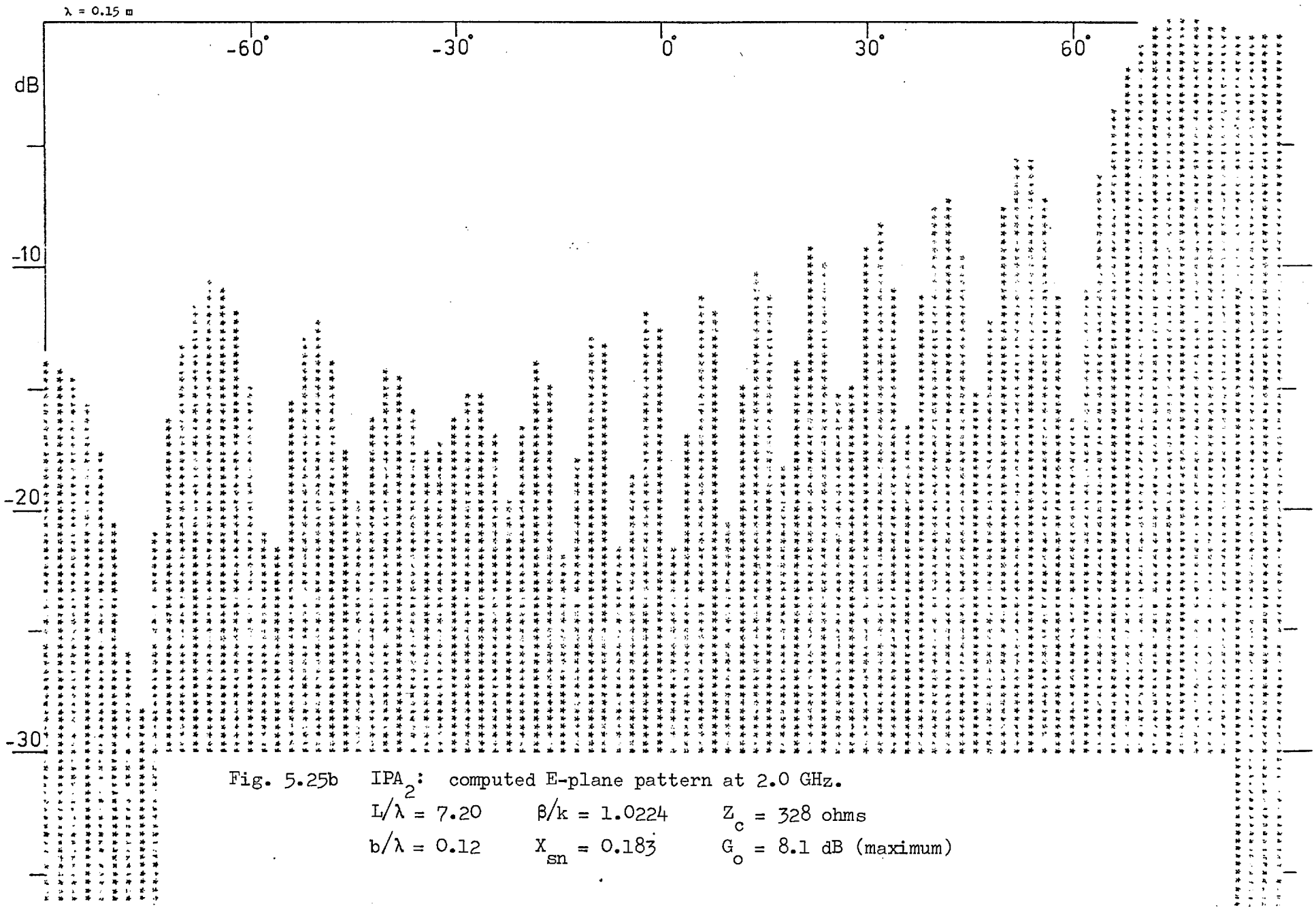


Fig. 5.25b IPA_2: computed E-plane pattern at 2.0 GHz.

$L/\lambda = 7.20$ $\beta/k = 1.0224$ $Z_c = 328$ ohms

$b/\lambda = 0.12$ $X_{sn} = 0.183$ $G_o = 8.1$ dB (maximum)

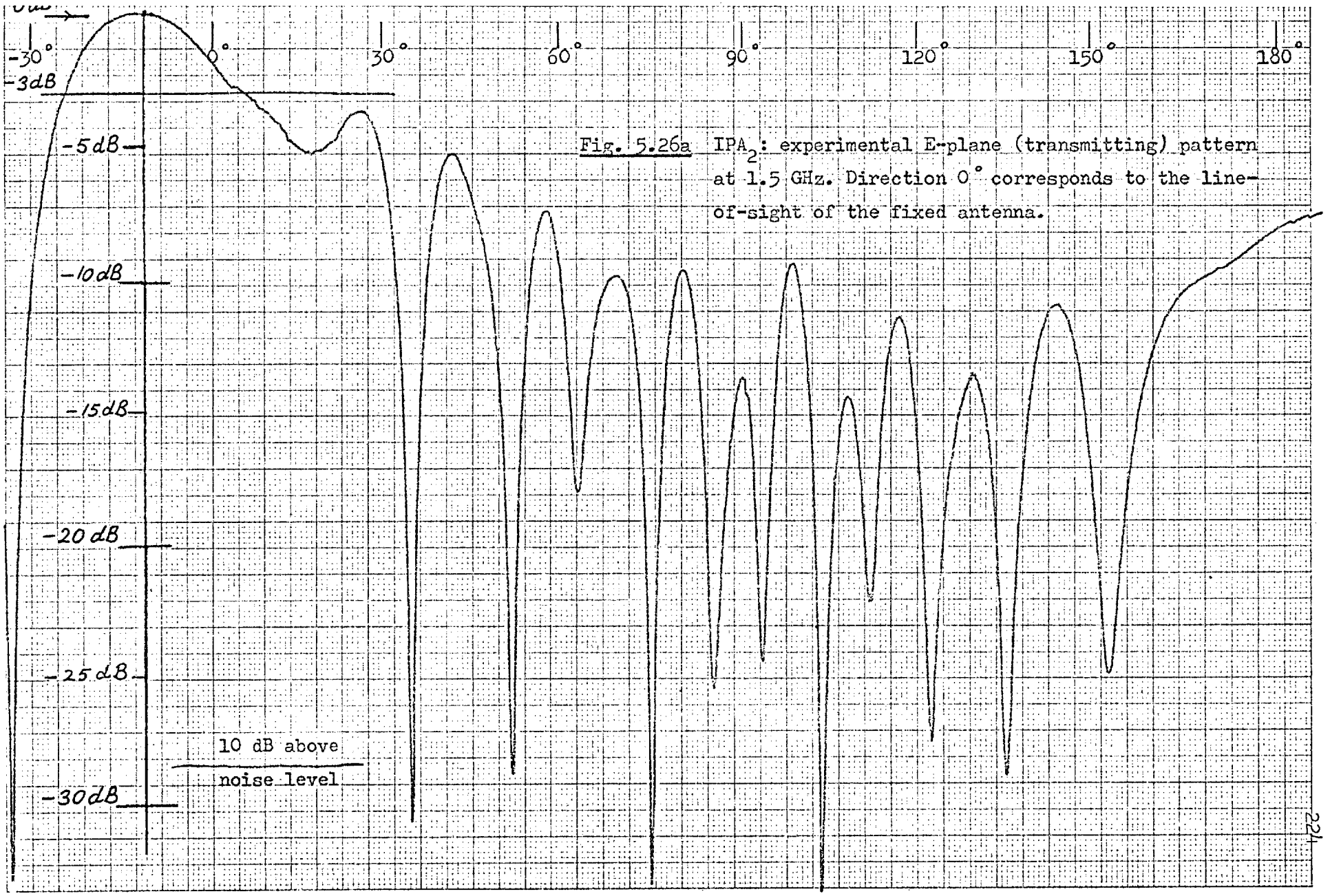


Fig. 5.26a IPA_2: experimental E-plane (transmitting) pattern at 1.5 GHz. Direction 0° corresponds to the line-of-sight of the fixed antenna.

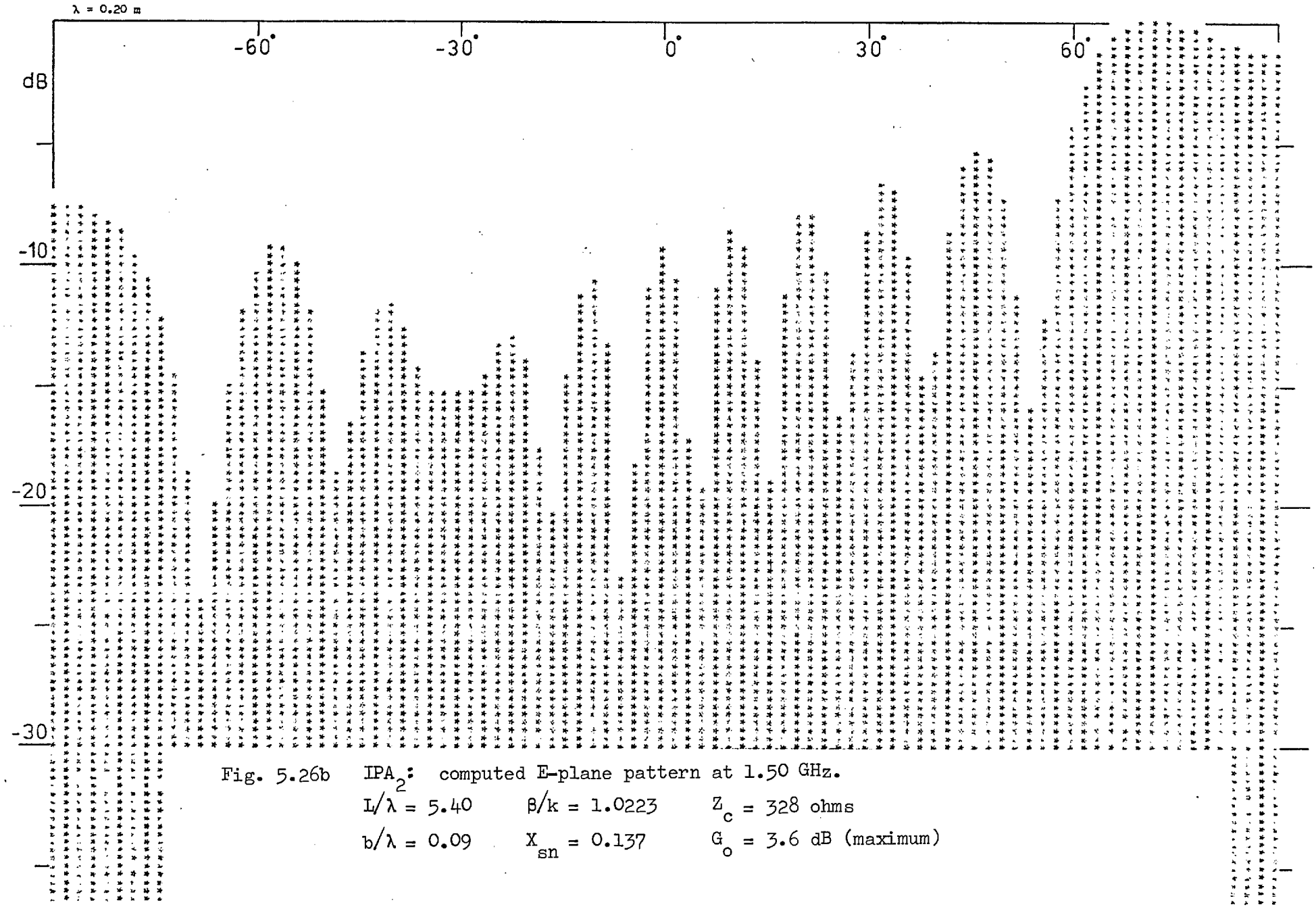


Fig. 5.26b IPA_2: computed E-plane pattern at 1.50 GHz.

$L/\lambda = 5.40$ $\beta/k = 1.0223$ $Z_c = 328$ ohms

$b/\lambda = 0.09$ $X_{sn} = 0.137$ $G_o = 3.6$ dB (maximum)

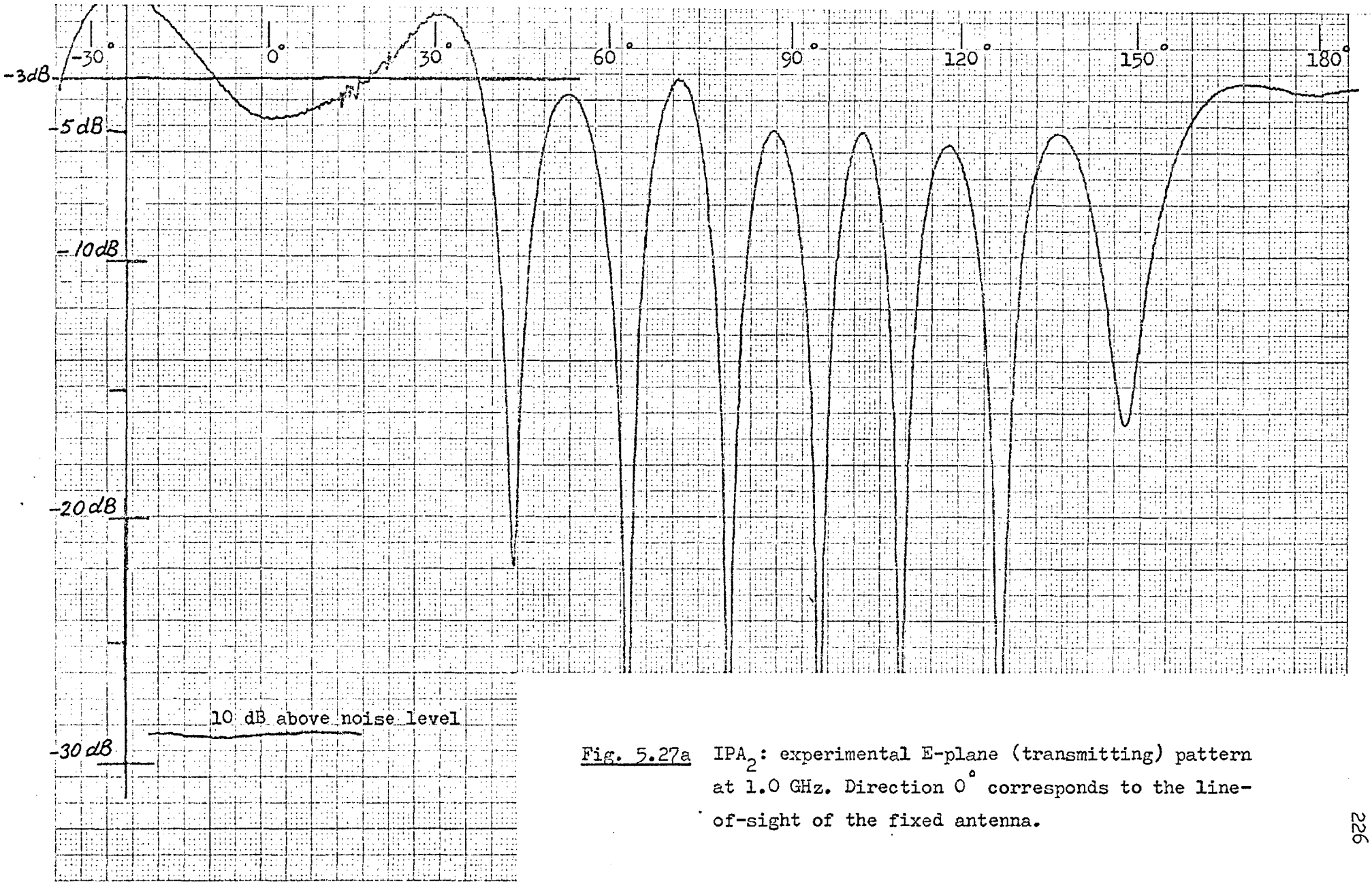


Fig. 5.27a IPA$_2$: experimental E-plane (transmitting) pattern at 1.0 GHz. Direction 0° corresponds to the line-of-sight of the fixed antenna.

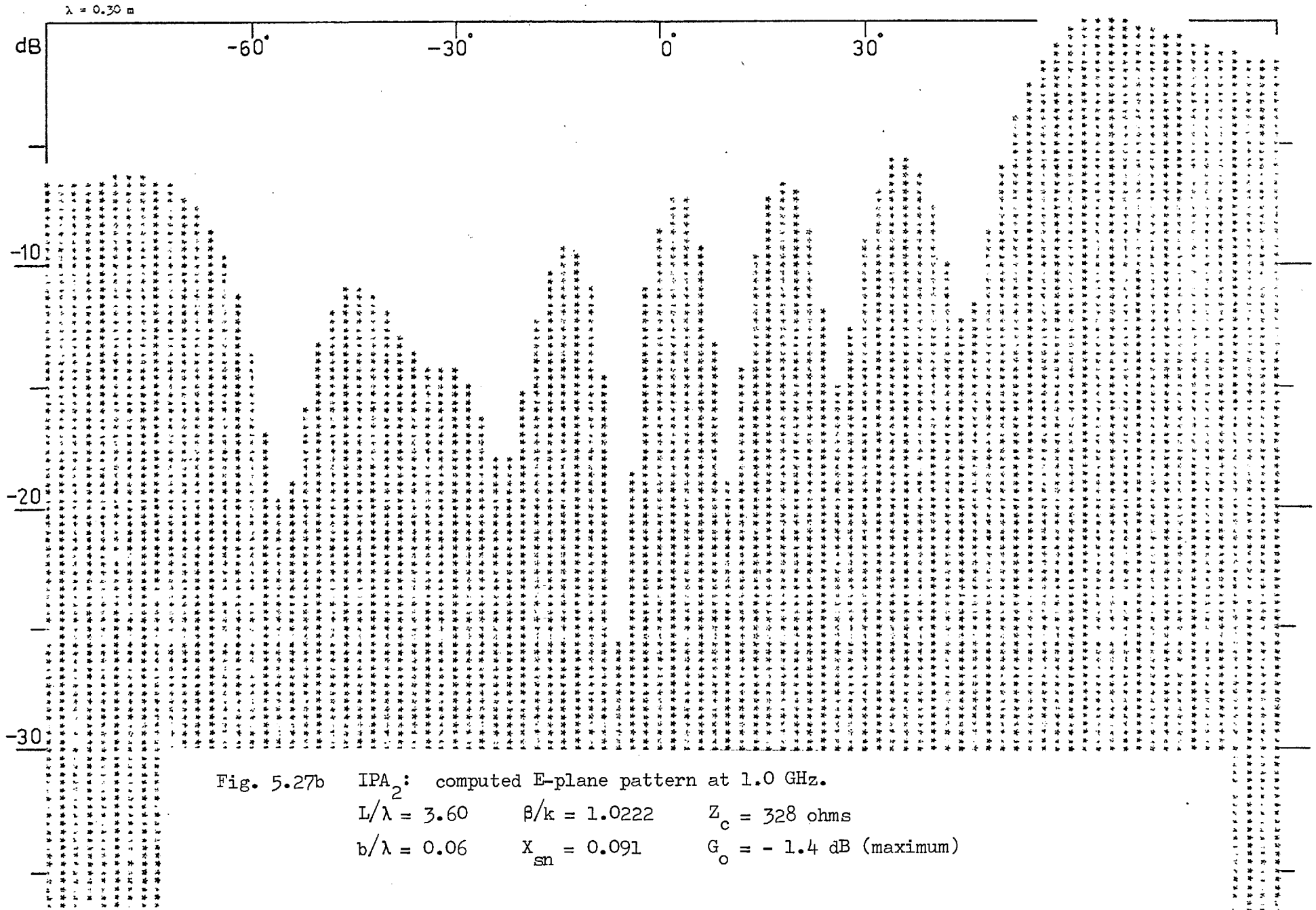


Fig. 5.27b IPA_2: computed E-plane pattern at 1.0 GHz.

$L/\lambda = 3.60$ $\beta/k = 1.0222$ $Z_c = 328$ ohms

$b/\lambda = 0.06$ $X_{sn} = 0.091$ $G_o = -1.4$ dB (maximum)

5.6.3. Concluding Remarks

Measurements of radiation characteristics were carried out in order to check the accuracy of analysis and computer programs developed for prediction of characteristics. The conclusion is that the theory is correct, the assumptions and approximations reasonably justified, and the results of computation accurate. This conclusion is principally on the basis of H-plane measurements. E-plane errors, due to site imperfections and asymmetries in the construction of the test antenna, prevented conclusive interpretation of experimental results; however, it must be emphasized that this limitation was confined to E-plane measurements only, and was partly compensated by a satisfactory analysis of errors, based on theory and supplementary measurements.

One class of errors has not been mentioned; that is, errors due to the non-infinite separation between the test and reference antennas [Ref. 5.4]. However, when these errors were significant their contribution to the overall errors became negligible, due to the presence of other sources of error. One particular effect is worth noting : side-lobe nulls became deeper as the frequency of measurement was decreased. This effect is readily seen by comparing experimental patterns at different frequencies, particularly in the H-plane.

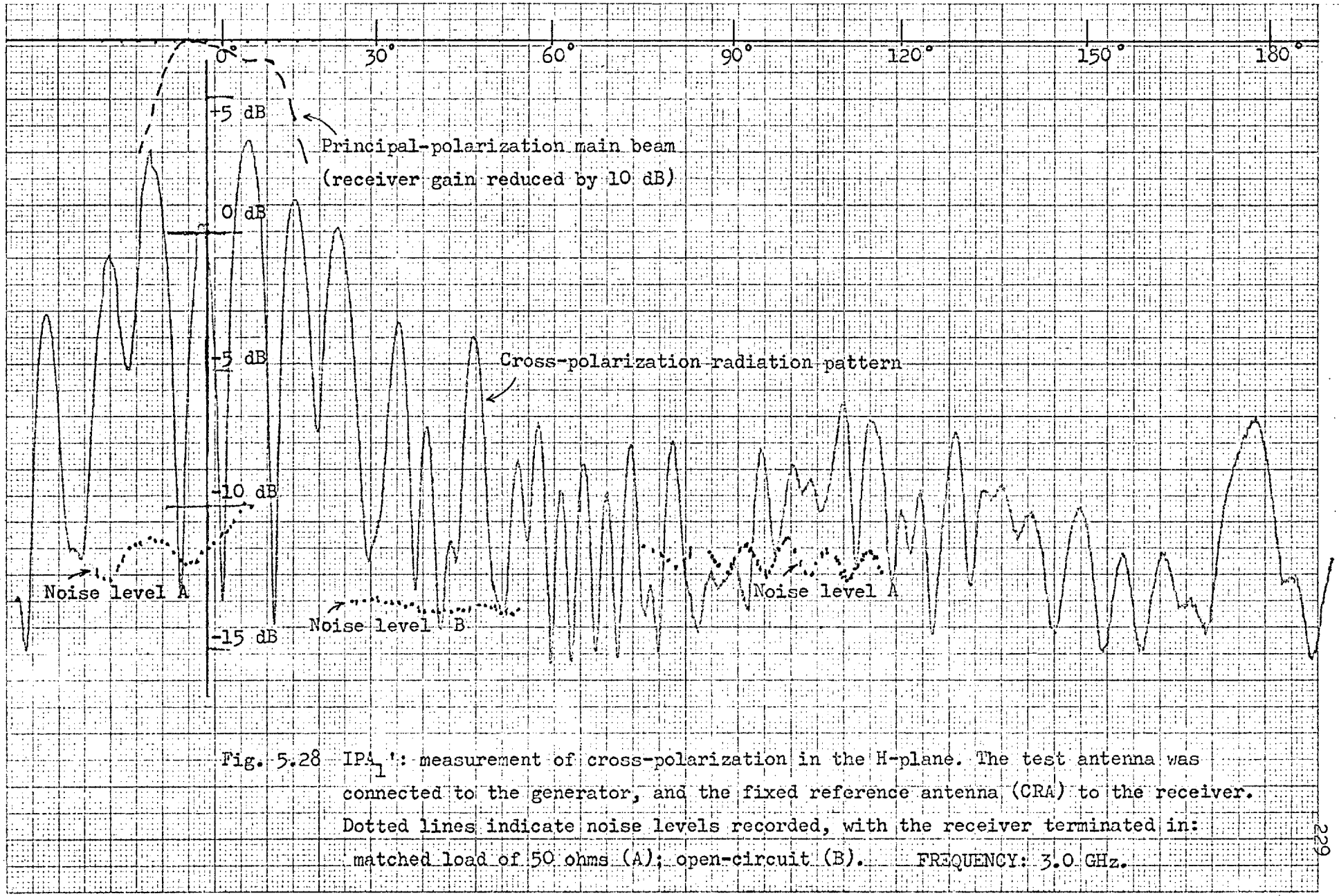


Fig. 5.28 IPA 1: measurement of cross-polarization in the H-plane. The test antenna was connected to the generator, and the fixed reference antenna (CRA) to the receiver. Dotted lines indicate noise levels recorded, with the receiver terminated in: matched load of 50 ohms (A); open-circuit (B). FREQUENCY: 3.0 GHz.

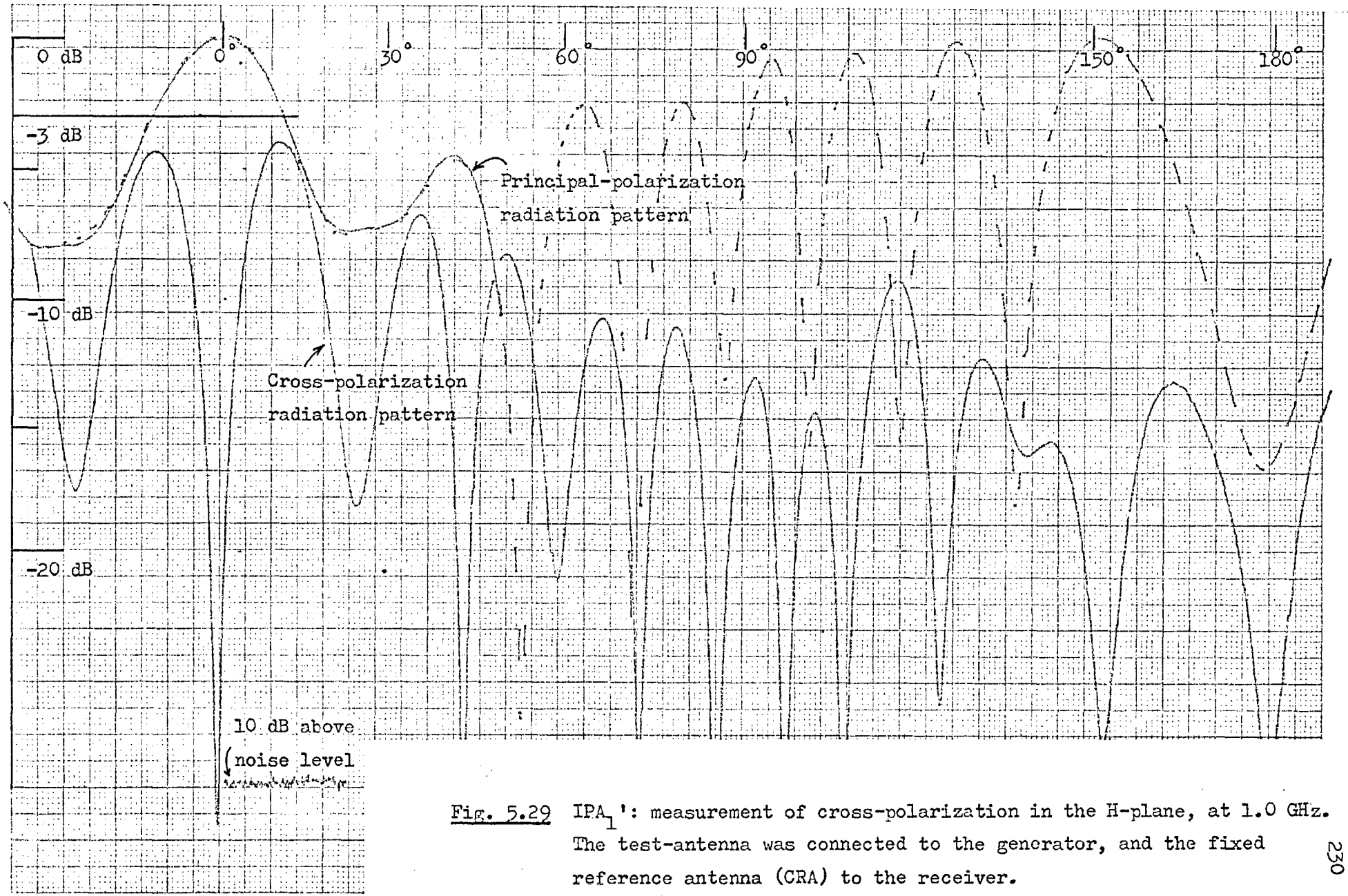


Fig. 5.29 IPA_1': measurement of cross-polarization in the H-plane, at 1.0 GHz. The test-antenna was connected to the generator, and the fixed reference antenna (CRA) to the receiver.

Freq. (GHz)	3.49	3.00	2.40	2.00	1.50	1.24	1.00
λ_o (m)	0.086	0.100	0.125	0.150	0.200	0.240	0.300
L/λ_o	12.79	11.00	8.80	7.33	5.50	4.58	3.67
b/λ_o	0.21	0.18	0.14	0.12	0.09	0.075	0.06
β/k	1.0229	1.0227	1.0225	1.0224	1.0223	1.0223	1.0222
X_{sn}	0.329	0.280	0.221	0.183	0.137	0.114	0.091
3 dB beam-width	22^o	26^o (27.5^o)	30^o (26.5^o)	32^o (34.5^o)	32^o (42^o)	30^o	32^o (25.5^o)
average side-lobe-level (dB)	- 15	- 13 (- 15)	- 11 (- 14)	- 8 (- 11)	- 6 (- 4)	- 5	- 4 (- 1)
maximum absolute gain G(dB)	17.7	15.1 (14.2)	11.0	7.6	2.5 (3.6)	-0.4	-2.7

Fig. 5.30 IPA_2 : Table of H-plane Characteristics. Quantities in Brackets Indicate Corresponding Experimental Values

[exception : instead of 2.4 GHz, experimental frequency of 2.5 GHz was used]

Freq. (GHz)	3.49	3.00	2.40	2.00	1.50	1.24	1.00
λ_o (m)	0.086	0.100	0.125	0.150	0.200	0.240	0.300
L/λ_o	12.56	10.80	8.64	7.20	5.40	4.50	3.60
b/λ_o	0.21	0.18	0.14	0.12	0.09	0.075	0.06
β/k	1.0229	1.0227	1.0225	1.0224	1.0223	1.0223	1.0222
X_{sn}	0.329	0.280	0.221	0.183	0.137	0.114	0.091
3 dB beam-width (dB)	29°	33° (13.5°)	41° (21°)	47° 24°	58° (27.5°)	64°	73° (75°)
average side-lobe-level (dB)	- 18	- 16 (- 12)	- 13 (- 12)	- 11 (-12.5)	- 9 (- 10)	- 7	- 7 (- 4)
maximum absolute Gain G(dB)	17.5	14.9	11.1	8.1	3.6	1.0	-1.4
main-beam dip (dB)	0	0	$1\frac{1}{3}$ (3.5)	$2\frac{2}{3}$ (7.5)	$11\frac{1}{3}$ (5)	$12\frac{2}{3}$	$12\frac{2}{3}$ (5)

Fig. 5.31 IPA_2 : Table of E-plane Characteristics.

Quantities in Brackets Indicate Experimental Values

[exception : instead of 2.4 GHz, experimental frequency of 2.5 GHz was used]

REFERENCES

5.1. Jasik, H. (editor): 'Antenna Engineering Handbook', McGraw-Hill, 1961, Sections 34.3 - 34.6.

5.2. Jasik, H.: Op. cit., Chapter 11.

5.3. Silver, S. (editor): 'Microwave Antenna Theory and Design', McGraw-Hill, 1949, pp 245-248.

5.4. Brown, J.: 'A Theoretical Analysis of Some Errors in Aerial Measurements', I.E.E. Monograph No. 285R, February, 1958.

CHAPTER VI

APPLICATIONS

6.1. Introduction

Two broad categories of research can generally be identified : first, 'basic research' which is concerned with determining the nature of a particular phenomenon, or with the evaluation of the general characteristics of a particular system. Second, 'applied research' which often requires the fulfilment of a particular specification, or the solution of a specific engineering problem.

The study reported in this thesis is more akin to the former research category (see Section 1.1). In Section 6.3 we propose some improvements to the IPA configurations considered in the previous chapters; and Section 6.4 contains a qualitative appraisal of the IPA for communication-systems applications.

The present study also overlaps with the 'applied research' category in two respects:

First, it should be recalled that the research study presented in this thesis was initially triggered off by a requirement for a wide--band directive antenna, for which the specification was given in Section 1.2. Even though, in the early stages of this study, this requirement was fulfilled by a different antenna (see Section 1.2), originally it was hoped that the IPA might turn out as a worthwhile contender. This expectation was based on the results of a first-order (perturbation) analysis which indicated that the velocity of propagation along the IPA should be invariant with the frequency of operation. However, further analysis, supported by near-field measurements (Section 3.6), indicated that the phase velocity decreases with frequency : i.e., β/k increases

with frequency (where β is the phase constant and k the free-space wave-number). This is in contrast with the requirement for optimum--directivity end-fire arrays, for which β/k should decrease with frequency [Ref. 6.1]. Consequently the IPA has a pattern band-width of 2:1 (approximately), which does not fulfil the specification of 7:1 bandwidth in the initial requirement (see Section 1.2).

Second, recently there has been a search for some means of improving the efficiency of the Beverage antenna, for transmission applications at HF and VHF (see Section 1.3). In this connection, we shall present a tentative proposal, which is based on the performance characteristics of the IPA, for increasing the efficiency of the (single-wire) Beverage antenna. This proposal and other pertinent material are contained in Section 6.2.

There are three aspects of the IPA design problem which have been omitted from consideration in this thesis. The first problem is related to the wide-band design of launching devices required to energize the antenna. However, this is essentially a question of wide-band design of baluns and impedance transformers, which has been treated extensively in the published literature [Refs. 6.2 - 6.4].

The second problem is associated with the availability of discrete impedance elements suitable for wide-band matching of the IPA at its load termination. This does not appear to be a serious practical problem, particularly as we successfully employed standard low-frequency resistors to provide the antenna with a matched termination above 1.0 GHz (see Section 5.3, and Fig. 5.6).

The third and final question is concerned with the mode of excitation of the IPA (Section 4.4). It has been shown that the anti-symmetric mode of excitation (Figs. 4.3 and 4.4b) yields wide-band radiation

characteristics, with the main beam directed along the wire axis. It turns out that the symmetric mode of excitation (Fig. 4.4a) would result in a deep null in the direction of the wire axis. This conclusion only applies to IPA_2, but similar results should also be obtained for IPA_1 if the single wire is replaced by two parallel wires excited in the balanced mode (see Appendix 3C.1).

The above property of the IPA makes it eminently suitable for direction-finding and position-fixing applications.

6.2. Proposals for Increasing the Efficiency of the Beverage Antenna

The motivation for attempting to improve the efficiency of the Beverage antenna was discussed in Section 1.3. It should be emphasized that the principal objective is to increase the antenna gain; reducing the antenna losses generally increases both the directivity and the radiation efficiency, with a consequent improvement in the antenna gain figures.

The problem of increasing the efficiency of the Beverage antenna can be approached in three different ways:

(1) The antenna wire is modified such that the radiated power along the length of the antenna is increased relative to the power dissipated in the ground.

(2) The ground is modified such that ground losses are reduced for (substantially) the same magnitude of surface impedance.

(3) The wire is modified such that the magnitude of tangential fields at the ground surface is reduced, thereby reducing the antenna losses.

The first method given above has already been employed by El-Enein and Professor Brown [Ref. 6.6]. El-Enein's proposal essentially consists

of periodic series loading of the horizontal wire with capacitive elements. The resulting structure is a leaky-wave antenna (LWA) which supports a fast-wave mode. This remarkable proposal appears to be the only effective solution to date to the problem of increasing the efficiency of the Beverage antenna. Because of the potential applications of the LWA, a critical appraisal of El-Enein's work is given in Appendix 6A.

El-Enein has presented a comparison between the radiation characteristics of the LWA and the Beverage antenna in the band 3-30 MHz. Unfortunately this comparison is not entirely realistic because the two antennas chosen for comparison had very different physical parameters. The heights of the LWA and the Beverage were 7.5 m and 3.0 m respectively; the lengths were 180 m and 300 m respectively. Nevertheless it is possible to conclude that series capactive loading of the wire would lead to a useful increase in the radiation efficiency, over a significant portion of the transmission band envisaged. Consequently a reduction in the overall length of the antenna is also possible, but only at the expense of reduced directivity at lower frequenceis.

It is worthwhile noting that Ege [Ref. 6.7] has solved both boundary--value problems (the Beverage antenna and the LWA) by numerical methods, employing point-matching techniques. His results indicate that El-Enein's analysis might yield inaccurate results above 20 MHz, for the particular configuration proposed.

The second method proposed for improving the efficiency of the Beverage antenna is directly related to the research work on the IPA reported in this thesis. For example, a set of conducting strips could be constructed at the ground surface (Fig. 6.1), beneath the wire, to simulate a corrugated-plane effect. This arrangement would have the

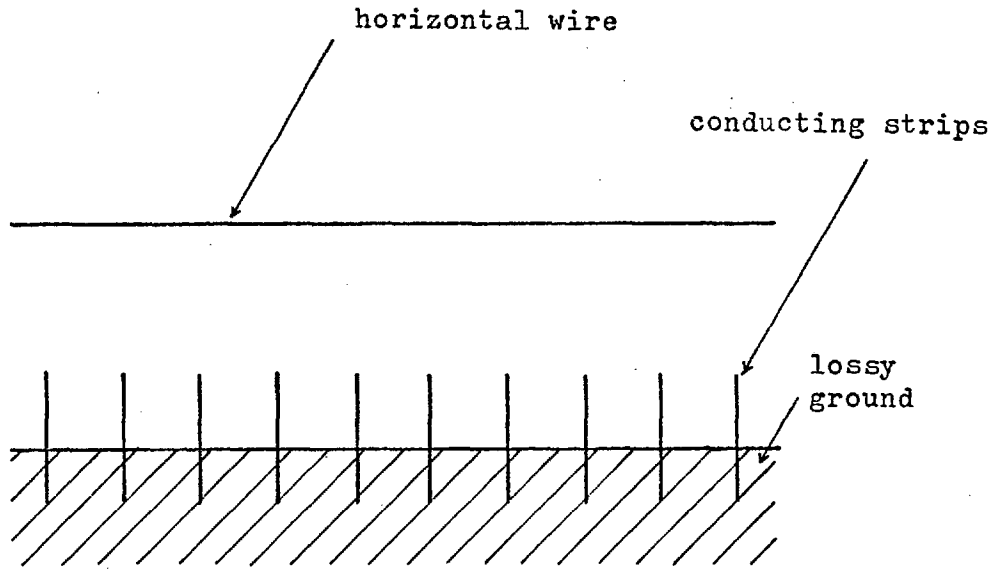


Fig. 6.1 Proposed Corrugated-Plane Geometry to Reduce Ground Losses

effect of reducing the ground losses by increasing the ratio X_s/R_s, where $Z_s = R_s + jX_s$ is the effective surface impedance of the ground. However, the realization of such a system might prove too costly at HF where antenna lengths of the order of 300 m would be required. However, it <u>might</u> be possible to obtain similar reductions in ground losses by employing grids of wires to simulate the conducting-strip arrangement, for example as indicated in Fig. 6.2.

The third proposal could be realized either by periodic series loading of the antenna wire with inductive elements, or by coating the wire with a thin layer of dielectric material. Both methods would yield a reduction in the phase velocity of the antenna; it is expected that there would be a significantly higher concentration of power density near the 'inductive wire', resulting in lower ground losses. It is likely that the dielectric coating would be a better practical proposition, and would result in lower ohmic losses than series loading with inductive elements.

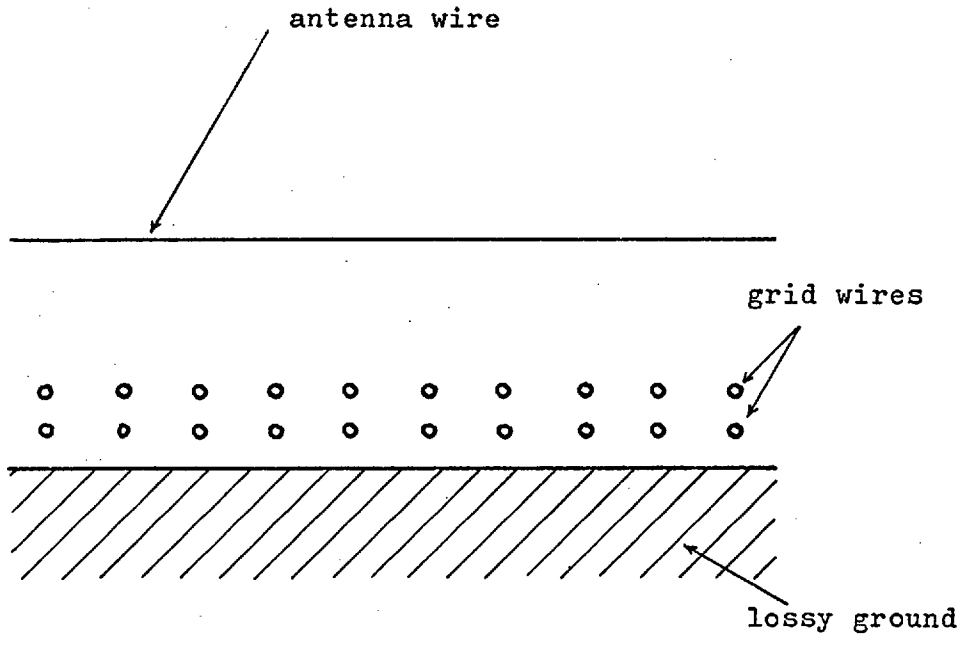


Fig. 6.2 Proposed Wire-Grid Geometry to Reduce Ground Losses

It is worth noting that proposals (2) and (3) have two distinct advantages over proposal (1), i.e., the LWA. Firstly, both proposals would reduce the <u>total</u> attenuation along the Beverage antenna : this would result in increased efficiency <u>and</u> increased directivity, in contrast to LWA's increased efficiency but <u>reduced</u> directivity at low frequencies. Secondly, proposals (2) and (3) would offer larger transient bandwidths than the LWA. This observation is based on a comparison of $\beta - \omega$ characteristics of the IPA and the LWA; the latter indicates greater non-linear behaviour.

Proposals (2) and (3) are both novel concepts, and consequently require further investigation to validate them. In particular it is likely that the antenna load termination might depict critical interaction

with radiation from the horizontal wire in proposal (3).

Finally it must be noted that horizontal arrays of closely spaced Beverage antennas have been investigated, also for the purpose of increasing the radiation efficiency [Ref. 6.8]. Theory indicates that an array of 11 parallel wires, with a regular spacing of 6 m, yields an increase of 5 dB approximately in antenna efficiency (at 6 MHz, η increases from 5% to 15%).

6.3. Proposed Modifications to the IPA

The geometric configuration of the IPA chosen for analysis and experimental evaluation, in the research study reported heretofore, had the advantage of simplicity - which facilitated validation of the theory and correlation between analytical and measured data. In this section we shall propose two simple modifications which should yield an improvement in the antenna characteristics; these proposals are equally applicable to IPA_1 and IPA_2.

The first modification is related to the input terminals and the load termination of the antenna : it is proposed to replace the wires which are perpendicular to the interface by sloping wires, as indicated in Figure 6.3. With this modification, broad-band matching would be easier, both at the load termination (to reduce standing waves along the antenna length) and at the input terminals (to match the antenna to the feeder cable).

The second modification consists of replacing the single wire parallel to the interface by an array of parallel wires, as indicated in Figure 6.4 which shows a periodic array of four wires.

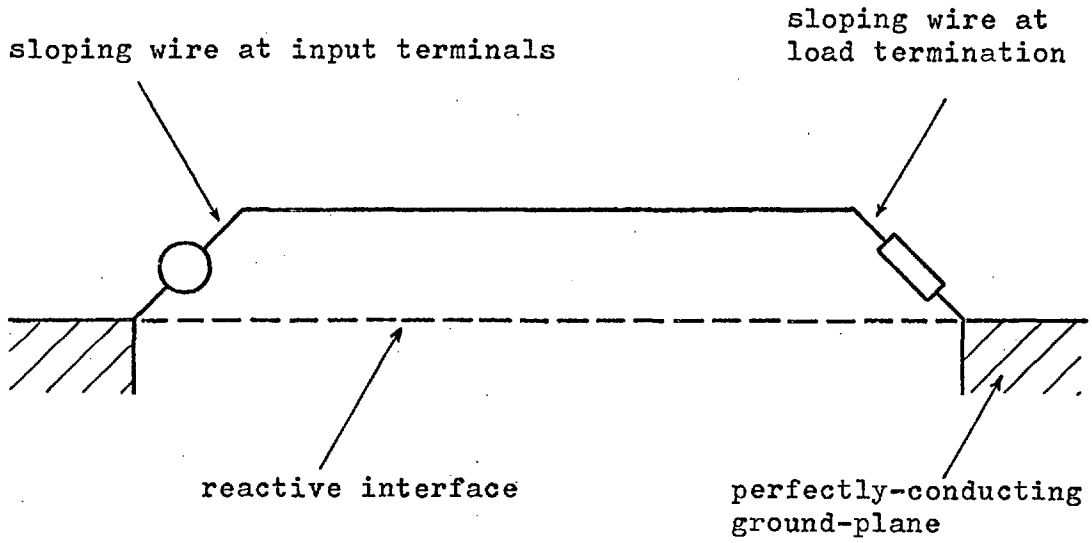


Fig. 6.3 Proposed Modification to the Input Terminals and the Load Termination of IPA_1

The array spacing S_A should be at least twice the wire-to-interface spacing b, so that adjacent wires are only loosely coupled. This modification has the following effects:

(1) Doubling the number of wires nearly halves the characteristic impedance Z_c, and therefore the input impedance. For example, if Z_c for the single-wire IPA_1 is 300 ohms, the corresponding value for the array of Fig. 6.4 is 75 ohms approximately. This would facilitate the design of a broad-band balun for feeding the antenna from a coaxial cable [Ref. 6.2].

(2) It seems that doubling the number of wires increases the antenna gain by nearly 3 dB (see (1) above and Eq. (4.94)]. From a mathematical view-point, this effect can be explained as follows; for a given <u>total</u> wire-current, the <u>maximum</u> power intensity remains constant in the far-field; whereas the <u>input</u> power to the antenna is reduced by increasing the number of wires. However, physical considerations of

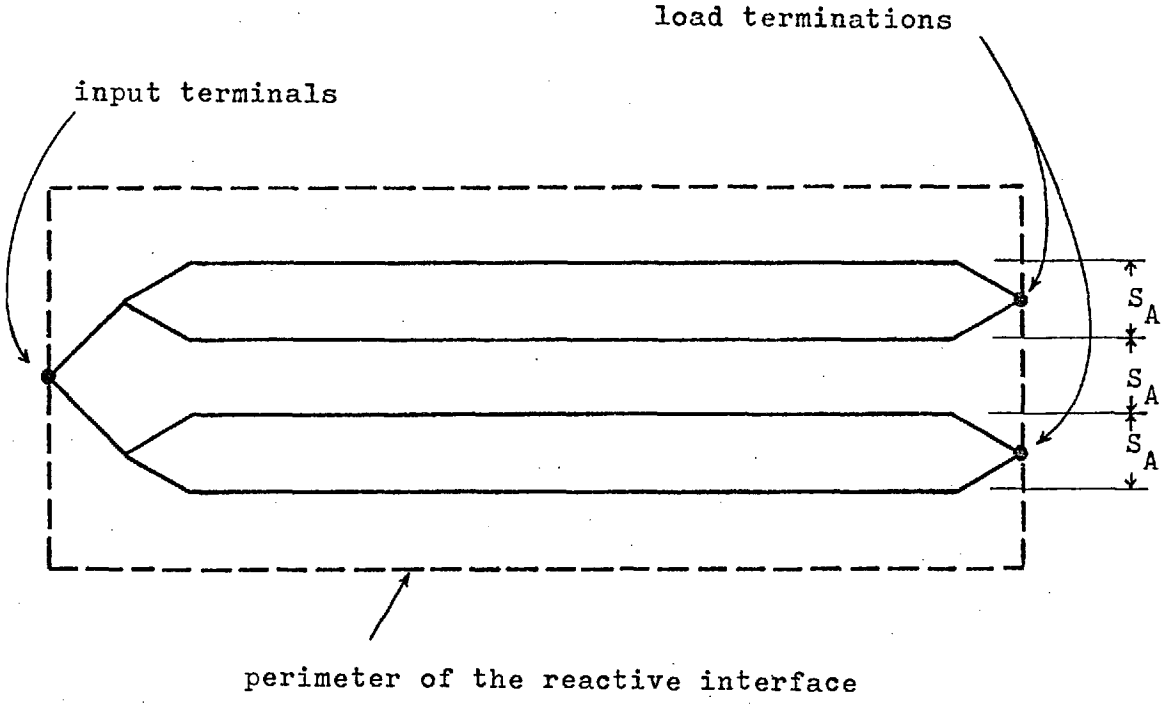


Fig. 6.4 Plan View of Array of Parallel Wires Equidistant From the Plane Interface

power conservation indicate that the increased gain can only arise from a corresponding improvement in directivity.

(3) Proper choice of array spacing S_A reduces the s.*l*.*l*. and increases the directivity : for optimum results from the four-wire array, S_A should approximately correspond to the free-space wavelength at the highest operating frequency. It should be noted that this improvement is directly related to the array space-factor.

The above results are based on the assumption of equal wire currents. Consequently the results somewhat depend on the method of interconnection between the wires, both at the input and at the load termination. The symmetrical arrangement of Fig. 6.4 should yield at least approximately equal wire currents.

A practical factor which has been neglected in the above considerations is the finite width of the reactive interface. This would reduce the relative contribution of the outside wires to the radiation field, particularly if the separation between the outside wires and the edges of the reactive interface is less than one-half the wavelength. For a particular application, it is expected that both the number of wires and the width of the reactive plane would be determined by practical physical constraints.

6.4. Comparison of the IPA with Other Antennas

In the design of any particular communication system, the antenna engineer is faced with the problem of choosing and optimizing one specific antenna system. The material of this section is pertinent to the above problem.

For comparison purposes we have chosen two antennas which have extensive applications in the VHF and UHF bands : the Yagi [Refs. 6.9 - 6.11], and the log-periodic dipole (LPD) antenna [Refs. 6.12 - 6.16]. The comparison presented is mainly qualitative since we are not concerned with the detailed analysis for only one specific system application.

The Yagi antenna has the advantage of simple construction, with relatively large tolerance requirements for manufacturing. In contrast the LPD antenna has the disadvantage that its construction requires small tolerances for satisfactory operation [Ref. 6.12]; for example, for a LPD operating in the band 0.45 - 0.85 GHz the element spacings have been specified to within 0.5×10^{-3} m ($\sim 1.5 \times 10^{-3}\ \lambda_o$ at the maximum frequency) [Ref. 6.16]. On the other hand, although the construction of the IPA is more complicated, the tolerances required are approximately one order

of magnitude larger. Both the Yagi and the LPD have the additional (mechanical) advantages of relatively low weight and low wind loading, compared to the IPA. However, IPA_1 can be flush mounted on a structure (e.g. on a building, ship, or sattelite), whereas the other two antennas generally require significant clearances for satisfactory operation.

The differences between the three antennas become even more significant when their electrical characteristics are considered. The most important difference is the (steady-state) bandwidth B_s, defined as the ratio of maximum to minimum frequencies. (The bandwidth is defined with reference to a specification of minimum required gain, or directivity, and maximum permissible standing-wave-ratio at the input; for example see the specification given in Section 1.2). Typical feasible values of B_s are 1.2, 10 and 2 for the Yagi, LPD and IPA respectively. However, the above figures refer to the <u>steady-state</u> bandwidth only. The <u>transient</u> bandwidth B_t of the LPD is much smaller than its B_s [Ref. 6.14]. This is predominantly due to the active region of the LPD moving along the antenna towards the apex with increasing frequency. Consequently, when a wideband signal (e.g., a narrow pulse) is transmitted the higher frequencies are radiated before the lower frequencies. The B_t of the IPA is expected to be much closer to its B_s due to two factors : its $\beta - \omega$ characteristics are fairly linear; and the phase centre of the antenna is almost fixed near its physical mid-point. Hence the IPA might be a more attractive proposition than the LPD for some wideband-signal (or pulse) applications.

Both Yagi and LPD antennas depict fairly constant gain characteristics over the bandwidth : typical gain variations are $\pm$ 1.5 dB and 0.5 dB respectively [Refs. 6.11 and 6.16]. In contrast, the gain of

the IPA increases with frequency. Again, this might be regarded as a desirable feature of the IPA if it is noted that the transmission loss between two isotropic antennas also increases with frequency [Ref. 6.17]. Furthermore, the gain-frequency characteristics of the IPA can be controlled by proper choice of the corrugation depths.

Finally we note that both Yagi and LPD antennas have more compact sizes than the IPA, for similar (average) gain figures. The LPD and the Yagi have the lowest and highest s.ℓ.ℓ.'s respectively : < -20 dB, and < -8 dB. On the other hand the LPD has the widest beam-width ($\sim 60^{\circ}$), whereas the IPA has the narrowest beam-width ($\sim 30^{\circ}$, at the maximum frequency).

6.5. Suggestions for Future Work

In the final analysis there remains one approach to resolve the controversy associated with the Beverage antenna (Sections 2.2 and 4.3) and that is the experimental technique. We suggest that the attenuation and phase constants should be measured along a prototype Beverage antenna, for a number of different launching devices, over the band 20 - 100 MHz. Furthermore, the variation with frequency of the tangential field components at the surface of the ground, say directly below the wire, should be determined. Another experiment, which would provide further insight into the mode of action of the antenna, would consist of determining the spatial variation of the field above the wire, preferably at a number of discrete distances from the antenna input terminals.

The two novel proposals for increasing the efficiency of the Beverage, Section 6.2, also constitute suggestions for future work.

As regards the IPA, there are many possibilities for further

research work. However, we shall confine ourselves to only two suggestions.

The theory presented in this thesis is relatively simple and depends on the validity of many physical approximations. It should be very useful to determine the quantitative limits of its validity by carrying out further complementary measurements on structures with deeper corrugations and different wire-to-interface spacings.

Finally, it might be possible to achieve shorter IPA lengths, or wider (steady-state) bandwidths, by departing from the uniform cross-section principle. In this connection, we offer two suggestions : a linear variation along the antenna length, of either the wire-to--interface spacing or the corrugation depths; and, secondly, a periodic variation of the corrugation depths to simulate a modulated surface reactance.

APPENDIX 6A

A CRITICAL APPRAISAL OF "A LEAKY-WAVE TRANSMITTING ANTENNA FOR THE BAND 3 - 30 MHz" [REF. 6.5]

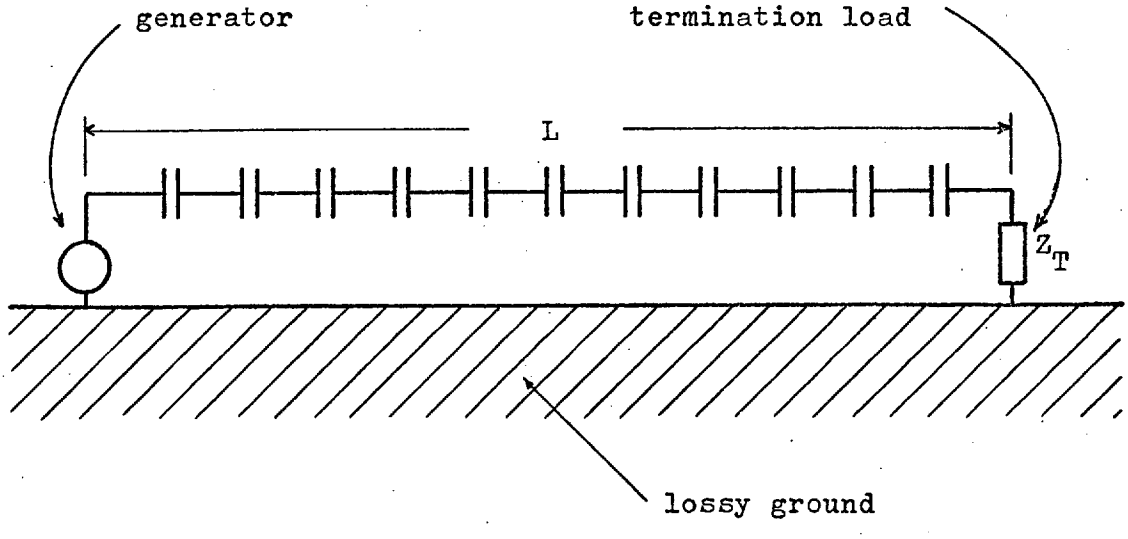


Fig. 6A.1 Schematic Representation of the Leaky-Wave Antenna (LWA)

The Leaky-Wave Antenna (LWA) has been proposed as a modification to the Beverage antenna, in order to increase the efficiency of the latter so that the same antenna can also be used for transmission (as well as reception) in the HF band [Ref. 6.6].

The basic form of El-Enein's proposed LWA is depicted in Fig. 6A.1. The antenna consists of a straight length of wire above plane ground; the wire height is b, radius a, and length L. The wire is series loaded with discrete impedance elements Z_L (normally capacitance elements), with periodic spacing S. When the antenna is used for transmission, the generator is connected between one end of the wire and ground; the

other end of the wire is grounded through a discrete termination load Z_T (which is normally open-circuit).

Unless otherwise stated, details given in square brackets refer to El-Enein's thesis [Ref. 6.6].

El-Enein's thesis can be divided into three main parts: part 1 [Chapters 2 and 3] consists of the analysis of the basic system (Fig. 6A.1) when both the wire and the plane ground are perfectly conducting; part 2 [Chapter 4] extends the analysis to plane ground with finite conductivity; and part 3 [Chapter 5] describes and evaluates various modifications to the basic system, such as multi-wire structures and distributed loading techniques. Experimental results presented in the above thesis are relevant to part 1 only, i.e., to the study of the basic system employing a perfectly-conducting ground plane.

The above thesis represents an important contribution to the field of antenna engineering, and the LWA concept is a remarkable solution to the problem of increasing the efficiency of the Beverage antenna. However, the thesis contains a number of errors and shortcomings which should be noted, if only because of the significant applications of the proposals. In the remainder of this appendix, some important sources of error in El-Enein's proposals will be enumerated; analytical errors not affecting the conclusions will be excluded. It is emphasized that these errors do not detract from the value of El-Enein's work; merely that specific applications arising from his proposals might require some modification in order to achieve optimum results.

Appraisal of Part I (perfectly-conducting ground)

The analysis of the basic system (with perfectly-conducting ground) is generally elegant and effective. The propagation constant

along the antenna is obtained by an iterative process involving three steps:

(1) The phase constant, β, along the antenna and the characteristic impedance, Z_c, are obtained by a circuit analysis of a uniform periodic section of the antenna which is regarded as a lossless transmission line with (periodic) series capactivie loading, jX_L [pp 20-24].

(2) The far-field of the antenna is represented as an angular spectrum of plane waves due to a horizontal line current above plane perfectly-conducting ground. Integration of the far field yields the attenuation constant corresponding to the total power radiated per unit length of the antenna [pp 26-31].

(3) A series resistance R_L is introduced into the equivalent circuit of the unit section of the antenna, in order to represent the radiation losses. The propagation constant $\gamma = \alpha + j\beta$ and the characteristic impedance Z_c are calculated again in terms of the new value of the loading impedance $Z_L = R_L + jX_L$ [pp 31-32].

There is excellent agreement between computed and measured values of the propagation constant [pp 49-50].

The far-field analysis for calculating the radiation pattern [pp 53-62] is similar to that presented in the present thesis, Sub-section 4.6.2. However, El-Enein assumes that the surface of the LWA is perfectly-conducting [p. 54]: this is incorrect, due to periodic capactive loading which requires non-zero gaps in the antenna wire-structure. Consequently, El-Enein's calculations in terms of an equivalent space distribution of electric current densities neglects possible contributions from the necessary distribution of magnetic current densities.

Another questionable approximation is El-Enein's assumption of uniform current distribution in the terminal wires [p. 58]. At best, this is a reasonable approximation for an antenna height less than one-quarter wavelength; the height of the proposed LWA is 7.5 m, i.e., three-quarters wavelength at 30 MHz [p. 16].

Comparison of El-Enein's computed and experimental radiation patterns indicate discrepancies exceeding 12 dB in the side-lobe levels; shapes and positions of computed and experimental side-lobes are also different [pp 70 - 73].

Appraisal of Part II (finite ground conductivity)

In this part [Chapter 4] the following sources of error can be identified:

(1) The ground losses are assumed to be the same for loaded-wire and unloaded wire structures [pp 79-81]. This assumption seems unjustified, because the magnetic field at the surface of ground is heuristically expected to be greater for a fast-wave line source than for a slow-wave line source; consequently, El-Enein's results for lossy ground could only be correct to the first order of approximation.

(2) The loading effect of lossy ground is calculated according to Knight's formula [pp 77 - 81]. Earlier in this thesis (Sections 2.2 and 3.3.3), it was emphasized that Knight's formulae yielded substantial errors at frequencies above 10 MHz. Consequently El-Enein's equivalent-circuit elements, representing the loading effect of the ground, are approximately correct below 10 MHz only.

(3) It is assumed that the attenuation α_R due to radiation is the same for perfectly-conducting and lossy grounds [p. 81]. This is incorrect, since an unloaded wire above lossy ground radiates. However,

it is possible that the change in α_R, due to ground loading effects, is negligible at some frequencies. Nevertheless the conclusion "the directivity of the aerial will decrease as the length increases" [p. 85] seems questionable.

(4) The direct comparison between the characteristics of loaded- and unloaded-wire antennas above lossy ground [pp 85 - 90] is somewhat misleading; because the height of the LWA above ground is 7.5 m, whereas the height of the Beverage antenna (unloaded wire above ground) is 3.0 m only. [The latter height is given by dos Santos: Ref. 6.8, p. 78].

REFERENCES

6.1 Walter, C.H.: 'Travelling Wave Antennas', McGraw-Hill Book Co., 1965, pp 322-325.

6.2 Oltman, G.: 'The Compensated Balun', I.E.E.E. Transactions on Microwave Theory and Technique, Vol. MTT-14, No. 3, pp 112-119, March 1966.

6.3 Duncan, J.W. and Minerva, V.P.: '100:1 Bandwidth Balun Transformer', Proc. I.R.E., Vol. 48, No. 2, pp 156-164, February 1960.

6.4 Evans, B.G.: 'Chebyshev Quarter-Wave Stepped Balun Transformer', Electronics Letters, Vol. 9, No. 22, pp 514-516, 1st. November, 1973.

6.5 C.C.I.R.: 'World Distribution and Characteristics of Atmospheric Radio Noise', Report 322, International Telecommunication Union, Geneva 1964.

6.6 El-Enein, M.H.: 'A Leaky-Wave Transmitting Antenna For The Band 3-30 MHz', Ph.D. Thesis, Imperial College, University of London, May, 1973.

6.7 Ege, T.: 'Application of Numerical Methods to Wire-Like Antenna Structures', Doctoral Thesis (to be presented), Imperial College, University of London.

6.8 dos Santos, A.F.: 'Multi-Beam Receiving Antenna For the Band 3-30 MHz', Ph.D. Thesis, Imperial College, University of London, September, 1970.

6.9 Jasik, H. (editor): 'Antenna Engineering Handbook', McGraw-Hill Book Co., 1961, Sections 5.6 and 24.6.

6.10 King, R.W.P., Mack, R.B. and Sandler, S.S.: 'Arrays of Cylindrical Dipoles', Cambridge University Press, 1968, Section 6.9.

6.11 J. Beam Aerials Limited: 'Production Bulletins', Northampton, England, 5th. June, 1963.

6.12 Jasik, H. (editor): Op. cit., Section 18.3.

6.13 King, R.W.P. et al.: Op. cit., Sections 6.14 - 6.16.

6.14 Mittra, R.: 'Log-Periodic Antennas', published as Chapter 22 of "Antenna Theory", Part II (edited by Collin, R.E. and Zucker, F.J.), McGraw-Hill Book Co., 1969, pp 378-380.

6.15 Weeks, W.L.: 'Antenna Engineering', McGraw-Hill Book Co., 1968, pp 275-288.

6.16 Eaton, J.L. and Thoday, R.D.C.: 'A U.H.F. Log-Periodic Receiving Aerial', B.B.C. Research Department Report No. 1969/20.

6.17 Livingston, D.C.: 'The Physics of Microwave Propagation', Prentice-Hall, Inc., New Jersey, 1970, pp 9-10.

LIST OF PRINCIPAL SYMBOLS

a, a_1	wire radius
b	spacing between the wire axis and the interface
c	free-space velocity of propagation
d	depth of corrugations
$\underline{E}$	electric field strength ($\underline{E}_t$ = transverse component)
$\underline{H}$	magnetic field strength ($\underline{H}_t$ = transverse component)
k	free-space wave number ($= 2\pi/\lambda_o$)
k_1	wave number of medium 1 ($= k$)
k_2	wave number of medium 2
K_r	complex relative permittivity of ground
S	corrugation periodic spacing
t	thickness of corrugation walls
v	phase velocity along the antenna
Z, Z_o, Z_1	intrinsic impedance of the dielectric medium (free--space)
$Z_c = R_c + jX_c$	characteristic impedance of the antenna
Z_{co}	characteristic impedance of the ideal transmission--line corresponding to the antenna geometry
$Z_{cn} = Z_{co}/Z_o$	normalized value of Z_{co}
$Z_s = R_s + jX_s$	surface impedance
$Z_{sn} = Z_s/Z_o$	normalized value of Z_s
$\gamma = \alpha + j\beta$	propagation constant along the antenna
γ_2	intrinsic propagation constant of medium 2
ϵ_r	dielectric constant of medium 2 (ground)
λ, λ_o	free-space wavelength ($= 2\pi/k$)
σ_2	conductivity of medium 2 (ground)
ω	angular frequency